Connectivity Design and Control of Multilateral Systems under Time Delay

August 2017

NISHIMURA, Satoshi

A Thesis for the Degree of Ph.D in Engineering

Connectivity Design and Control of Multilateral Systems under Time Delay

August 2017

Graduate School of Science and Technology
Keio University

NISHIMURA, Satoshi

Acknowledgements

This dissertation is a summary of my research from April 2012 to September 2017 as the member of Katsura Laboratory, the Faculty of Science and Technology, Keio University. In the five and a half years since I entered the laboratory, I have had many valuable experiences and I was supported by a lot of people. Here, I would like to express my gratitude to the all people who have given me the supports and advices.

First of all, I would like to be deeply grateful from my heart for my supervisor Associate Professor Dr. Seiichiro Katsura, Department of System Design Engineering, Keio University. His dedicated teaching has grown me and provided a lot of precious things. Moreover, his passion for the academic research has inspired me to do research activity and to develop the novelty. Besides, he provided a lot of opportunities such as making the presentation of my research at domestic and international conference, participating in exhibitions. I can never imagine that I could accomplish this work without this kind help.

I would like to offer my special thanks to the members of my Ph. D. dissertation committee, Professor Dr. Toru Namerikawa, Department of System Design Engineering, Keio University, Professor Dr. Hideo Saito, Department of System Design Engineering, Keio University, and Associate Professor Dr. Takahiro Yakoh, Department of System Design Engineering, Keio University, who also gave me fruitful advices at regular research meetings.

I would like to show my appreciation to Professors who always gave precious comments at the research meetings. I would like to thank Professor Dr. Kouhei Ohnishi in Keio University, Professor Dr. Toshiyuki Murakami in Keio University, Professor Dr. Hiroaki Nishi in Keio University, and Assitant Professor Dr. Takahiro Nozaki in Keio University.

I would like to thank to Mr. Yoshitaka Abe, Mr. Hiroki Onoyama, Mr. Yusuke Kawamura, Mr. Koichiro Nagata, Mr. Takami Miyagi, and Mr. Bagus Rezandi Mohammad who are my colleagues. I had great experiences collaborating with you during the life in the laboratory. I was able to go through my research life because we were able to cooperate with each other.

As my career of research activities, the Japan Society for the Promotion of Science (JSPS) has provided me the financial support. I would like to show my gratitude to the organization. By the support, I could get various opportunities to conduct my research and to make the presentation at the academic

conferences.

Let me appreciate everyone who collaborated with and help me in Katsura Laboratory. The things which I obtained at this laboratory are treasurable for me.

Finally, I would like to express my gratitude to my family who bring me up and help me a lot. Your kind and warm-hearted assistance have enabled me to study without any inconvenience, and I would like to thank you from my heart.

August, 2017

Satoshi Nishimura

Table of Contents

List of Figures

List of Tables

Chapter 1

Introduction

Chapter 1 describes the background, motivation and chapter organization of this dissertation. Section 1.1 shows the background of this dissertation, which consists of three subsections. Section 1.2 explains the motivation of this dissertation, then chapter organization is written in Section 1.3. For explaining the previous two parts, the related studies are introduced.

1.1 Background of This Dissertation

This section firstly shows the research background. Research of networked control systems is showed first, then related research regarding control of multilateral systems is highlighted. As one of the applications of multilateral systems, research of telehaptics is explained.

1.1.1 Control through Network

Networked control systems (NCS) are the research field that has been widely studied for years [1,2]. In NCS, controllers and controlled plants are placed in spatially separated locations and connected through communication networks. Several reasons can be regarded as the cause of the development of NCS, for example, the improvement regarding network equipment, progress of computational processing speed. One of the biggest benefits of NCS is that it can realize remote control operation. An operator does not have to go further to control a system directly. An operator of the system does not directly have to go to the operated area; meaning that the range of activity can be expanded.

Because of the remote operation, delays comes inside the control loop. One particular feature of NCS is that it contains a time delay element inside the system, which makes the whole control system unstable and deteriorates control performance. Network delay and packet dropout problem are one of the important research topics. Time delay compensation itself is a well-researched topic even outside of NCS as one of the examples is a delay in an actuator and sensor [3]. Connection to remote places requires transmission time that information arrives at the remote system, which ends up as time delay element in the control system. Control that contains time delay inside the control loop is a challenging research for its serious phase delay. A situation where dropout problem occurs is also required to be considered, especially in wireless connection.

A compensation method for time delay can be divided into two types: whether the model of the delay time is used in a controller or not. One of the most popular delay compensation methods that use a delay time model is the Smith predictor [4]. It uses the model to remove the delay element from the poles of a transfer function, and if the model perfectly matches the delay time, the system becomes stable. Two degrees of freedom structure was proposed in [5] by extending the structure of the Smith predictor. The Smith predictor was applied to multivariable systems in [6]. In NCS, the delay time varies because of the jitter in a communication line, and sometimes information from the remote system is lost because there might occur packet loss. A jitter buffer approach is a rational method to attenuate the effect of the variation of a delay time. It enables to linearize the nonlinearity of time-varying delay at the cost of enlarging the delay time [7]. The buffer size is adapted based on the condition of the delay so that the delay time can be shortened [8]. A feedback controller to adjust the queuing delay in the jitter buffer and the interval of receiving packets is determined by implementing a low-pass filter in [9].

The other type of the delay compensation is the way without the use of a delay time model. A communication disturbance observer (CDOB) was proposed in [10, 11]. The delay is modeled as a network disturbance, and the effect was compensated by an observer structure. This method has high stability performance; however, command tracking performance and disturbance rejection performance are not satisfying. Various methods were proposed to enhance the tracking performance in CDOB. The Q-filter in CDOB was modified to realize position tracking in the steady state in [12]. Model error feedback base on H_2/H_∞ control to compensate the plant modeling error was proposed in [13]. A jitter buffer is used in CDOB to enhance the command tracking performance in [14]. There are other methods that do not use the delay model. A model-based prediction approach is proposed in [15] to ensure both closed-loop stability and tracking performance. A random dropout packet is assumed in [16], and the

setpoint is dynamically compensated for following the desired objective.

1.1.2 Control of Multilateral Systems

Control of multi-agent systems has been recently attracting attention as a society becoming more broad and complex. Connectivity between agents and how the connectivity affects the motion of an agent and the overall motion of a system is a primary interest in the research field. Numbers of applications can be expected in multi-agent systems: microgrids [17], sensor networks [18], formation control of multiple spacecrafts [19], etc.

One of the backgrounds why the research field has increased interest is that agents are gaining more and more mobility thanks to the improvement of network technologies [20]. It has become much easier to connect distant points and cooperate with agents in remote places. A research field that tries to realize cooperative motion with multiple agents is called decentralized control [21]. There are two main topics in multi-agent systems: control technique to conduct a transferring motion and control to achieve consensus. To realize transferring motion with many subsystems, a COG position of a whole system has to be controlled. On the contrary, the consensus problem is trying to control the formation of an entire system because consensus problem only focuses on regulating position errors to 0. In this dissertation, motions mentioned above are named as a COG motion and formation motion, respectively.

Research in [22] realized to achieve cooperative motion by using optimal control. [23] realized stable flocking motion in fixed topology.

The consensus problem is a well-researched topic for realizing the agreement between systems [24]. The study in [25] shows useful results how the connectivity of the system affects the performance and the stability of the whole system in the consensus problem through a network, and the detailed proof is reported in [26]. Passivity based control was introduced in [27] to realize formation stabilization. Then the stability margin of the system was newly defined in [28]. Event based consensus problem was studied in [29]. Observer-based consensus control under time delay was proposed in [30]. Average consensus problems with delayed communications are discussed in [31] to show the condition to reach an agreement under time-varying delay. Research in [32] showed some notation to consider the center of gravity which is called centroid in multi-agent systems.

1.1.3 Haptics through Network

One of the particular application of multi-agent systems through a network is bilateral or multilateral teleoperation. In bilateral teleoperation, there are two systems: which is a master system and the other is a slave system. Robot manipulators are used as an actuator to transmit the tactile sensation.

Research of bilateral teleoperation has a long history. Goertz *et al*. firstly proposed a master-slave system manipulator who was mechanically connected [33]. As the research progressed, bilateral teleoperation that electrically connects the systems has emerged. To evaluate how well the impedance of a contact object is transmitted to the other system, the evaluation index called transparency was proposed in [34]. As for more specific indices, operationality and reproducibility were introduced in [35] to evaluate both operational force and impedance reproduction performance. Based on the indices, a 4ch bilateral control scheme is said to have the best transparency in bilateral teleoperation when there is no delay between the systems.

When assuming the haptic sensation sharing between remote places, communication delay inevitably occurs between the systems. It is well known that the delay time destabilizes the whole control system and the tactile sensation transmission performance becomes deteriorated [36]. The main reason for the problem is that the information flow is bilateral, resulting in including the delay time inside the control loop.

Numbers of studies that compensates the effect of time delay has been reported [37]. Mainly, there are two classifications in bilateral teleoperation: whether the method is based on passivity approach or not. Passivity-based bilateral control is a well-known control technique to stabilize the system. Many researchers have applied wave variable control to bilateral teleoperation systems [38]. Two channel system that transmits only position or velocity responses was firstly used to realize position synchronization. The μ synthesis was introduced in [39] to design both control performance and stability margin. Position drift problem, which occurs in passivity-based bilateral teleoperation system, is solved [40] to realize position synchronization. The wave variable method was applied in robust acceleration controlled systems in [41]. A method to reduce the reflections in wave based teleoperation was proposed in [42]. Time domain passivity approach (TDPA) was proposed in [43]. A passive observer (PO) and passive controller (PC) are newly defined. The PO measures energy flow that comes in and goes out of a system, and the PC dissipates the energy output of a system. This approach is aimed to overcome the conservativeness of a wave variable bilateral teleoperation system designed in a frequency domain that assumes linearity of a

system. The method is extended to 2 port systems in [44]. To enhance both stability and transparency of the wave variable system, 4 channel bilateral controllers are also proposed [45]. Wave-based reflection is reduced by modifying wave-transformation controllers in [46]. 4 channel TDPA system is proposed in [47].

There are also numbers of reported works that aim to construct non-passive bilateral teleoperation. Impedance based control was used in [48]. The Smith predictor-based bilateral teleoperation was also reported [49] by Hashtrudi-Zaad *et al*. Sirouspour *et al.* proposed model predictive control in a bilateral teleoperation system [50]. Bilateral control through a wireless network has also been studied [51]. CDOB was applied in bilateral teleoperation [52]. Position symmetric type bilateral teleoperation with time varying gains was proposed in [53]. Open loop bilateral teleoperation that optionally feedbacks high-frequency force response was proposed to enhance the stability [54]. A bilateral control system that considers bandwidth constraint was proposed [55]. A bilateral teleoperation system is expressed in a state space equation, and controllers are designed to converge the error state in [56]. 3ch bilateral teleoperation structure was proposed to reduce the operational force in [57].

One of the challenging problem in bilateral control system under communication delay is the contact motion to the environment. Especially, the contact motion to the hard environment is a complicated issue. Contact motion to a hard object using force reflecting type bilateral teleoperation was studied in [58]. There is a trade-off between the operational force performance and the stable contact motion performance. The concept of frequency domain damping (FDD) was presented by Suzuki *et al.* [59, 60], stabilizing the control system even in contact with hard environment without additionally enlarging the operational force. Energy monitor was proposed by Tian *et al.* [61] to change the structure of the control system to perform better position tracking performance and stabilize the contact motion. Asymmetric position synchronization in bilateral teleoperation was proposed in [62]. The study reported by Hyodo *et al.* [63] proposed position control decoupling method. The concept of modal space in bilateral teleoperation is implicitly considered, and the paper assumed asymmetric use.

Bilateral teleoperation or multilateral teleoperation can be applied to telerehabilitation systems. [64] shows some challenges and technical requirement for realizing telerehabilitation. Group synchronization to conduct cooperative tasks to operate a virtual environment was proposed in [65]. Bilateral control for thermal rendering was also studied in [66].

Multilateral teleoperation is a research topic which is new compared to bilateral teleoperation. It is a control technique that shares tactile sensation being more than three points [67]. In multilateral

teleoperation, there are several situations: multi-master and single-slave case, or single-master and multi-slave case, or multi-master and multi-slave case. Multilateral teleoperation can be used for realizing cooperative tasks through a network. Trilateral control whose mobility is different in master and slave systems is proposed in [68]. Haptic transmission ratio was introduced in [69] to adjust the influence or operators in multilateral control using 4ch structure. Dominance factor was proposed in [70, 71] to determine the authority of the operators. Multilateral control for transmitting thermal sensation was proposed in [72].

The transmission performance depends on the distance between the subsystems in multilateral control. When subsystems are placed far from each other, controllers interfere and degrade the tactile sensation transmission performance [36]. Several methods to improve the performance or ensure the stability of multilateral control under a time delay have been proposed [73]. Adaptive impedance control was used to compensate the unknown time-varying delay in [74]. Passivity approach is employed in [75] to ensure the stability of the system. The concept of wave variable is applied to multilateral teleoperation in [76]. Force reflected type multilateral teleoperation was proposed in [77]. A class of absolute stability in trilateral teleoperation was studied in [78]. Operational force in multilateral teleoperation was considered in [79] by removing position controllers. Connectivity of the subsystems in multilateral teleoperation is considered based on the condition of each communication path was evaluated, and connection topology was optimized in [80] to reduce the operational force. The desired task is divided and allocated in multi-master-single-slave multilateral teleoperation in [81] and the stability of the system is guaranteed by using passivity. The modal transformation matrix that is newly defined in the study reported in [82] is named a network quarry matrix to decouple the role of controllers. Multilateral control also Multilateral teleoperation system using state convergence is proposed in [83]. Neural network based multilateral teleoperation was proposed in [84]. Adaptive robust control was implemented in [85] to realize n master and n slave systems in multilateral teleoperation.

1.2 Motivation of This Dissertation

Even there are many researches that were previously proposed, there are few research that has a explicit structure of a control system that defines the modal space in multilateral systems. Modal decomposition is an effective method to control multi-agent systems. A modal space is a virtual control space that transforms the real world's value and generates the reference value for the actuator [86]. The num-

ber of modes that can be controlled is the same as the number of actuators. Usually, the quarry matrix is designed to contain one common mode, and the rest of the modes are defined as the differential mode. There is very few research that explicitly defines the mode in network systems to separately control each motion. One reason why modal space has not been explicitly defined in a bilateral and multilateral teleoperation system is that the modal space becomes complicated because of the time delay element.

Based on these backgrounds, the aim of this dissertation is to design the connectivity between systems to decouple the controllers for each motion. The connectivity stands for the mode that can be defined in network systems. The definition of COG motion and relative motion is given as follows:

- COG motion: the motion of the center of gravity position of the overall system
- Relative motion: the motion of the relative position between systems

The desired motion which is defined by a designer is created by the connectivity matrix. It is hard to change how other systems transmit the response to the own system; therefore, in this dissertation, the response of the own system is going to be transmitted through a network to feedback it to the own system. This dissertation mostly treats a double integrator system; therefore, COG motion must have double integrator characteristics even there are delays between systems. In a connected graph, it is able to divide the motions of multilateral systems into two. In this dissertation, the two motions are defined as a COG motion and relative motion. The relative motion is defined as the relative motion between the systems, and the corresponding COG motion that is orthogonal to the defined relative motion becomes the motion of an overall system.

In some situations, the delay times in every link can be viewed as the same value; however, in order not to lose the generality of the propsoed method, this dissertation assuems every delay time as a different value.

One of the aspects of this dissertation is to extend the utility of the modal transformation. The mode, or motion, is defined in network systems in this dissertation, and each motion is separately controlled by controllers assigned to each motion. The interesting point of this dissertation is that the connectivity shows how to send or receive the information from the other systems by looking at the connectivity matrix. The design methodology of the connectivity is presented. It will realize to separately control each motion by using the delay in the network or a delay time model.

One of the main advantages of the proposed method is that it realizes to enhance the transient response. Although the interference effect does not appear in the steady state since it has high-pass filter

characteristics, it is very difficult to separately realize both control goals in conventional methods, which limits the bandwidth that can realize the control goals. In order to uniquely assign controllers to each control goal, the motions must be firstly defined. Since the proposed method in this dissertation mainly focuses on the definition and decoupling of motions in network systems, controller interference does not structurally occur. Even though the stability margin is limited compared to the conventional methods, control goals can be realized in wide bandwidth because the proposal is free of controller interference.

1.3 Chapter Organization of This Dissertation

Fig. 1-1 shows the chapter organization of this dissertation. Chapter 2 proposes the method to design the connectivity of the relative motion so that the COG motion gains the characteristics of a double integrator in multi-agent systems through a network. Since position tracking control is the same in multi-agent systems and bilateral/multilateral teleoperation, in this chapter, the proposed method is applied in multi-agent systems. This dissertation shows it can be realized by designing the connectivity of the relative motion to set the determinant of a graph Laplacian that contains delay elements as 0 [87].

In Chapter 3, the design method of the COG motion in order not to affect the relative motion in bilateral control is proposed. It can be realized by using a buffer to a control input for COG motion [88]. Also, controllers are designed so that an operator can operate the system with small operational force in a low-frequency area. Both the performance and stability is analyzed.

In Chapter 4, this dissertation discusses the integrated design method of both connectivities for bilateral/multilateral control. Each motion can be decoupled by mapping the response in the work space to a virtual space [82, 89]. The space transformation matrix is newly proposed, and it is designed to contain the delay element between the systems.

In Chapter 5, bilateral control using a flexible manipulator is conducted. This is one of the applications of the proposed method described in Chapter 4. By modeling the manipulator using the wave equation, the system can be viewed as an equivalent time delay system. The transformation matrix is applied to realize the motion decoupling [90].

Chapter 6 proposes the relative motion topology design method in multilateral control. When the number of system for tactile sensation communication increases, the connectivity matrix becomes complex. In this situation, the method proposes to design the topology for the relative motion, which is much simple compared to the method shown in Chapter 4. This dissertation reveals that the eigenvector of the

maximum eigenvalue of an adjacency matrix expresses the equivalent amount of information that each system contains [88]. The value is defined as Influence Value (IV) in this dissertation. It is based on an index which is called centrality in graph theory. Centrality is an index that quantitatively measures the importance of each node in a network. This dissertation uses eigenvector centrality to quantify the influence that each system has in an overall system. Page Rank [91] which was established by Google Inc. is also based on eigenvector centrality. IV is used to design the topology to regain the tactile sensation transmission performance.

In Chapter 7, this dissertation proposes the method to present thermal and tactile sensations using multilateral control simultaneously. In remote communication, it can achieve more realistic feeling when not only tactile sensation but also thermal sensation can be transmitted. However, the response speed of the Peltier device that is used as an actuator for thermal sensation presentation is slow compared to robot manipulators. Therefore, in order to compensate the difference, the additional buffer is used to correct the timing of the presentation.

Finally, Chapter 8 concludes this dissertation.

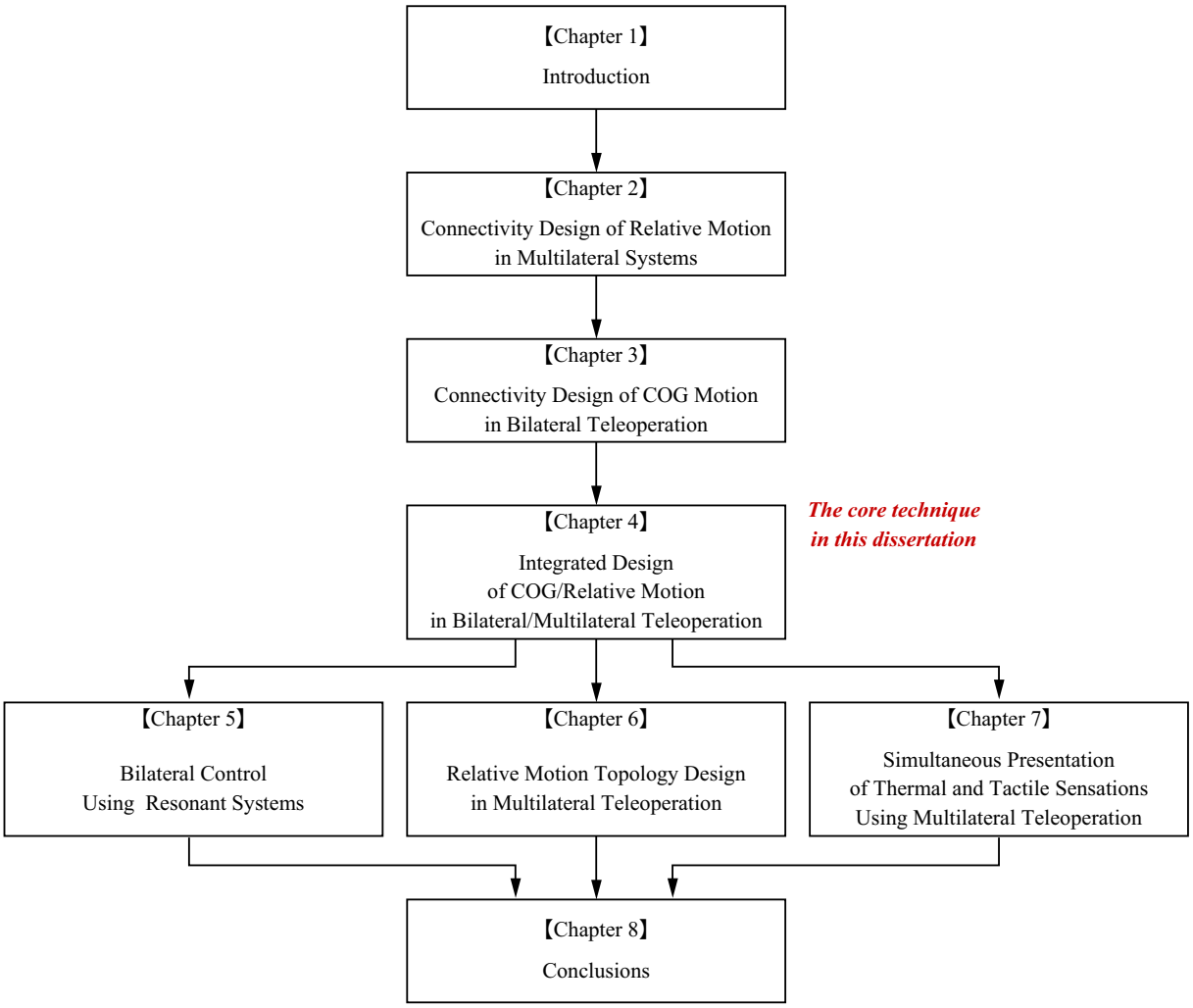

Fig. 1-1: Chapters constructed in this dissertation.

Chapter 2

Connectivity Design of Relative Motion in Multilateral Systems

---

In this chapter, the connectivity design method of the relative motion in multilateral systems is proposed. The following sections explain the connectivity of multi-agents by using the determinant of a graph Laplacian. Each agent is assumed to have a double integrator characteristics by the utilization of the disturbance observer in this dissertation. The aim is to regain the double integrator characteristics in network systems.

2.1 Introduction of Chapter 2

In Section 2.1, mathematical expression of the connectivity and the dynamics of a system is explained. The condition to regain the double integrator characteristics in the COG motion is to design the determinant of the graph Laplacian in network systems as 0 [87]. Section 2.2 shows the connectivity design when the number of the system is two, which is the most simple case in multilateral systems. The connectivity proposed in Section 2.2 becomes the fundamental unit to realize the purpose. Then, the design method is extended to a multilateral system with various topologies in Section 2.3. Section 2.4 shows the numerical results whether the double integrator characteristics is regained in the proposed method.

2.2 Preliminary

Some of the fundamental characteristics of a graph Laplacian is introduced in this section.

2.2.1 Graph Laplacian

The definition of a graph is firstly explained. Let $\mathcal{G} = (\boldsymbol{V}, \boldsymbol{E}, \boldsymbol{A})$ be a weighted directed graph of order n composed of a set nodes $\mathcal{V} = \{1, 2, \cdots, n\}$, set on edges $\mathcal{E} \subset \mathcal{V} \times \mathcal{V}$, and a weighted adjacency matrix $\boldsymbol{A} = (a_{ij})$ that is nonnegative adjacency elements a_{ij}. If there is no time delay between any subsystems, the elements will be given as

$$a_{ij} = \begin{cases} 1, & \text{if connected} \\ 0, & \text{otherwise} \end{cases} . \tag{2.1}$$

As for the diagonal elements, each element will be the summation of off-diagonal elements of corresponding column:

$$d_{ij} = \begin{cases} \sum_{k=1}^{n} a_{ik}, & j = i \\ 0, & j \neq i \end{cases} , \tag{2.2}$$

where d_{ij} is the elements of the dimensional matrix $\boldsymbol{D}$.

The graph Laplacian $\boldsymbol{L}_{\mathrm{p}}$ shows the connectivity between each subsystem, and the definition is

$$\boldsymbol{L}_{\mathrm{p}} = \boldsymbol{D} - \boldsymbol{A}. \tag{2.3}$$

This dissertation assumes a connected graph. In the connected graph, the number of the smallest eigenvalue of the graph Laplacian is one, which means there is one COG motion defined by the graph Laplacian [93].

In the following, some basic property of a graph Laplacian is shown. Since the summation of all row of $\boldsymbol{L}_{\mathrm{p}}$ is 0,

$$\boldsymbol{L}_{\mathrm{p}} c\mathbf{1} = 0, \tag{2.4}$$

where $\mathbf{1} = [1\ 1\ \cdots\ 1]^T$ and c is the constant value. By modifying (2.4),

$$\begin{aligned} \boldsymbol{L}_{\mathrm{p}} \boldsymbol{v}_1 &= \lambda \boldsymbol{v}_1 \\ &= 0 \cdot \boldsymbol{v}, \end{aligned} \tag{2.5}$$

where $\boldsymbol{v}_1$ is the right eigenvector of the corresponding eigenvalue. Therefore, the eigenvalue of a graph Laplacian has 0 and the corresponding eigenvector is $\mathbf{1}$.

A real quadratic form of a graph Laplacian is given as

$$\begin{aligned}\boldsymbol{q}_n^T \boldsymbol{L}_{\mathrm{p}} \boldsymbol{q}_n &= \sum_{i=1}^{n} q_i (\boldsymbol{L}_{\mathrm{p}} \boldsymbol{q})_i \\ &= \sum_{i=1}^{n} q_i \sum_{j=1}^{n} A_{ij}(q_i - q_j) \\ &= \frac{1}{2} \sum_{i,j} (q_i A_{ij} - q_j A_{ji})(q_i - q_j) \\ &= \frac{1}{2} \sum_{i,j} A_{ij}(q_i - q_j)^2 \\ &\geq 0, \end{aligned} \tag{2.6}$$

where $\boldsymbol{q}_n$ is the arbitrary $n \times 1$ vector. Since the real quadratic form is nonnegative, a graph Laplacian is positive semi-definite.

Assume $\boldsymbol{L}_{\mathrm{p}n}$ as a $n \times n$ matrix. When a graph is not a connected graph, $\boldsymbol{L}_{\mathrm{p}n}$ can be divided into some block matrices whose block consists of a graph Laplacian. By renumbering the system, the matrix can be rewritten as

$$\boldsymbol{L}_{\mathrm{p}n} = \begin{bmatrix} \boldsymbol{L}_{\mathrm{p}w} & & & \boldsymbol{0} \\ & \boldsymbol{L}_{\mathrm{p}x} & & \\ & & \ddots & \\ \boldsymbol{0} & & & \boldsymbol{L}_{\mathrm{p}y} \\ & & & & \boldsymbol{L}_{\mathrm{p}z} \end{bmatrix}, \tag{2.7}$$

where $\boldsymbol{L}_{\mathrm{p}i}$ is the $i \times i$ matrix whose graph is connected. By using the property of a block matrix, he characteristic equation of $\boldsymbol{L}_{\mathrm{p}}$ is calculated as

$$\begin{aligned}\det(s\boldsymbol{I}_n - \boldsymbol{L}_{\mathrm{p}n}) &= \det(s\boldsymbol{I}_w - \boldsymbol{L}_{\mathrm{p}w}) \cdot \det(s\boldsymbol{I}_x - \boldsymbol{L}_{\mathrm{p}x}) \cdot \cdots \cdot \det(s\boldsymbol{I}_y - \boldsymbol{L}_{\mathrm{p}y}) \cdot \det(s\boldsymbol{I}_z - \boldsymbol{L}_{\mathrm{p}z}) \\ &= \prod_{k=1}^{w} (s - \lambda_{w_k}) \cdot \prod_{k=1}^{x} (s - \lambda_{x_k}) \cdot \cdots \cdot \prod_{k=1}^{y} (s - \lambda_{y_k}) \cdot \prod_{k=1}^{z} (s - \lambda_{z_k}). \end{aligned} \tag{2.8}$$

Since a connected graph contains only one smallest eigenvalue which is 0, the number of the smallest eigenvalue 0 becomes the number of the connected components.

2.2.2 Dynamics of Multilateral System without Time Delay

The motion equation of a motor is expressed as

$$M\ddot{x}^{\mathrm{res}} = f^{\mathrm{ref}} - f^{\mathrm{dis}}, \tag{2.9}$$

where M, $\ddot{x}^{\mathrm{res}}$, f^{ref}, and f^{dis} stand for the mass of a motor, acceleration response, driving force reference, disturbance force, respectively. The driving force is given by

$$f^{\mathrm{ref}} = K_{\mathrm{t}} I^{\mathrm{ref}}, \tag{2.10}$$

where K_{t} and I^{ref} stand for the thrust constant and current reference, respectively. Throughout the dissertation, robust acceleration control is constructed by using the DOB [92]. By using the DOB, the motor mass and torque constant can be nominalized. Also, the DOB eliminates disturbance applied to the motor within the frequency area of a low-pass filter:

$$\ddot{x}^{\mathrm{res}} = \frac{K_{\mathrm{tn}}}{M_{\mathrm{n}}} I^{\mathrm{ref}} - \frac{s}{s + g_{\mathrm{dis}}} f^{\mathrm{dis}}, \tag{2.11}$$

where the subscript $_n$ and g_{dis} stand for the nominal value and the cut-off frequency of the DOB, respectively. M_{n} shows the nominal mass of a system. When the acceleration reference $\ddot{x}^{\mathrm{ref}}$ is set as

$$\ddot{x}^{\mathrm{ref}} = \frac{M_{\mathrm{n}}}{K_{\mathrm{tn}}} I^{\mathrm{ref}}, \tag{2.12}$$

and if the cut-off frequency of the low-pass filter is high enough, the acceleration reference becomes the acceleration response:

$$\ddot{x}^{\mathrm{res}} = \ddot{x}^{\mathrm{ref}}. \tag{2.13}$$

Hereafter, the control input for the motor is obtained as the acceleration reference. The dynamics of the motor becomes a simple double integrator characteristics when implementing DOB.

Acceleration reference for each system is obtained based on the states of other systems. Control input for subsystem i is given as

$$\ddot{x}_i^{\mathrm{ref}} = -\sum_{j=1}^{n} [K_{\mathrm{p}} a_{ij}(x_j - x_i) + K_{\mathrm{d}} a_{ij}(s x_j - s x_i)], \tag{2.14}$$

where K_{p} is the proportional gain, and K_{d} is the derivative gain. s stands for the Laplace operator. Then the overall dynamics of a system is defined as

$$\ddot{\boldsymbol{x}}^{\mathrm{ref}} = -K_{\mathrm{p}} \boldsymbol{L}_{\mathrm{p}} \boldsymbol{x} - s K_{\mathrm{d}} \boldsymbol{L}_{\mathrm{p}} \boldsymbol{x}. \tag{2.15}$$

$\boldsymbol{L}_{\mathrm{p}}$ shows the connectivity of relative motions. In a directed graph, all of the eigenvalues of $\boldsymbol{L}_{\mathrm{p}}$ are real numbers and are nonnegative values. It is well known that all of the eigenvalues of $\boldsymbol{L}_{\mathrm{p}}$ is non-negative

value, and the smallest eigenvalue becomes 0. Define the order of eigenvalues by $0 = \lambda_1, \lambda_2, \cdots \lambda_n$. Then, the poles of the system described in (2.15) is obtained as follows [93]:

$$s = \frac{1}{2}\left(K_{\mathrm{d}}\lambda_i \pm \sqrt{(K_{\mathrm{d}}\lambda_i)^2 - 4K_{\mathrm{p}}\lambda_i} \right). \tag{2.16}$$

It indicates there are two eigenvalues for each eigenvalue λ_i of L. One of the fundamental characteristics regarding the eigenvalues of the graph Laplacian is that the smallest eigenvalue λ_1 is 0.

Let $\boldsymbol{w}_1$ be a left eigenvector of $\boldsymbol{L}_{\mathrm{p}}$ for λ_1. Then,

$$\boldsymbol{w}_1^T \boldsymbol{L}_{\mathrm{p}} = \boldsymbol{w}_1^T \cdot 0. \tag{2.17}$$

Therefore,

$$\begin{aligned} \boldsymbol{w}_1^T \ddot{\boldsymbol{x}}^{\mathrm{ref}} &= -K_{\mathrm{p}} \boldsymbol{w}_1^T \boldsymbol{L}_{\mathrm{p}} \boldsymbol{x} - sK_{\mathrm{d}} \boldsymbol{w}_1^T \boldsymbol{L}_{\mathrm{p}} \boldsymbol{x} \\ &= 0. \end{aligned} \tag{2.18}$$

It indicates that $\boldsymbol{w}_1^T \boldsymbol{x}$ is invariant. $\boldsymbol{L}_{\mathrm{p}}$ does not affect the motion of $\boldsymbol{w}_1^T \boldsymbol{x}$, which is described as decoupled in this dissertation.

2.2.3 Dynamics of Multilateral System under Time Delay

The expression of the adjacency matrix is extended in order to consider communication delay in every link. Considering the communication delay (CD), (i, j) element a_{ij}^{CD} of the adjacency matrix $\boldsymbol{A}^{\mathrm{CD}}$ is defined as follows [80]:

$$a_{ij}^{\mathrm{CD}} = \begin{cases} e^{-Ts} & : \text{ if there is a connection from subsystem } j \text{ to subsystem } i \text{ with time delay } T \text{ s} \\ 0 & : \text{ there is no connection} \end{cases}. \tag{2.19}$$

As for the diagonal elements, each element will be the summation of off-diagonal elements of corresponding column:

$$d_{ij}^{\mathrm{CD}} = \begin{cases} \text{summation of the number of incomming path}, & j = i \\ 0, & j \neq i \end{cases}, \tag{2.20}$$

where d_{ij} is the elements of the dimensional matrix. The graph Laplacian with delay elements $\boldsymbol{L}_{\mathrm{p}}^{\mathrm{CD}}$ shows the connectivity that contains communication delay between subsystems:

$$\boldsymbol{L}_{\mathrm{p}}^{\mathrm{CD}} = \boldsymbol{D}^{\mathrm{CD}} - \boldsymbol{A}^{\mathrm{CD}}. \tag{2.21}$$

Control input for subsystem i is given as

$$\ddot{x}_i = \sum_{j=1}^{n}[K_{\mathrm{p}}a_{ij}(e^{-T_{ij}s}x_j - x_i) + K_{\mathrm{d}}a_{ij}(e^{-T_{ij}s}sx_j - sx_i)]. \tag{2.22}$$

The state space expression of a multi-agent system through network is expressed as

$$\ddot{\boldsymbol{x}}^{\mathrm{ref}} = -K_{\mathrm{p}}\boldsymbol{L}_{\mathrm{p}}^{\mathrm{CD}}\boldsymbol{x} - sK_{\mathrm{d}}\boldsymbol{L}_{\mathrm{p}}^{\mathrm{CD}}\boldsymbol{x}. \tag{2.23}$$

The structure of the graph Laplacian becomes with delay elements different from the previous ones, where the delay elements appear in the off-diagonal part.

Define the equivalent eigenvalue λ^{CD} of $\boldsymbol{L}_{\mathrm{p}}^{\mathrm{CD}}$ as a value that satisfies

$$\det(s\boldsymbol{I} - \boldsymbol{L}_{\mathrm{p}}^{\mathrm{CD}}) = \prod_{i=1}^{n}\left(s - \lambda_i^{\mathrm{CD}}\right). \tag{2.24}$$

Based on the definition, λ^{CD} contains a delay element. Then, the poles of the overall system can be derived by the same manner as (2.16):

$$s = \frac{1}{2}\left(K_{\mathrm{d}}\lambda_i^{\mathrm{CD}} \pm \sqrt{(K_{\mathrm{d}}\lambda_i^{\mathrm{CD}})^2 - 4K_{\mathrm{p}}\lambda_i^{\mathrm{CD}}}\right). \tag{2.25}$$

2.3 Connectivity Design of Two Agents

2.3.1 Problem Definition

To make the problem clear and simple, the number of the subsystem is limited to two in this subsection. At first, the problem is stated, and then it solved by modifying the structure of the graph Laplacian.

The graph Laplacian when there is no time delay is expressed by

$$\boldsymbol{L}_{\mathrm{p2}} = \begin{bmatrix} 1 & -1 \\ -1 & 1 \end{bmatrix}. \tag{2.26}$$

The subscript 2 indicates the order of the matrix. The eigenvalues are

$$\lambda = 0, 2. \tag{2.27}$$

One simple way to examine whether the eigenvalues contain 0 or not is to calculate the determinant of a graph Laplacian.

$$\begin{cases} \det(\boldsymbol{L}_{\mathrm{p}}) = 0, & \lambda_1 = 0 \\ \det(\boldsymbol{L}_{\mathrm{p}}) \neq 0, & \lambda_1 \neq 0 \end{cases}. \tag{2.28}$$

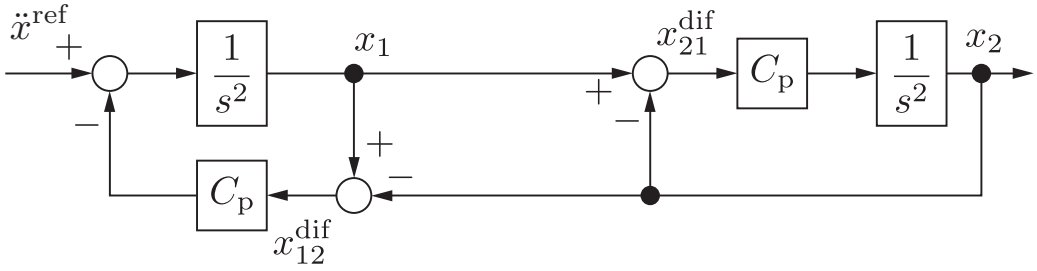

Fig. 2-1: Block diagram of two agent system without time delay.

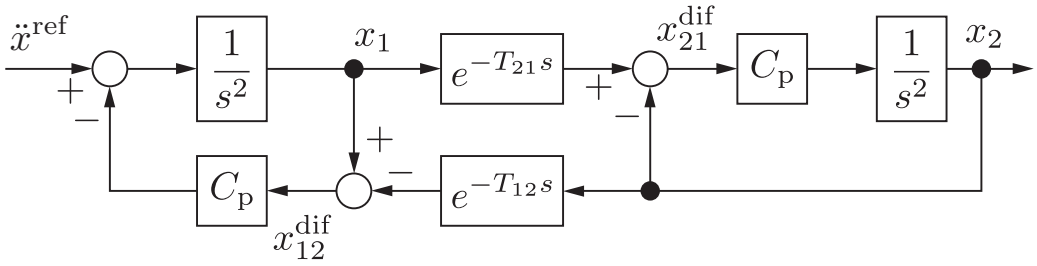

Fig. 2-2: Block diagram of two agent system when there is time delay.

The determinant in the two agent system is

$$\det(\boldsymbol{L}_{\mathrm{p2}}) = 0. \tag{2.29}$$

It indicates that the relative motion does not affect the COG motion of the system. The block diagram of a two agent system when there is no time delay is shown in Fig. 2-1. In Fig. 2-1, $C_{\mathrm{p}} = K_{\mathrm{p}} + K_{\mathrm{d}}s$. Position difference between subsystems will be an input generated by the multiplication of the gain C_{p} and position difference x^{dif}. The characteristic polynomial of the system is given as

$$G(s) = s^2\left(s^2 + 2C_{\mathrm{p}}\right). \tag{2.30}$$

When there is delay between agents, the graph Laplacian is expressed by

$$\boldsymbol{L}_{\mathrm{p2}}^{\mathrm{CD}} = \begin{bmatrix} 1 & -e^{-T_{12}s} \\ -e^{-T_{21}s} & 1 \end{bmatrix}, \tag{2.31}$$

and the eigenvalues and the determinant of L_{n} are

$$\begin{aligned} \lambda &= (1 - e^{-\frac{T_{12}+T_{21}}{2}s}), (1 + e^{-\frac{T_{12}+T_{21}}{2}s}), \\ \det(\boldsymbol{L}_2^{\mathrm{CD}}) &= 1 - e^{-(T_{12}+T_{21})s} \neq 0. \end{aligned} \tag{2.32}$$

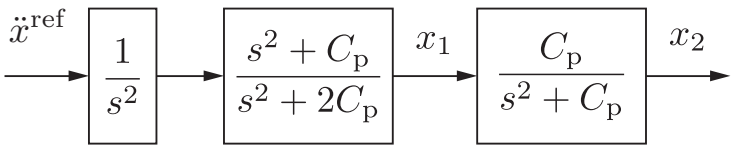

Fig. 2-3: Equivalent transfer function of Fig. 2-1.

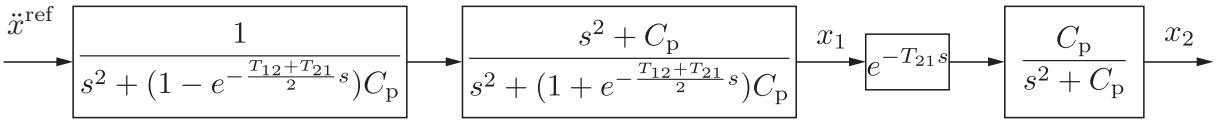

Fig. 2-4: Equivalent transfer function of Fig. 2-2.

It clearly shows the eigenvalues of the network two-agent system do not have 0. It indicates that the vibration caused by the equivalent torsional force affects the COG position of the system, where the same problem was reported in bilateral teleoperation [88]. The block diagram of a network two-agent system is shown in Fig. 2-2. The characteristic polynomial of the system is given as

$$G(s) = \left(s^2 + \left(1 - e^{-\frac{T_{12}+T_{21}}{2}s}\right) C_\mathrm{p}\right) \left(s^2 + \left(1 + e^{-\frac{T_{12}+T_{21}}{2}s}\right) C_\mathrm{p}\right). \tag{2.33}$$

The difference between Figs. 2-1 and 2-2 can be seen when obtaining the transfer functions which is shown in Figs. 2-3 and 2-4. When there is no time delay, the double integrator characteristics appears because the eigenvalue of $\boldsymbol{L}_{\mathrm{p2}}$ contains 0, which indicates the COG motion of the system. However, the characteristics do not appear, and the controller aimed to control the relative motion of the system affects to the COG motion of the system. Impulse response is compared in Fig. 2-5. Simulation parameters are listed in Table 2.1. The impulse input was applied to subsystem 1. It clearly shows the overall motion does not follow the double integrator characteristics when there is a delay.

2.3.2 Modification of Connectivity

In order not to make the relative motion controller affect the COG motion of the system, the connection between two subsystems needs to be modified. Rewrite the graph Laplacian as

$$\boldsymbol{L}_{\mathrm{p2}}^{\mathrm{CD}} = \begin{bmatrix} 1 & 0 \\ 0 & 1 \end{bmatrix} - \begin{bmatrix} 0 & e^{-T_{12}s} \\ e^{-T_{21}s} & 0 \end{bmatrix}. \tag{2.34}$$

a_{ij} $(i \neq j)$, which is the off-diagonal element in the graph Laplacian shows the information that comes from the other subsystem, while d_{ii} shows the information of the local subsystem. What can be changed

Table 2.1: Simulation parameters for impulse input.

Parameter	Description	Value
T_{12}	Delay time from subsystem 2 to 1	100 ms
T_{21}	Delay time from subsystem 1 to 2	300 ms
K_{p}	Proportional gain for position control	100
K_{d}	Differential gain for position control	20

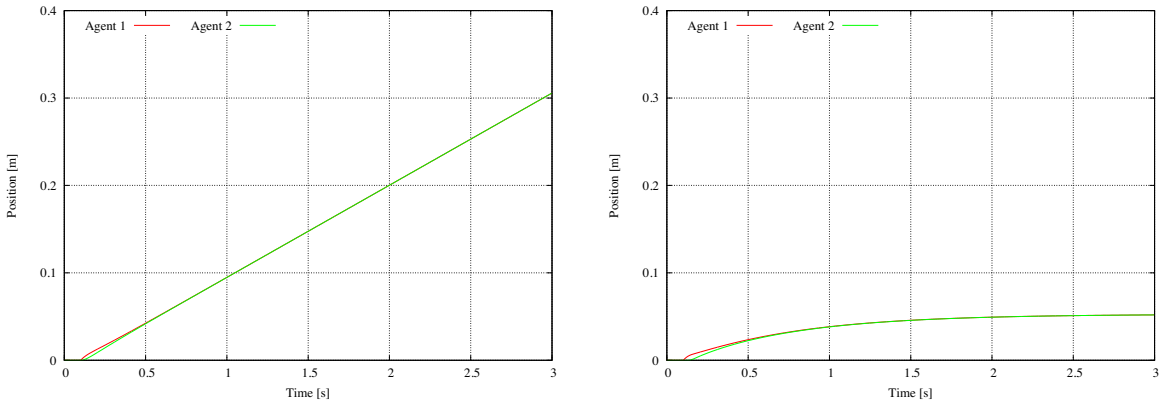

(a) When there is no delay.

(b) When there is delay.

Fig. 2-5: Comparison of impulse response in two-agent system.

is the information of the local subsystem; therefore, the elements of the dimensional matrix are modified to make the determinant of the graph Laplacian $\boldsymbol{L}_{\mathrm{p}}^{\mathrm{CD}}$ as 0.

In order to determine the values, let d_{ii} set as $\mathrm{diag}\{\alpha, \beta\}$, which is the modified dimensional matrix $\boldsymbol{\mathcal{D}}_2$, then the determinant is calculated by

$$\det(\boldsymbol{\mathcal{L}}_{\mathrm{p}2}^{\mathrm{CD}}) = \alpha\beta - e^{-(T_{12}+T_{21})s}. \tag{2.35}$$

α and β are assumed to be 1 or $e^{-T_{12}s}$ or $e^{-T_{21}s}$ or $e^{-(T_{12}+T_{21})s}$ for a reason which is explained later. By calculating $\det(\boldsymbol{\mathcal{L}}_{\mathrm{p}2}^{\mathrm{CD}}) = 0$, pairs of α and β are obtained as

$$\begin{aligned}\boldsymbol{\mathcal{D}}_2^{\mathrm{CD}} =& \mathrm{diag}\{e^{-(T_{12}+T_{21})s}, 1\},\ \mathrm{diag}\{e^{-T_{12}s}, e^{-T_{21}s}\},\\ & \mathrm{diag}\{e^{-T_{21}s}, e^{-T_{12}s}\},\ \mathrm{diag}\{1, e^{-(T_{12}+T_{21})s}\}.\end{aligned} \tag{2.36}$$

There are four ways to select the pair of α and β. The lower two pairs in (2.36) are symmetric to the upper two pairs, so that the lower two pairs is excluded hereafter. The pairs $\boldsymbol{\mathcal{D}}_2^{\mathrm{CD}} = \mathrm{diag}\{e^{-(T_{12}+T_{21})s}, 1\}$ and $\boldsymbol{\mathcal{D}}_2^{\mathrm{CD}} = \{e^{-T_{12}s}, e^{-T_{21}s}\}$ are named as type 1 and type 2, respectively.

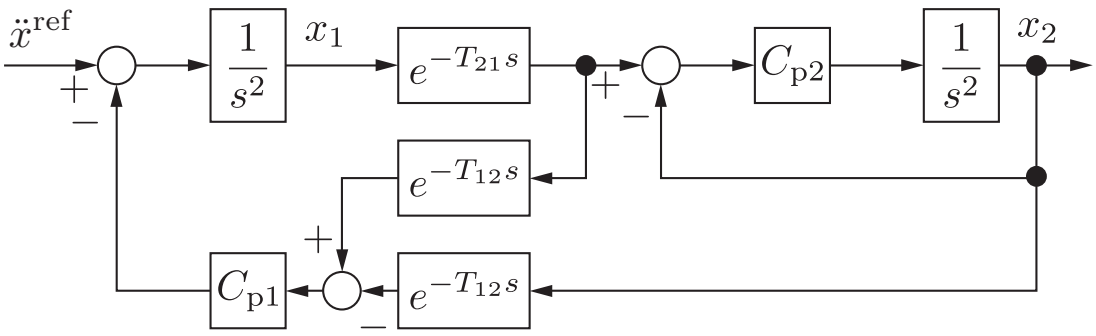

Fig. 2-6: Motion decoupled two agent system (type 1).

The block diagram of type 1 two-agent system is shown in Fig. 2-6. All of the delay elements are between the subsystems; therefore, this structure does not require any delay time model in local subsystems. This is the reason why the choice of α and β were limited to four. It enables to derive a solution which can be realized by transmitting the response through a network. The graph Laplacian of this structure is given as

$$\boldsymbol{\mathcal{L}}_{\mathrm{p2}}^{\mathrm{CD1}} = \begin{bmatrix} e^{-(T_{12}+T_{21})s} & -e^{-T_{12}s} \\ -e^{-T_{21}s} & 1 \end{bmatrix}. \tag{2.37}$$

The eigenvalues of this type is

$$\lambda^{\mathrm{CD1}} = 0, 1 + e^{-(T_{12}+T_{21})s}. \tag{2.38}$$

It means that the structure has a decoupled COG position, and when all of the delay times are 0, eigenvalues becomes similar to the case when there is no delay which is shown in (2.27). The characteristic polynomial of the system $G^1(s)$ is calculated by

$$G^1(s) = s^2\left(s^2 + (1 + e^{-(T_{12}+T_{21})s})C_{\mathrm{p}}\right), \tag{2.39}$$

when $C_{\mathrm{p1}} = C_{\mathrm{p2}} = C_{\mathrm{p}}$. (2.39) indicates that having the smallest eigenvalues as 0 in the graph Laplacian means the same as having two poles at the origin. In other words, the system contains a double integrator inside.

Since both equivalent eigenvalues λ^{CD1} are not negative values, the matrix $\boldsymbol{\mathcal{L}}_{\mathrm{p2}}^{\mathrm{CD1}}$ is positive semi-definite. The rank of $\boldsymbol{\mathcal{L}}_{\mathrm{p2}}^{\mathrm{CD1}}$ becomes 1 by using the elementary transformation of a matrix which is shown in the following.

$$\boldsymbol{\mathcal{L}}_{\mathrm{p2}}^{\mathrm{CD1}} = \begin{bmatrix} e^{-(T_{12}+T_{21})s} & -e^{-T_{12}s} \\ -e^{-T_{21}s} & 1 \end{bmatrix} \rightarrow \begin{bmatrix} -e^{-T_{21}s} & 1 \\ 0 & 0 \end{bmatrix}. \tag{2.40}$$

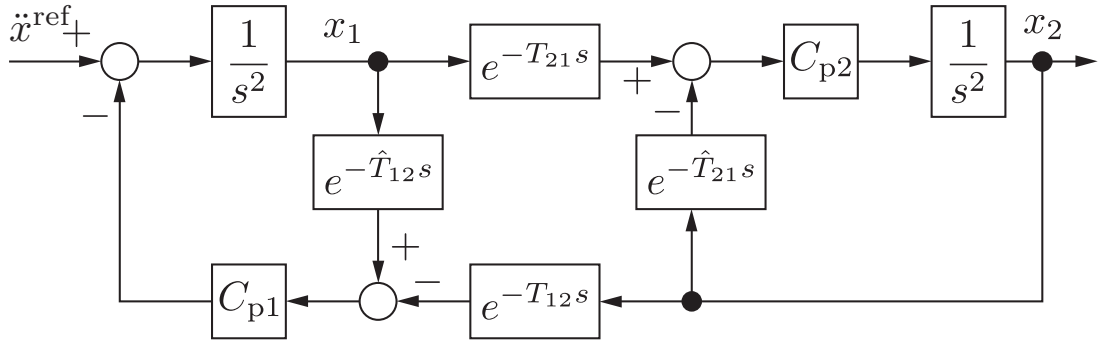

Fig. 2-7: Motion decoupled two agent system (type 2).

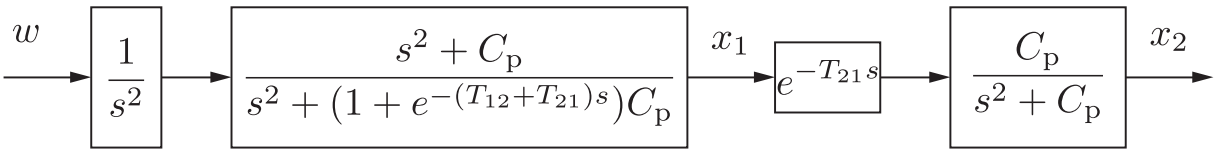

Fig. 2-8: Equivalent transformation of Fig. 2-6.

The block diagram of type 2 system is shown in Fig. 2-7. The graph Laplacian of this structure is given as

$$\boldsymbol{\mathcal{L}}_{\mathrm{p2}}^{\mathrm{CD2}} = \begin{bmatrix} e^{-\hat{T}_{12}s} & -e^{-T_{12}s} \\ -e^{-T_{21}s} & e^{-\hat{T}_{21}s} \end{bmatrix}, \tag{2.41}$$

where $\hat{}$ stands for the model of a value. The eigenvalues λ^{CD2} and the characteristic polynomial $G^2(s)$ are

$$\lambda^{\mathrm{CD2}} = 0, e^{-T_{12}s} + e^{-T_{21}s} \tag{2.42}$$

$$G^2(s) = s^2 \left(s^2 + (e^{-T_{12}s} + e^{-T_{21}s})C_{\mathrm{p}}\right), \tag{2.43}$$

when $C_{\mathrm{p1}} = C_{\mathrm{p2}} = C_{\mathrm{p}}$. The result also shows the system has the characteristic of a double integrator.

Same characteristics as type 1 can be also said in $\boldsymbol{\mathcal{L}}_{\mathrm{p2}}^{\mathrm{CD2}}$. The eigenvalues λ^{CD2} do not become negative value so that $\boldsymbol{\mathcal{L}}_{\mathrm{p2}}^{\mathrm{CD2}}$ is also positive semi-definite. The rank of $\boldsymbol{\mathcal{L}}_{\mathrm{p2}}^{\mathrm{CD2}}$ is also 1 which is explained in the following.

$$\boldsymbol{\mathcal{L}}_{\mathrm{p2}}^{\mathrm{CD2}} = \begin{bmatrix} e^{-\hat{T}_{12}s} & -e^{-T_{12}s} \\ -e^{-T_{21}s} & e^{-\hat{T}_{21}s} \end{bmatrix} \rightarrow \begin{bmatrix} e^{-\hat{T}_{12}s} & -e^{-T_{12}s} \\ 0 & 0 \end{bmatrix}. \tag{2.44}$$

The equivalent block diagram of Figs. 2-6 and 2-7 when $C_{\mathrm{p1}} = C_{\mathrm{p2}} = C_{\mathrm{p}}$ are shown in Figs. 2-8 and 2-9.

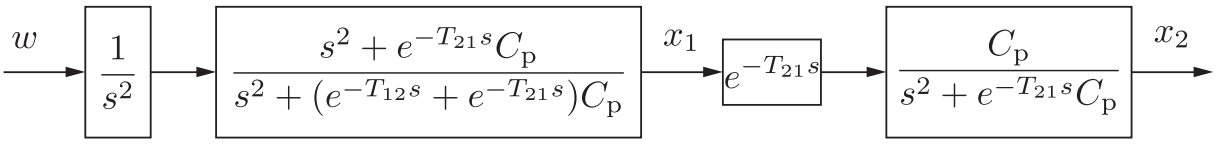

Fig. 2-9: Equivalent transformation of Fig. 2-7.

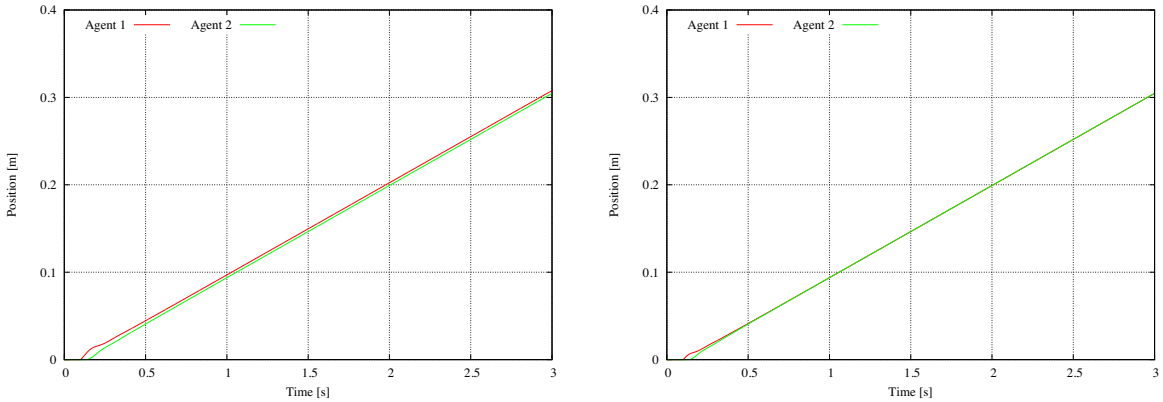

(a) Type 1. (b) Type 2.

Fig. 2-10: Impulse response in the proposed structure.

The impulse response is given in Fig. 2-10. The parameters are same as the previous simulation that is listed in Table 2.1. In this situation, there is no COG controller in both systems. Both structures show that the double integrator characteristics is regained. In Fig. 2-10(a), agent 1 is moving ahead of agent 2 compared to Fig. 2-10(b). The reason is that the timing of the synchronization is modified so that agent 2 tracks T_{12} s delayed motion of agent 1.

2.3.3 Controller Parameter Design for Relative and COG Motion

Controllers are placed based on the inspiration of resonant ratio control [94] for the type 1 motion decoupled system, which is a famous method to suppress vibration of a two mass resonant system. A PD controller with equivalent torsional is used in the method, and a torsional force feedback gain is newly inserted to the feedback of torsional force. As for type 2 system, since the structure is often studied in other reports, the design methodology is omitted. From Figs. 2-8 and 2-9, it is necessary to set the position controllers for the relative motion the same between two agents. Based on the fact, Fig. 2-6 can be rewritten into Fig. 2-11.

The controller placement of 1st and 2nd agents is expressed in Fig. 2-12. Controller gains $K_\mathrm{p}^\mathrm{cog}$,

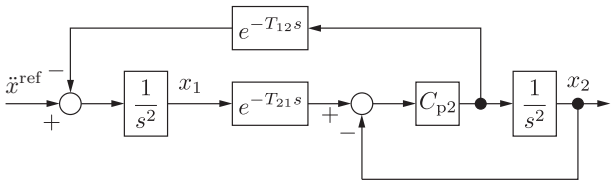

Fig. 2-11: Equivalent transformation of Fig. 2-6 when $C_{\mathrm{p1}} = C_{\mathrm{p2}}$.

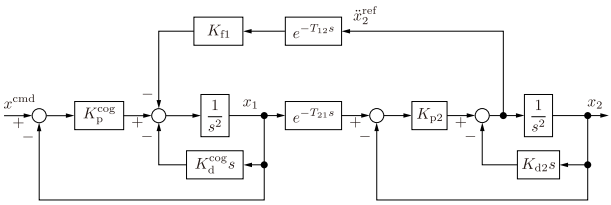

Fig. 2-12: Controller placement for Fig. 2-11.

$K_{\mathrm{d}}^{\mathrm{cog}}$, and K_{f1} is for controlling the relative motion, while K_{p1} and K_{d1} is the controller for the COG motion. The transfer function of the 1st agent $G_1(s)$ that is from x^{cmd} to x_1 is calculated as

$$G_1(s) = \frac{n_2 s^2 + n_1 s + n_0}{d_4 s^4 + d_3 s^3 + d_2 s^2 + d_1 s + d_0}, \tag{2.45}$$

$$n_2 = 1, \tag{2.46}$$

$$n_1 = K_{\mathrm{d2}}, \tag{2.47}$$

$$n_0 = K_{\mathrm{p2}}, \tag{2.48}$$

$$d_4 = 1, \tag{2.49}$$

$$d_3 = K_{\mathrm{d}}^{\mathrm{cog}} + K_{\mathrm{d2}}, \tag{2.50}$$

$$d_2 = (1 + e^{-(T_{12}+T_{21})s} K_{\mathrm{f1}}) K_{\mathrm{p2}} + K_{\mathrm{p}}^{\mathrm{cog}} + K_{\mathrm{d}}^{\mathrm{cog}} K_{\mathrm{d2}}, \tag{2.51}$$

$$d_1 = K_{\mathrm{p}}^{\mathrm{cog}} K_{\mathrm{d2}} + K_{\mathrm{p2}} K_{\mathrm{d}}^{\mathrm{cog}}, \tag{2.52}$$

$$d_0 = K_{\mathrm{p}}^{\mathrm{cog}} K_{\mathrm{p2}}. \tag{2.53}$$

The transfer function from x_1 to x_2 is obtained as

$$G_2(s) = \frac{K_{\mathrm{p2}}}{s^2 + K_{\mathrm{d2}} s + K_{\mathrm{p2}}}. \tag{2.54}$$

The pole placement method is used to determine every gain. The desired characteristic equation from the position command x^{cmd} to x_2 is defined as

$$\begin{aligned} G(s) &= (s + p_1)^4 \\ &= s^4 + 4p_1 s^3 + 6p_1^2 s^2 + 4p_1^3 s + p_1^4. \end{aligned} \tag{2.55}$$

By comparing the coefficients, the controller gains and the pole of 1st agent is determined as

$$K_{\mathrm{p}}^{\mathrm{cog}} = K_{\mathrm{p2}}, \tag{2.56}$$

$$K_{\mathrm{d}}^{\mathrm{cog}} = 4\sqrt{K_{\mathrm{p2}}} - K_{\mathrm{d2}}, \tag{2.57}$$

$$K_{\mathrm{f1}} = e^{(T_{21}+T_{12})s}\frac{(K_{\mathrm{d2}} - 2\sqrt{K_{\mathrm{p2}}})^2}{K_{\mathrm{p2}}}, \tag{2.58}$$

$$p^{\mathrm{cog}} = \sqrt{K_{\mathrm{p2}}}. \tag{2.59}$$

In (2.87), it requires the future value which is shown as $e^{(T_{12}+T_{21})s}$. It is difficult to obtain the future value; therefore, $e^{(T_{12}+T_{21})s}$ is approximated as 1 in this dissertation. Even though the controller parameters were determined based on the gain of the relative motion controller, the role of each controller is clearly decoupled. K_{f1} mainly determines the stability of the whole system because the delay element $e^{-(T_{12}+T_{21})s}$ is multiplied by the value. In actual cases, for example, where there are jitters in a communication line, the stability can be assured by the lowering the gain.

2.4 Connectivity Design of Multi-Agent Systems

The design procedure of the graph Laplacian in the multi-agent system is the same as the one when the number of the agent is two. Two types that are shown in the previous section to decouple COG and relative motions is the fundamental set to realize motion decoupling in multi-numbered agent systems.

2.4.1 Line-Shaped Multi-Agent Systems

Consider a line graph whose number of subsystems is three. The graph Laplacian is expressed by

$$\boldsymbol{L}_{\mathrm{p3}}^{\mathrm{CD}} = \begin{bmatrix} 1 & -e^{-T_{12}s} & 0 \\ -e^{-T_{21}s} & 2 & -e^{-T_{23}s} \\ 0 & -e^{-T_{23}s} & 1 \end{bmatrix}. \tag{2.60}$$

The elements that are changeable are the diagonal terms, which expresses an information of the local subsystems. Let $\boldsymbol{\mathcal{D}}_3^{\mathrm{CD}}$ set as $\mathrm{diag}\{\delta, \epsilon, \zeta\}$, then the determinant is calculated by

$$\det(\boldsymbol{\mathcal{L}}_{\mathrm{p3}}^{\mathrm{CD}}) = \delta\epsilon\zeta - e^{-(T_{23}+T_{32})s}\delta - e^{-(T_{12}+T_{21})s}\zeta. \tag{2.61}$$

The set of δ, ϵ, and ζ can be obtained by solving $\det(\boldsymbol{\mathcal{L}}_{\mathrm{p3}}^{\mathrm{CD}}) = 0$. By solving a backward calculation, the modified dimensional matrix is obtained by

$$\begin{aligned}\boldsymbol{\mathcal{D}}_3^{\mathrm{CD}} =& \mathrm{diag}\{e^{-(T_{12}+T_{21})s}, 1+e^{-(T_{23}+T_{32})s}, 1\},\\ & \mathrm{diag}\{e^{-T_{12}s}, e^{-T_{21}s}+e^{-T_{23}s}, e^{-T_{32}s}\},\\ & \mathrm{diag}\{e^{-T_{21}s}, e^{-T_{12}s}+e^{-T_{32}s}, e^{-T_{23}s}\},\\ & \mathrm{diag}\{1, 1+e^{-(T_{12}+T_{21})s}, e^{-(T_{23}+T_{32})s}\}. \end{aligned} \tag{2.62}$$

The backward calculation was conducted so that a delay time model is not required in the first and the last sets shown in (2.62). The determinant of the modified graph Laplacian is calculated as

$$\det(\boldsymbol{\mathcal{L}}_{\mathrm{p3}}^{\mathrm{CD}}) = 0. \tag{2.63}$$

It can be seen that even in three-agent systems, the connectivity design to realize motion decoupling has two ways. Therefore, it can be said that the decoupling of the COG motion and formation motion has been succeeded.

Characteristics of $\boldsymbol{\mathcal{L}}_{\mathrm{p3}}^{\mathrm{CD}}$ are given in the following. At first, the rank of the proposed matrix $\boldsymbol{\mathcal{L}}_{\mathrm{p3}}^{\mathrm{CD}}$ is 2. It can be derived by using the elementary transformation of a matrix:

$$\begin{aligned}\boldsymbol{L}_{\mathrm{p3}}^{\mathrm{CD}} =& \begin{bmatrix} e^{-(T_{12}+T_{21})s} & -e^{-T_{12}s} & 0\\ -e^{-T_{21}s} & 1+e^{-(T_{23}+T_{32})s} & -e^{-T_{23}s}\\ 0 & -e^{-T_{23}s} & 1\end{bmatrix} \to \begin{bmatrix} e^{-(T_{12}+T_{21})s} & -e^{-T_{12}s} & 0\\ -e^{-T_{21}s} & 1 & 0\\ 0 & -e^{-T_{23}s} & 1\end{bmatrix}\\ & \to \begin{bmatrix} -e^{-T_{21}s} & 1 & 0\\ 0 & -e^{-T_{23}s} & 1\\ 0 & 0 & 0\end{bmatrix}. \end{aligned} \tag{2.64}$$

The real quadratic form of $\boldsymbol{\mathcal{L}}_{\mathrm{p3}}^{\mathrm{CD}}$ is calculated as

$$\boldsymbol{q}_3^T \boldsymbol{\mathcal{L}}_{\mathrm{p3}}^{\mathrm{CD}} \boldsymbol{q}_3 = (e^{-T_{12}s}q_1 - q_2)(e^{-T_{21}s}q_1 - q_2) + (e^{-T_{23}s}q_2 - q_3)(e^{-T_{32}s}q_2 - q_3). \tag{2.65}$$

When $T_{12} = T_{21}$ and $T_{23} = T_{32}$, the quadratic form of $\boldsymbol{\mathcal{L}}_{\mathrm{p3}}^{\mathrm{CD}}$ becomes nonnegative. Therefore, if $T_{ij} = T_{ji}$, $\boldsymbol{\mathcal{L}}_{\mathrm{p3}}^{\mathrm{CD}}$ becomes positive semi-definite.

Finally, the graph Laplacian to decouple the COG motion and formation motion is inductively given by

$$\boldsymbol{\mathcal{L}}_{\mathrm{p}n}^{\mathrm{CD}} = \boldsymbol{\mathcal{D}}_n^{\mathrm{CD}} - \boldsymbol{A}_{\mathrm{n}}^{\mathrm{CD}}, \tag{2.66}$$

where

$$
\begin{aligned}
\boldsymbol{\mathcal{D}}_n^{\mathrm{CD}} = \quad & \mathrm{diag}\Big\{ \quad e^{-(T_{12}+T_{21})s},\ \left(1+e^{-(T_{23}+T_{32})s}\right),\ \left(1+e^{-(T_{34}+T_{43})s}\right), \\
& \qquad \cdots,\ \left(1+e^{-(T_{(n-1)n}+T_{n(n-1)})s}\right),\ 1 \qquad\qquad \Big\}, \\
& \mathrm{diag}\Big\{ \quad e^{-T_{12}s},\ \left(e^{-T_{21}s}+e^{-T_{23}s}\right),\ \left(e^{-T_{32}s}+e^{-T_{34}s}\right)\}, \\
& \qquad \cdots,\left(e^{-T_{(n-1)(n-2)}s}+e^{-T_{(n-1)n}s}\right),\ e^{-T_{n(n-1)}s} \qquad\qquad \Big\}, \\
& \mathrm{diag}\Big\{ \quad e^{-T_{21}s},\ \left(e^{-T_{12}s}+e^{-T_{32}s}\right),\ \left(e^{-T_{34}s}+e^{-T_{43}s}\right)\}, \\
& \qquad \cdots,\left(e^{-T_{(n-2)(n-1)}s}+e^{-T_{n(n-1)}s}\right),\ e^{-T_{(n-1)n}s} \qquad\qquad \Big\}, \\
& \mathrm{diag}\Big\{ \quad 1,\ \left(1+e^{-(T_{12}+T_{21})s}\right),\ \left(1+e^{-(T_{23}+T_{32})s}\right),\ \left(1+e^{-(T_{34}+T_{43})s}\right), \\
& \qquad \cdots,\ \left(1+e^{-(T_{(n-2)(n-1)}+T_{(n-1)(n-2)})s}\right),\ e^{-(T_{(n-1)n}+T_{n(n-1)})s} \qquad\qquad \Big\}.
\end{aligned}
\tag{2.67}
$$

The determinant of the modified graph Laplacian can be also inductively obtained by $\det(\boldsymbol{\mathcal{L}}_{\mathrm{p}n}^{\mathrm{CD}}) = 0$.

The proof of the determinant of the structure above is 0 is shown in the following by using the mathematical induction. The graph Laplacian using the first and second diagonal elements shown in (2.67) is defined as$\boldsymbol{\mathcal{L}}_{\mathrm{p}n}^{\mathrm{CD1}}$ and $\boldsymbol{\mathcal{L}}_{\mathrm{p}n}^{\mathrm{CD2}}$, respectively.

Theorem 1: for any n, $\det(\boldsymbol{\mathcal{L}}_{\mathrm{p}n}^{\mathrm{CD1}}) = 0$ holds.

Proof. When $n = 2$, $\det(\boldsymbol{\mathcal{L}}_{\mathrm{p2}}^{\mathrm{CD1}}) = 0$ holds as it was shown in (2.38). Assume $\det(\boldsymbol{\mathcal{L}}_{\mathrm{p}n}^{\mathrm{CD1}}) = 0$. It means the following equation holds:

$$
\begin{aligned}
& \det(\boldsymbol{\mathcal{L}}_{\mathrm{p}n}^{\mathrm{CD1}}) \\
& = \begin{vmatrix}
e^{-(T_{12}+T_{21})s} & -e^{-T_{12}s} & \cdots & 0 & 0 \\
-e^{-T_{21}s} & 1+e^{-(T_{23}+T_{32})s} & \cdots & 0 & 0 \\
\vdots & \vdots & \ddots & \vdots & \vdots \\
0 & \cdots & \cdots & e^{-T_{(n-2)(n-1)}s} & 0 \\
0 & 0 & \cdots & 1+e^{-(T_{(n-1)n}+T_{n(n-1)})s} & -e^{-T_{(n-1)n}s} \\
0 & 0 & 0 & -e^{-T_{n(n-1)}s} & 1
\end{vmatrix} \\
& = 0.
\end{aligned}
\tag{2.68}
$$

If the same connectivity design was applied to $n+1$ numbered multi-agent system and the determinant also becomes 0, the connectivity design can be extended to multi-agent systems with any number of

agents. When the number of the agents is $n+1$, the determinant becomes

$$\det(\boldsymbol{\mathcal{L}}^{\mathrm{CD1}}_{\mathrm{p}n+1}) = \begin{vmatrix} e^{-(T_{12}+T_{21})s} & \cdots & 0 & 0 & 0 & 0 \\ -e^{-T_{21}s} & \cdots & 0 & 0 & 0 & 0 \\ \vdots & \vdots & \ddots & \vdots & \vdots & \vdots \\ 0 & \cdots & \cdots & -e^{-T_{(n-2)(n-1)}s} & 0 & 0 \\ 0 & 0 & \cdots & 1+e^{-(T_{(n-1)n}+T_{n(n-1)})s} & -e^{-T_{(n-1)n}s} & 0 \\ 0 & 0 & 0 & -e^{-T_{n(n-1)}s} & 1+e^{-(T_{n(n+1)}+T_{(n+1)n})s} & -e^{-T_{n(n+1)}s} \\ 0 & 0 & 0 & 0 & -e^{-T_{(n+1)n}s} & 1 \end{vmatrix}. \tag{2.69}$$

By using the characteristics of the determinant, the determinant does not change when adding elements of one row to the elements of another row with the multiplication of constant value. Eq. (2.69) can be modified as

$$\begin{aligned} &\det(\boldsymbol{\mathcal{L}}^{\mathrm{CD1}}_{\mathrm{p}n+1}) \\ &= \begin{vmatrix} e^{-(T_{12}+T_{21})s} & \cdots & 0 & 0 & 0 & 0 \\ -e^{-T_{21}s} & \cdots & 0 & 0 & 0 & 0 \\ \vdots & \vdots & \ddots & \vdots & \vdots & \vdots \\ 0 & \cdots & \cdots & -e^{-T_{(n-2)(n-1)}s} & 0 & 0 \\ 0 & 0 & \cdots & 1+e^{-(T_{(n-1)n}+T_{n(n-1)})s} & -e^{-T_{(n-1)n}s} & 0 \\ 0 & 0 & 0 & -e^{-T_{n(n-1)}s} & 1 & -e^{-T_{n(n+1)}s} \\ 0 & 0 & 0 & 0 & 0 & 1 \end{vmatrix} && (2.70) \\ &= 1 \times \begin{vmatrix} e^{-(T_{12}+T_{21})s} & -e^{-T_{12}s} & \cdots & 0 & 0 \\ -e^{-T_{21}s} & 1+e^{-(T_{23}+T_{32})s} & \cdots & 0 & 0 \\ \vdots & \vdots & \ddots & \vdots & \vdots \\ 0 & \cdots & \cdots & e^{-T_{(n-2)(n-1)}s} & 0 \\ 0 & 0 & \cdots & 1+e^{-(T_{(n-1)n}+T_{n(n-1)})s} & -e^{-T_{(n-1)n}s} \\ 0 & 0 & 0 & -e^{-T_{n(n-1)}s} & 1 \end{vmatrix} && (2.71) \\ &= 1 \times \det(\boldsymbol{\mathcal{L}}^{\mathrm{CD1}}_{\mathrm{p}n}) && (2.72) \\ &= 0. && (2.73) \end{aligned}$$

The modification from (2.70) to (2.71) is done by adding the $n+1$th row to n th row with the multiplication of $e^{-T_{(n+1)n}s}$. It showed that if $\det(\boldsymbol{\mathcal{L}}^{\mathrm{CD1}}_{\mathrm{p}n}) = 0$ holds, $\det(\boldsymbol{\mathcal{L}}^{\mathrm{CD1}}_{\mathrm{p}n+1}) = 0$ also holds. Therefore, $\det(\boldsymbol{\mathcal{L}}^{\mathrm{CD1}}_{\mathrm{p}n}) = 0$ holds for any n in this line-shaped multi-agent system. □

The rank of the proposed matrix with order n becomes $n-1$ by using the same procedure when the order is three. The proposed matrix is also semi-definite when $T_{ij} = T_{ji}$. The real quadratic form is

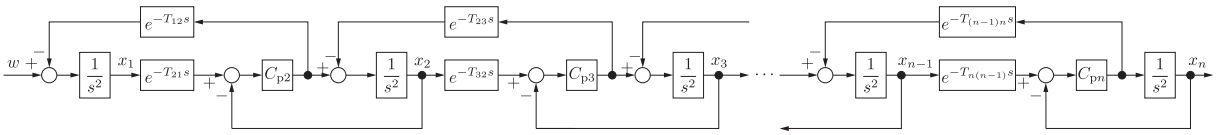

Fig. 2-13: Motion decoupled multi-agent system as a line structure.

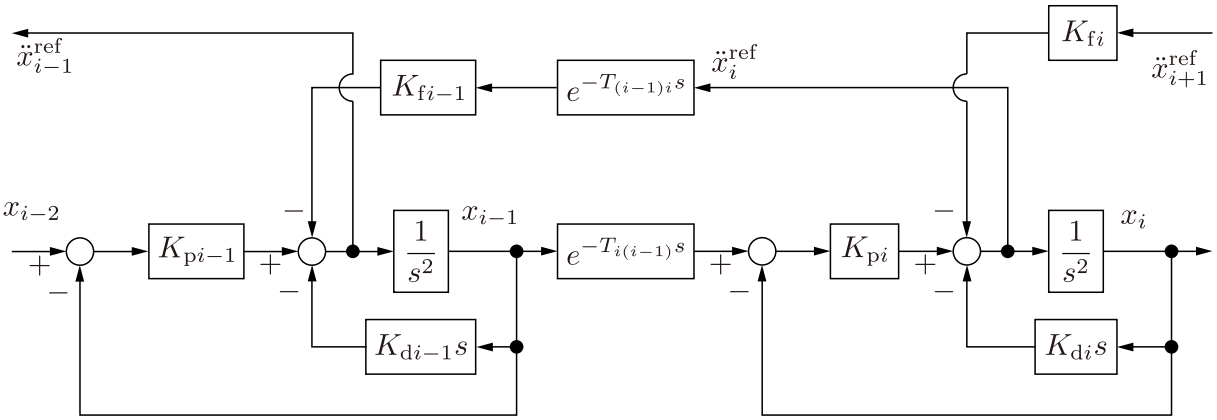

Fig. 2-14: Controller placement in $i-1$th system.

calculated as

$$\begin{aligned}\boldsymbol{q}^T\boldsymbol{\mathcal{L}}_{pn}^{\mathrm{CD}}\boldsymbol{q} =&(e^{-T_{12}s}q_1-q_2)(e^{-T_{21}s}q_1-q_2)+(e^{-T_{23}s}q_2-q_3)(e^{-T_{32}s}q_2-q_3)\cdots\\ &(e^{-T_{(n-1)n}s}q_{n-1}-q_n)(e^{-T_{n(n-1)}s}q_{n-1}-q_n).\end{aligned} \tag{2.74}$$

The block diagram of the motion decoupled multi-agent system is shown in Fig. 2-13. The connected structure is very similar to a multi-mass resonant system [94]. Since the connectivity of the proposed method became similar to that of a multi-mass resonant system, controller design based on vibration control can be used to the proposed method. Poles of the proposed control structure are designed to be placed on the real axis.

Controller design method is explained in the following. Fig. 2-14 shows the controller placement of

$i-1$th system. The transfer function of the $i-1$ th agent is calculated as

$$G_{i-1}(s) = \frac{n_2 s^2 + n_1 s + n_0}{d_4 s^4 + d_3 s^3 + d_2 s^2 + d_1 s + d_0} \tag{2.75}$$

$$n_2 = 1, \tag{2.76}$$

$$n_1 = K_{\mathrm{d}i}, \tag{2.77}$$

$$n_0 = K_{\mathrm{p}i}, \tag{2.78}$$

$$d_4 = 1, \tag{2.79}$$

$$d_3 = K_{\mathrm{d}i-1} + K_{\mathrm{d}i}, \tag{2.80}$$

$$d_2 = (1 + e^{-(\tau_{i,i-1}+\tau_{i-1,i})s} K_{\mathrm{f}i}) K_{\mathrm{p}i} + K_{\mathrm{p}i-1} + K_{\mathrm{d}i-1} K_{\mathrm{d}i}, \tag{2.81}$$

$$d_1 = K_{\mathrm{p}i-1} K_{\mathrm{d}i} + K_{\mathrm{p}i} K_{\mathrm{d}i-1}, \tag{2.82}$$

$$d_0 = K_{\mathrm{p}i-1} K_{\mathrm{p}i}. \tag{2.83}$$

The pole placement method is used to determine every gain which is the same as the case with two agent systems. The desired characteristic equation is defined as

$$\begin{aligned} G(s) &= (s + p_{i-1})^4 \\ &= s^4 + 4p_{i-1}s^3 + 6p_{i-1}^2 s^2 + 4p_{i-1}^3 s + p_{i-1}^4. \end{aligned} \tag{2.84}$$

By comparing the coefficients, the controller gains and the pole of $i-1$ th agent is determined as

$$K_{\mathrm{p}i-1} = K_{\mathrm{p}i} \tag{2.85}$$

$$K_{\mathrm{d}i-1} = 4\sqrt{K_{\mathrm{p}i}} - K_{\mathrm{d}i} \tag{2.86}$$

$$K_{\mathrm{f}i-1} = e^{(\tau_{i,i-1}+\tau_{i-1,i})s} \frac{(K_{\mathrm{d}i} - 2\sqrt{K_{\mathrm{p}i}})^2}{K_{\mathrm{p}i}} \tag{2.87}$$

$$p_{i-1} = \sqrt{K_{\mathrm{p}i}}. \tag{2.88}$$

2.4.2 Tree-Shaped Multi-Agent Systems

The fundamental unit are used to decouple each motion of the tree shaped system. The example is given in Fig. 2-15. The graph Laplacian with delay elements is expressed by

$$\boldsymbol{L}_{\mathrm{p6}}^{\mathrm{CD}} = \begin{bmatrix} 1 & -e^{-T_{12}s} & 0 & 0 & 0 & 0 \\ -e^{-T_{21}s} & 3 & -e^{-T_{23}s} & 0 & -e^{-T_{25}s} & 0 \\ 0 & -e^{-T_{32}s} & 3 & -e^{-T_{34}s} & 0 & -e^{-T_{36}s} \\ 0 & 0 & -e^{-T_{43}s} & 1 & 0 & 0 \\ 0 & -e^{-T_{52}s} & 0 & 0 & 1 & 0 \\ 0 & 0 & -e^{-T_{63}s} & 0 & 0 & 1 \end{bmatrix}. \tag{2.89}$$

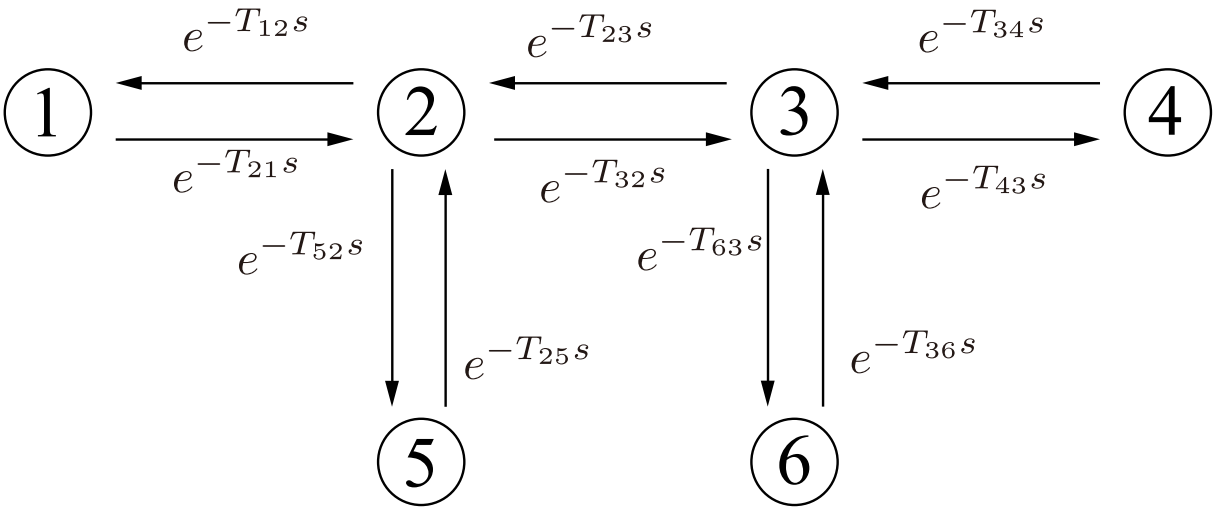

Fig. 2-15: Tree shaped multi-agent system.

The obtained sets of the elements are obtained as follows:

$$
\begin{aligned}
\boldsymbol{\mathcal{D}}_6^{\mathrm{CD}} = \quad & \mathrm{diag}\Big\{ \quad e^{-(T_{12}+T_{21})s}, 1+e^{-(T_{23}+T_{32})s}+e^{-(T_{25}+T_{52})s}, \\
& \qquad\quad 1+e^{-(T_{34}+T_{43})s}+e^{-(T_{36}+T_{63})s}, 1, 1, 1 \qquad\quad \Big\}, \\
& \mathrm{diag}\Big\{ \quad e^{-T_{12}s}, e^{-T_{21}s}+e^{-T_{23}s}+e^{-T_{25}s}, \\
& \qquad\quad e^{-T_{32}s}+e^{-T_{34}s}+e^{-T_{36}s}, e^{-T_{43}s}, e^{-T_{52}s}, e^{-T_{63}s} \qquad\quad \Big\}, \\
& \mathrm{diag}\Big\{ \quad e^{-T_{21}s}, e^{-T_{12}s}+e^{-T_{32}s}+e^{-T_{52}s}, \\
& \qquad\quad e^{-T_{23}s}+e^{-T_{43}s}+e^{-T_{63}s}, e^{-T_{34}s}, e^{-T_{25}s}, e^{-T_{36}s} \qquad\quad \Big\}, \\
& \mathrm{diag}\Big\{ \quad 1, 2+e^{-(T_{12}+T_{21})s}, 2+e^{-(T_{23}+T_{32})s}, e^{-(T_{34}+T_{43})s}, \\
& \qquad\quad e^{-(T_{25}+T_{52})s}, e^{-(T_{36}+T_{63})s} \qquad\quad \Big\}.
\end{aligned}
\tag{2.90}
$$

The values are obtained by using some characteristics of the determinant.

The modification procedure of the determinant is to translate the determinant to the line-shaped structured systems. The same procedure is used to obtain the motion decoupled connectivity that is to determine the diagonal elements of the matrix so that the determinant becomes 0.

$$
\begin{aligned}
&\det(\boldsymbol{\mathcal{L}}_{\mathrm{p6}}^{\mathrm{CD1}}) \\
&= \begin{vmatrix}
e^{-(T_{12}+T_{21})s} & -e^{-T_{12}s} & 0 & 0 & 0 & 0 \\
-e^{-T_{21}s} & 1+e^{-(T_{23}+T_{32})s}+e^{-(T_{25}+T_{52})s} & -e^{-T_{23}s} & 0 & -e^{-T_{25}s} & 0 \\
0 & -e^{-T_{32}s} & 1+e^{-(T_{34}+T_{43})s}+e^{-(T_{36}+T_{63})s} & -e^{-T_{34}s} & 0 & -e^{-T_{36}s} \\
0 & 0 & -e^{-T_{43}s} & 1 & 0 & 0 \\
0 & -e^{-T_{52}s} & 0 & 0 & 1 & 0 \\
0 & 0 & -e^{-T_{63}s} & 0 & 0 & 1
\end{vmatrix} && (2.91) \\
&= 1 \times \begin{vmatrix}
e^{-(T_{12}+T_{21})s} & -e^{-T_{12}s} & 0 & 0 & 0 \\
-e^{-T_{21}s} & 1+e^{-(T_{23}+T_{32})s}+e^{-(T_{25}+T_{52})s} & -e^{-T_{23}s} & 0 & -e^{-T_{25}s} \\
0 & -e^{-T_{32}s} & 1+e^{-(T_{34}+T_{43})s} & -e^{-T_{34}s} & 0 \\
0 & 0 & -e^{-T_{43}s} & 1 & 0 \\
0 & -e^{-T_{52}s} & 0 & 0 & 1
\end{vmatrix} && (2.92) \\
&= 1 \times \begin{vmatrix}
e^{-(T_{12}+T_{21})s} & -e^{-T_{12}s} & 0 & 0 \\
-e^{-T_{21}s} & 1+e^{-(T_{23}+T_{32})s} & -e^{-T_{23}s} & 0 \\
0 & -e^{-T_{32}s} & 1+e^{-(T_{34}+T_{43})s} & -e^{-T_{34}s} \\
0 & 0 & -e^{-T_{43}s} & 1
\end{vmatrix} && (2.93) \\
&= 1 \times \begin{vmatrix}
e^{-(T_{12}+T_{21})s} & -e^{-T_{12}s} & 0 \\
-e^{-T_{21}s} & 1+e^{-(T_{23}+T_{32})s} & -e^{-T_{23}s} \\
0 & -e^{-T_{32}s} & 1
\end{vmatrix} && (2.94) \\
&= 0. && (2.95)
\end{aligned}
$$

The controller design method was the same in the line shaped multi-agent system, therefore, the description is omitted.

2.5 Simulation Results of Various Types of Multi-Agent Systems

2.5.1 Simulation Conditions

Simulations are conducted to examine whether COG motion and formation motion are decoupled. The number of subsystems in the simulations is set as 10. The delay times that are assumed in the simulations are constant values between 100 ms to 900 ms.

$$
\begin{aligned}
&T_{12} = 100 \text{ ms}, \;\; T_{i,i+1} = 100 + 100(i-1) \text{ ms} \\
&T_{21} = 100 \text{ ms}, \;\; T_{i+1,i} = 100 + 100(i-1) \text{ ms} \\
&\quad (i = 2,\ 3,\ \cdots,\ 9).
\end{aligned}
$$

Table 2.2: Simulation parameters for multilateral systems.

Parameter	Description	Value
p	Pole for every motion	80 rad/s
K_{p}	Proportional gain for every motion	6400
K_{d}	Differential gain for every motion	120
K_{f}	Torsional feedback gain for every motion	20

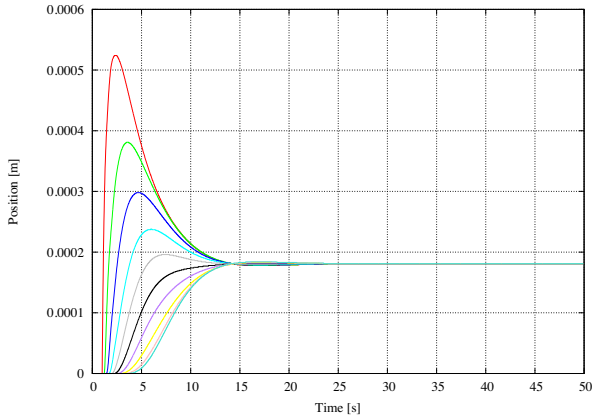

Fig. 2-16: Impulse response when the motions are not decoupled.

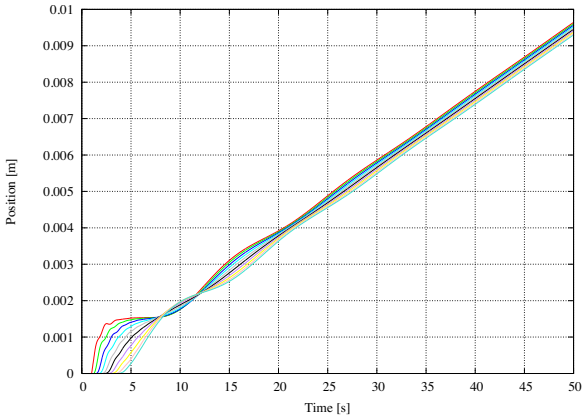

Fig. 2-17: Impulse response when the motions are decoupled.

The value becomes large as agent number increases. Two control structures were compared in the simulations: the structures whether the motions are decoupled or not. The designed control parameter was set as shown in Table 2.2.

2.5.2 Simulation Results

At first, the impulse input was applied to subsystem 1 in both methods. In this situation, there is no controller for the COG motion. The results are shown in Figs. 2-16 and 2-17. These results mostly show the effectiveness of decoupling the motions. As for the control structure where the motions are not decoupled since the characteristic polynomial does not have double poles at the origin, the COG motion stops in the steady state. On the contrary, the response regarding the structure where the motions are decoupled shows that COG motion is moving at constant speed. This is because the structure has a characteristics of a double integrator.

At next, step response results are applied to both conventional and proposed methods. The results are

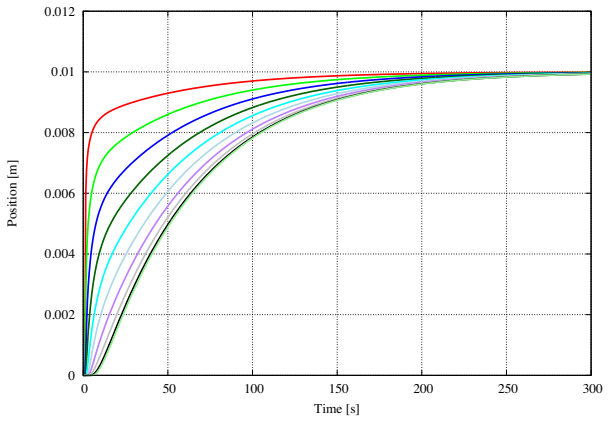

Fig. 2-18: Step command response when the motions are not decoupled.

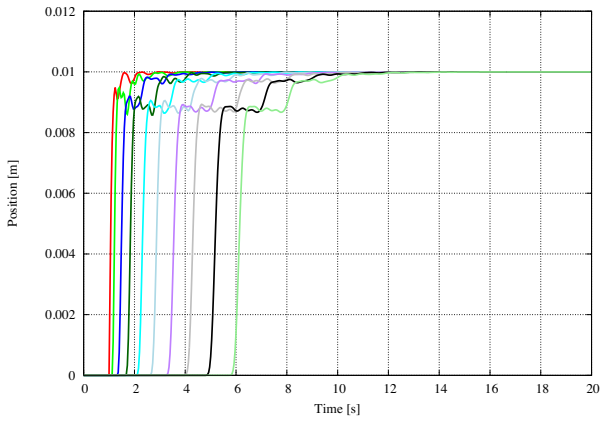

Fig. 2-19: Step command response when the motions are decoupled.

shown in Figs. 2-18 and 2-19. The position command for COG position was set as

$$x^{\mathrm{cmd}} = 0.01\ [\mathrm{m}].$$

Both methods converged to the command value; however, in the conventional method, it took about 300 s for all of the agents to converge to the command while it took only 15 s in the proposed method to converge. The reason for the slow convergence of the conventional method is the interference between the controllers. The pulling back motion in the proposed method is to reduce the vibration in the formation position, which is often seen in vibration control.

Next, sinusoidal wave was applied to each method. The command was

$$x^{\mathrm{cmd}} = 0.01 \sin(0.1t)\ [\mathrm{m}].$$

The results are shown in Figs. 2-20 and 2-21, respectively. In the conventional method, there are large position errors in every agent compared to the command. However, in the proposed method, every agent well tracks the command of COG motion even the controller gains are the same with the conventional method.

At next, both step and sinusoidal wave commands were applied to a tree-shaped multi-agent system whose structure is shown in Fig. 2-22. The results are expressed in Figs. 2-23 and 2-24. Both responses is very similar to the responses of the proposed tree shaped system that are shown in Figs. 2-19 and 2-21. It indicates that the COG and formation motion in both line and tree shaped systems are decoupled by using the proposed connectivity design. Therefore, the validity of the proposed method was confirmed.

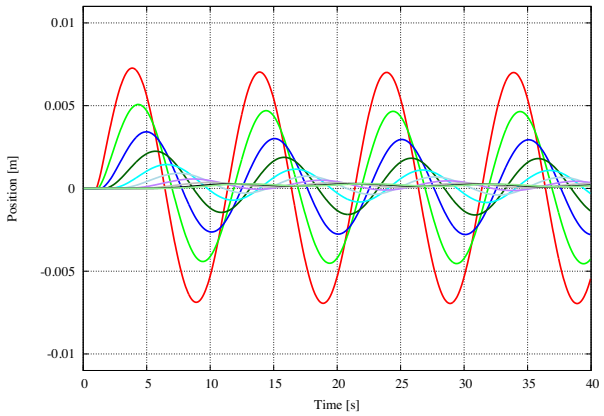

Fig. 2-20: Sinusoidal wave command response in motion coupled structure.

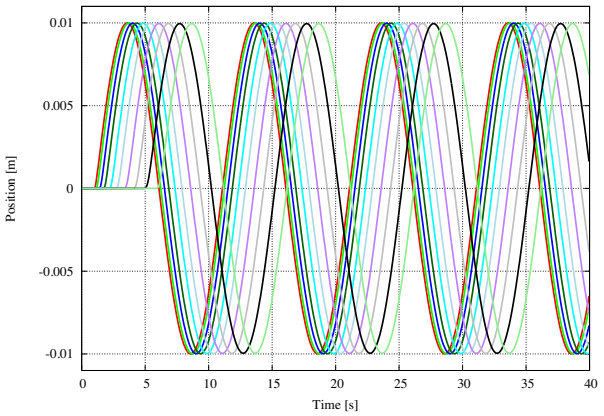

Fig. 2-21: Sinusoidal wave command response in motion decoupled structure.

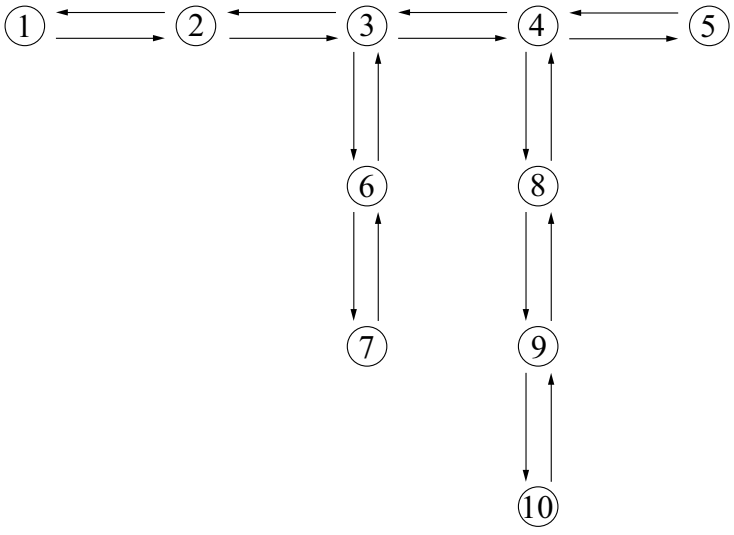

Fig. 2-22: Tree shaped system used in the simulation.

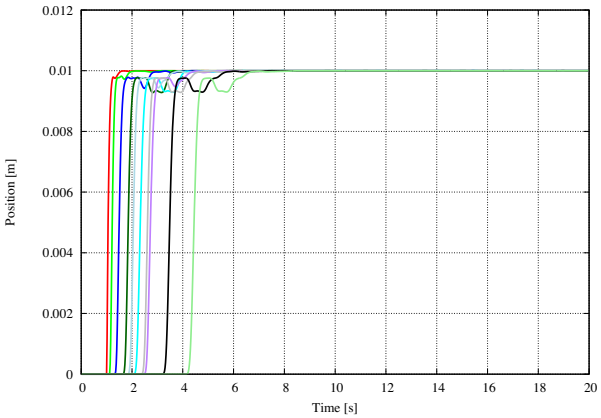

Fig. 2-23: Step command response to tree shaped system (proposed method).

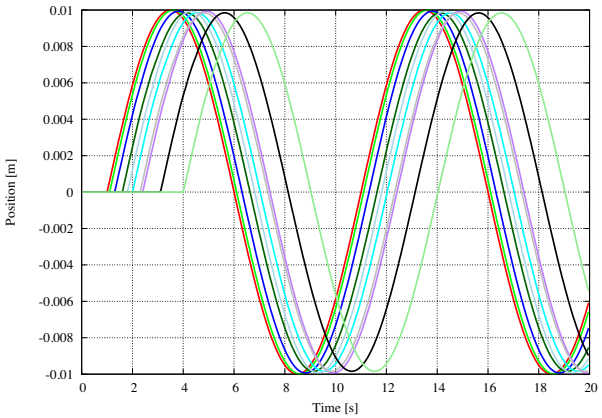

Fig. 2-24: Sinusoidal wave command response to tree shaped system (proposed method).

2.6 Summary of Chapter 2

In this chapter, the connectivity design method for the relative motion in multilateral systems was proposed. The connectivity was designed to make the determinant of the graph Laplacian as 0 so that the COG motion in the system has the double integrator characteristics. Firstly, the design was established in a system whose number of systems is two. It became clear that there are two ways to design the connectivity to realize the desired characteristics in the COG motion. Controller parameter design was done by using the concept of resonant ratio control, which is one of the famous methods in vibration control. Then, the connectivity design method was extended to n agent system based on the fundamental connectivity set obtained in the two-agent system. The numerical results showed that the desired characteristics were regained in the proposed method.

Chapter 3

Connectivity Design of COG Motion in Bilateral Teleoperation

In this chapter, The connectivity for controlling the COG motion in bilateral teleoperation is proposed. Controllers in bilateral teleoperation interfere because of a time delay between the systems [36]. At first, the interference that is affected by the force controller to the position controller is eliminated by inserting a buffer to the force response of their own system.

3.1 Introduction of Chapter 3

The contents of this chapter are given as follows. The effect of the interference is firstly discussed in Section 3.1. In Section 3.2, the connectivity design of the COG motion is described. It can be realized by using the delay element to the force input of each local system. The conceptual figure is shown in Fig. 3-1. Since the method requires the model, the effect of the modeling error and the compensation method is described in Section 3.3. Section 3.4 shows the experiment results to verify the effect of the proposed method. Finally, Section 3.5 concludes this chapter.

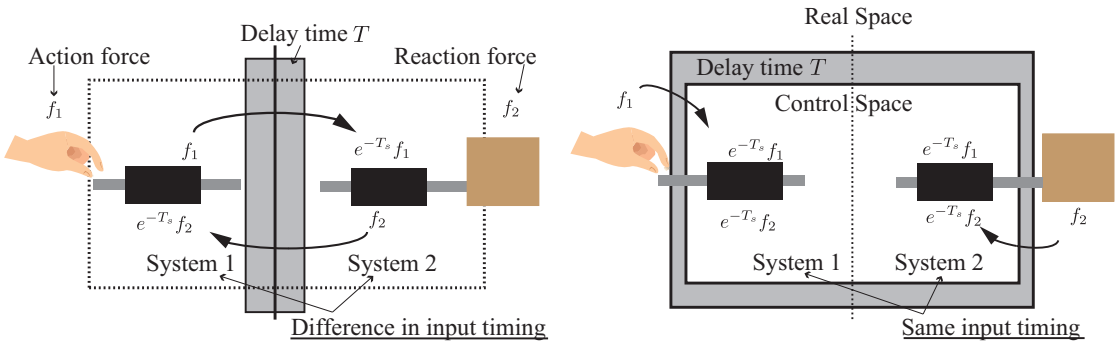

(a) Conventional method. (b) Proposed method.

Fig. 3-1: Conceptual figure of comparison between conventional and proposed method.

3.2 Problem Definition

3.2.1 Control Goals

As mentioned in Chapter 1, bilateral control realizes tactile sensation transmission between two subsystems by fulfilling two control goals. The control goals of a bilateral control system are defined as

$$f_1 + f_2 = 0, \tag{3.1}$$

$$x_1 - x_2 = 0, \tag{3.2}$$

where x and f stand for the position and force response, respectively. The subscript $_i$ represents the value of ith subsystem. Position and force responses are separately controlled to realize the control goals. As for the local subsystems, the DOB [95] is used to realize robust acceleration control. In this dissertation, external force f is estimated by using the RFOB [96].

3.2.2 Bilateral Control without Time Delay

In order to separately control the values, the work space responses are transmitted to another space which is called a modal space. The matrix to transform the coordinates are called the quarry matrix [86], and it is defined as

$$\boldsymbol{Q}_2 = \begin{bmatrix} 1 & 1 \\ -1 & 1 \end{bmatrix}. \tag{3.3}$$

$$\begin{bmatrix} x_c \\ x_d \end{bmatrix} = \boldsymbol{Q}_2 \begin{bmatrix} x_1 \\ x_2 \end{bmatrix}, \tag{3.4}$$

$$\begin{bmatrix} f_c \\ f_d \end{bmatrix} = \boldsymbol{Q}_2 \begin{bmatrix} f_1 \\ f_2 \end{bmatrix}, \tag{3.5}$$

where subscript $_c$ and $_d$ stand for the value of the common and differential modes, respectively. The subscript of $\boldsymbol{Q}$ (in this case, 2) indicates the order of the quarry matrix. The coordinate transformation realizes to transform the motion of two subsystems to view as one rigid motion that describes the center of gravity motion of the overall system, and the relative motion that describes the inner motion of the overall system. By modifying the control goals in the modal space, (3.1) and (3.2) are rewritten as

$$f_c = 0, \tag{3.6}$$

$$x_d = 0. \tag{3.7}$$

Controllers for realizing each control goals are placed at each modes. The acceleration references for each modes are given as

$$\ddot{x}_c^{\mathrm{ref}} = C_{\mathrm{f}}(f_c^{\mathrm{cmd}} - f_c), \tag{3.8}$$

$$\ddot{x}_d^{\mathrm{ref}} = C_{\mathrm{p}}(x_d^{\mathrm{cmd}} - x_d), \tag{3.9}$$

where C_{f} and C_{p} stand for the force and position controllers, respectively. As seen in (3.6) and (3.7), $f_c^{\mathrm{cmd}} = x_d^{\mathrm{cmd}} = 0$. In this dissertation, a proportional controller is used as C_{f}, and a proportional and differential controller is used as C_{p}. The acceleration reference for each subsystem in the work space can be calculated by multiplying the acceleration reference in the mode space with the inverse transformation matrix $\boldsymbol{Q}_2^{-1}$ that is given as

$$\begin{aligned}
\begin{bmatrix} \ddot{x}_1^{\mathrm{ref}} \\ \ddot{x}_2^{\mathrm{ref}} \end{bmatrix} &= \boldsymbol{Q}_2^{-1} \begin{bmatrix} \ddot{x}_c^{\mathrm{ref}} \\ \ddot{x}_d^{\mathrm{ref}} \end{bmatrix} \\
&= -\frac{1}{2} \begin{bmatrix} C_{\mathrm{f}}(f_1 + f_2) + C_{\mathrm{p}}(x_1 - x_2) \\ C_{\mathrm{f}}(f_1 + f_2) + C_{\mathrm{p}}(-x_1 + x_2) \end{bmatrix} \\
&= -\frac{1}{2} C_{\mathrm{f}} \begin{bmatrix} 1 & 1 \\ 1 & 1 \end{bmatrix} \begin{bmatrix} f_1 \\ f_2 \end{bmatrix} - \frac{1}{2} C_{\mathrm{p}} \begin{bmatrix} 1 & -1 \\ -1 & 1 \end{bmatrix} \begin{bmatrix} x_1 \\ x_2 \end{bmatrix} \\
&= -\frac{1}{2} C_{\mathrm{f}} \boldsymbol{L}_{\mathrm{f}} \boldsymbol{f} - \frac{1}{2} C_{\mathrm{p}} \boldsymbol{L}_{\mathrm{p}} \boldsymbol{x}.
\end{aligned} \tag{3.10}$$

$\boldsymbol{L}_{\mathrm{f}}$ and $\boldsymbol{L}_{\mathrm{p}}$ indicates the connectivity of the force response and position response, respectively. The determinants of $\boldsymbol{L}_{\mathrm{f}}$ and $\boldsymbol{L}_{\mathrm{p}}$ are calculated as

$$\det(\boldsymbol{L}_{\mathrm{f}}) = 0, \tag{3.11}$$

$$\det(\boldsymbol{L}_{\mathrm{p}}) = 0. \tag{3.12}$$

As for $\boldsymbol{L}_{\mathrm{p}}$, the determinant becomes 0 when there is no delay between the systems because it is a standard graph Laplacian. It means the position controller does not affect the COG motion. Here, the determinant of $\boldsymbol{L}_{\mathrm{f}}$ is also 0. It shows the double integrator characteristics is maintained in the COG motion because the force controller is a proportional controller. It indicates that COG motion is actuated only by the force controller, and the relative motion is controlled by the response of position difference between subsystems.

3.2.3 Bilateral Control under Time Delay

In this chapter, the delay time between system 1 and system 2 is assumed to be symmetric as T. When there is delay between the systems, the acceleration reference for each system is modified as

$$\begin{aligned}\begin{bmatrix} \ddot{x}_1^{\mathrm{ref}} \\ \ddot{x}_2^{\mathrm{ref}} \end{bmatrix} &= -\frac{1}{2}\begin{bmatrix} C_{\mathrm{f}}(f_1 + e^{-Ts}f_2) + C_{\mathrm{p}}(x_1 - e^{-Ts}x_2) \\ C_{\mathrm{f}}(e^{-Ts}f_1 + f_2) + C_{\mathrm{p}}(-e^{-Ts}x_1 + x_2) \end{bmatrix} \\ &= -\frac{1}{2}C_{\mathrm{f}}\begin{bmatrix} 1 & e^{-Ts} \\ e^{-Ts} & 1 \end{bmatrix}\begin{bmatrix} f_1 \\ f_2 \end{bmatrix} - \frac{1}{2}C_{\mathrm{p}}\begin{bmatrix} 1 & -e^{-Ts} \\ -e^{-Ts} & 1 \end{bmatrix}\begin{bmatrix} x_1 \\ x_2 \end{bmatrix}. \end{aligned} \tag{3.13}$$

The block diagram of the conventional bilateral teleoperation is given in Fig. 3-2. Here, the determinant of each connectivity matrix is calculated as

$$\det(\boldsymbol{L}_{\mathrm{f}}^{\mathrm{CD}}) = 1 - e^{-2Ts} \neq 0, \tag{3.14}$$

$$\det(\boldsymbol{L}_{\mathrm{p}}^{\mathrm{CD}}) = 1 - e^{-2Ts} \neq 0. \tag{3.15}$$

The determinant of $\boldsymbol{L}_{\mathrm{f}}^{\mathrm{CD}}$ must become 0; otherwise, the controller for COG motion affects the relative motion.

In order to analyze the performance of each controller, modal space analysis is an effective method. The conceptual figure that describes the information flow that is sent to each system are shown in Fig.3-3. From this figure, it is obvious that four states are controlled in the conventional bilateral teleoperation system, which are the states of system 1 and 2 of the present time and that of T second previous state, respectively. The same fact can be found in (3.13). The states that are controlled are the same four

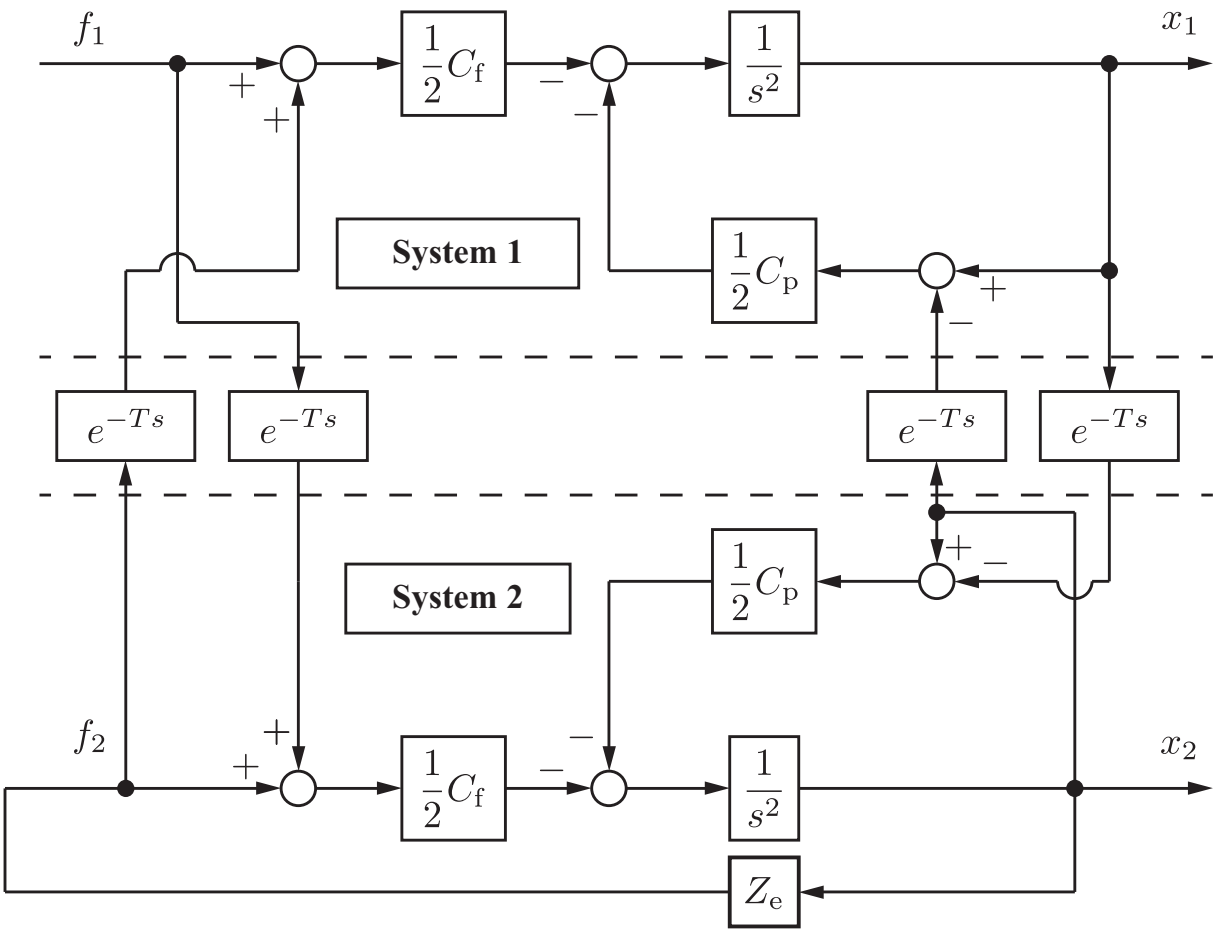

Fig. 3-2: Block diagram of the conventional bilateral teleoperation.

states that are noted above. What is different from the bilateral control system without time delay is that delayed information that is sent from the other system can be regarded as same as the present information because the transmission time is small enough to be neglected.

In this section, four state values are transformed into a modal state values as defined as follows:

$$\begin{bmatrix} f_{\mathrm{com,p}} \\ f_{\mathrm{dif,p}} \\ f_{\mathrm{com,d}} \\ f_{\mathrm{dif,d}} \end{bmatrix} = \begin{bmatrix} 1 & 1 \\ 1 & -1 \\ e^{-Ts} & e^{-Ts} \\ e^{-Ts} & -e^{-Ts} \end{bmatrix} \begin{bmatrix} f_1 \\ f_2 \end{bmatrix}, \tag{3.16}$$

$$\begin{bmatrix} x_{\mathrm{com,p}} \\ x_{\mathrm{dif,p}} \\ x_{\mathrm{com,d}} \\ x_{\mathrm{dif,d}} \end{bmatrix} = \begin{bmatrix} 1 & 1 \\ 1 & -1 \\ e^{-Ts} & e^{-Ts} \\ e^{-Ts} & -e^{-Ts} \end{bmatrix} \begin{bmatrix} x_1 \\ x_2 \end{bmatrix}, \tag{3.17}$$

where subscript $_{\mathrm{com}}$ and $_{\mathrm{dif}}$ stand for the common mode and differential mode, while subscript $_{\mathrm{p}}$ and $_{\mathrm{d}}$

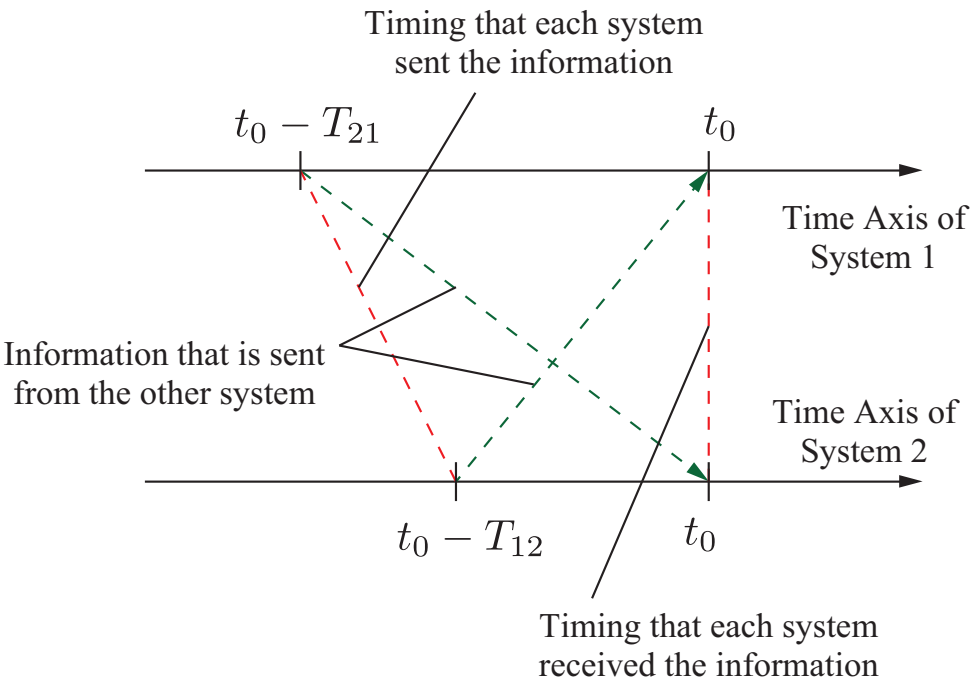

Fig. 3-3: Relationship among four states.

denote the present value or delayed value respectively. The relationship between each state is

$$\begin{cases} x_{\mathrm{com,d}} &= e^{-Ts}x_{\mathrm{com,p}} \\ x_{\mathrm{dif,d}} &= e^{-Ts}x_{\mathrm{dif,p}} \\ x_{\mathrm{com,d}} &= e^{-Ts}x_{\mathrm{com,p}} \\ x_{\mathrm{dif,d}} &= e^{-Ts}x_{\mathrm{dif,p}} \end{cases}. \tag{3.18}$$

The acceleration references for each modal state values can be calculated by using (3.13). At first, acceleration references for the delayed states is derived by multiplying $\mathrm{diag}\{e^{-Ts},\ e^{-Ts}\}$ to both side, which is obtained as

$$\begin{aligned} \begin{bmatrix} e^{-Ts}\ddot{x}_1^{\mathrm{ref}} \\ e^{-Ts}\ddot{x}_2^{\mathrm{ref}} \end{bmatrix} = &-\frac{1}{2}C_{\mathrm{f}}\begin{bmatrix} e^{-Ts} & e^{-2Ts} \\ e^{-2Ts} & e^{-Ts} \end{bmatrix}\begin{bmatrix} f_1 \\ f_2 \end{bmatrix} \\ &-\frac{1}{2}C_{\mathrm{p}}\begin{bmatrix} e^{-Ts} & -e^{-2Ts} \\ -e^{-2Ts} & e^{-Ts} \end{bmatrix}\begin{bmatrix} x_1 \\ x_2 \end{bmatrix}. \end{aligned} \tag{3.19}$$

Since the acceleration references for each state were obtained, acceleration references for each modal

state value can be calculated, which are shown as (3.20) and (3.21):

$$\begin{aligned}\ddot{x}^{\mathrm{ref}}_{\mathrm{com,p}} &= -\frac{1}{2}C_{\mathrm{f}}f_{\mathrm{com,p}} - \frac{1}{2}C_{\mathrm{p}}x_{\mathrm{com,p}} - \frac{1}{2}C_{\mathrm{f}}f_{\mathrm{com,d}} + \frac{1}{2}C_{\mathrm{p}}x_{\mathrm{com,d}} \\ &= -\frac{1}{2}(1+e^{-Ts})C_{\mathrm{f}}f_{\mathrm{com,p}} - \frac{1}{2}(1-e^{-Ts})C_{\mathrm{p}}x_{\mathrm{com,p}}, \qquad (3.20)\\ \ddot{x}^{\mathrm{ref}}_{\mathrm{dif,p}} &= -\frac{1}{2}C_{\mathrm{p}}x_{\mathrm{dif,p}} - \frac{1}{2}C_{\mathrm{f}}f_{\mathrm{dif,p}} - \frac{1}{2}C_{\mathrm{p}}x_{\mathrm{dif,d}} + \frac{1}{2}C_{\mathrm{f}}f_{\mathrm{dif,d}} \\ &= -\frac{1}{2}(1+e^{-Ts})C_{\mathrm{p}}x_{\mathrm{dif,p}} - \frac{1}{2}(1-e^{-Ts})C_{\mathrm{f}}f_{\mathrm{dif,p}}. \qquad (3.21)\end{aligned}$$

Eqs. (3.20) and (3.21) are obtained by adding and subtracting the first and second rows of (3.13) and (3.19).

As shown in all equations, it is obvious that every modes are interfering each other, meaning that the role of each controller is not decoupled in each mode. This is the reason why tactile sensation transmission performance is degraded in a bilateral control system under communication delay.

3.3 Connectivity Design of COG Motion

It is important to robustly control the relative motion in bilateral control because high stiffness controller in the relative motion can transmit precise impedance of a contact object. In order to separately control the relative motion from COG motion, the connectivity of the COG motion that does not interfere with relative motion is proposed in this section. What can be changed is the information of the local subsystem; therefore, the elements of the dimensional matrix are modified to make the determinant of the connectivity matrix of COG motion as 0.

The design procedure is the same as the one proposed in the previous chapter. In order not to make the COG motion controller affect the relative motion of the system, the connection between two subsystems needs to be modified. In this chapter, the connectivity matrix $\boldsymbol{L}_{\mathrm{f}}$ is designed. In order to determine the diagonal elements of d_{ii} of the COG motion connectivity matrix, let d_{ii} set as $\mathrm{diag}\{\alpha, \beta\}$, which is the modified dimensional matrix $\boldsymbol{\mathcal{D}}^{\mathrm{CD}}_{\mathrm{2f}}$, then the determinant is calculated by

$$\det(\boldsymbol{\mathcal{L}}^{\mathrm{CD}}_{\mathrm{2f}}) = \alpha\beta - e^{-2Ts}. \qquad (3.22)$$

By calculating $\det(\boldsymbol{\mathcal{L}}^{\mathrm{CD}}_{\mathrm{2f}}) = 0$, pairs of α and β are obtained as

$$\boldsymbol{\mathcal{D}}^{\mathrm{CD}}_{\mathrm{2f}} = \mathrm{diag}\{e^{-2Ts}, 1\},\ \mathrm{diag}\{1, e^{-2Ts}\},\ \mathrm{diag}\{e^{-Ts}, e^{-Ts}\}. \qquad (3.23)$$

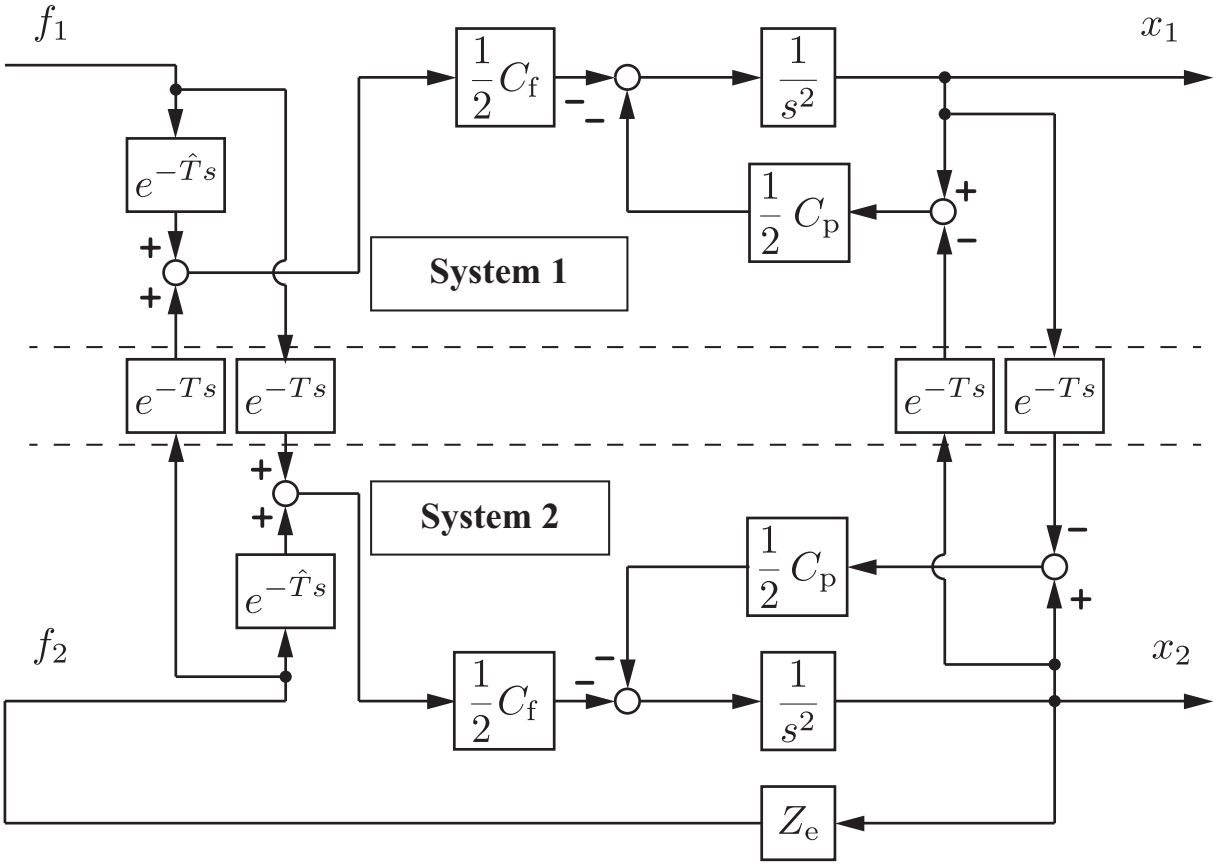

Fig. 3-4: Block diagram of the proposed method.

There are three ways to select the pair of α and β. The first two pairs in (3.23) are already proposed in [63]. In this section, the last set is used hereafter.

The acceleration reference of the proposed method is given as

$$\begin{aligned}\begin{bmatrix} \ddot{x}_1^{\mathrm{ref}} \\ \ddot{x}_2^{\mathrm{ref}} \end{bmatrix} &= -\frac{1}{2}\begin{bmatrix} C_\mathrm{f}(e^{-Ts}f_1 + e^{-Ts}f_2) + C_\mathrm{p}(x_1 - e^{-Ts}x_2) \\ C_\mathrm{f}(e^{-Ts}f_1 + e^{-Ts}f_2) + C_\mathrm{p}(-e^{-Ts}x_1 + x_2) \end{bmatrix} \\ &= -\frac{1}{2}C_\mathrm{f}\begin{bmatrix} e^{-\hat{T}s} & e^{-Ts} \\ e^{-Ts} & e^{-\hat{T}s} \end{bmatrix}\begin{bmatrix} f_1 \\ f_2 \end{bmatrix} - \frac{1}{2}C_\mathrm{p}\begin{bmatrix} 1 & -e^{-Ts} \\ -e^{-Ts} & 1 \end{bmatrix}\begin{bmatrix} x_1 \\ x_2 \end{bmatrix}. \end{aligned} \tag{3.24}$$

The block diagram of the proposed method is shown in Fig. 3-4.

The block diagrams of the differential and common modal space are shown in Figs. 3-5 and 3-6 respectively. When $\hat{T}$ is the same as T, the interference in the position differential mode becomes 0. It means the force differential mode does not interfere with the position differential mode, realizing ideal position tracking even there exists a time delay between the systems. Realization of simultaneity also eliminates the interference from the position differential mode to the force common mode, achieving a

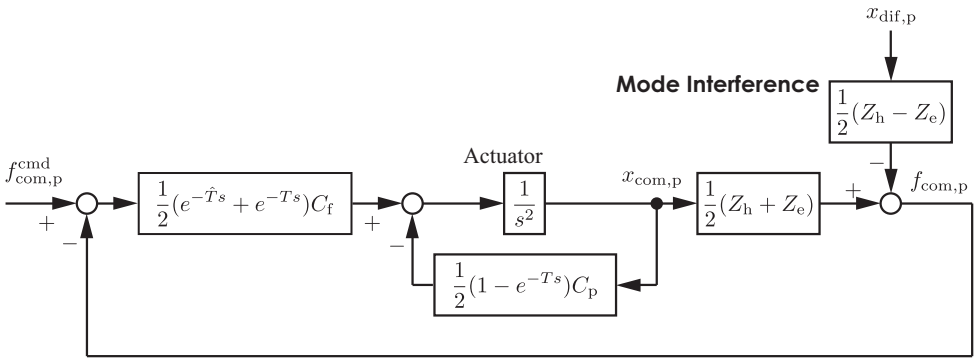

Fig. 3-5: Block diagram of the COG motion considering the modeling error.

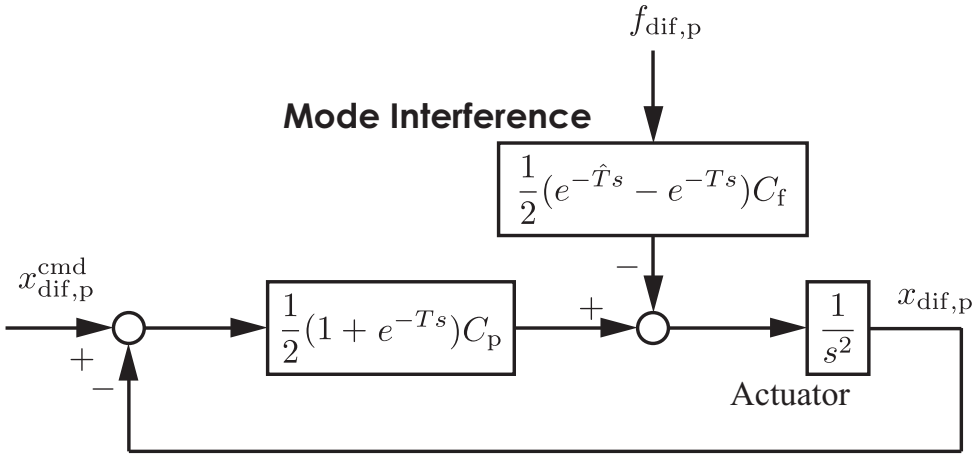

Fig. 3-6: Block diagram of the relative motion considering the modeling error.

decoupled bilateral control system under a communication delay.

However, it is well known that the delay time in network control systems varies because of jitter problem or packet loss. A situation that there exists a modeling error between the estimated delay time $\hat{T}$ and the actual delay time might also occur. The difference between the values results in the interferences between the modes. The effect of the modeling error is analyzed in the following section, and the compensation method using a phase compensator is also expressed.

3.4 Analysis and Compensation of Modeling Error

3.4.1 Performance Analysis

Performance analysis considering the effect of the modeling error of a delay time is firstly conducted. The relationship of the four values that are sent between the systems is expressed in a fundamental matrix

Table 3.1: Control parameters for Bode plot.

Parameter	Description	Value
T	Actual delay time	100 ms
K_{p}	Proportional gain for position control	400.0
K_{d}	Differential gain for position control	40.0
C_{f}	Proportional gain for force control	1.0

as shown as

$$\begin{bmatrix} f_1 \\ x_1 \end{bmatrix} = \frac{1}{F_{\mathrm{den}}} \begin{bmatrix} F_{11} & F_{12} \\ F_{21} & F_{22} \end{bmatrix} \begin{bmatrix} x_2 \\ f_2 \end{bmatrix}, \tag{3.25}$$

$$\begin{cases} F_{11} &= -(2s^2 + C_{\mathrm{p}})^2 - e^{-2Ts} {P_{\mathrm{p}}}^2 {C_{\mathrm{p}}}^2 \\ F_{12} &= -\left(e^{-\hat{T}s}(2s^2 + C_{\mathrm{p}}) + e^{-2Ts} P_{\mathrm{p}} C_{\mathrm{p}}\right) \\ F_{21} &= -F_{12} \\ F_{22} &= \left(e^{-2\hat{T}s} - e^{-2Ts}\right) P_{\mathrm{f}} C_{\mathrm{f}} \\ F_{\mathrm{den}} &= e^{-Ts} P_{\mathrm{f}} C_{\mathrm{f}} \left(2s^2 + (1 + e^{-\hat{T}s} P_{\mathrm{p}}) C_{\mathrm{p}}\right). \end{cases} \tag{3.26}$$

A fundamental matrix is usually used in two-port network systems to express the relationship between four values. The Bode diagrams for each element when a delay time model becomes different from the actual delay time are shown in Fig. 3-7. Control parameters that are used for the Bode plot are shown in Table 3.1. The delay time model is changed from 60 ms to 140 ms. F_{11} stands for the operational force performance in free motion. Since F_{12} and F_{21} indicate whether the system can realize the control goals, the frequency response should be flat at 0 dB. When $\hat{T}$ is equal to T, the frequency response in F_{22}, which indicates the interference of the position control and the force control, becomes $-\infty$ dB.

From the figure, it can be seen that the control performance of the system becomes worse in front of modeling error. The performance behavior becomes different according to the magnitude correlation between the modeled delay time and the actual delay time. As the delay time becomes larger, the low frequency component in F_{11} and F_{21} becomes worse, which means operational force becomes large, and position tracking performance gets degraded. When the model delay time is set larger than the actual delay time, the gain of F_{11}, F_{12}, and F_{21} around 20 Hz, which is a human operation frequency area, becomes large.Therefore, the model delay time should be the same or smaller than the actual delay time. In order to consider the worse case, the compensation is conducted in a situation where the actual delay time is larger than the delay time model.

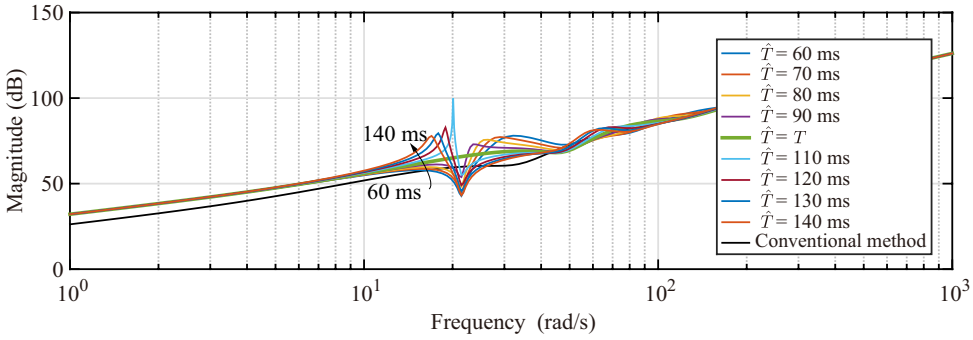

(a) F_{11}

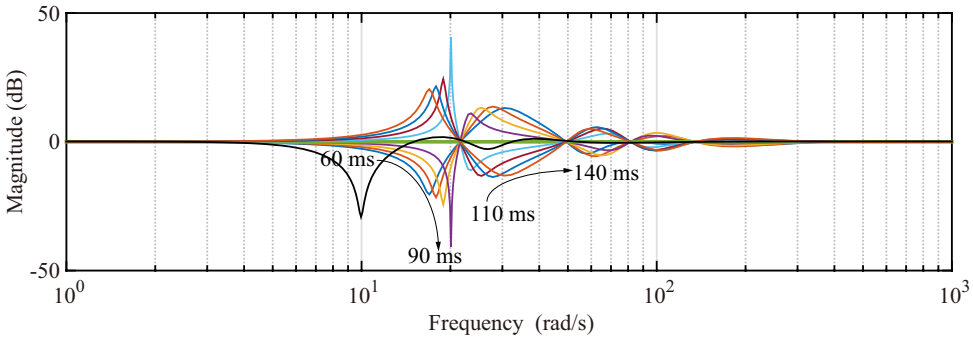

(b) F_{12}, F_{21}

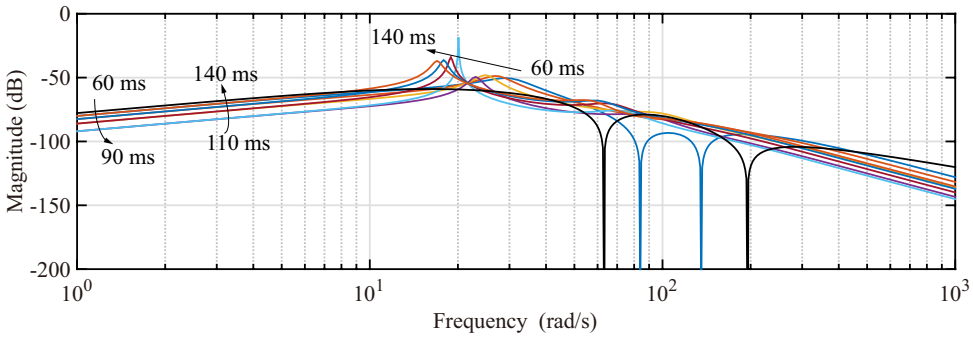

(c) F_{22}

Fig. 3-7: Parameters of $\boldsymbol{F}$ matrix without any compensation.

3.4.2 Modeling Error Compensation

In this subsection, the control design of the phase compensator for the modeling error compensation is explained. Since the biggest merit of the proposed method is that the system realizes high position tracking performance in spite of a communication delay between the systems, the modeling error compensator is designed to regain the position tracking performance. As for the comparison, frequency domain damp-

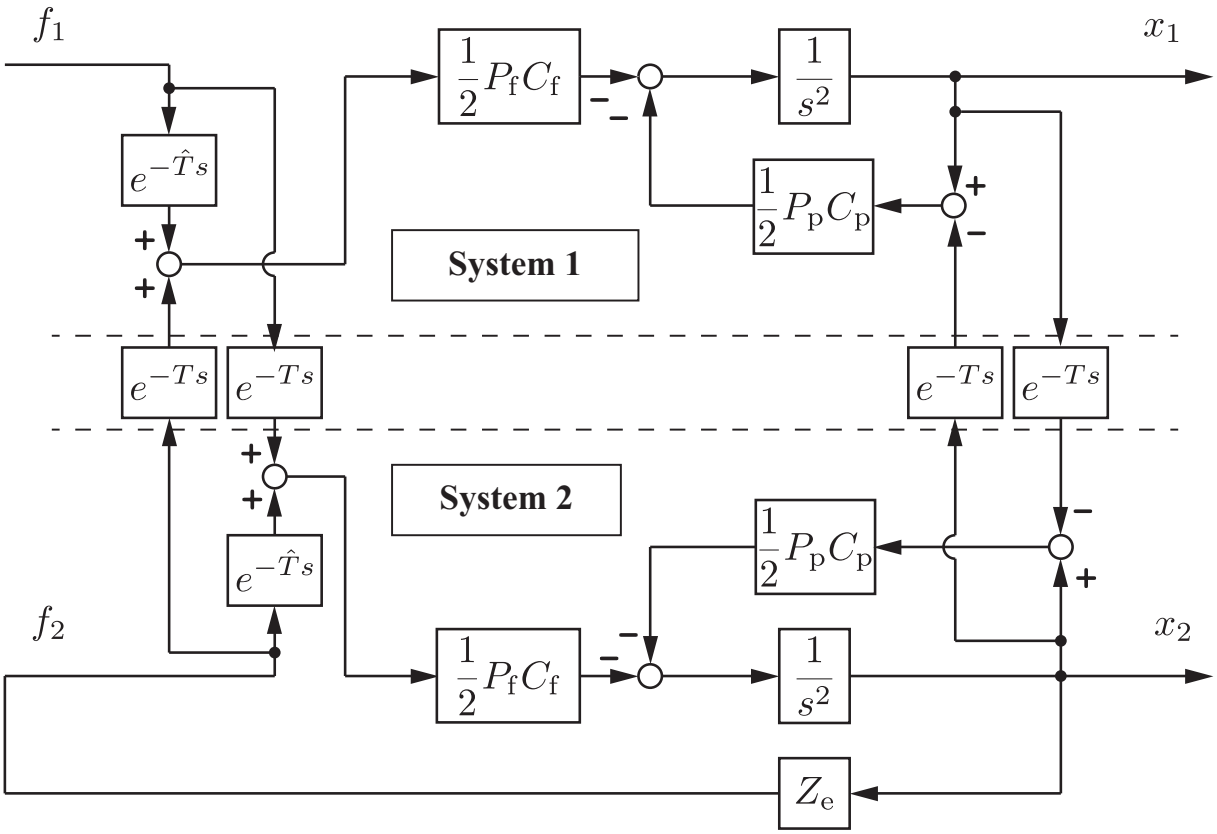

Fig. 3-8: Block diagram of the proposed method with compensation.

Table 3.2: Parameters for the compensators.

Parameter	Description	Value
α_{f}	Gain of P_{f} (phase-lag compensator)	0.1
g_{f}	Cut-off frequency of P_{f}	18.84 rad/s
α_{p}	Gain of P_{p} (phase-lead compensator)	2.5
g_{p}	Cut-off frequency of P_{p}	50 rad/s
K_{vm}	Gain of FDD	160
g_{h}	Cut-off frequency of HPF in FDD	25 rad/s

ing (FDD) [60] is used as the conventional method in the paper. Phase compensators are inserted to both position and force control. The merit of using the compensators is it can change the character of each controller separately. A situation where 20 ms error exists, concretely speaking, $\hat{T}$ is set as 100 ms while T is 120 ms, is assumed from now. This is a worse case because the actual delay time is larger than the delay time model.

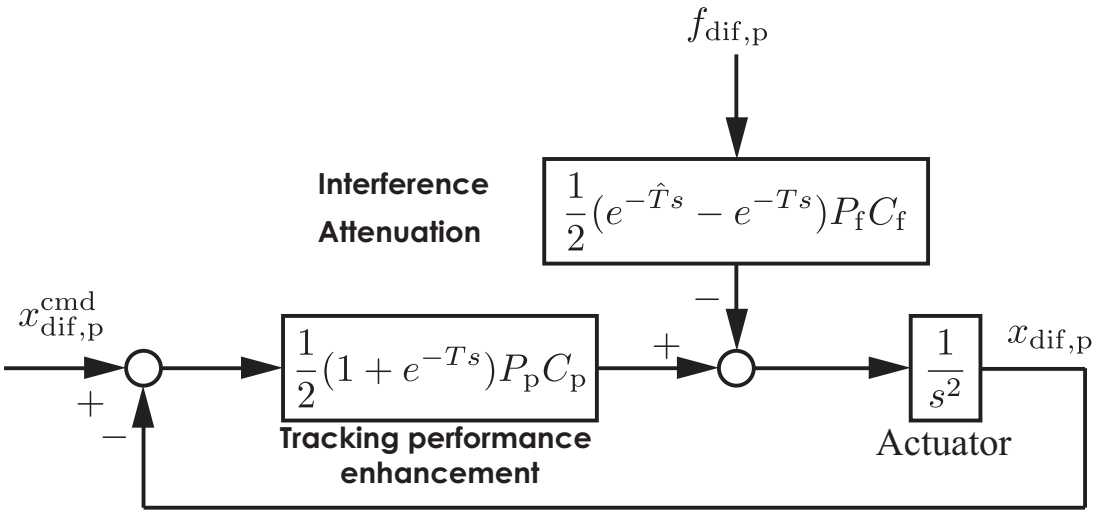

Fig. 3-9: The differential mode in the proposed method with compensation.

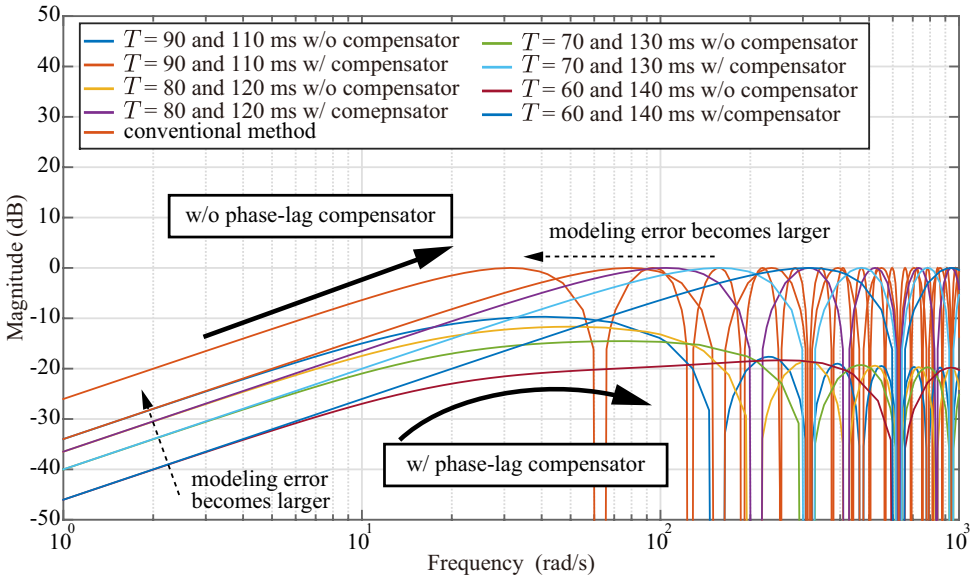

Fig. 3-10: Gain diagram of the coefficient of the force differential mode.

Acceleration references for the proposed connectivity using phase compensators are shown as

$$\begin{bmatrix} s^2 x_1^{\mathrm{ref}} \\ s^2 x_2^{\mathrm{ref}} \end{bmatrix} = -\frac{1}{2}P_{\mathrm{f}}C_{\mathrm{f}} \begin{bmatrix} e^{-\hat{T}s} & e^{-Ts} \\ e^{-Ts} & e^{-\hat{T}s} \end{bmatrix} \begin{bmatrix} f_1 \\ f_2 \end{bmatrix} - \frac{1}{2}P_{\mathrm{p}}C_{\mathrm{p}} \begin{bmatrix} 1 & -e^{-Ts} \\ -e^{-Ts} & 1 \end{bmatrix} \begin{bmatrix} x_1 \\ x_2 \end{bmatrix}, \tag{3.27}$$

where P_{p} and P_{f} stand for the phase-lead compensator in position control and the phase-lag compensator in force control, respectively. Block diagrams of the whole control structure of the proposed method, and the differential modal space of the proposed connectivity is shown in Figs. 3-8 and 3-9.

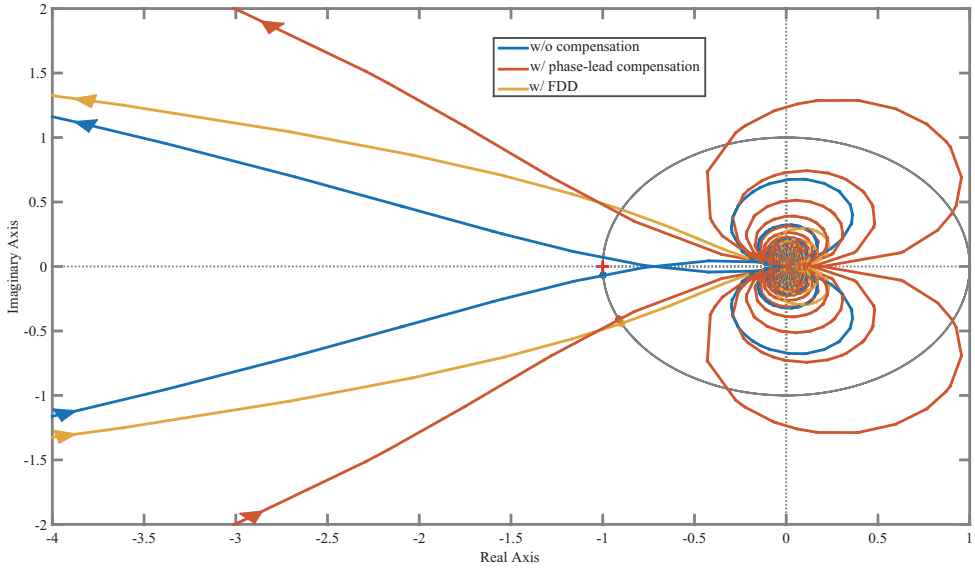

Fig. 3-11: Nyquist plot of the differential modal space.

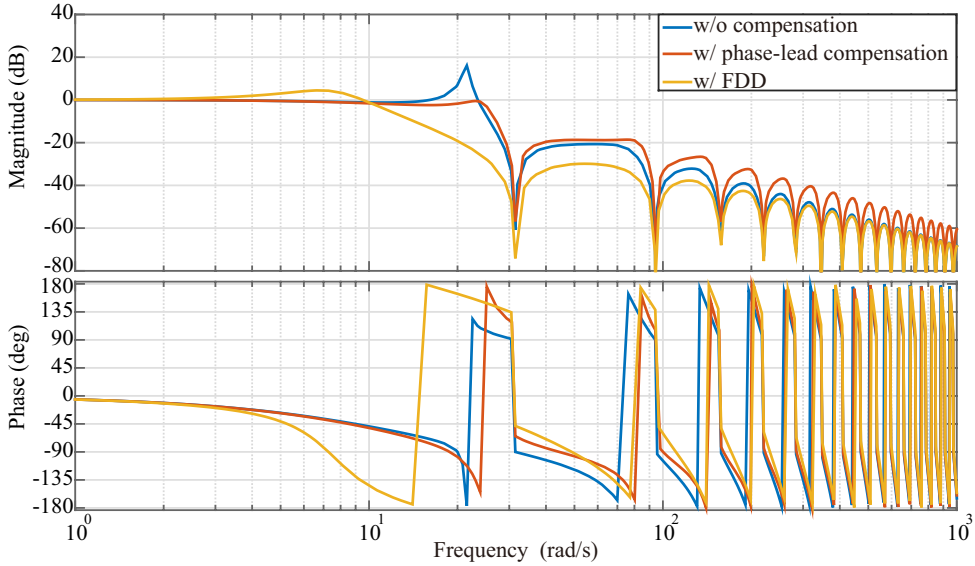

Fig. 3-12: Closed loop Bode diagram for the differential modal space.

At first, P_{f} is designed to attenuate the mode space interference. Since P_{f} is serially connected to C_{f}, it is easy to say these terms determine the equivalent mass of the system [88]. In order not to enlarge the operational force in low-frequency area that human operates where the cut-off frequency is defined as 3 Hz in this paper, the gain and cut-off frequency of P_{f} is determined as shown in Table 3.2. The effect of P_{f} is shown in Fig. 3-10. The gain of the force differential mode coming inside the position differential

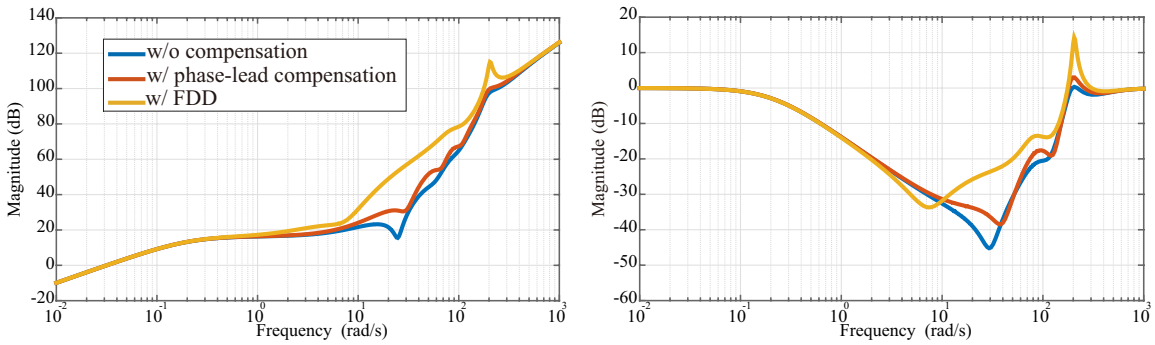

(a) Operationality. (b) Reproducibility.

Fig. 3-13: Operationality and reproducibility.

mode is attenuated by the use of P_{f}.

At next, the parameters of P_{p} are designed so as to have same phase margin in the open loop transfer function of the differential modal space. Nyquist plot of the transfer function of the differential mode in each method is shown in Fig. 3-11. The phase margin value of the phase-lead compensator method is 24.1 rad, while FDD method has 26.2 rad margin. The parameters of each method are shown in Table 3.2. The difference of each method appears in the closed-loop characteristics of the differential mode, which is shown in Fig. 3-12. It is easy to say that the bandwidth that simultaneity property is achieved is wider in the proposed method than in the conventional method.

The operationality and reproducibility are compared between the three methods which are shown in Fig. 3-13. The impedance of an environment is assumed as $Z_{\mathrm{e}} = 100000 + 100s$. The results show that the proposed method has better performance in operational force in all frequency and the reproducibility has the same performance within 10 rad/s.

3.5 Experiments

In this section, some experiments are conducted to verify the validity of the proposed method.

3.5.1 Experimental Setup

Three motions, that are free motion and contact motion operated by an input motor, and free and contact motion operated by human are compared between the conventional method and the proposed method. System 1 is assumed as the master system, and system 2 is assumed as the slave system. In the first motion, both 1 Hz and 2 Hz input was applied to the system. As for the first two motions, two

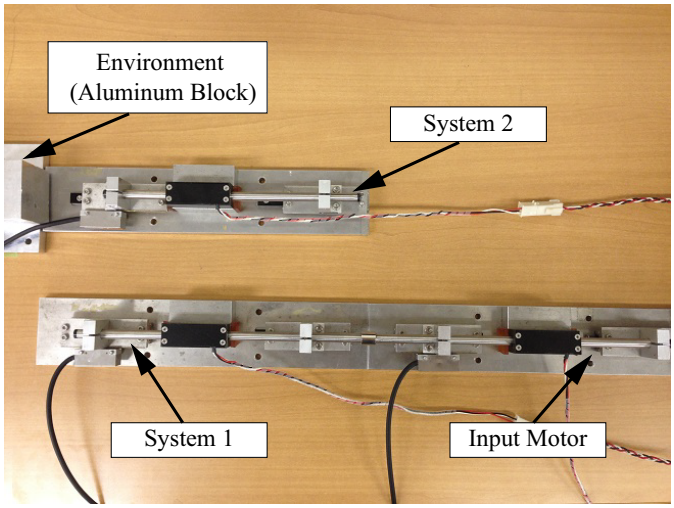

Fig. 3-14: Experimental setup.

situations where $T = \hat{T} = 100$ ms and $T = 120$ ms $\neq \hat{T}$ are assumed. An aluminum block is chosen as the environment for contact motion. Experimental parameters are the one shown in Tables 3.1 and 3.2, and the experimental setup is shown in Fig. 3-14.

3.5.2 Free Motion Results

Fig. 3-15 shows the free motion results when the actual delay time is the same as the modeled delay time. The tracking errors are the almost the same between the two methods. However, the phase delay is larger in FDD method, which is because of the position tracking bandwidth, as shown in Fig. 3-12. The amplitude of the sinusoidal wave is larger in the proposed method because the operational force is smaller than the conventional method. Fig. 3-16 shows the results when the actual delay time is different from the modeled delay time. The tracking error in both inputs is smaller in the proposed method compared to the amplitude that the system was operated. From the experiments, it can be said that the proposed method is superior to the conventional method in operational force and position tracking perspective.

3.5.3 Contact Motion Results

At next, contact motion is compared in Fig. 3-17. In both situations, a settling time of position and force errors was shorter in the proposed method than the conventional method. This is mainly because the operational force is small and position tracking performance is better in the proposed method. The faster the errors converge, the better it is for the tactile sensation transmission point of view.

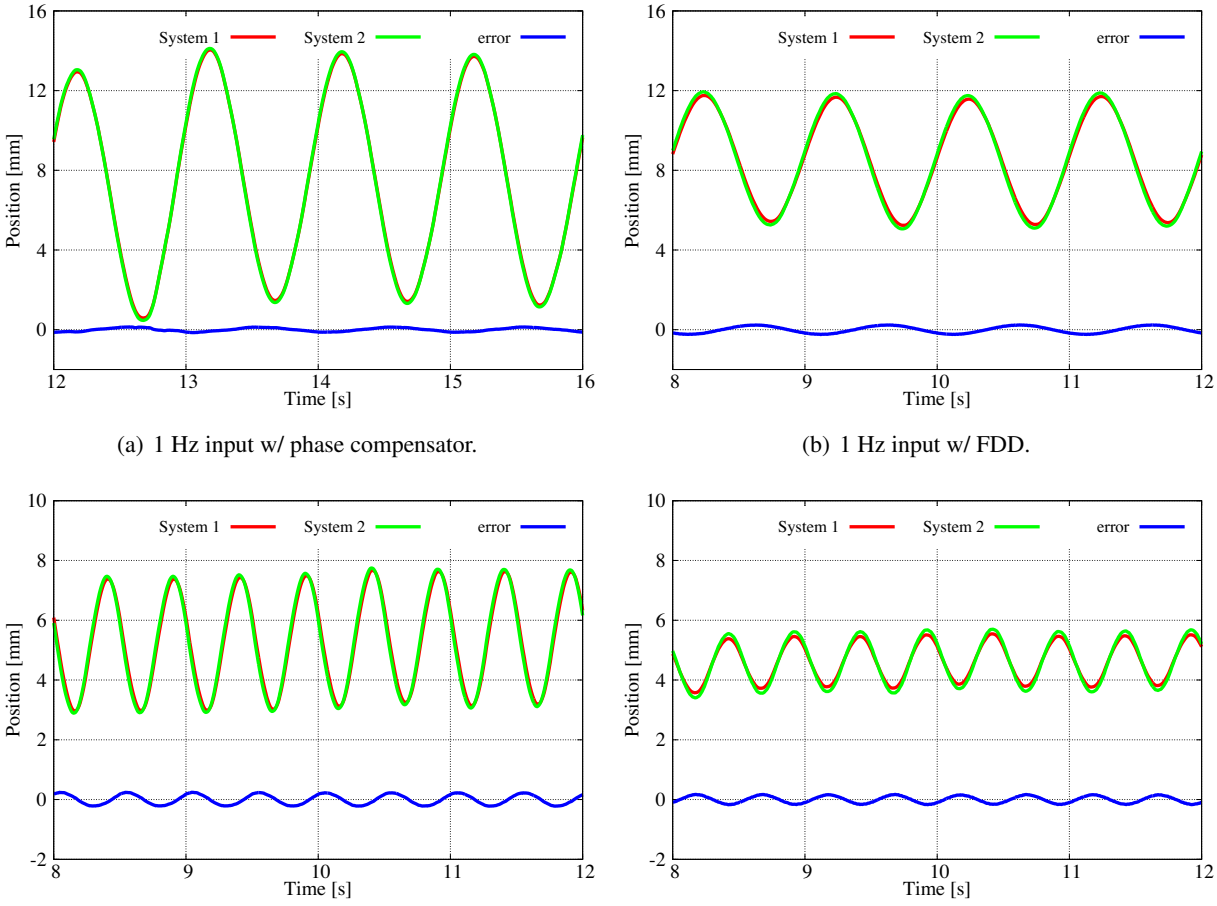

(a) 1 Hz input w/ phase compensator.

(b) 1 Hz input w/ FDD.

(c) 2 Hz input w/ phase compensator.

(d) 2 Hz input w/ FDD.

Fig. 3-15: Free motion results when $T = 100$ ms.

While the position error convergence is fast in the proposed method compared to the conventional method, the overshoot in the transient response became large. This is due to the small operational force. As shown in Fig. 3-13(a), the operational force is smaller than that of the conventional method, which makes the position error large during the transient response.

3.5.4 Experimental Results with Jitter

At last, the results that the system was operated by human are shown in Figs. 3-18, and 3-19. This case considered the jitter effect, where T randomly varied between 120 and 130 ms. Both methods could realize stable contact motion while the proposed method had smaller position error compared to the conventional method.

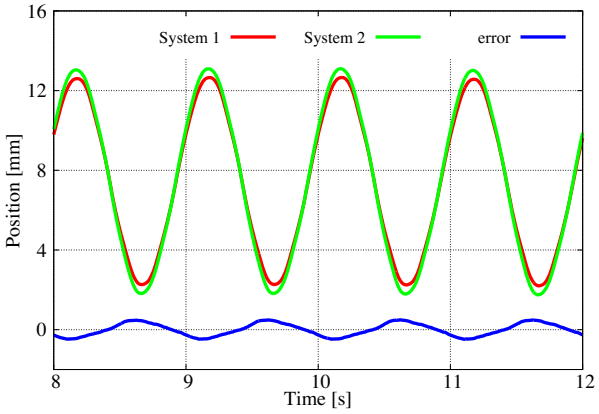

(a) 1 Hz input w/ phase compensator.

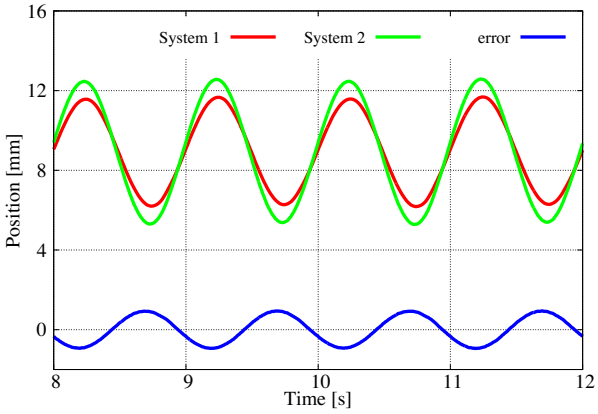

(b) 1 Hz input w/ FDD.

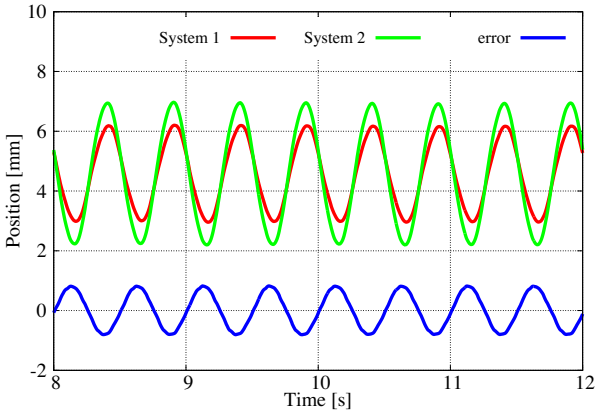

(c) 2 Hz input w/ phase compensator.

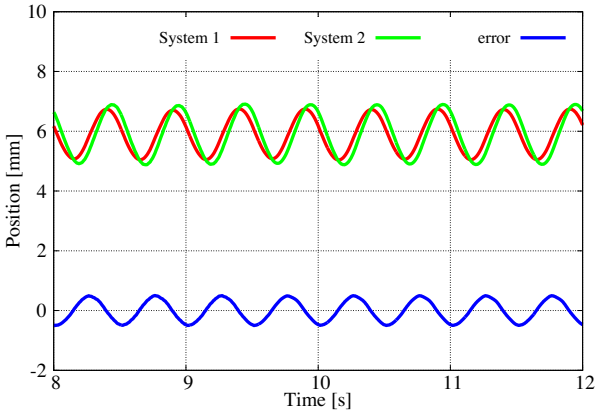

(d) 2 Hz input w/ FDD.

Fig. 3-16: Free motion results when $T = 120$ ms.

From the experiments, it is confirmed that the operational force and position tracking performance of the proposed method were superior to the conventional method.

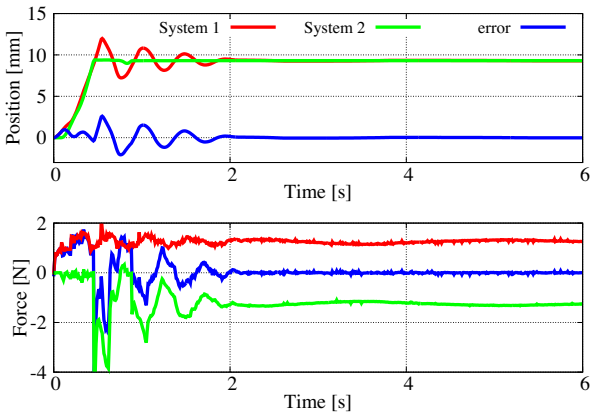

(a) w/ phase compensator when $T = 100$ ms.

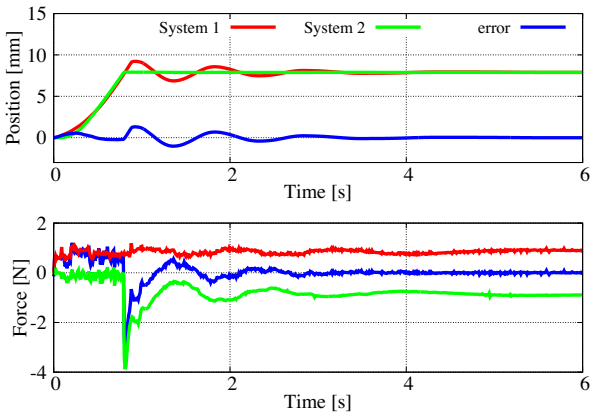

(b) w/ FDD when $T = 100$ ms.

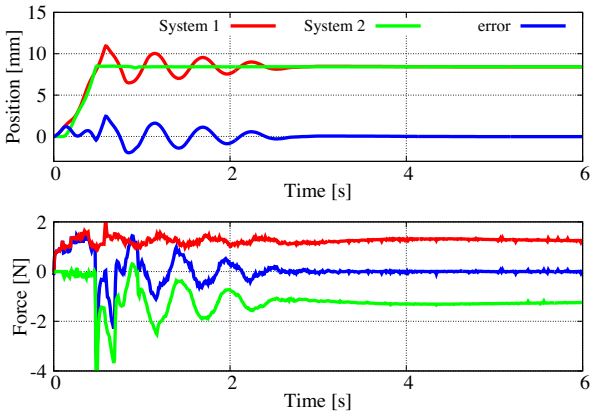

(c) w/ phase compensator when $T = 120$ ms.

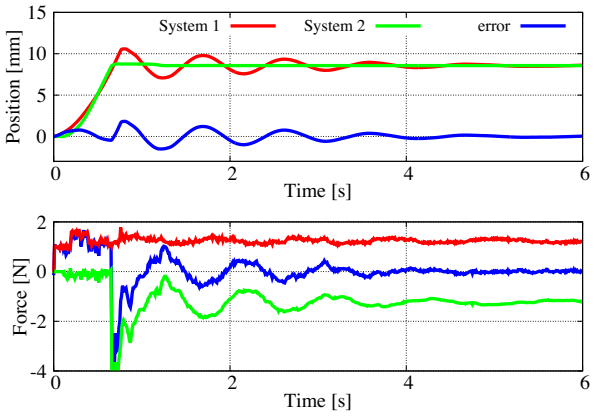

(d) w/ FDD when $T = 120$ ms.

Fig. 3-17: Contact motion results.

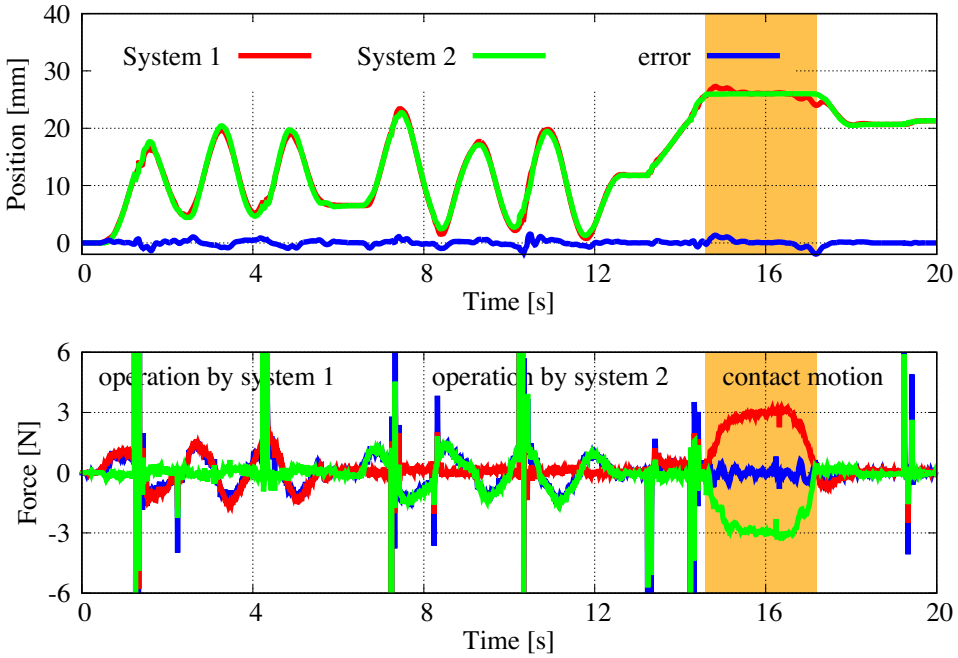

Fig. 3-18: Human operation result using phase compensator.

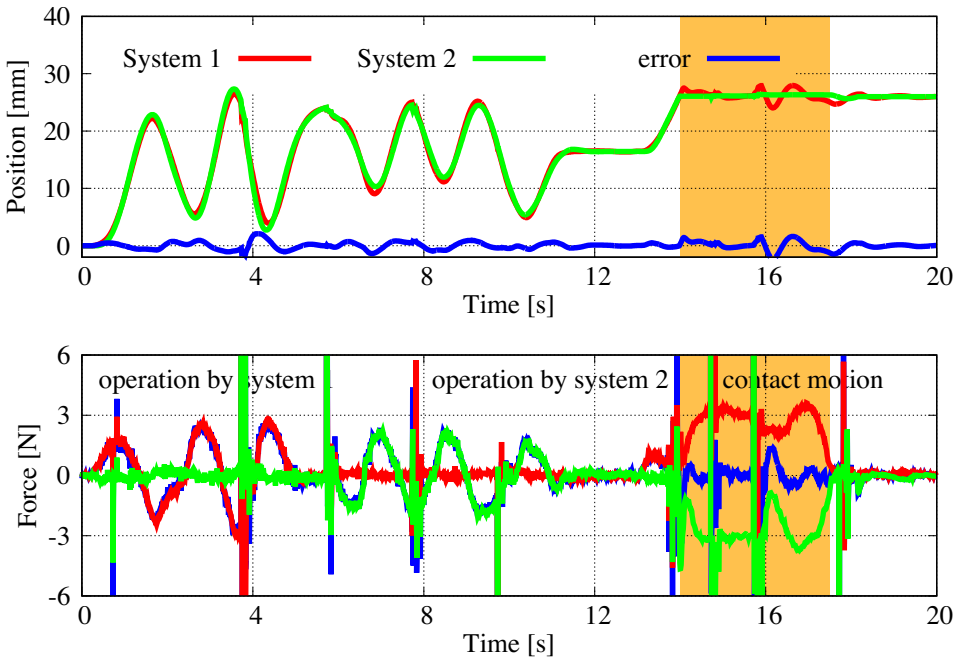

Fig. 3-19: Human operation result using FDD.

3.6 Summary of Chapter 3

In this chapter, force response in bilateral teleoperation was modified to change the connectivity of the COG motion. Firstly, this chapter described the problem in bilateral teleoperation. It was revealed that the number of the mode defined to control was exceeding the number of the controllable mode. In order to eliminate the interference, the connectivity for the COG motion was designed so that the COG motion does not affect to relative motion. It was realized by inserting the artificial buffer to the force response of their own system. Consequently, the force controller does not affect the motion of the relative motion when there is no modeling error. The effect of the modeling error was analyzed using the fundamental matrix, the effect of the error was attenuated by using phase compensation controllers to both position and force controllers. Finally, experimental results showed that the proposed method could realize synchronized motion.

Chapter 4

Integrated Design of COG/Relative Motion in Bilateral/Multilateral Teleoperation

---

This chapter proposes the integrated design of connectivity for both COG and relative motions in bilateral and multilateral teleoperation systems. It will be the extension of Chapter 2 and 3. The concept of modal transformation is extended in network systems in this chapter. The modal space is defined along the delay time between the systems. It shows that the modal transformation matrix and the inverse transformation matrix illustrates how to route the information to other systems.

4.1 Introduction of Chapter 4

The contents of this chapter are given as follows. In Section 4.2, connectivity design for bilateral teleoperation is proposed. The performance of the proposed method is analyzed in Section 4.3. Then, the number of the agents are extended to realize the motion decoupled control in multilateral teleoperation in Section 4.4. The topology is assumed to be fully connected in this section. Experiments are conducted to show the validity of the proposed method. Section 4.5 concludes the chapter.

4.2 Integrated Connectivity Design for Bilateral Teleoperation

4.2.1 Bilateral Teleoperation Based on Modal Transformation

In the previous chapter, bilateral control using the modal transformation matrix was introduced. By inserting a selection matrix $\boldsymbol{S}$, (3.10) can be rewritten as

$$\begin{aligned}\ddot{\boldsymbol{x}}^{\mathrm{ref}} &= -\boldsymbol{Q}_2^{-1}\left(C_{\mathrm{f}}\boldsymbol{S}_{\mathrm{f}}\boldsymbol{Q}\boldsymbol{f} + C_{\mathrm{p}}\boldsymbol{S}_{\mathrm{p}}\boldsymbol{Q}\boldsymbol{x}\right)\\ &= -C_{\mathrm{f}}\boldsymbol{Q}_2^{-1}\boldsymbol{S}_{\mathrm{f}}\boldsymbol{Q}\boldsymbol{f} - C_{\mathrm{p}}\boldsymbol{Q}_2^{-1}\boldsymbol{S}_{\mathrm{p}}\boldsymbol{Q}\boldsymbol{x},\end{aligned} \tag{4.1}$$

where

$$\boldsymbol{S}_{\mathrm{f}} = \begin{bmatrix} 1 & 0 \\ 0 & 0 \end{bmatrix}, \boldsymbol{S}_{\mathrm{p}} = \begin{bmatrix} 0 & 0 \\ 0 & 1 \end{bmatrix}. \tag{4.2}$$

As it is obvious, the determinant of each connectivity matrix becomes 0 because the determinant of $\boldsymbol{S}_{\mathrm{f}}$ and $\boldsymbol{S}_{\mathrm{p}}$ is 0. It means that if it is possible to derive the modal transformation matrix for network control systems, then the motion defined by the transformation matrix will be decoupled. Then, the problem becomes how the define the modal transformation matrix in the network systems.

In Chapter 2, it was revealed that there are two ways to design the connectivity. From the design, the COG motion was able to regain the double integrator characteristics. In order to realize complete motion decoupling in network systems when the number of the system is two, at least the relative motion must be decoupled from the COG motion. Therefore, one of the solutions that will be obtained will have (2.37).

By solving the corresponding common mode vector for the relative motion connectivity matrices proposed in Chapter 2, it is able to derive the coordinate transformation matrix that completely decouples both motions. By using the fundamental characteristics that are shown in Chapter 2, a vector ${\boldsymbol{w}_1^{\mathrm{CD1}}}^T$ that is orthogonal to the relative motions can be derived. By solving the left eigenvectors of $\boldsymbol{\mathcal{L}}_{\mathrm{p2}}^{\mathrm{CD1}}$,

$${\boldsymbol{w}_1^{\mathrm{CD1}}}^T = \begin{bmatrix} 1 & e^{-T_{12}s} \end{bmatrix}, \tag{4.3}$$

$${\boldsymbol{w}_2^{\mathrm{CD1}}}^T = \begin{bmatrix} -e^{-T_{21}s} & 1 \end{bmatrix}. \tag{4.4}$$

The left eigenvector ${\boldsymbol{w}_1^{\mathrm{CD1}}}^T$ is orthogonal to the left eigenvector ${\boldsymbol{w}_2^{\mathrm{CD1}}}^T$ because of the fundamental characteristics of a matrix.

Therefore, the obtained modal transformation matrix is given as

$$\boldsymbol{\mathcal{Q}}^{\mathrm{CD1}} = \begin{bmatrix} 1 & e^{-T_{12}s} \\ -e^{-T_{21}s} & 1 \end{bmatrix}. \tag{4.5}$$

Based on the obtained modal transformation matrix, the acceleration reference is obtained as

$$\begin{aligned}\begin{bmatrix} \ddot{x}_1^{\mathrm{ref}} \\ \ddot{x}_2^{\mathrm{ref}} \end{bmatrix} = &- \frac{1}{\det(\boldsymbol{\mathcal{Q}}^{\mathrm{CD1}})} C_{\mathrm{f}} \begin{bmatrix} 1 & e^{-T_{12}s} \\ e^{-T_{21}s} & e^{-(T_{12}+T_{21})s} \end{bmatrix} \begin{bmatrix} f_1 \\ f_2 \end{bmatrix} \\ &- \frac{1}{\det(\boldsymbol{\mathcal{Q}}^{\mathrm{CD1}})} C_{\mathrm{p}} \begin{bmatrix} e^{-(T_{12}+T_{12})s} & -e^{-T_{12}s} \\ -e^{-T_{21}s} & 1 \end{bmatrix} \begin{bmatrix} x_1 \\ x_2 \end{bmatrix}. \end{aligned} \tag{4.6}$$

The determinant of both connectivity matrix becomes 0; therefore, it can be said that the modal transformation matrix for COG and relative motion decoupling was derived. The same procedure can be used to obtain the solution for type 2. In this case, the modal transformation matrix that the relative motion connectivity matrix is expressed as (2.41) is obtained. Solving the left eigenvectors of $\boldsymbol{\mathcal{L}}_{\mathrm{p2}}^{\mathrm{CD2}}$ gives

$$\boldsymbol{w}_1^{\mathrm{CD2}T} = \begin{bmatrix} e^{-T_{21}s} & e^{-T_{12}s} \end{bmatrix}, \tag{4.7}$$

$$\boldsymbol{w}_2^{\mathrm{CD2}T} = \begin{bmatrix} -1 & 1 \end{bmatrix}, \tag{4.8}$$

and the modal transformation matrix is obtained as

$$\boldsymbol{\mathcal{Q}}^{\mathrm{CD2}} = \begin{bmatrix} e^{-T_{21}s} & e^{-T_{12}s} \\ -1 & 1 \end{bmatrix}. \tag{4.9}$$

The acceleration reference is obtained as

$$\begin{aligned}\begin{bmatrix} \ddot{x}_1^{\mathrm{ref}} \\ \ddot{x}_2^{\mathrm{ref}} \end{bmatrix} = &- \frac{1}{\det(\boldsymbol{\mathcal{Q}}^{\mathrm{CD2}})} C_{\mathrm{f}} \begin{bmatrix} e^{-T_{12}s} & e^{-T_{12}s} \\ e^{-T_{21}s} & e^{-T_{21}s} \end{bmatrix} \begin{bmatrix} f_1 \\ f_2 \end{bmatrix} \\ &- \frac{1}{\det(\boldsymbol{\mathcal{Q}}^{\mathrm{CD2}})} C_{\mathrm{p}} \begin{bmatrix} e^{-T_{21}s} & -e^{-T_{12}s} \\ -e^{-T_{21}s} & e^{-T_{12}s} \end{bmatrix} \begin{bmatrix} x_1 \\ x_2 \end{bmatrix}. \end{aligned} \tag{4.10}$$

It is obvious that both matrices have 0 as the determinant. It shows that if $T_{12} = T_{21}$, the connectivity matrix for the force response is the same as the one in Chapter 3.

This subsection obtained for the modal transformation matrix that satisfies the connectivity that was proposed in Chapter 2. The inverse determinant includes requiring future value of position and force response, which is impossible to obtain. Therefore, in this dissertation, the delay element in the determinant of the proposed modal transformation is implemented as 1 for the simplicity. Final acceleration references for each system using $\boldsymbol{\mathcal{Q}}^{\mathrm{CD1}}$ are derived as

$$\begin{aligned}\begin{bmatrix} \ddot{x}_1^{\mathrm{ref}} \\ \ddot{x}_2^{\mathrm{ref}} \end{bmatrix} = &- \frac{1}{2} C_{\mathrm{f}} \begin{bmatrix} 1 & e^{-T_{12}s} \\ e^{-T_{21}s} & e^{-(T_{12}+T_{21})s} \end{bmatrix} \begin{bmatrix} f_1 \\ f_2 \end{bmatrix} - \frac{1}{2} C_{\mathrm{p}} \begin{bmatrix} e^{-(T_{12}+T_{12})s} & -e^{-T_{12}s} \\ -e^{-T_{21}s} & 1 \end{bmatrix} \begin{bmatrix} x_1 \\ x_2 \end{bmatrix}. \end{aligned} \tag{4.11}$$

The equation indicates that the relative motion is controlled in system 2 which is the same result in Chapter 2. As for the COG motion, it is controlled in system 1. The references generated at each system

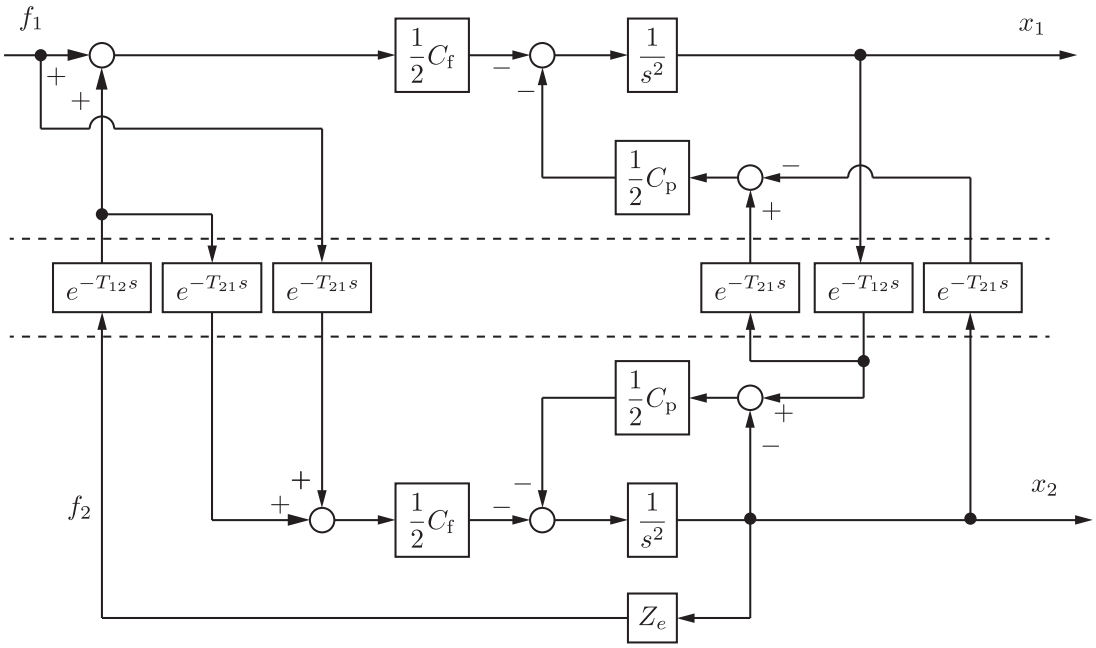

Fig. 4-1: Block diagram of the proposed bilateral teleoperation using $\mathcal{Q}^{\mathrm{CD1}}$.

is transmitted to the other system to realize the 4ch structure. The important point is that it is required to control each motion at each system. The corresponding block diagram is shown in Fig. 4-1. Z_e stands for an impedance of an environment. The figure shows that the control system does not require the model of a delay time, while the control structure is asymmetric.

The other acceleration references using $\mathcal{Q}^{\mathrm{CD2}}$ are calculated as

$$\begin{bmatrix} \ddot{x}_1^{\mathrm{ref}} \\ \ddot{x}_2^{\mathrm{ref}} \end{bmatrix} = -\frac{1}{2}C_{\mathrm{f}} \begin{bmatrix} e^{-\hat{T}_{12}s} & e^{-T_{12}s} \\ e^{-T_{21}s} & e^{-\hat{T}_{21}s} \end{bmatrix} \begin{bmatrix} f_1 \\ f_2 \end{bmatrix} - \frac{1}{2}C_{\mathrm{p}} \begin{bmatrix} e^{-\hat{T}_{21}s} & -e^{-T_{12}s} \\ -e^{-T_{21}s} & e^{-\hat{T}_{12}s} \end{bmatrix} \begin{bmatrix} x_1 \\ x_2 \end{bmatrix}. \tag{4.12}$$

and the block diagram is shown in Fig. 4-2. The structure requires to control both motions at each system. It can also be seen by the fact that the block diagram shown in Fig. 2-7 cannot be modified to the similar structure of Fig. 2-11. Both diagram shows the relative motion connectivity for both bilateral teleoperation systems. The relative motion controller is separately placed in Fig. 2-7, meaning that controllers are required at each system. The bilateral teleoperation using $\mathcal{Q}^{\mathrm{CD2}}$ requires delay time model, however, the structure is symmetric.

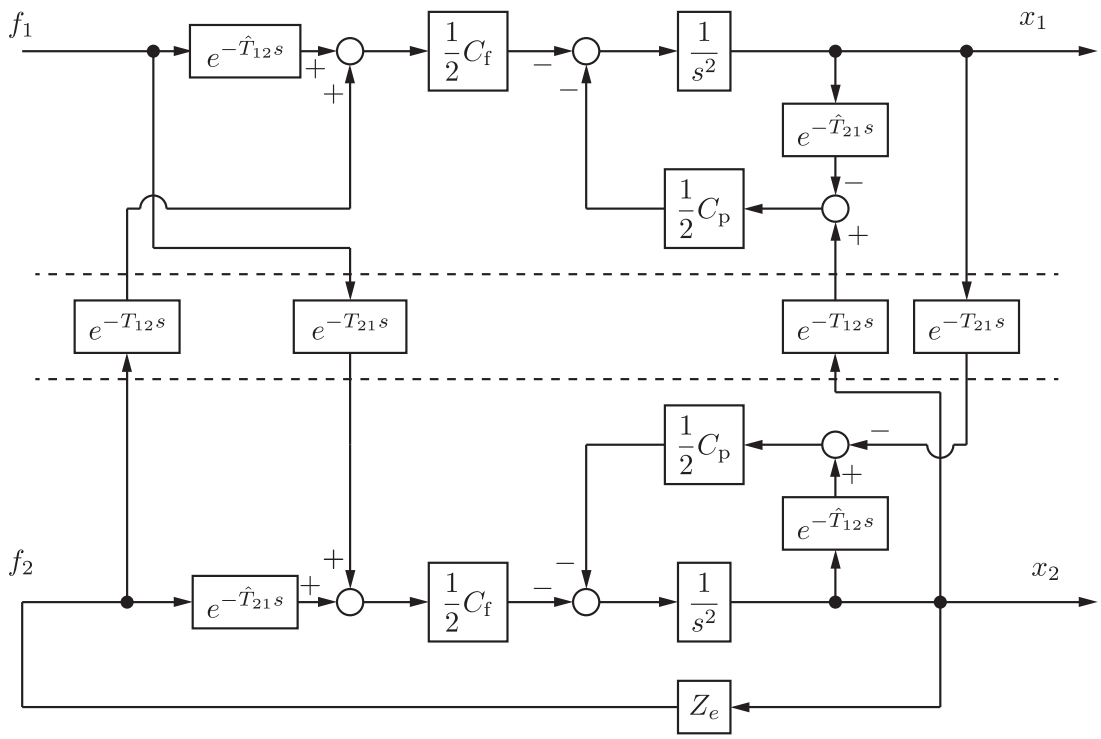

Fig. 4-2: Block diagram of the proposed bilateral teleoperation using $\boldsymbol{\mathcal{Q}}^{\mathrm{CD2}}$.

4.2.2 Controller Design in Modal Space

This subsection shows the controller design method based on modal transformation. At first, the values in motor space are transformed to the modal space by the defined transformation matrices.

The acceleration reference in the modal space using the modal transformation $\boldsymbol{\mathcal{Q}}^{\mathrm{CD}i}$ is obtained as

$$\ddot{\boldsymbol{x}}_m^{\mathrm{ref}} = -\frac{1}{2}\det(\boldsymbol{\mathcal{Q}}^{\mathrm{CD}i})C_\mathrm{f}\boldsymbol{S}\boldsymbol{f}_m - \frac{1}{2}\det(\boldsymbol{\mathcal{Q}}^{\mathrm{CD}i})C_\mathrm{p}(\boldsymbol{I}-\boldsymbol{S})\boldsymbol{x}_m, \tag{4.13}$$

where the subscript $_m$ stands for the value of the modal space. Assume the impedance of human as Z_h. Then the impedance matrix $\boldsymbol{Z}$ will be transformed as

$$\boldsymbol{Z}_m = \boldsymbol{\mathcal{Q}}^{\mathrm{CD}i}\boldsymbol{Z}\boldsymbol{\mathcal{Q}}_\mathrm{n}^{\mathrm{CD}i\,-1}, \tag{4.14}$$

in the modal space where $\boldsymbol{\mathcal{Q}}_\mathrm{n}^{\mathrm{CD}i\,-1} = \det(\boldsymbol{\mathcal{Q}}^{\mathrm{CD1}})\cdot\boldsymbol{\mathcal{Q}}^{\mathrm{CD}i\,-1}$. The block diagrams of the modal space is given in Figs. 4-3 and 4-4. In Fig. 4-3, the cut-off frequency of RFOB is also expressed. Z_{11}^i and Z_{12}^i are the elements of $\boldsymbol{Z}_m$.

It is obvious that each mode is decoupled, consequently, the role of the controllers are uniquely determined. The controller gains and the cut-off frequency of RFOB is determined to fulfill the stability of

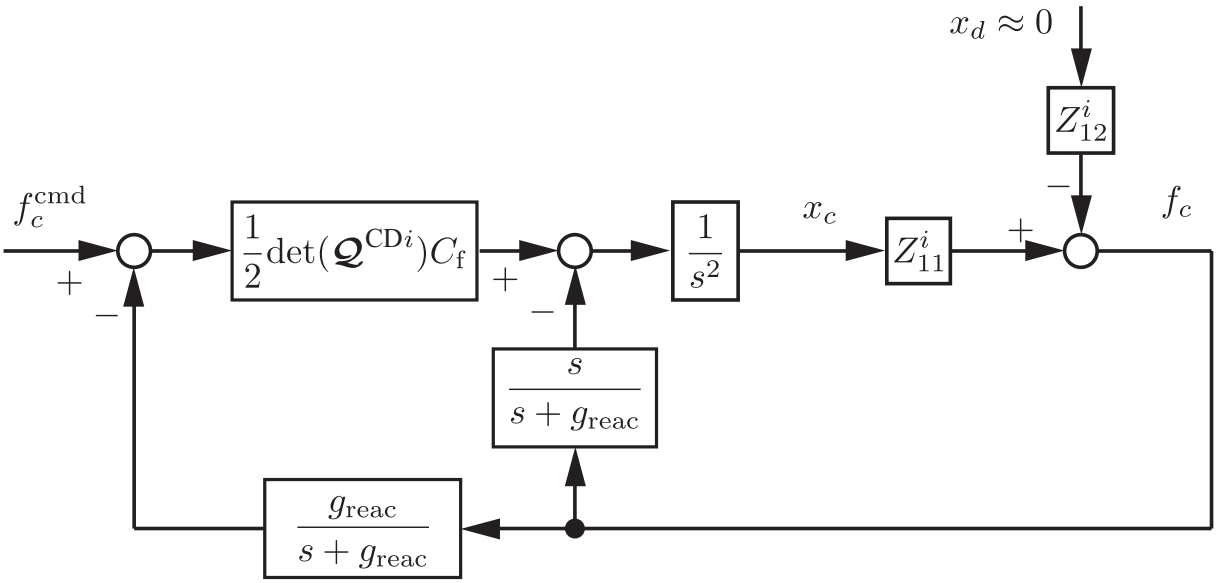

Fig. 4-3: Block diagram of the proposed COG mode.

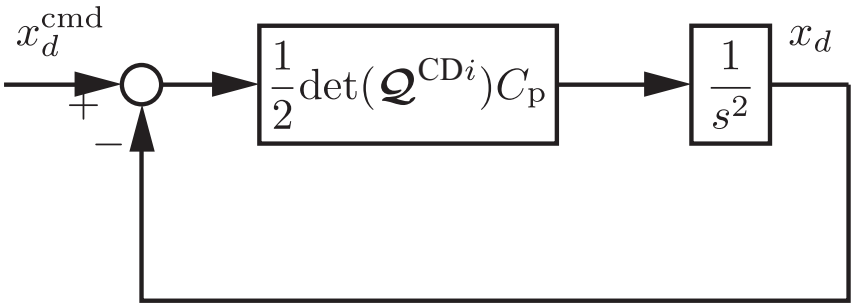

Fig. 4-4: Block diagram of the proposed relative mode.

each controller.

4.3 Performance Analysis

4.3.1 Overall Characteristic of the Control Structures

At first, overall characteristic of both control systems when cut-off frequencies of a disturbance observer and a reaction force observer are large enough to be regarded as infinite are expressed. In order to analyze the performance of bilateral teleoperation, a notation based on the fundamental matrix is often used. The fundamental matrix for the conventional bilateral teleoperation is calculated as

Table 4.1: Control parameters for $\boldsymbol{\mathcal{Q}}^{\mathrm{CD1}}$.

Parameter	Description	Value
$T_{12},\ T_{21}$	Delay time	75 ms
K_{p}	Proportional gain for position control	100.0
K_{d}	Differential gain for position control	20.0
C_{f}	Proportional gain for force control	0.5
g_{dis}	Cut-off frequency of DOB	1200.0 rad/s
g_{reac}	Cut-off frequency of RFOB	1200.0 rad/s

Table 4.2: Control parameters for $\boldsymbol{\mathcal{Q}}^{\mathrm{CD2}}$.

Parameter	Description	Value
$T_{12},\ T_{21}$	Delay time	75 ms
K_{p}	Proportional gain for position control	81.0
K_{d}	Differential gain for position control	18.0
C_{f}	Proportional gain for force control	0.3
g_{dis}	Cut-off frequency of DOB	250.0 rad/s
g_{reac}	Cut-off frequency of RFOB	250.0 rad/s

$$\begin{bmatrix} f_1 \\ x_1 \end{bmatrix} = \begin{bmatrix} F_{11} & F_{12} \\ F_{21} & F_{22} \end{bmatrix} \begin{bmatrix} x_2 \\ f_2 \end{bmatrix} \tag{4.15}$$

$$\begin{cases} F_{11} = -\dfrac{(2s^2 + C_{\mathrm{p}})^2 - e^{-T_{\mathrm{rtt}}s}{C_{\mathrm{p}}}^2}{2e^{-T_{21}s}C_{\mathrm{f}}(s^2 + C_{\mathrm{p}})} \\ F_{12} = -F_{21} = -\dfrac{2s^2 + (1 + e^{-T_{\mathrm{rtt}}s})C_{\mathrm{p}}}{2e^{-T_{21}s}(s^2 + C_{\mathrm{p}})} \\ F_{22} = \dfrac{(1 - e^{-T_{\mathrm{rtt}}s})C_{\mathrm{f}}}{2e^{-T_{21}s}(s^2 + C_{\mathrm{p}})} \end{cases}, \tag{4.16}$$

where T_{rtt} stands for the round trip delay time. It is obvious that position and force controllers are interfering with each other, and this is because the role of each controller is not decoupled. The fundamental matrices for the proposed methods are given as

$$\boldsymbol{F}_1 = \begin{bmatrix} -\dfrac{2s^2}{e^{-T_{21}s}C_{\mathrm{f}}} & -\dfrac{1}{e^{-T_{21}s}} \\ e^{-T_{12}s} & 0 \end{bmatrix}, \tag{4.17}$$

$$\boldsymbol{F}_2 = \begin{bmatrix} -\dfrac{2s^2}{e^{-T_{21}s}C_{\mathrm{f}}} & -e^{-(T_{12}-T_{21})s} \\ 1 & 0 \end{bmatrix}. \tag{4.18}$$

Each element of the fundamental matrix is compared in Fig. 4-5. As for the comparison, bilateral teleoperation without compensation and 3ch bilateral teleoperation are also plotted [57]. Control parameters

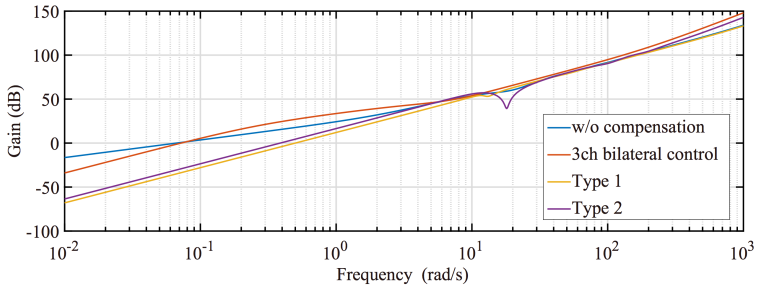

(a) F_{11}

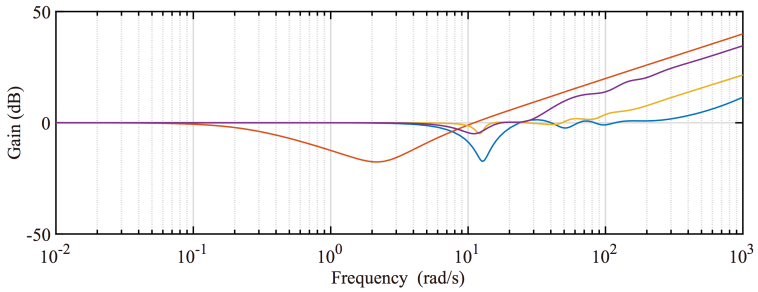

(b) F_{12}

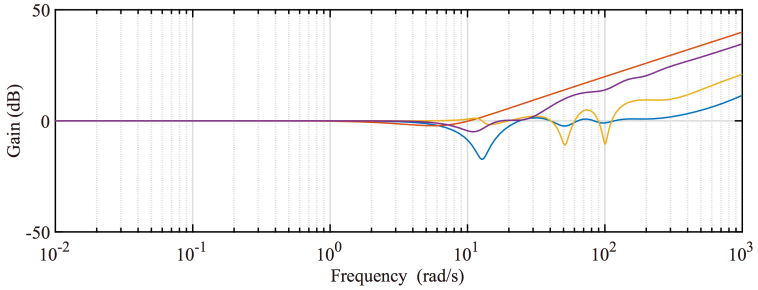

(c) F_{21}

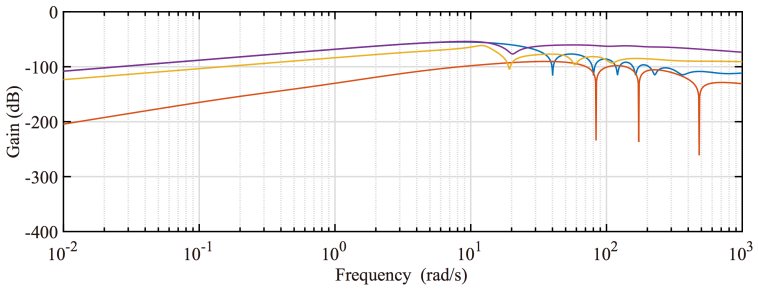

(d) F_{22}

Fig. 4-5: Parameters of $\boldsymbol{F}$ matrix.

of both methods are tuned so that the representative pole of every method are almost placed in the same place. 3ch bilateral control is famous for its small operational force performance; however, it is also

known that stable contact to a hard environment is difficult in the control structure. In order to realize stable contact motion, force gain was set low, consequently enlarging the operational force. The validity of the introduced methods are shown especially in Fig.4-5 (a). Both methods have smaller operational force compared with the rest of the methods. The reason for type 2 ($\boldsymbol{\mathcal{Q}}^{\mathrm{CD2}}$) bilateral teleoperation having little larger operational force is due to stability improvement by lowering the force gain.

Transfer functions when contacting an environment show the characteristics of each proposed method. The transfer functions of the control structure based on $\boldsymbol{\mathcal{Q}}^{\mathrm{CD1}}$ when operating from system 1 and 2 are respectively shown as

$$x_1 = \frac{C_{\mathrm{f}}}{2s^2 + e^{-T_{\mathrm{rtt}}s} Z_e C_{\mathrm{f}}} f_1, \tag{4.19}$$

$$x_2 = \frac{e^{-T_{\mathrm{rtt}}s} C_{\mathrm{f}}}{2s^2 + Z_e C_{\mathrm{f}}} f_2. \tag{4.20}$$

The biggest merit of the control system is that there is no delay element in the denominator when operating from the system 2. It indicates that the stability of the contact motion is not affected by the delay element, which can realize wide-band tactile transmission performance. When contacting to a soft object, the operator should operate system 1, while the operator is suitable to operate system 2 when contacting to a hard object. On the other hand, the transfer functions of the control structure based on $\boldsymbol{\mathcal{Q}}^{\mathrm{CD2}}$ are given as

$$x_1 = \frac{e^{-T_{21}s} C_{\mathrm{f}}}{2s^2 + e^{-T_{12}s} Z_e C_{\mathrm{f}}} f_1, \tag{4.21}$$

$$x_2 = \frac{e^{-T_{12}s} C_{\mathrm{f}}}{2s^2 + e^{-T_{21}s} Z_e C_{\mathrm{f}}} f_2. \tag{4.22}$$

The denominators in both transfer functions are similar to each other, which means that even stability of the contact motion is affected by the delay element, the control performance is almost the same regardless of the system to operate. The control structure is suitable for a situation where there is a possibility that a human operates from both systems.

Performance characteristics of bilateral teleoperation can be analyzed through operationality and reproducibility, which is defined as

$$f_1 = \frac{F_{11} + F_{12} Z_e}{F_{21} + F_{22} Z_e} x_1 \tag{4.23}$$

$$= \left(\frac{F_{11}}{F_{21} + F_{22} Z_e} + \frac{F_{12}}{F_{21} + F_{22} Z_e} Z_e \right) x_1 \tag{4.24}$$

$$= (P_o + P_r Z_e) x_1, \tag{4.25}$$

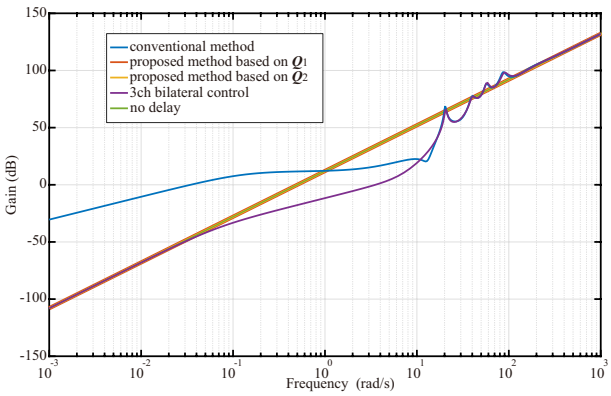

Fig. 4-6: Operationality.

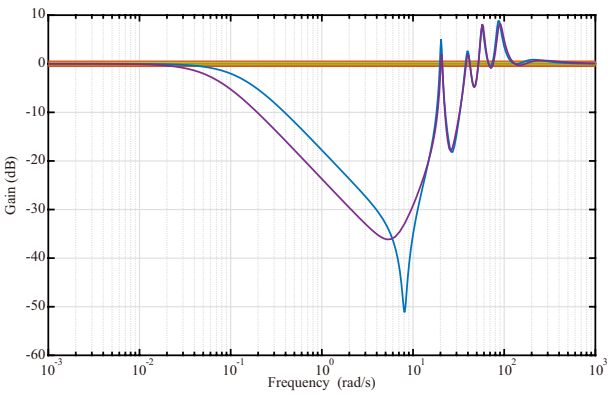

Fig. 4-7: Reproducibility.

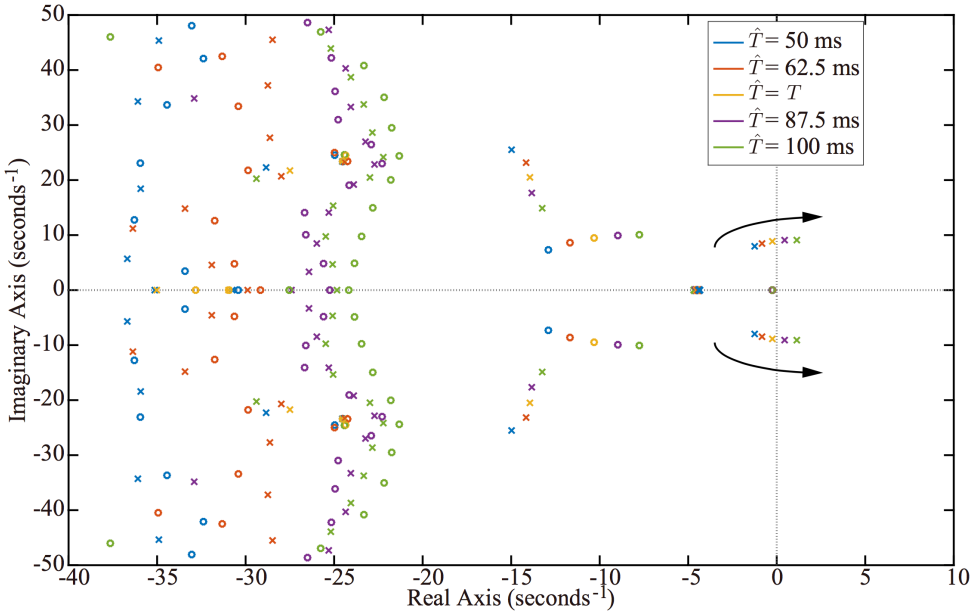

Fig. 4-8: Pole zero placement of $\mathcal{Q}^{\mathrm{CD2}}$ bilateral teleoperation in case of delay time modeling error.

where P_o and P_r stand for operationality and reproducibility, respectively. The Bode diagrams for both indices are given in Figs. 4-6 and 4-7. The parameters are set as , $T_{12} = 0.05$ s, $T_{21} = 0.1$ s, $C_{\mathrm{p}} = 100 + 20s$, $C_{\mathrm{f}} = 0.5$, $Z_e = 10000 + 10s$, respectively. The proposed methods are compared with the conventional method and 3ch bilateral control [57]. The results show the proposed methods have the best performance in both operationality and reproducibility. It indicates that the performance is same as bilateral control without time delay.

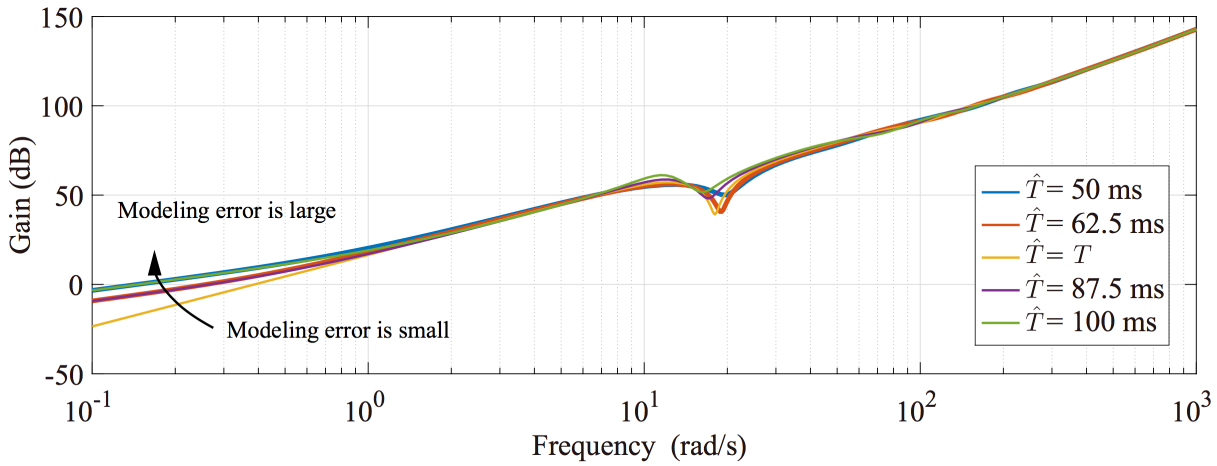

Fig. 4-9: F_{11} in case of modeling error.

4.3.2 Effect of Modeling Error

Bilateral teleoperation with $\mathcal{Q}^{\mathrm{CD2}}$ requires a delay time model in each system. Pole-zero placement in case of modeling error in delay time is shown in Fig. 4-8. Actual delay time was set as 75 ms. The results show that the bigger delay time model is, the more unstable the system will become. Therefore, if the delay time varies, the model of the delay time should be set at the smaller value. Effect of modeling error in operational force performance is shown in Fig. 4-9.

4.4 Integrated Connectivity Design for Fully Connected Multilateral Teleoperation

This section explains the proposed method for mode decoupled multilateral teleoperation. In multilateral teleoperation, the topology is assumed to be fully connected; therefore, in the following, fully connected link is assumed. The topology is shown in Fig. 4-10.

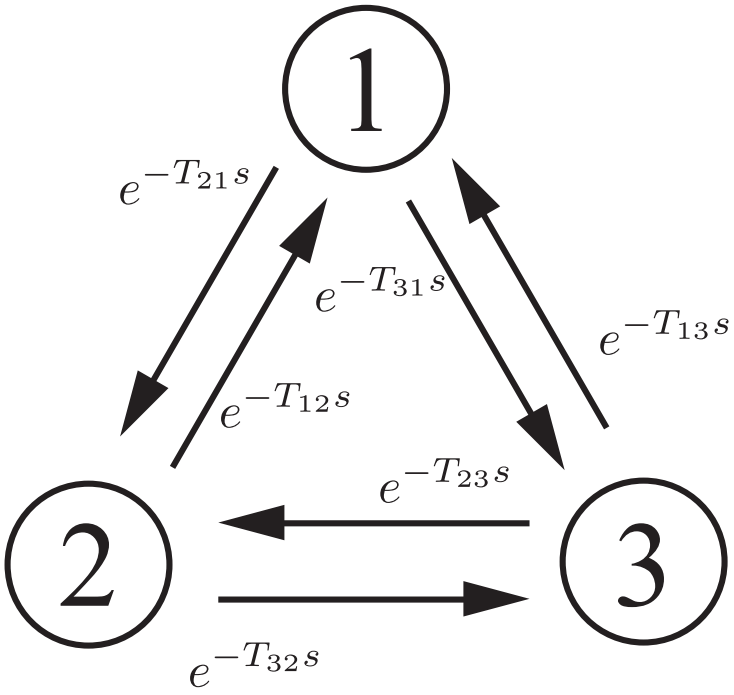

Fig. 4-10: Topology between the systems and its delay time.

The acceleration reference in the conventional multilateral teleoperation is written as

$$\begin{aligned}
\begin{bmatrix} \ddot{x}_1^{\mathrm{ref}} \\ \ddot{x}_2^{\mathrm{ref}} \\ \ddot{x}_3^{\mathrm{ref}} \end{bmatrix} &= -\frac{1}{3}\begin{bmatrix} C_{\mathrm{f}}(f_1 + e^{-T_{12}s}f_2 + e^{-T_{13}s}f_3) + C_{\mathrm{p}}(2x_1 - e^{-T_{12}s}x_2 - e^{-T_{13}s}x_3) \\ C_{\mathrm{f}}(e^{-T_{21}s}f_1 + f_2 + e^{-T_{23}s}f_3) + C_{\mathrm{p}}(-e^{-T_{21}s}x_1 + 2x_2 - e^{-T_{23}s}x_3) \\ C_{\mathrm{f}}(e^{-T_{31}s}f_1 + e^{-T_{32}s}f_2 + f_3) + C_{\mathrm{p}}(-e^{-T_{31}s}x_1 - e^{-T_{32}s}x_2 + 2x_3) \end{bmatrix} \\
&= -\frac{1}{3}C_{\mathrm{f}}\begin{bmatrix} 1 & e^{-T_{12}s} & e^{-T_{13}s} \\ e^{-T_{21}s} & 1 & e^{-T_{23}s} \\ e^{-T_{31}s} & e^{-T_{32}s} & 1 \end{bmatrix}\begin{bmatrix} f_1 \\ f_2 \\ f_3 \end{bmatrix} \\
&\quad -\frac{1}{3}C_{\mathrm{p}}\begin{bmatrix} 2 & -e^{-T_{12}s} & -e^{-T_{13}s} \\ -e^{-T_{21}s} & 2 & -e^{-T_{23}s} \\ -e^{-T_{31}s} & -e^{-T_{32}s} & 2 \end{bmatrix}\begin{bmatrix} x_1 \\ x_2 \\ x_3 \end{bmatrix}. \qquad (4.26)
\end{aligned}$$

It shows that the determinant of each connectivity matrix is not 0, meaning that the controller interference occurs.

In the following, system 2 and 3 are assumed as a master system while the slave system is defined as system 1. All of the communication paths are required to be used to construct motion decoupled multilateral teleoperation.

As the previous parts show, there are two ways to realize motion decoupled teleoperation systems. The first type divides the role of the system to control each motion, while the second type requires to control each motion at both systems. Therefore, the same thing can be said in multilateral teleoperation: when

making each system control one motion, the structure becomes asymmetric and it becomes symmetric if every system tries to control every motion in each system. Based on this fact, the first proposed motion decoupling matrix $\mathcal{Q}_3^{\mathrm{CD1}}$ is defined in the following:

$$\mathcal{Q}_3^{\mathrm{CD1}} = \begin{bmatrix} 1 & e^{-T_{12}s} & e^{-T_{13}s} \\ -e^{-T_{21}s} & 2 & -e^{-T_{23}s} \\ -e^{-T_{31}s} & -e^{-T_{32}s} & 2 \end{bmatrix}. \tag{4.27}$$

Control goals in the first proposed multilateral teleoperation system are modified into

$$f_1 + e^{-T_{12}s} f_2 + e^{-T_{13}s} f_3 = 0, \tag{4.28}$$

$$-e^{-T_{21}s} x_1 + 2x_2 - e^{-T_{23}s} x_3 = 0, \tag{4.29}$$

$$-e^{-T_{31}s} x_1 - e^{-T_{32}s} x_2 + 2x_3 = 0. \tag{4.30}$$

As for the second matrix, it is given as

$$\mathcal{Q}_3^{\mathrm{CD2}} = \begin{bmatrix} e^{-(T_{12}+T_{13})s} & e^{-(T_{21}+T_{23})s} & e^{-(T_{31}+T_{32})s} \\ -1 & 2 & -1 \\ -1 & -1 & 2 \end{bmatrix}. \tag{4.31}$$

Control goals for the second proposed system are given as

$$e^{-(T_{12}+T_{13})s} f_1 + e^{-(T_{21}+T_{23})s} f_2 + e^{-(T_{31}+T_{32})s} f_3 = 0, \tag{4.32}$$

$$-x_1 + 2x_2 - x_3 = 0, \tag{4.33}$$

$$-x_1 - x_2 + 2x_3 = 0. \tag{4.34}$$

However, as it was obvious in bilateral teleoperation, the stability margin in the symmetric type structure when contacting to a hard object is limited compared to the asymmetric structure, the explanation of $\mathcal{Q}_3^{\mathrm{CD2}}$ is omitted.

In the following, how to generate the matrix is explained. Most important part in designing the mode is the definition of the COG motion [89]. External force is used to control the COG motion and the previous section showed that it is required to gather all of the force responses to one system to generate the acceleration reference for controlling the COG mode. Therefore, the COG mode in the proposed multilateral teleoperation is determined as

$$\boldsymbol{f}_c = \begin{bmatrix} 1 & e^{-T_{12}s} & e^{-T_{13}s} \end{bmatrix}. \tag{4.35}$$

It indicates that a force controller is placed at the slave system.

As for the relative modes, the two modes are determined based on the following theorem.

Theorem 2: In 3rd order motion decoupled multilateral teleoperation, a subsystem cannot have more than two controllers.

Proof. Consider the inverse transformation of the matrix. A coefficient of acceleration reference for the COG mode in subsystem 1 is given as

$$\det\boldsymbol{Q}_3(q_{22}q_{33} - q_{23}q_{32}), \tag{4.36}$$

where q_{ij} stands for the element in i th row and j th column of $\boldsymbol{Q}_3$. The element cannot be summarized by a delay element not to put a delay element as a coefficient of the slave system's force; therefore, either $q_{22}q_{33}$ or $q_{23}q_{32}$ cannot include a delay element. If a position controller is placed in subsystem 1 along with the force controller, at least one of the four elements q_{22}, q_{23}, q_{32}, and q_{33} will have a delay element. Thereupon, all of the combinations of the differential modes can be summarized by a delay element. It indicates that (4.36) will be summarized by a delay element. □

Based on *Theorem 2*, the position controllers must be placed in subsystems 2 and 3. Accordingly, the relative motions in the proposed multilateral teleoperation are defined as

$$\boldsymbol{x}_{d_1} = \begin{bmatrix} -e^{-T_{21}s} & 2 & -e^{-T_{23}s} \end{bmatrix} \tag{4.37}$$

$$\boldsymbol{x}_{d_2} = \begin{bmatrix} -e^{-T_{31}s} & -e^{-T_{32}s} & 2 \end{bmatrix}, \tag{4.38}$$

where $\boldsymbol{x}_{d_i}$ stands for the relative motion matrix.

$$\det(\boldsymbol{\mathcal{Q}}_3^{\mathrm{CD1}}) = \frac{1}{3}\left(4 - e^{-(T_{12}+T_{21})s} + 2e^{-(T_{23}+T_{32})s} + 2e^{-(T_{13}+T_{31})s} + e^{-(T_{12}+T_{23}+T_{31})s} + e^{-(T_{13}+T_{32}+T_{21})s}\right) \tag{4.39}$$

$$\boldsymbol{\mathcal{Q}}_3^{\mathrm{CD1}\,-1} = \frac{1}{\det(\boldsymbol{\mathcal{Q}}_3^{\mathrm{CD1}})} \begin{bmatrix} 4 - e^{-(T_{23}+T_{32})s} & -2e^{-T_{12}s} - e^{-(T_{13}+T_{32})s} & -2e^{-T_{13}s} - e^{-(T_{12}+T_{23})s} \\ 2e^{-T_{21}s} + e^{-(T_{23}+T_{31})s} & 2 + e^{-(T_{13}+T_{31})s} & e^{-T_{23}s} - e^{-(T_{23}+T_{31})s} \\ 2e^{-T_{31}s} + e^{-(T_{32}+T_{21})s} & -e^{-T_{32}s} + e^{-(T_{31}+T_{12})s} & 2 + e^{-(T_{12}+T_{21})s} \end{bmatrix} \tag{4.40}$$

The determinant and the inverse matrix of (4.27) are calculated as (4.39) and (4.40). It is required to implement the inverse of the determinant to fully realize the motion decoupling; however, it is quite

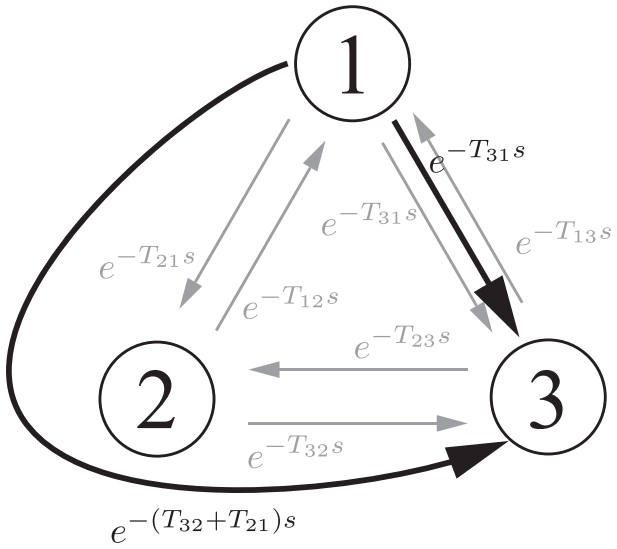

Fig. 4-11: Example of sending the acceleration reference from system 1 to system 3.

difficult to implement it because of the complexity of the term. Therefore, all of the delay times in (4.39) are modified into one so that the nominal inverse network quarry matrix is given as

$$\boldsymbol{\mathcal{Q}}_{3\mathrm{n}}^{\mathrm{CD1}\,-1} = \det(\boldsymbol{\mathcal{Q}}_{3}^{\mathrm{CD1}}) \cdot \boldsymbol{\mathcal{Q}}_{3}^{\mathrm{CD1}\,-1}, \tag{4.41}$$

where the subscript $_{\mathrm{n}}$ is the nominal value.

Acceleration references for each system are calculated by

$$\ddot{\boldsymbol{x}}^{\mathrm{ref}} = -C_{\mathrm{f}}\boldsymbol{\mathcal{Q}}_{3\mathrm{n}}^{\mathrm{CD1}\,-1}\boldsymbol{S}_{\mathrm{f}}\boldsymbol{\mathcal{Q}}_{3}^{\mathrm{CD1}}\boldsymbol{f} + C_{\mathrm{p}}\boldsymbol{\mathcal{Q}}_{3\mathrm{n}}^{\mathrm{CD1}\,-1}\boldsymbol{S}_{\mathrm{p}}\boldsymbol{\mathcal{Q}}_{3}^{\mathrm{CD1}}\boldsymbol{x}. \tag{4.42}$$

As same as the case in bilateral teleoperation, controllers are designed in the modal space. The acceleration reference in the modal space is given as

$$\ddot{\boldsymbol{x}}_{m}^{\mathrm{ref}} = -\frac{1}{3}\det(\boldsymbol{\mathcal{Q}}_{3}^{\mathrm{CD1}})C_{\mathrm{f}}\boldsymbol{S}_{\mathrm{f}}\boldsymbol{f}_{m} - \frac{1}{3}\det(\boldsymbol{\mathcal{Q}}_{3}^{\mathrm{CD1}})C_{\mathrm{p}}\boldsymbol{S}_{\mathrm{p}}\boldsymbol{x}_{m}, \tag{4.43}$$

Since the acceleration reference is the extension from the proposed bilateral teleoperation, the block diagram of the modal space becomes the same as the one shown in the previous section. Controller gains are determined based on the Nyquist plots of the mode spaces.

An example to send acceleration reference that is generated at one system to another system is shown in the following. Assume the case when sending the acceleration reference of the force controller generated at system 1 to system 3. q_{31}^{-1} in $\boldsymbol{\mathcal{Q}}_{3\mathrm{n}}^{\mathrm{CD1}\,-1}$ which is $2e^{-T_{31}s} + e^{-(T_{32}+T_{21})s}$ shows how to send the

value, and Fig. 4-11 shows the flow of sending the reference. There exist two paths to send the response, one that directly sends from system 3 to system1 and the other one that goes through system 2 to send to system 1. It means that it does not require a delay time model to send back the acceleration reference. The same thing can be said to every case except generating the acceleration reference of the own system. q_{11}^{-1}, q_{22}^{-1}, and q_{33}^{-1} in $\boldsymbol{\mathcal{Q}}_{3\mathrm{n}}^{\mathrm{CD1}^{-1}}$ indicate how to send the reference generated at the own system. All of the three elements includes a round trip delay time between the other systems. It can be implemented only when a delay time model is used in each system. It does not require any delay time model when sending the position and force responses to calculate the reference values. Therefore, the proposed method requires only the round trip delay time as a delay time model when implementing.

Since the modal spaces are decoupled, the response of the relative motion mode does not affect to the COG mode. The relationship between force and position values are given as

$$\begin{bmatrix} f_1 & x_2 & x_3 \end{bmatrix}^T = \boldsymbol{F} \begin{bmatrix} x_1 & f_2 & f_3 \end{bmatrix}^T$$

$$\boldsymbol{F} = \begin{bmatrix} \dfrac{C_{\mathrm{f}} s^2}{e^{-(T_{13}+T_{31})s}} & -\dfrac{e^{-T_{12}s}}{e^{-T_{31}s}} & -\dfrac{1}{e^{-T_{31}s}} \\ \dfrac{e^{-(T_{12}+T_{21})s} + 2e^{-T_{13}s}}{e^{-(T_{13}+T_{31})s} + 2e^{-T_{23}s}} & 0 & 0 \\ \dfrac{4 - e^{-(T_{23}+T_{32})s}}{e^{-(T_{13}+T_{31})s} + 2e^{-T_{23}s}} & 0 & 0 \end{bmatrix}. \tag{4.44}$$

As shown in (4.44), the proposed method is free from the interference because F_{22}, F_{23}, F_{32}, and F_{33}, which show the interference term, is 0. As for the fully connected topology, this method can be extended to n number multilateral teleoperation.

4.5 Experiments

4.5.1 Experimental Setup for Bilateral Teleoperation

The following section experimentally analyzes the two structures in bilateral teleoperation. The experimental parameters are the same values as shown in Tables 4.1 and 4.2. Input motor was used for applying an external force, and all of the systems was a one-DOF system. The experimental setup is the same that is shown in Chapter 3. In order to have the same condition with the theoretical analysis, T_{12} and T_{21} are the same, meaning that the system with $\boldsymbol{\mathcal{Q}}^{\mathrm{CD2}}$ becomes pure symmetric structure. Therefore, operation from system 2 using $\boldsymbol{\mathcal{Q}}^{\mathrm{CD2}}$ is not conducted. Free motion, contact motion to a high stiff environment (aluminum block) are compared respectively between the bilateral teleoperation without

compensation and the two structures. Experimental parameters for the bilateral teleoperation without compensation are same as bilateral teleoperation using $\mathcal{Q}^{\mathrm{CD1}}$. In the following, the system using $\mathcal{Q}^{\mathrm{CD1}}$ is listed as type 1, and the system using $\mathcal{Q}^{\mathrm{CD2}}$ is named as type 2.

4.5.2 Experimental Results of Bilateral Teleoperation

At first, free motion results where same sinusoidal 0.5 Hz force was applied are shown in Fig. 4-12. The results show that both methods have smaller operational force than the one without compensation. Fig. 4-12(c) and (d) demonstrates that type 1 can be operated from both systems in the free motion. The results of Fig. 4-12(b) show that the amplitude of the position response is smaller compared to Fig. 4-12(c) and (d) and the position error is large. These are because the force gain is small and the bandwidth that robust acceleration control is realized is limited due to the stability problem in the contact motion. Bilateral teleoperation using $\mathcal{Q}^{\mathrm{CD2}}$ requires to have low cut-off frequency in DOB to achieve stable contact.

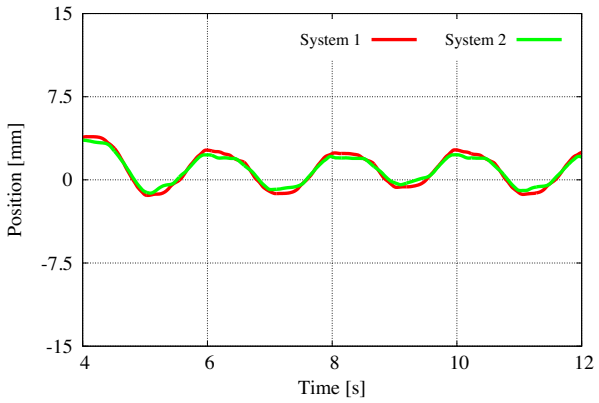

(a) w/o compensation.

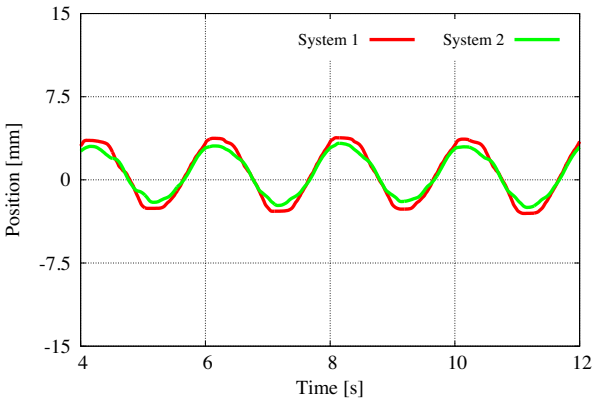

(b) type 2.

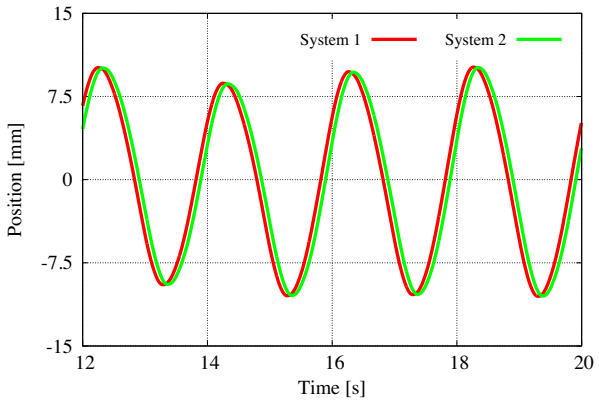

(c) type 1 (operation from system 1).

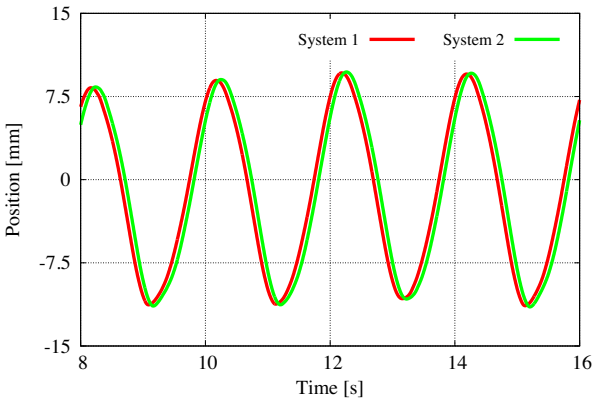

(d) type 1 (operation from system 2).

Fig. 4-12: Free motion results.

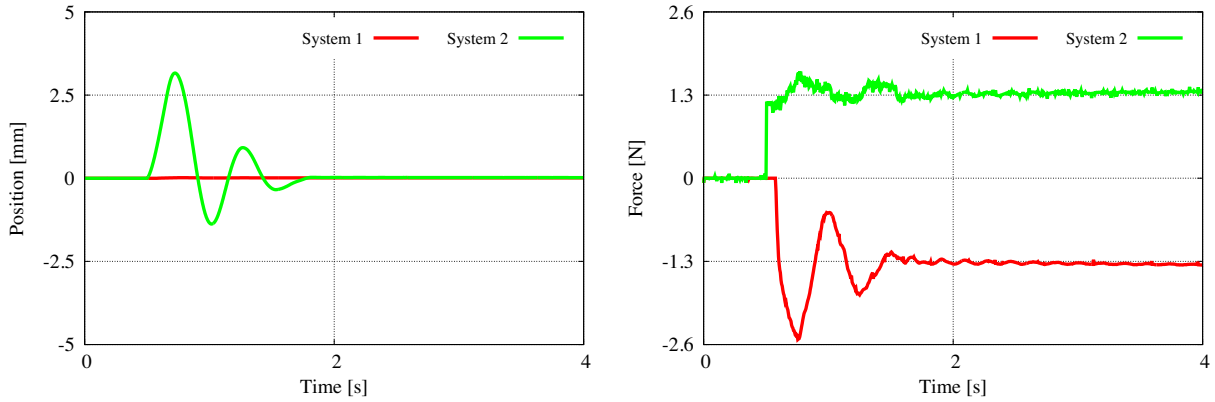

(a) Position response. (b) Force response.

Fig. 4-13: Contact motion results w/o compensation.

At next, experimental results for the contact motion are compared. The aluminum block was placed next to the system 1 so that the block was pushed without any reaching movement. The experimental results are shown in Figs. 4-13, 4-14, and 4-15. The result of type 1 operating from the system 2 has the best performance. When operating from the system 1, the contact motion becomes unstable. Since force gain is smaller in type 2 compared to other methods, the error convergence is relatively slow, though peak error was smaller compared to the system without compensation.

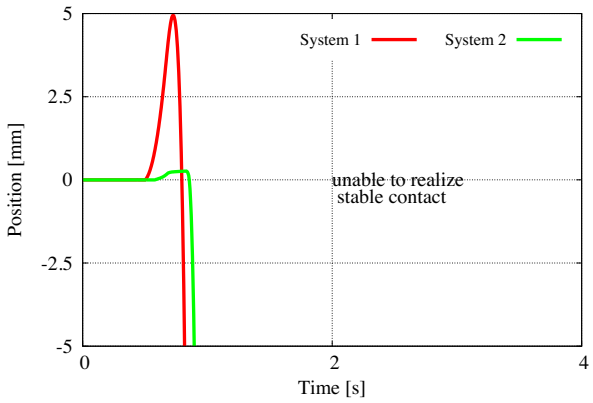

(a) Position response (operation from system 1).

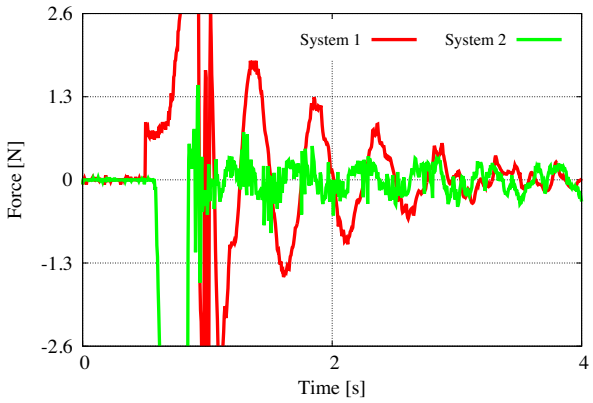

(b) Force response (operation from system 1).

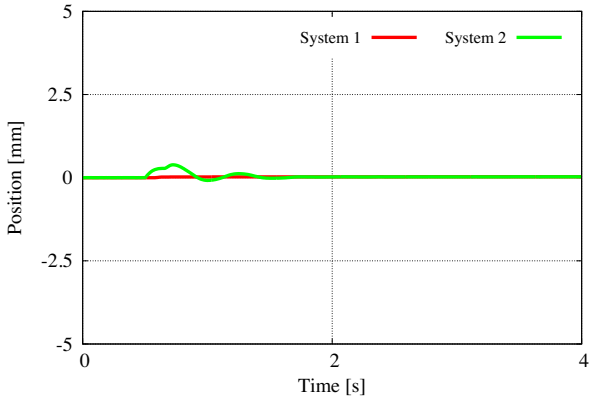

(c) Position response (operation from system 2).

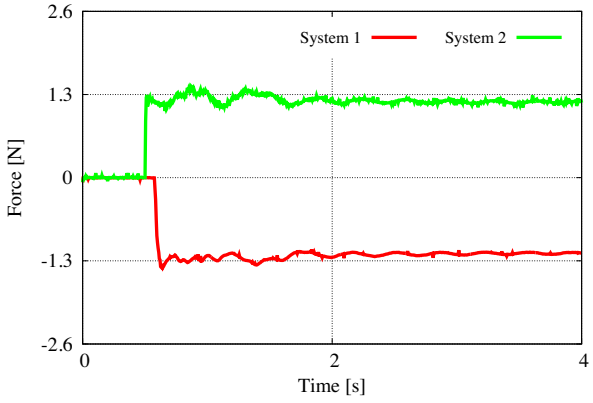

(d) Force response (operation from system 2).

Fig. 4-14: Contact motion results of type 1.

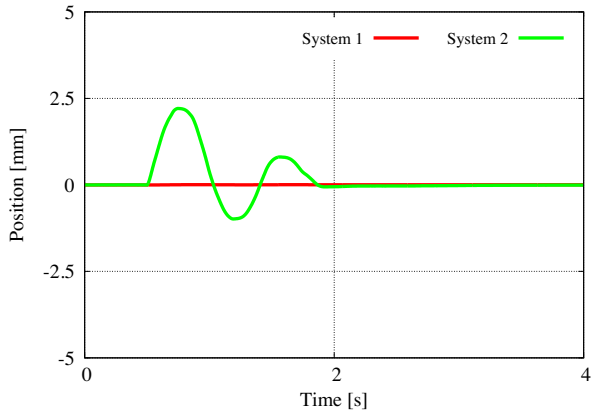

(a) Position response.

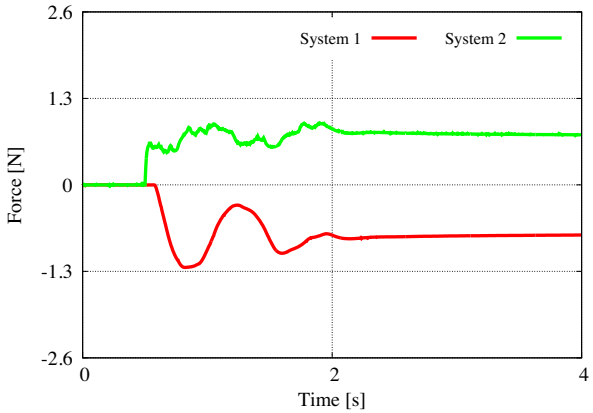

(b) Force response.

Fig. 4-15: Contact motion results of type 2.

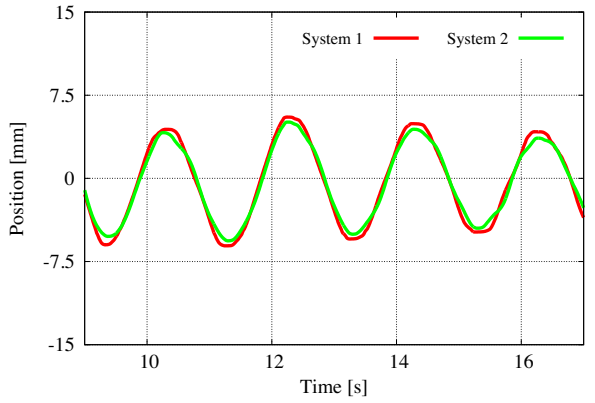

(a) When $\hat{T} = 100$ ms.

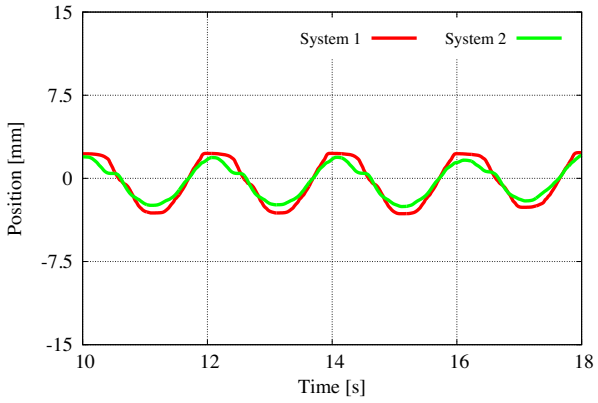

(b) When $\hat{T} = 50$ ms.

Fig. 4-16: Free motion results in case of modeling error.

The effect of modeling error was also experimentally analyzed. The reason for the operational force becoming smaller when delay time model is larger than the actual delay time is because of the stability issue. As for the contact motion, stable contact was realized when delay time model is smaller than the actual delay time. The result matches the analytical results of pole placement.

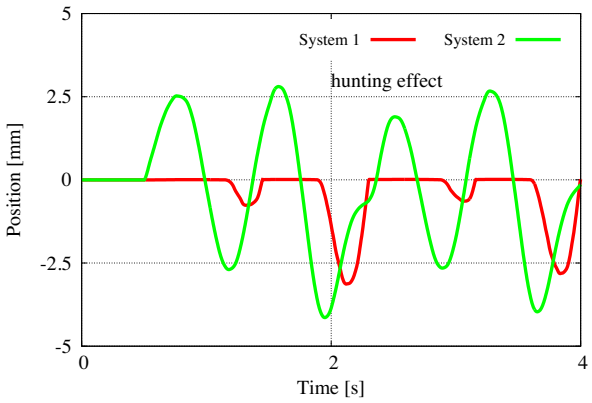

(a) Position response when $\hat{T} = 100$ ms.

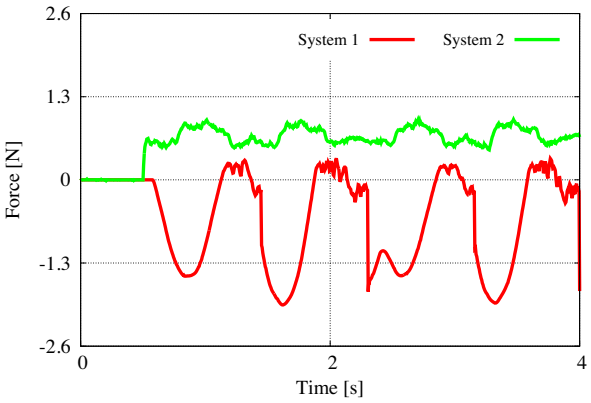

(b) Force response when $\hat{T} = 100$ ms.

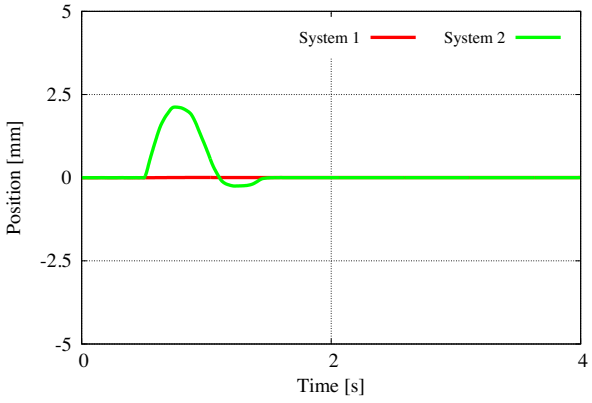

(c) Position response hen $\hat{T} = 50$ ms.

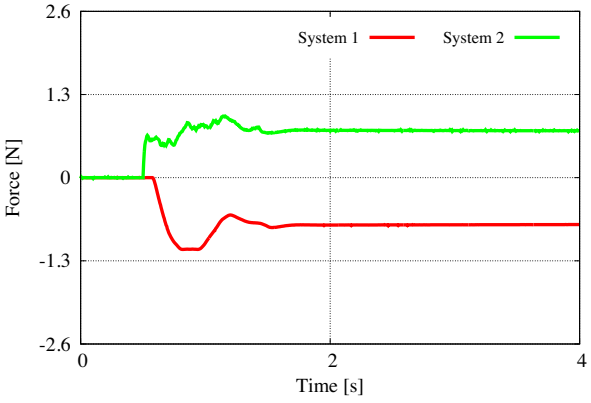

(d) Force response when $\hat{T} = 50$ ms.

Fig. 4-17: Contact motion results in case of modeling error.

Table 4.3: Experimental parameters for multilateral teleoperation.

Parameter	Description	Value
K_{p}	Proportional gain for position control	9.0
K_{d}	Differential gain for position control	6.0
$C_{\mathrm{f}}^{\mathrm{conv}}$	Proportional gain for force control (conv. method)	0.6
C_{f}	Proportional gain for force control	0.2
g_{dis}	Cut-off frequency of DOB	1500.0 rad/s
g_{reac}	Cut-off frequency of RFOB	1500.0 rad/s

4.5.3 Experimental Setup for Multilateral Teleoperation

Experimental parameters used in the experiments are shown in Table 4.3. Superscript $^{\mathrm{conv}}$ indicates the value of the conventional method. The values of parameters without any superscript represents same controller gain was used in every method. The force gain in the conventional method is 3 times larger than the proposed methods to imitate the role of the inverse quarry matrix.

As for the condition of the delay times, two situations are considered. In case 1, it is assumed that all of the delay time is the same as

$$T = 50 \text{ ms}, \tag{4.45}$$

and case 2 is the one that all of the delay time are different as shown as

$$T_{12} = 20 \text{ ms}, T_{21} = 60 \text{ ms}, T_{31} = 70 \text{ ms}, \tag{4.46}$$

$$T_{13} = 30 \text{ ms}, T_{23} = 60 \text{ ms}, T_{32} = 50 \text{ ms}. \tag{4.47}$$

4.5.4 Experimental Results for Multilateral Teleoperation in Case 1

At first, free motion results are shown in Figs. 4-18 and 4-19. 1 Hz sinusoidal wave was the input to the systems. Since same input was applied, force response was not shown in the results. In the conventional method, the amplitude of the position response is smaller than the proposed methods, and the position errors are large. This is due to the interference of the controllers, generating additional velocity constraint in the force control loop. Slight position errors in the proposed methods are due to the limitation of the position controller gains due to the modification of the determinants.

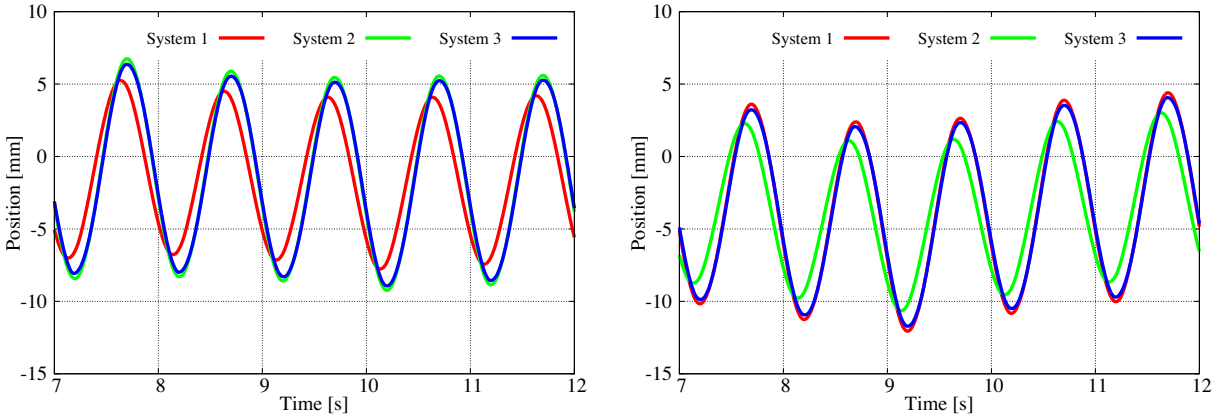

(a) Operation from system 1. (b) Operation from system 2.

Fig. 4-18: Free motion results of the conventional method in case 1.

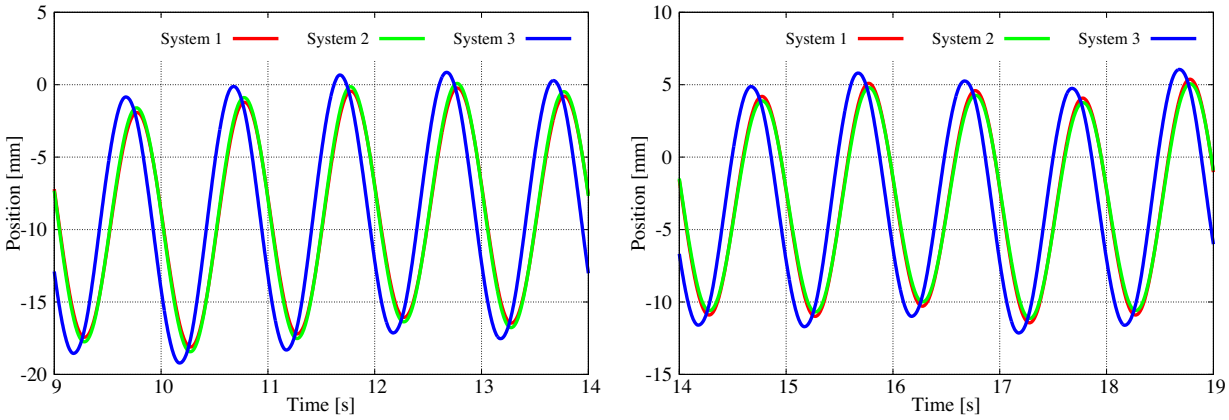

(a) Operation from system 1. (b) Operation from system 2.

Fig. 4-19: Free motion results of the proposed multilateral teleoperation in case 1.

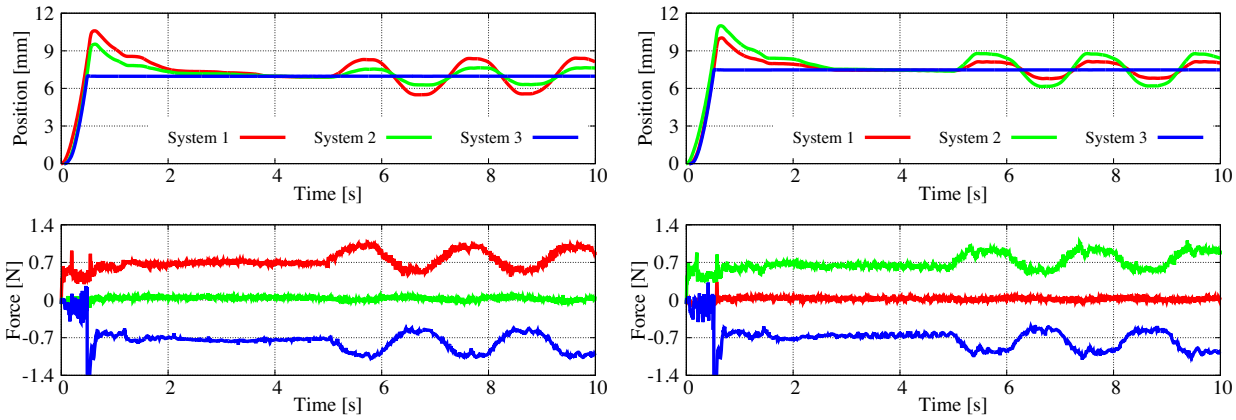

(a) Operation from system 1. (b) Operation from system 2.

Fig. 4-20: Contact motion results of the conventional method in case 1.

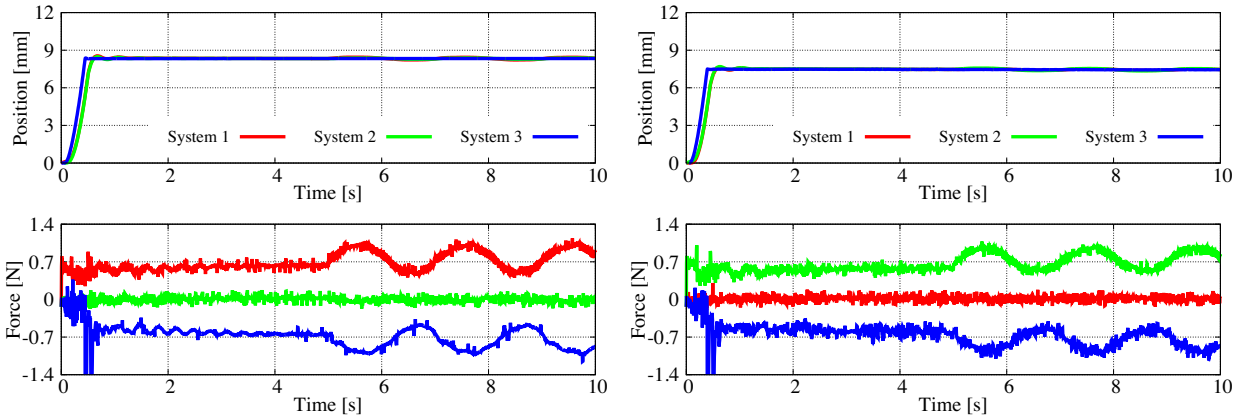

(a) Operation from system 1. (b) Operation from system 2.

Fig. 4-21: Contact motion results of the proposed multilateral teleoperation in case 1.

Contact motion results are shown in Figs. 4-20 and 4-21. Input was based on Sigmoid function to imitate the input of human, and after 4 s, 0.5 Hz sinusoidal wave input was additionally applied. In the contact motion, the cut-off frequencies of a disturbance observer and a reaction force observer were reduced to 150 rad/s for stable contact motion. In the conventional method, the error convergence in the position response is slow compared to the asymmetric multilateral teleoperation. The position error during push and pull motion was also large. As for the symmetric type multilateral teleoperation, both convergence speed and the position error during the push and pull motion was the largest. The is due to the limitation of the cut-off frequencies of the observers. The results of the proposed method showed the better performance than the conventional method.

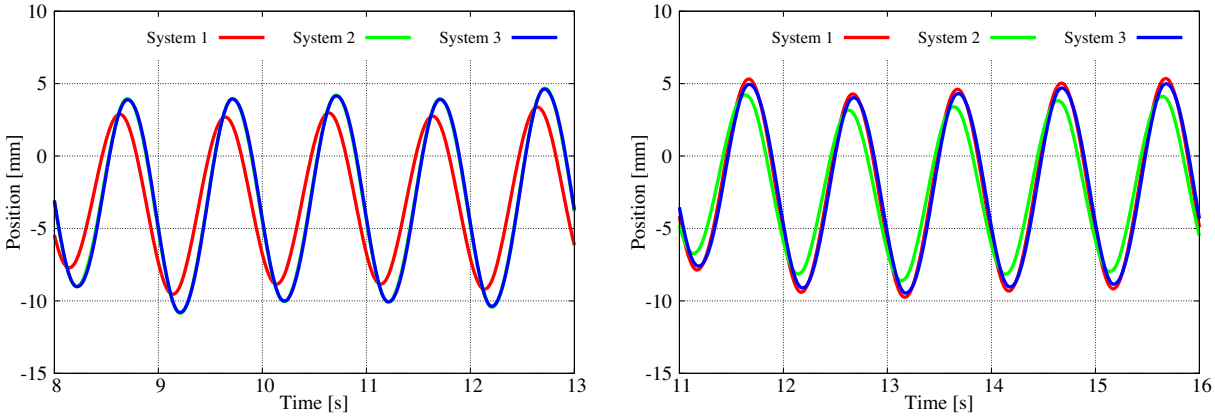

(a) Operation from system 1.

(b) Operation from system 2.

Fig. 4-22: Free motion results of the conventional method in case 2.

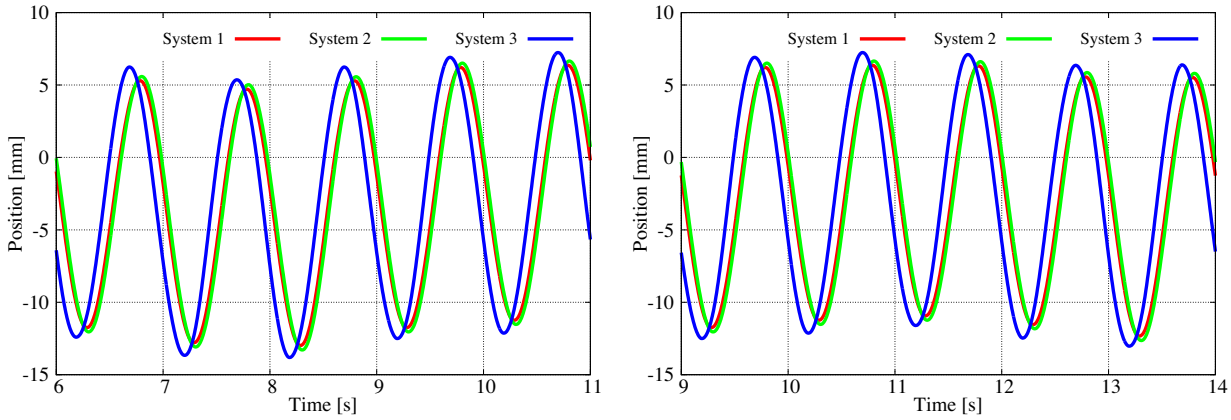

(a) Operation from system 1.

(b) Operation from system 2.

Fig. 4-23: Free motion results of the proposed multilateral teleoperation in case 2.

4.5.5 Experimental Results for Multilateral Teleoperation in Case 2

In case 2, the delay time of every communication link was randomly selected. At first, the free motion results are shown in Figs. 4-22 and 4-23. The overall results are almost the same between case 1 and case2. The difference in the position response between Figs. 4-22(a) and 4-22(b) is because the delay time is no longer symmetric. However, in the proposed methods, the results shows that the performance is not affected by the difference between the delay times.

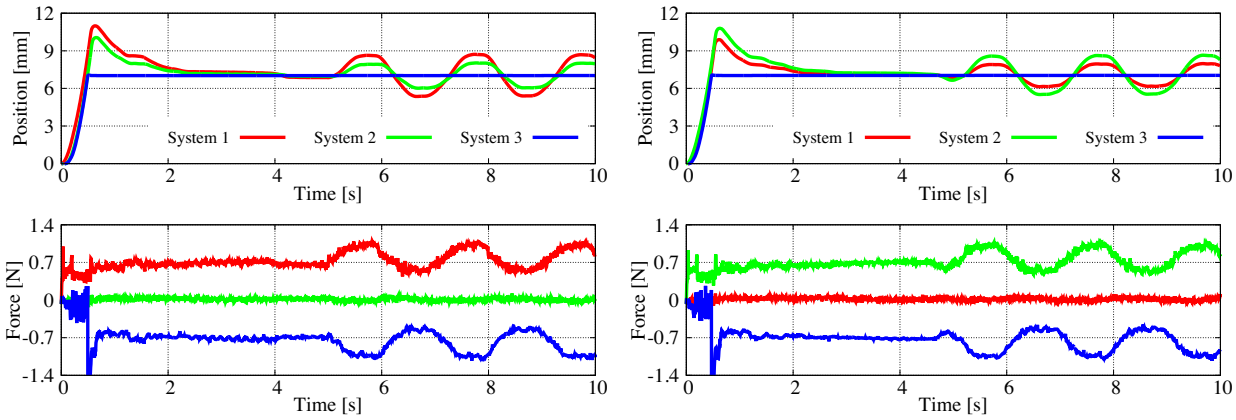

(a) Operation from system 1. (b) Operation from system 2.

Fig. 4-24: Contact motion results of the conventional method in case 2.

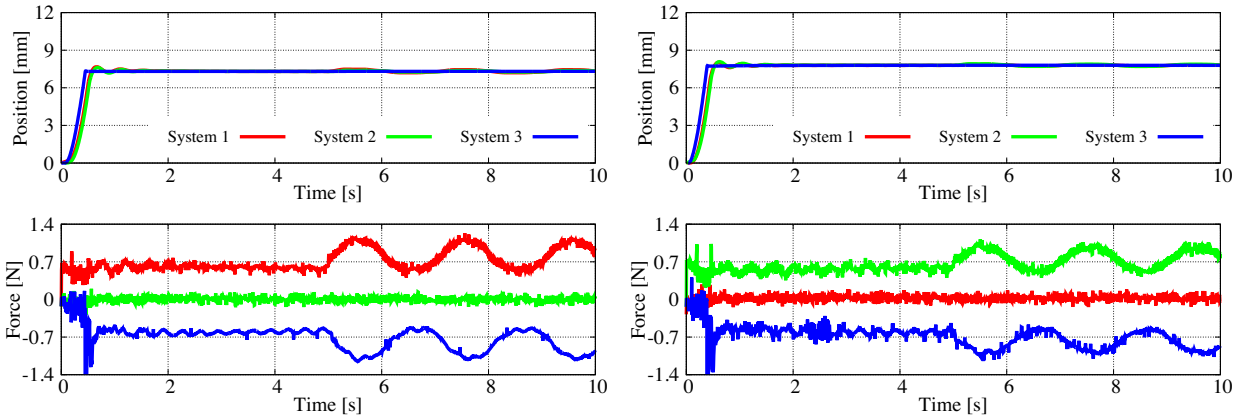

(a) Operation from system 1. (b) Operation from system 2.

Fig. 4-25: Contact motion results of the proposed multilateral teleoperation in case 2.

The contact motion results are shown in Figs. 4-24 and 4-25. The position and force results in the proposed method showed that it could transmit precise haptic sensation to remote places.

4.6 Summary of Chapter 4

In this chapter, the integrated design method of both connectivities for bilateral/multilateral teleoperation was proposed. As same as the design in Chapter 2, the dissertation showed that there are two ways to realize motion decoupling in bilateral teleoperation. The modal transformation matrix of the proposed method was obtained based on the necessary condition in Chapter 2. And one of the connectivity matrix for force response that was derived from the proposed modal transformation matrix became the same as the matrix proposed in Chapter 3 when the delay time between the uplink and the downlink is the same. The interesting characteristics of the proposed method is that the modal transformation matrix determines the route to realize motion decoupling. In bilateral teleoperation, the structure without the use of delay model was proposed. The design method was then extended to multilateral teleoperation. If the topology of a system is fully connected, the method can be extended to n numbered multilateral teleoperation. The determinant of the connectivity matrix for both motions became 0 in the proposed method. It indicates that the double integrator characteristics in COG motion is realized. The performance analysis showed that the proposed method has complete transmissibility even in the presence of time delay.

Chapter 5

Bilateral Control Using Resonant System

This chapter describes bilateral control using flexible manipulators. For example, the mechanical structure contains some flexibility because of the safety. Even in this situation, it is required to transmit precise haptic sensation.

5.1 Introduction of Chapter 5

The contents of this chapter are given as follows. In Section 5.2, the flexible system is modeled by using the wave equation, and control goals in this chapter are described. Section 5.3 describes control of resonant systems based on wave equation. Vibration caused by the flexibility is compensated by rejecting a reflected wave inside the system.In this case, the system can be viewed as an equivalent input time delay system. Therefore, in Section 5.4, integrated connectivity design to eliminate the controller interference caused by the delay element is proposed. The connectivity design method proposed in Chapter 4 was applied. Section 5.5 shows the experimental results to verify the validity of the proposed method. Finally, this chapter is concluded in Section 5.6.

5.2 System Modeling and Control Goals in Bilateral Control

5.2.1 System Modeling

The following subsection describes the modeling of master and slave systems. The master and slave systems used in this Chapter are shown in Fig. 5-1. In Fig. 5-1, θ, τ, L, and $\theta(t, x)$ stand for the angle,

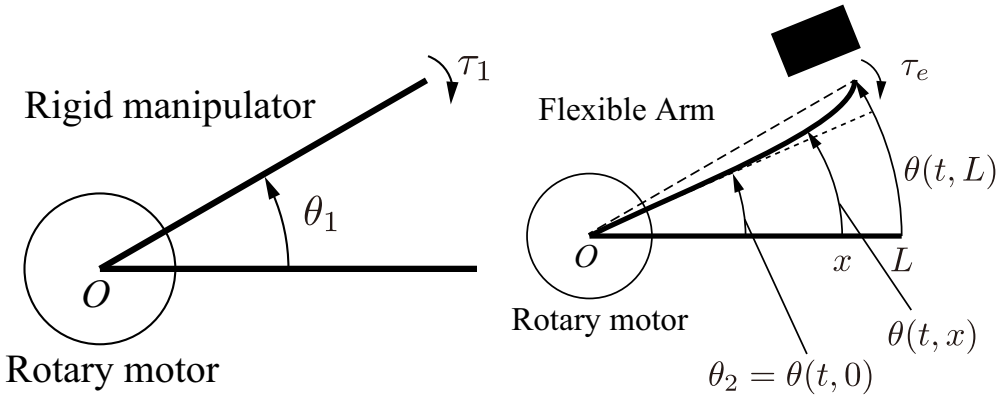

(a) Master system. (b) Slave system.

Fig. 5-1: Model for master and slave systems.

torque, length of the load in the slave system, and the distributed angle, respectively. The master system is assumed as a rigid body system, while the slave system is assumed as a mechanically resonant system.

The modeling of the master system is explained in the following. Since the DOB is used as explained in Chapter 2, the motion equation of the master system can be described as

$$\theta_1 = \frac{1}{s^2}\ddot{\theta}_1^{\mathrm{ref}}. \tag{5.1}$$

The dynamics becomes the same even the system is a rotating body. The cut-off frequency of the DOB is set high enough so that it eliminates the effect of the disturbance.

While the master system is a rigid body, the slave system is assumed to have a flexible structure in this section. In order to consider high-order vibration, the system is modeled by using the wave equation which is one of the distributed parameter models. An equation of bending vibration such as a Euler-Bernoulli beam usually becomes the model for flexible manipulators. Modeling of a flexible system by the wave equation assumes there is no bending moment, and it only considers the propagation of shear force. The wave-based disturbance observer [97] compensates the modeling error caused by the neglected term, and the next section explains the structure. Additionally, the deflection at each position on the flexible arm is converted to the angle for the simplicity. The wave equation is represented as

$$s^2\theta(s, x) = c^2\frac{\partial^2\theta(s, x)}{\partial x^2}, \tag{5.2}$$

where $c = \sqrt{k'G/\rho}$ stands for the propagation velocity of the wave, and the coefficient k' determines the term, the shear modulus of rigidity G and the line density ρ. The boundary conditions for the slave

system are given as

$$\begin{aligned}\theta(s,0) &= \theta_2 \\ &\approx \frac{1}{s^2}\ddot{\theta}_2^{\mathrm{ref}}, \end{aligned} \tag{5.3}$$

$$\frac{\partial\theta(s,L)}{\partial x} = -\frac{1}{\kappa}\tau_e, \tag{5.4}$$

where $\kappa = k'G$ stands for the elastic coefficient. Eq. (5.3) indicates that the rotary motor is located at the boundary $x = 0$. Since the motor in the slave system also uses the DOB, the motor is robust against the motion of the flexible arm. Eq. (5.4) indicates that the external force generated by the environment acts on the boundary $x = L$.

By using the wave equation and boundary conditions, the transfer function from the motor angle to the tip angle can be obtained as

$$\theta(s,L) = G(s)\theta_2 + H(s)\tau_e, \tag{5.5}$$

$$G(s) = \frac{2e^{-T_w s}}{1+e^{-2T_w s}}, \tag{5.6}$$

$$H(s) = -\frac{1}{s\sqrt{\rho\kappa}}\frac{1-e^{-T_w s}}{1+e^{-2T_w s}}, \tag{5.7}$$

where T_w stand for the propagation time of the wave, which is represented as

$$T_w = \frac{L}{c}. \tag{5.8}$$

As shown in (5.5), the transfer function contains time-delay elements. Block diagram of the transfer function is shown in Fig. 5-2. In Fig. 5-2, there is a feedback loop that includes the time delay element. The term represents a reflected wave. When a system is modeled by the wave equation, vibration is induced by the reflected wave. Therefore, the reflected wave is needed to be compensated to suppress the vibrations caused by mechanical resonances in the slave system.

5.2.2 Control Goals

Control objective in this section is to transmit haptic sensation between the systems which contain mechanical resonance in the slave system. It means it is important to control the tip of each system because the law of action and reaction is required to be realized at the position. Therefore, the control

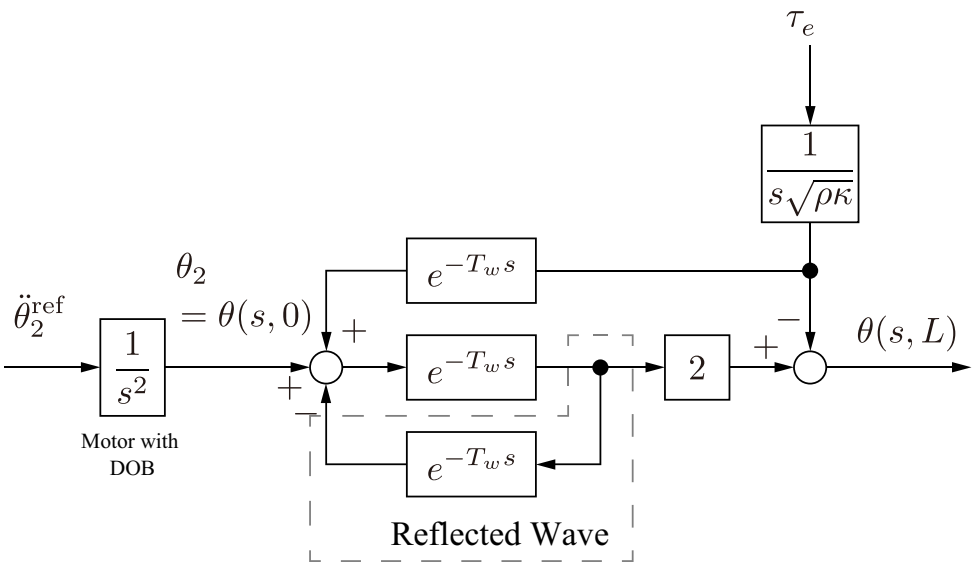

Fig. 5-2: Block diagram of slave system modeled as wave equation.

goals will be expressed as

$$\theta_1 - \theta(s,L) = 0, \tag{5.9}$$

$$\tau_1 + \tau_e = 0. \tag{5.10}$$

The bilateral teleoperation structure will be constructed in order to realize the control goals.

5.3 Control of Resonant System based on Wave Equation

At first, the reflected wave rejection is described to suppress the vibration [98]. Secondly, the disturbance rejection method based on a wave-based disturbance observer is explained.

As described previously, the reason for a flexible system to vibrate is the reflected wave that goes back to the motor side. Therefore, if the slave system is free from the reflected wave, there will be no vibration. Reflected wave θ_{rfl} is defined as

$$\theta_{\mathrm{rfl}} = \theta_2 - e^{-T_w s}\theta(s,L). \tag{5.11}$$

The reflected wave rejection can estimate the reflected wave by using the nominal value of propagation time and can compensate the actual reflected wave. The block diagram of the reflected wave rejection is shown in Fig. 5-3. In Fig. 5-3, g_{r}, $\hat{\theta}_{\mathrm{rfl}}$, and $\ddot{\theta}_{\mathrm{rfl}}^{\mathrm{cmp}}$ stand for the cut-off frequency, estimated reflected

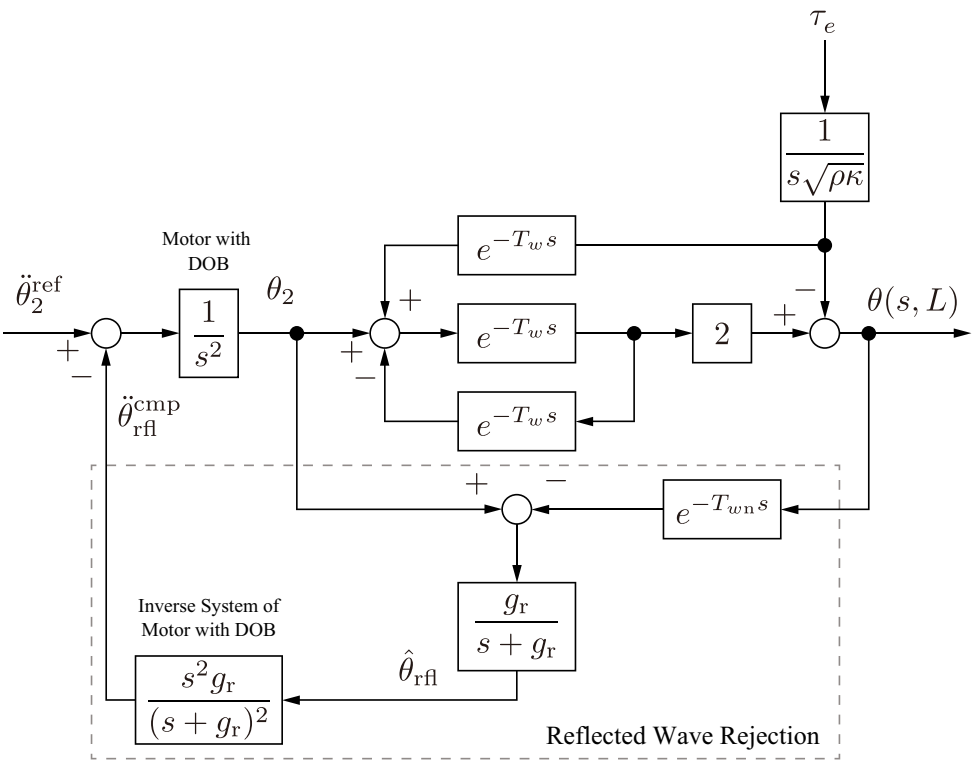

Fig. 5-3: Block diagram of reflected wave rejection.

wave, and compensation value for the reflected wave, respectively. The nominal value of the propagation velocity is set as

$$T_{wn} = \frac{\pi}{2\tilde{\omega}_1}, \tag{5.12}$$

where $\tilde{\omega}_1$ is the identified first-order resonant frequency. The transfer function when the reflected wave rejection is implemented is calculated as

$$\begin{aligned}\theta(s, L) =& \frac{1}{s^2} e^{-T_{wn} s} \ddot{\theta}_2^{\mathrm{ref}} \\ & - \frac{1}{s\sqrt{\rho\kappa}} (1 - e^{-2T_{wn} s}) \tau_e.\end{aligned} \tag{5.13}$$

From (5.13), the system does not induce vibration because there is no time delay element in the denominator.

The vibrations are suppressed by the reflected wave rejection; however, the effect of disturbance still exists. Therefore, a wave-based disturbance observer (WDOB) is used to eliminate the effect of the

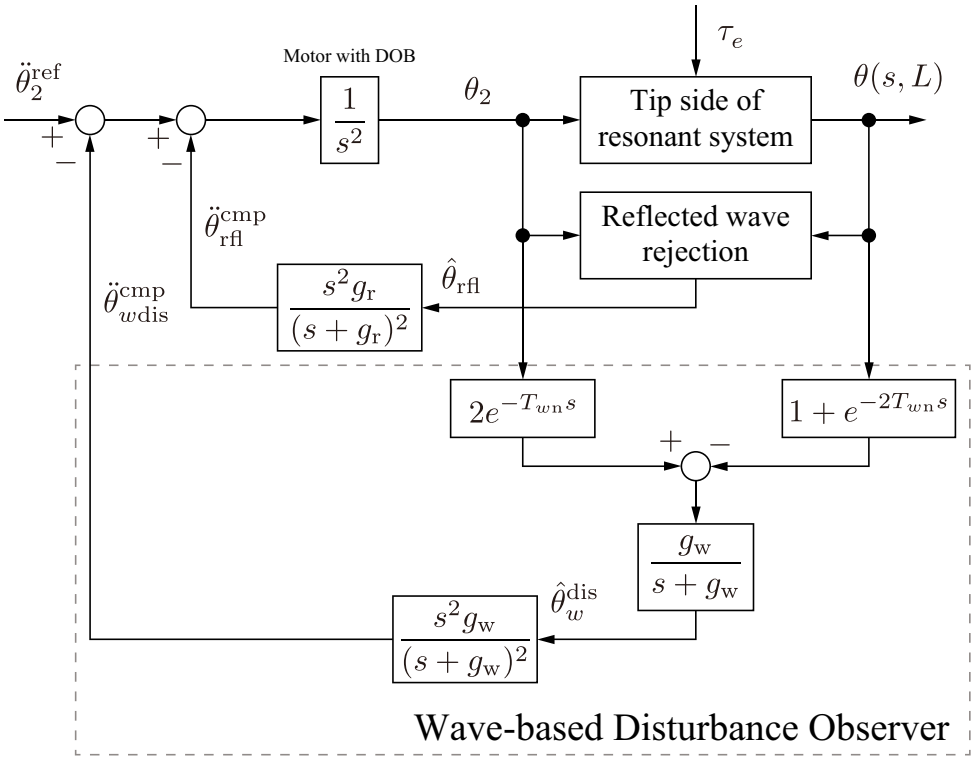

Fig. 5-4: Block diagram of wave-based disturbance observer.

disturbance. The disturbance including the effect of the external torque is defined as

$$\hat{\theta}_w^{\mathrm{dis}} = \frac{g_{\mathrm{w}}}{s+g_{\mathrm{w}}}\left[2e^{-T_{wn}s}\theta_s - (1+e^{-2T_{wn}s})\theta(s,L)\right], \tag{5.14}$$

where $\hat{\theta}_w^{\mathrm{dis}}$ stands for the estimated disturbance. Block diagram of the disturbance compensation by the WDOB is shown in Fig. 5-4. In Fig. 5-4, the disturbance is estimated by the WDOB because of (5.14). Then, the estimated disturbance multiplied by the inverse system of the slave system with the reflected wave rejection is fedback to the acceleration reference. The inverse system of the slave system with the reflected wave rejection $s^2 e^{+T_{wn}s}$ is approximated as s^2 because it is hard to implement the future value. Finally, the estimated disturbance eliminates the actual disturbance acting on the tip of the flexible system. If the cut-off frequencies of the reflected wave rejection and WDOB are high enough, the transfer function from the acceleration reference to the tip position is represented as

$$\theta(s,L) = \frac{1}{s^2}e^{-T_{wn}s}\ddot{\theta}_2^{\mathrm{ref}}. \tag{5.15}$$

Eq. (5.15) shows that the resonant system with the reflected wave rejection and the WDOB represents

the double integrator and a time delay. Therefore, the slave system can be regarded as an equivalent time delay system.

Besides, the disturbance estimated by WDOB includes the external torque from an environment. Hence, under the assumption that modeling error is not so much, the WDOB can also calculate the external torque from an environment. From the definitionwith $\theta^{\mathrm{err}} \approx 0$, the environmental torque can be estimated as

$$\begin{aligned}\hat{\tau}_e &= \frac{s\sqrt{\rho_{\mathrm{n}}\kappa_{\mathrm{n}}}}{1-e^{-2T_{w\mathrm{n}}s}}\hat{\theta}_w^{\mathrm{dis}} \\ &= \frac{\sqrt{\rho_{\mathrm{n}}\kappa_{\mathrm{n}}}}{2T_{w\mathrm{n}}s}\hat{\theta}_w^{\mathrm{dis}}.\end{aligned} \tag{5.16}$$

The above estimation (5.16) is used to constructing torque control in the bilateral control system. The relationship between τ_e and τ_2 will be obtained as

$$\tau_e = e^{-T_{w\mathrm{n}}s}\tau_2, \tag{5.17}$$

where τ_2 is the equivalent external torque viewed from a motor point of view.

5.4 Bilateral Control of Equivalent Time-Delay System

Bilateral control using rigid/flexible systems is constructed in this subsection. By using the method explained in the previous subsection, the resonant system became a double integrator with a time delay element. It is important to decouple the role of each controller when constructing bilateral control. However, it is known that there will be interference in the case of the delay between the systems [36]. The paper explains a control design procedure to realize controller decoupling when there is a delay element in the slave system by considering modal transformation considering the delay element. Control goals will be modified according to the transformation matrix.

The equivalent delay element exists between the motor of the slave system and the tip of the flexible arm as shown in (5.15). As for the master system, there is no the delay element because it is rigid. The delay element can be expressed as a transformation matrix by transforming the coordinate from motor space to tip space. The matrix $\boldsymbol{D}^{-1}$ can be defined as

$$\boldsymbol{D}^{-1} = \begin{bmatrix} 1 & 0 \\ 0 & e^{-T_{w\mathrm{n}}s} \end{bmatrix}. \tag{5.18}$$

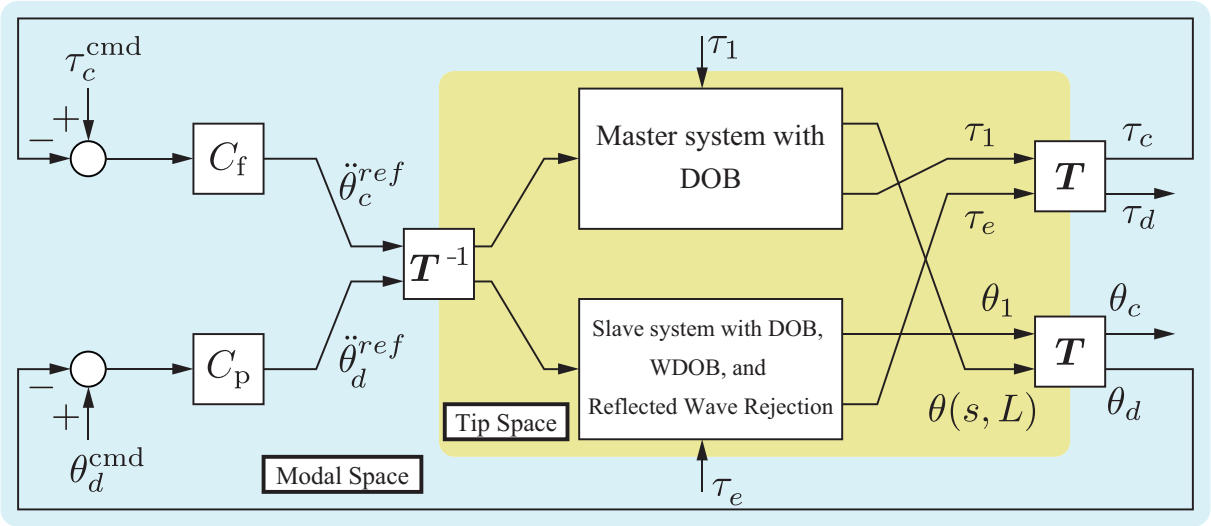

Fig. 5-5: Block diagram of the proposed bilateral control system.

The transformation matrix from the modal space to the work space is given as

$$\boldsymbol{Q}^{-1} = \frac{1}{2}\begin{bmatrix} 1 & -1 \\ 1 & 1 \end{bmatrix}. \tag{5.19}$$

Therefore, the coordinate transformation from the modal space to the tip space is calculated as

$$\boldsymbol{T}^{-1} = \boldsymbol{D}^{-1}\boldsymbol{Q}^{-1} \tag{5.20}$$

$$= \frac{1}{2}\begin{bmatrix} 1 & -1 \\ e^{-T_{\mathrm{wn}}s} & e^{-T_{\mathrm{wn}}s} \end{bmatrix}. \tag{5.21}$$

The transformation matrix from the tip space to the modal space is inversely calculated as

$$\boldsymbol{T} = \frac{1}{e^{-T_{\mathrm{wn}}s}}\begin{bmatrix} e^{-T_{\mathrm{wn}}s} & 1 \\ -e^{-T_{\mathrm{wn}}s} & 1 \end{bmatrix}. \tag{5.22}$$

However, it is difficult to implement the future value $e^{+T_w s}$. Therefore, the value is expressed as 1 in this section. Based on the matrix, the control goals are modified as follows to decouples two controllers:

$$e^{-T_{\mathrm{wn}}s}\tau_1 + \tau_e = 0, \tag{5.23}$$

$$e^{-T_{\mathrm{wn}}s}\theta_1 - \theta(s,L) = 0. \tag{5.24}$$

A position and force controllers are placed in the modal space for the regulation. Acceleration reference for the common mode is expressed as

$$\ddot{\theta}_c^{\mathrm{ref}} = C_{\mathrm{f}}(\tau_c^{\mathrm{cmd}} - \tau_c), \tag{5.25}$$

while acceleration reference for the differential mode is expressed as

$$\ddot{\theta}_d^{\mathrm{ref}} = C_{\mathrm{p}}(\theta_d^{\mathrm{cmd}} - \theta_d). \tag{5.26}$$

Since the control goals for the bilateral control are (5.23) and (5.24) in this paper, both commands will be 0. The block diagram of the proposed bilateral control system is shown in Fig. 5-5.

Final acceleration references for each motor will be given as

$$\begin{aligned}\begin{bmatrix} \ddot{\theta}_1^{\mathrm{ref}} \\ \ddot{\theta}_e^{\mathrm{ref}} \end{bmatrix} &= -\frac{1}{2}\det(\boldsymbol{L})C_{\mathrm{f}}\boldsymbol{T}^{-1}\boldsymbol{S}\boldsymbol{T}\boldsymbol{\tau} - \frac{1}{2}\det(\boldsymbol{L})C_{\mathrm{p}}\boldsymbol{T}^{-1}(\boldsymbol{I}-\boldsymbol{S})\boldsymbol{T}\boldsymbol{\theta} \\ &= \frac{1}{2}C_{\mathrm{f}}\begin{bmatrix} e^{-T_{w\mathrm{n}}s} & 1 \\ e^{-2T_{w\mathrm{n}}s} & e^{-T_{w\mathrm{n}}s} \end{bmatrix}\begin{bmatrix} \tau_1 \\ \tau_e \end{bmatrix} - \frac{1}{2}C_{\mathrm{p}}\begin{bmatrix} e^{-T_{w\mathrm{n}}s} & -1 \\ -e^{-2T_{w\mathrm{n}}s} & e^{-T_{w\mathrm{n}}s} \end{bmatrix}\begin{bmatrix} \theta_1 \\ \theta(s,L) \end{bmatrix}. \end{aligned} \tag{5.27}$$

The determinant of both connectivity matrix shown in (5.27) is 0, the motions are decoupled and both controllers are able to control each desired motion. Since (5.27) is the acceleration reference for the tip space, the acceleration reference for the motor is calculated by

$$\begin{aligned}\begin{bmatrix} \ddot{\theta}_1^{\mathrm{ref}} \\ \ddot{\theta}_2^{\mathrm{ref}} \end{bmatrix} &= -\frac{1}{2}\det(\boldsymbol{L})\boldsymbol{Q}^{-1}\boldsymbol{S}\boldsymbol{T}\boldsymbol{\tau} - \frac{1}{2}\det(\boldsymbol{L})\boldsymbol{Q}^{-1}(\boldsymbol{I}-\boldsymbol{S})\boldsymbol{T}\boldsymbol{\theta} \\ &= \frac{1}{2}C_{\mathrm{f}}\begin{bmatrix} e^{-T_{w\mathrm{n}}s} & e^{-T_{w\mathrm{n}}s} \\ e^{-T_{w\mathrm{n}}s} & e^{-T_{w\mathrm{n}}s} \end{bmatrix}\begin{bmatrix} \tau_1 \\ \tau_e \end{bmatrix} - \frac{1}{2}C_{\mathrm{p}}\begin{bmatrix} e^{-T_{w\mathrm{n}}s} & -e^{-T_{w\mathrm{n}}s} \\ -e^{-T_{w\mathrm{n}}s} & e^{-T_{w\mathrm{n}}s} \end{bmatrix}\begin{bmatrix} \theta_1 \\ \theta(s,L) \end{bmatrix}. \end{aligned} \tag{5.28}$$

5.5 Experiments

In order to verify the effectiveness of the proposed method, the experiments of bilateral control are performed. The experimental setup is shown in Fig. 5-6. Fig. 5-6(a) shows the master system which is composed of a rigid link and a direct drive rotary motor with encoder. An operator operates the master system. On the other hand, the slave system has a flexible mechanism as shown in Fig. 5-6(b). A position sensitive detector (PSD) and a laser diode measure the tip angle. Experimental parameters are shown in Table 5.1.

Fig. 5-7 shows the experimental results without the reflected wave rejection and the transformation $\boldsymbol{D}^{-1}$. The angle response in Fig. 5-7 indicates that the response of tip angle is oscillating because of the mechanical resonance. Because of the vibration, the force responses shown in Fig. 5-7 also has an oscillatory response, which makes difficult to operate and recognize the reaction torque from the slave system.

On the other hand, Fig. 5-8 shows the experimental results of the proposed method. From the angle response shown in Fig. 5-8, it can be seen that the vibration is well suppressed by the reflected wave

Table 5.1: Experimental parameters for bilateral control.

Parameter	Description	Value
T_s	Sampling time	0.5 ms
$J_{1\mathrm{n}}$ and $J_{2\mathrm{n}}$	Motor inertia	2.8×10^3 kgm^2
$\tilde{\omega}_1$	First-order resonant frequency	37.7 rad/s
$T_{w\mathrm{n}}$	Nominal propagation time	41.7 ms
K_{p}	Proportional gain for position control	196
K_{d}	Differential gain for position control	625
C_{f}	Proportional gain for force control	25
g_{r}	Cut-off frequency of RFOB	70 rad/s
g_{w}	Cut-off frequency of WDOB	45 rad/s
g_{dis}	Cut-off frequency of DOB	500 rad/s

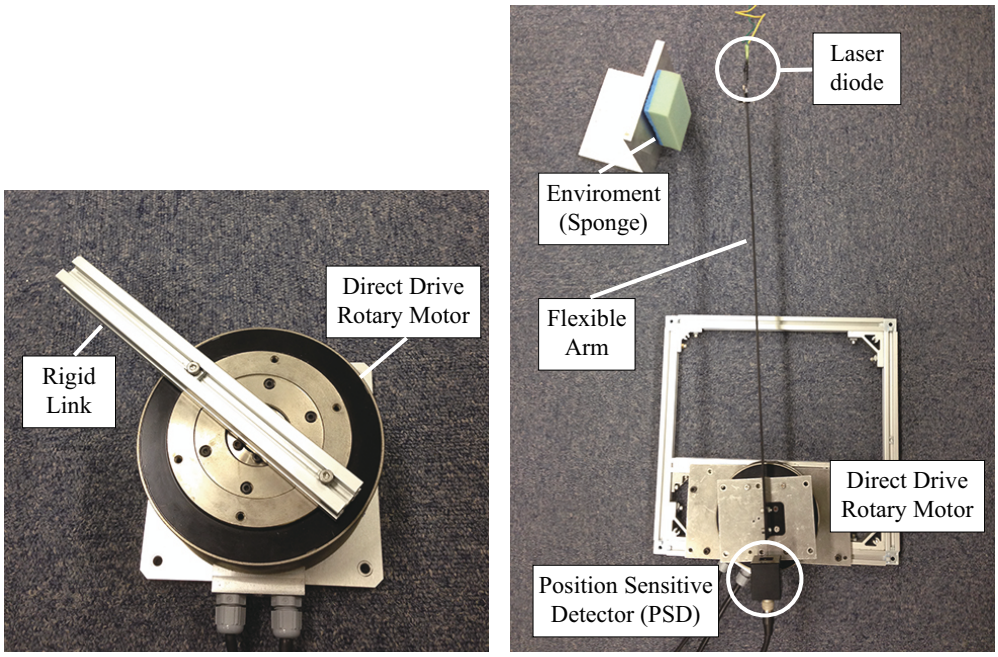

(a) Master system. (b) Slave system.

Fig. 5-6: Experimental setup.

rejection and the appropriate coordinate transformation $\boldsymbol{D}^{-1}$. The torque response in Fig. 5-8 shows that the law of action-reaction is realized in the contact motion. When the direction of the movement changes, the large operational torque is observed because of frictional torque. It is required to identify the friction more precisely for decreasing the operational torque.

The validity of the proposed method is confirmed by these experimental results.

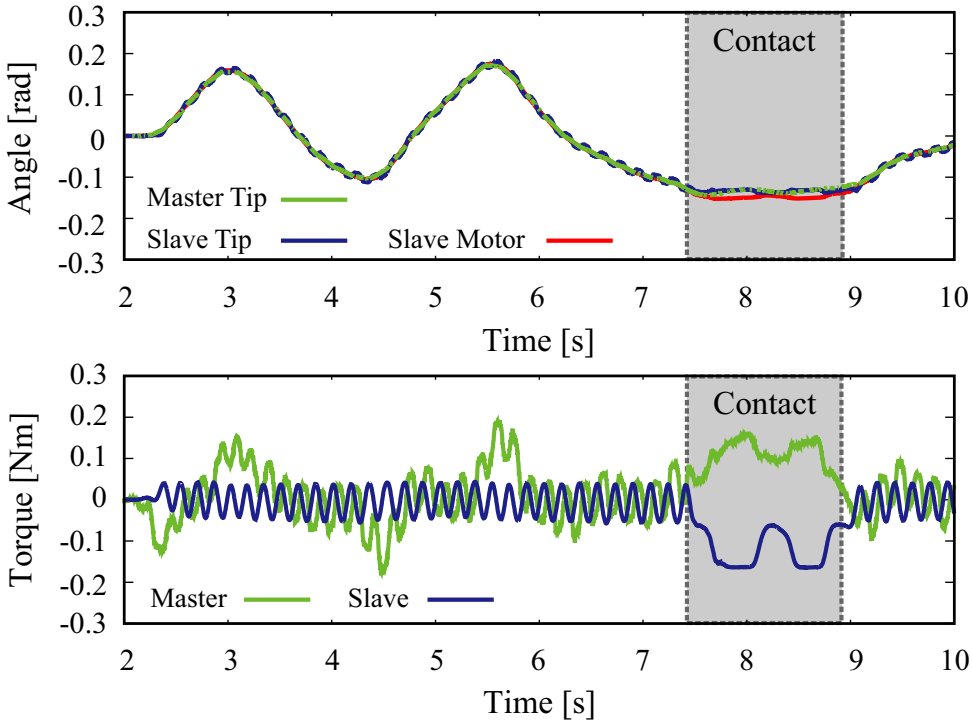

Fig. 5-7: Experimental result of the conventional method.

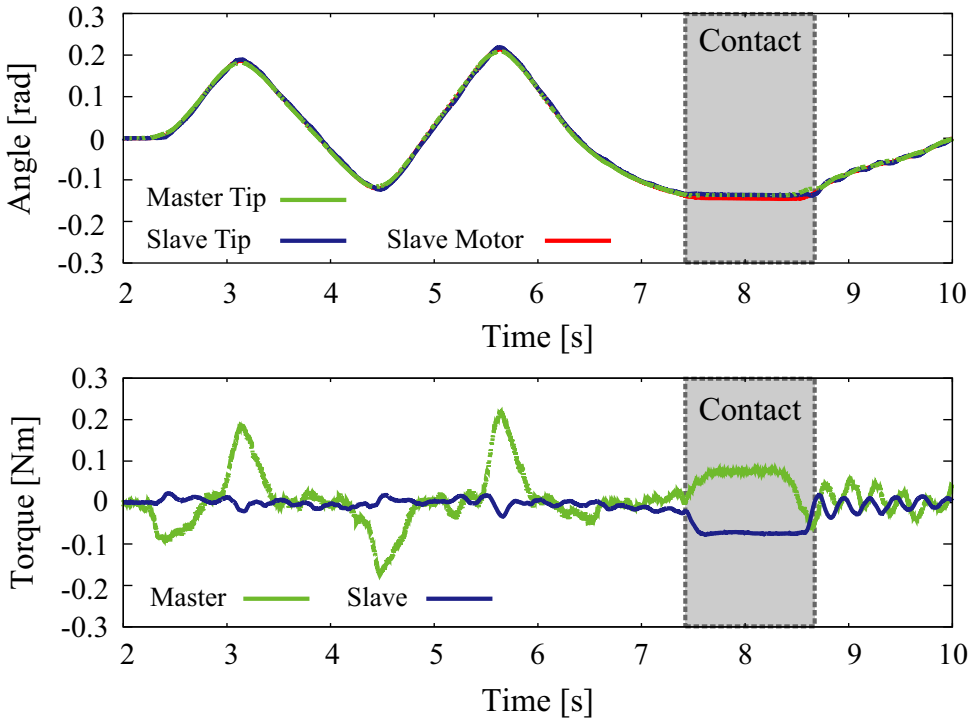

Fig. 5-8: Experimental result of the proposed method.

5.6 Summary of Chapter 5

In this chapter, the design methodology to construct bilateral control using a flexible manipulator was proposed. The flexible system was modeled by using the wave equation. Then, reflected wave rejection and wave-based disturbance observer was implemented to eliminate the vibration and load side disturbance, respectively. Consequently, the system that contains mechanical vibration can be viewed as an equivalent time delay system. The integrated connectivity design matrix proposed in Chapter 4 was applied to decouple controllers for COG/relative motions. It revealed that the connectivity design method is also valid in input delay systems. The experimental results show that precise tactile sensation transmission was realized in the proposed method.

Chapter 6

Relative Motion Topology Design in Multilateral Teleoperation

---

This chapter describes topology design method for relative motion in multilateral teleoperation. It is known that the change in the topology makes the system to perform differently in decentralized systems. Therefore, the best topology considering the delay time in a communication link is required to be realized.

6.1 Introduction of Chapter 6

The contents of this chapter are given as follows. In Section 6.2, the value is firstly defined. In Section 6.3, the topology is designed by removing the unnecessary links. The design flow for realizing the designed topology is proposed in Section 6.4. Section 6.5 shows the experimental results to verify the validity of the proposed method. Finally, this chapter is concluded in Section 6.6.

6.2 Definition of Topological Influence Value

This section firstly defines the influence value (IV). It is an index that represents the relative amount of information which each system contains [99]. When a system receives more information, it indicates that the system transmits more information. Therefore, a communication link that directs from a system with more IV to a system with less IV includes more information than a link from a system with less IV to a system with more IV. It can be said that the index shows the amount of the influence that a system

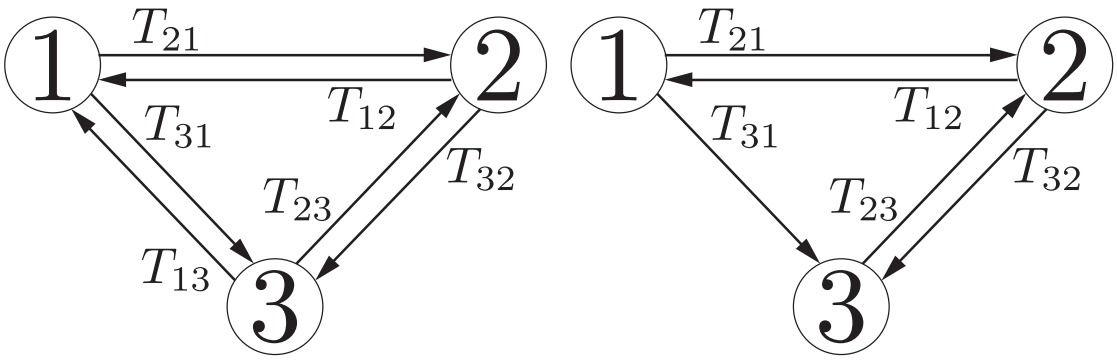

(a) Topology 1. (b) Topology 2.

Fig. 6-1: Examples of topology when there are three systems.

has in the overall system. Thus, the amount of the information that goes through each communication link can be quantified by considering the amount of information that each system includes. Similar index is used in [100].

This index is actually calculated by using an adjacency matrix. The eigenvector of the maximum eigenvalue regarding the adjacency matrix is regarded as the index of how much information each subsystem contains. The maximum eigenvalue of the adjacency matrix expresses overall strength of system connection. If the maximum eigenvalue is a large value, it indicates the connection of the overall system is strong. The maximum eigenvalue of the adjacency matrix is calculated, and then its eigenvectors are nominalized so that the sum of the vector elements is one.

An example using the topology shown in Fig. 6-1(b) is briefly described. When ignoring the communication delay, the adjacency matrix becomes

$$\boldsymbol{A} = \begin{bmatrix} 0 & 1 & 0 \\ 1 & 0 & 1 \\ 1 & 1 & 0 \end{bmatrix}. \tag{6.1}$$

When the effect of the delay is included, the matrix can be rewritten as

$$\boldsymbol{A}^{\mathrm{CD}} = \begin{bmatrix} 0 & e^{-T_{12}} & 0 \\ e^{-T_{21}} & 0 & e^{-T_{23}} \\ e^{-T_{31}} & e^{-T_{32}} & 0 \end{bmatrix}. \tag{6.2}$$

The Laplace operator in (2.19) is removed to obtain the index. Eq. (6.2) contains the delay time and it can be viewed as an scaling factor depending on the delay. When there is no time delay in Fig. 6-1(b) (which means $T_{12} = T_{21} = T_{23} = T_{32} = T_{31} = 0$ s), the adjacency matrix becomes the same as the

normal adjacency matrix:

$$\begin{aligned}\boldsymbol{A}^{\mathrm{CD}} &= \begin{bmatrix} 0 & e^{-0} & 0 \\ e^{-0} & 0 & e^{-0} \\ e^{-0} & e^{-0} & 0 \end{bmatrix} \\ &= \begin{bmatrix} 0 & 1 & 0 \\ 1 & 0 & 1 \\ 1 & 1 & 0 \end{bmatrix} \\ &= \boldsymbol{A}. \end{aligned} \tag{6.3}$$

6.2.1 Calculation of Influence Value

It is able to obtain the amount of the influence that each system has by the use of the adjacency matrix that contains the delay. The eigenvectors of the maximum eigenvalue is defined as $\boldsymbol{IV}$ that quantitatively represents the strength of a connection. Assume the delay times in each link shown in Fig. 6-1(a) are $T_{12} = T_{21} = 0.05$ s, $T_{23} = T_{32} = 0.15$ s, $T_{13} = T_{31} = 0.1$ s. The following equations compares the maximum eigenvalue and the influence value for Fig. 6-1(a) when not considering and considering the delay:

$$\lambda_{\max} = 2.00, \quad \boldsymbol{IV} = [0.333, 0.333, 0.333]^T, \tag{6.4}$$

$$\lambda_{\max}^{\mathrm{CD}} = 1.81, \quad \boldsymbol{IV}^{\mathrm{CD}} = [0.339, 0.333, 0.328]^T. \tag{6.5}$$

where $\lambda_{\max}$ and $\boldsymbol{IV}$ stand for the maximum eigenvalue of the adjacency matrix and the influence value of a system, and i th row of $\boldsymbol{IV}$ expresses the influence value of i th system IV_i. All of the IV becomes the same when the delay is ignored that is expressed in (6.4). On the other hand, as it is shown in (6.5), IV_1^{CD} is the the largest when taking the delay into account. The total delay time it takes to transmit the information of system 1 is the smallest in the three. It indicates that the system whose connection link has smaller delay time will have strong influence in the overall system when the topology is fully connected. It means the index reflects not only the number of connection links but also the delay in each link.

At next, four examples of the topologies are shown in Fig. 6-2. The delay time in each link is $T_{12} = T_{21} = 0.3$ s, $T_{23} = T_{32} = 0.2$ s, $T_{34} = T_{43} = 0.15$ s, $T_{14} = T_{41} = 0.05$ s, $T_{13} = T_{31} = 0.1$ s, $T_{24} = T_{42} = 0.2$ s. The maximum eigenvalue $\lambda_{\max}^{\mathrm{CD}}$ and the influence value $\boldsymbol{IV}^{\mathrm{CD}}$ are shown

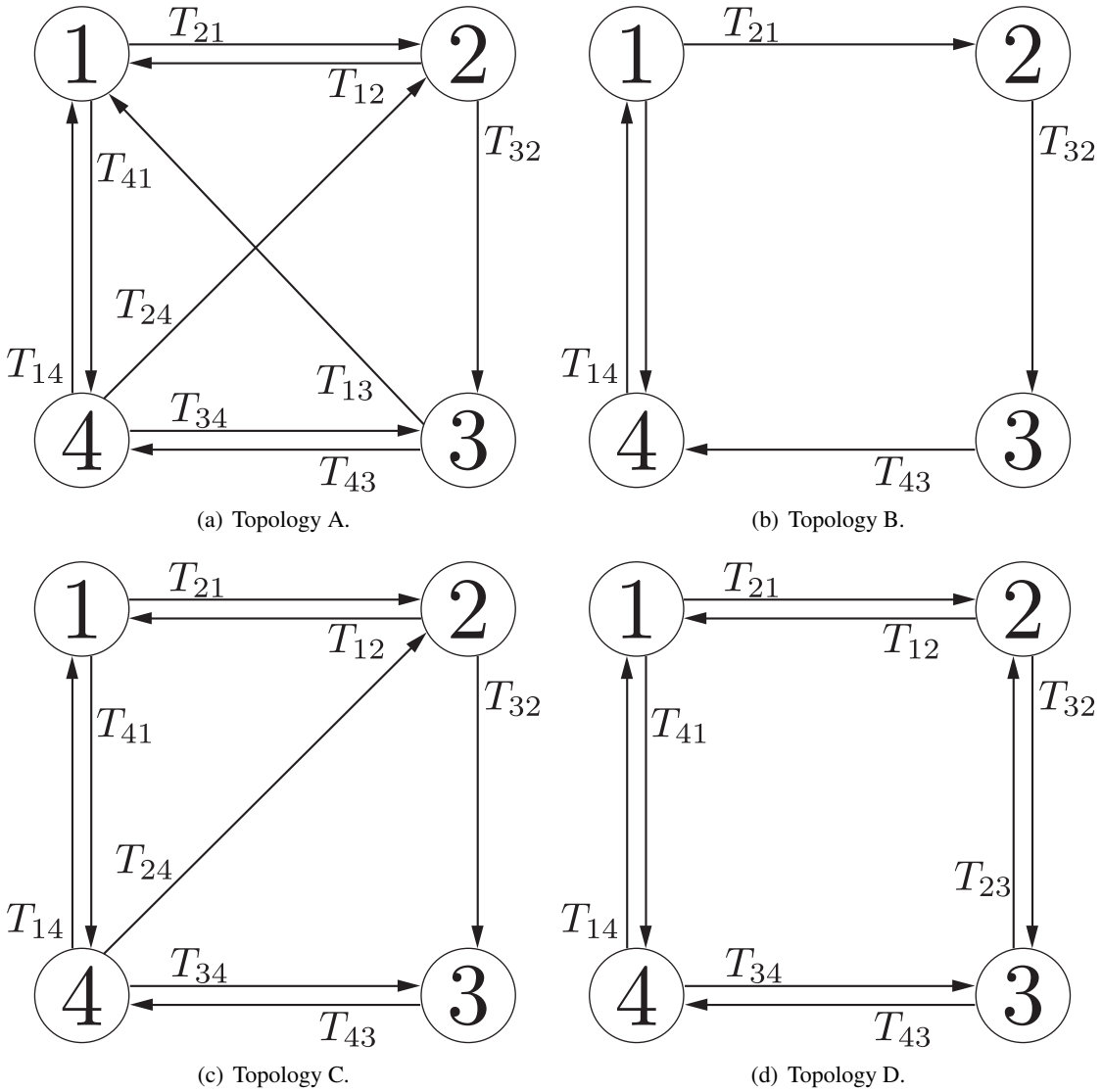

(a) Topology A.

(b) Topology B.

(c) Topology C.

(d) Topology D.

Fig. 6-2: Examples of topology when there are four systems.

from (6.6) to (6.9), respectively.

$$\lambda^{\mathrm{CD}}_{\max_{\mathrm{A}}} = 1.91,\ \boldsymbol{IV}^{\mathrm{CD}}_{\mathrm{A}} = [0.312, 0.228, 0.210, 0.250]^T, \tag{6.6}$$

$$\lambda^{\mathrm{CD}}_{\max_{\mathrm{B}}} = 0.84,\ \boldsymbol{IV}^{\mathrm{CD}}_{\mathrm{B}} = [0.277, 0.243, 0.237, 0.243]^T, \tag{6.7}$$

$$\lambda^{\mathrm{CD}}_{\max_{\mathrm{C}}} = 1.71,\ \boldsymbol{IV}^{\mathrm{CD}}_{\mathrm{C}} = [0.251, 0.236, 0.248, 0.265]^T, \tag{6.8}$$

$$\lambda^{\mathrm{CD}}_{\max_{\mathrm{D}}} = 1.69,\ \boldsymbol{IV}^{\mathrm{CD}}_{\mathrm{D}} = [0.252, 0.231, 0.246, 0.269]^T. \tag{6.9}$$

In Fig. 6-2(a), system 1 has the largest influence and the influence of system 3 is the smallest.

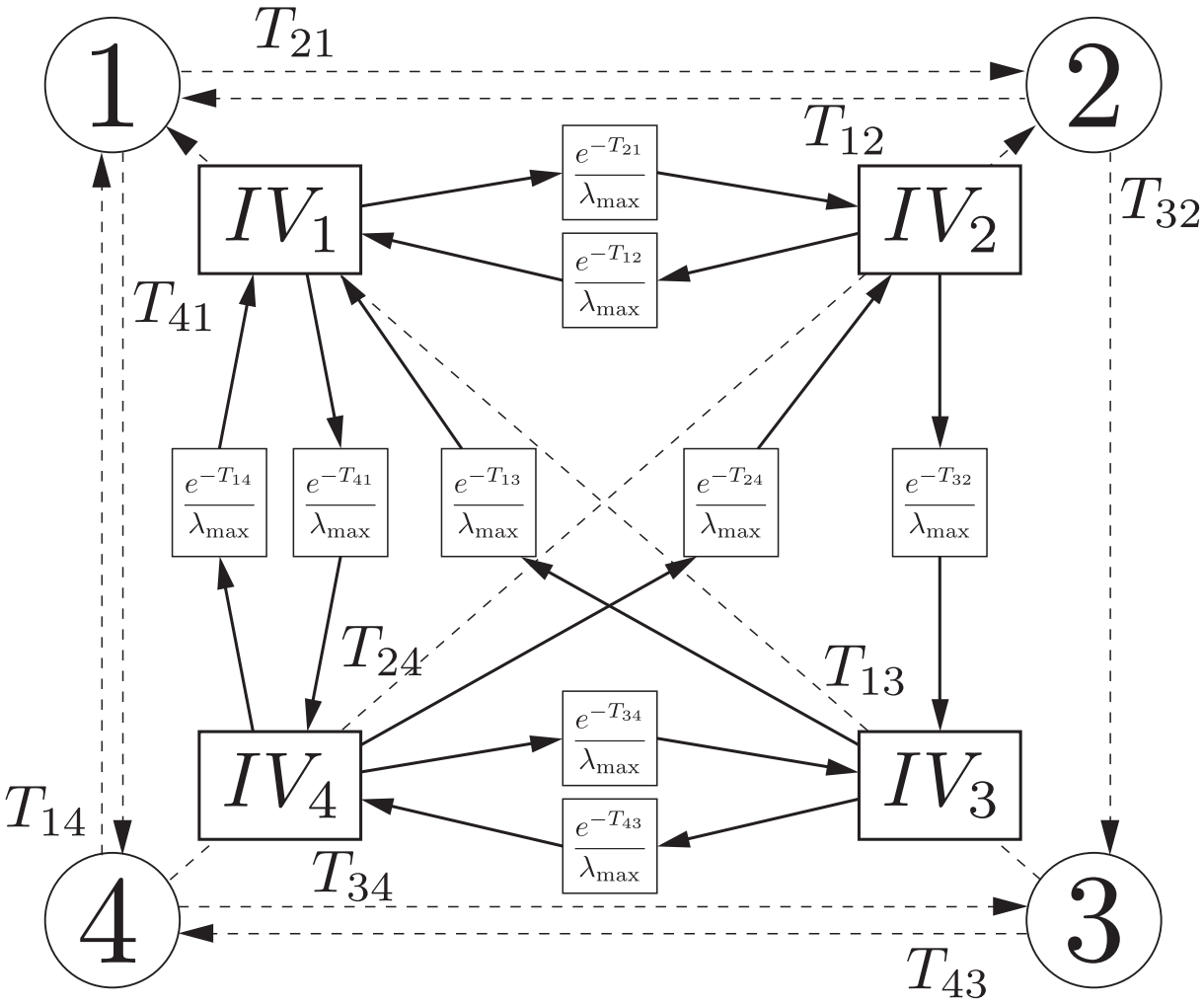

Fig. 6-3: Relation among IVs of each system and maximum eigenvalue under communication delay.

Removing the link which heads from system 3 to 1 in Fig. 6-2(a) is shown in Fig. 6-2(c). Comparing Fig. 6-2(a) and 6-2(c), the dispersion of the IV in each system shown in Fig. 6-2(c) is smaller than that of the IV shown in Fig. 6-2(a). This means that in order to equalize the IV, it is effective to remove the link which is headed from a system which has the least IV to a system which has the most IV. Comparing the value $\lambda_{\max}^{\mathrm{CD}}$ of Fig. 6-2(a) and 6-2(c) shows removing a link also decreases the maximum eigenvalue of the adjacency matrix. It indicates taking a communication link away weakens the overall strength of the connectivity as a whole system.

The IV has a relationship between each other. Since the IV is the eigenvectors of the maximum

eigenvalue, its relationship can be written in the following equation:

$$(\boldsymbol{A} - \lambda_{\max}^{\mathrm{CD}} \boldsymbol{I})\boldsymbol{IV}^{\mathrm{CD}} = \boldsymbol{0}. \tag{6.10}$$

The example of the relationship in Fig. 6-2(a) is shown as follows:

$$\boldsymbol{IV}_{\mathrm{A}}^{\mathrm{CD}} = \begin{bmatrix} IV_2^{\mathrm{CD}} \dfrac{e^{-T_{12}}}{\lambda_{\max}^{\mathrm{CD}}} + IV_3^{\mathrm{CD}} \dfrac{e^{-T_{13}}}{\lambda_{\max}^{\mathrm{CD}}} + IV_4^{\mathrm{CD}} \dfrac{e^{-T_{14}}}{\lambda_{\max}^{\mathrm{CD}}} \\ IV_1^{\mathrm{CD}} \dfrac{e^{-T_{21}}}{\lambda_{\max}^{\mathrm{CD}}} + IV_4^{\mathrm{CD}} \dfrac{e^{-T_{24}}}{\lambda_{\max}^{\mathrm{CD}}} \\ IV_2^{\mathrm{CD}} \dfrac{e^{-T_{32}}}{\lambda_{\max}^{\mathrm{CD}}} + IV_4^{\mathrm{CD}} \dfrac{e^{-T_{34}}}{\lambda_{\max}^{\mathrm{CD}}} \\ IV_1^{\mathrm{CD}} \dfrac{e^{-T_{41}}}{\lambda_{\max}^{\mathrm{CD}}} + IV_3^{\mathrm{CD}} \dfrac{e^{-T_{43}}}{\lambda_{\max}^{\mathrm{CD}}} \end{bmatrix}. \tag{6.11}$$

The IV of a system can be calculated by adding the IVs of the receiving systems and then divide it by the maximum aigenvalue.

Fig. 6-3 shows the the relationship between IVs that is mathematically expressed in (6.11). The IV of one system is affected by other IVs of the systems that is directly connected. For example, the IVs of system 1 and 4 affect the IV of system 2 because there is a connection that is towards system 2; however, the value is not affected by system 3 because there is no direct connection.

To verify the fact that the IV represents the strength of the connection links, the proof is shown in order to clarify that it stands for the relative influence to other systems. This proof is based on the paper from Uchimura et al. [100].

Let $\boldsymbol{D}$ be a diagonal matrix with the eigenvalues of $\boldsymbol{A}^{\mathrm{CD}}/\lambda_{\max}^{\mathrm{CD}}$, $\boldsymbol{V}$ be a matrix that has the corresponding eigenvectors in the column, and $\boldsymbol{V}_m = (v_1^m, \cdots, v_n^m)$ be the eigenvector corresponding to $\lambda = \lambda_{\max}^{\mathrm{CD}}$. One element of $\boldsymbol{D}$ is 1, and all other elements are less than 1. Also define $\hat{\boldsymbol{V}} = \boldsymbol{V}/\sum_{i=1}^{n} v_i$. The relationship between $\boldsymbol{V}_m$ and $\boldsymbol{IV}^{\mathrm{CD}}$ is shown as $\boldsymbol{IV}^{\mathrm{CD}} = \boldsymbol{V}_m/\sum_{i=1}^{n} v_i^m = \hat{\boldsymbol{V}}_m$.

Transforming $\boldsymbol{A}^{\mathrm{CD}}/\lambda_{\max}^{\mathrm{CD}}$ by the eigenvalue decomposition gives $\boldsymbol{A}^{\mathrm{CD}}/\lambda_{\max}^{\mathrm{CD}} = \boldsymbol{V}\boldsymbol{D}\boldsymbol{V}^{-1}$. Hence, the following equation is obtained:

$$\left(\frac{1}{\lambda_{\max}^{\mathrm{CD}}}\boldsymbol{A}^{\mathrm{CD}}\right)^k = \boldsymbol{V}\boldsymbol{D}^k\boldsymbol{V}^{-1}. \tag{6.12}$$

Since only one element is 1 and all other less than 1, the following equation follows:

$$\lim_{k\to\infty} \boldsymbol{D}^k = diag(0, \cdots, 1, \cdots, 0). \tag{6.13}$$

Apparently, $\boldsymbol{V}\boldsymbol{D}^k\boldsymbol{V}^{-1} = \hat{\boldsymbol{V}}\boldsymbol{D}^k\hat{\boldsymbol{V}}^{-1}$, and since all elements on the ith row of $\hat{\boldsymbol{V}}^{-1}$ are equal to 1, as for the arbitrary vector $\boldsymbol{X} = (x_1, \cdots, x_n)^T$ such that $\sum_{i=1}^{n} x_i = 1$, the equation in the following stands:

$$\begin{aligned}
\hat{\boldsymbol{V}}^{-1}\boldsymbol{X} &= (*, \cdots, 1, \cdots, *)^T, \\
\lim_{k\to\infty} \boldsymbol{D}^k\hat{\boldsymbol{V}}^{-1}\boldsymbol{X} &= (0, \cdots, 1, \cdots, 0)^T, \\
\lim_{k\to\infty} \hat{\boldsymbol{V}}\boldsymbol{D}^k\hat{\boldsymbol{V}}^{-1}\boldsymbol{X} &= \hat{\boldsymbol{V}}_m = \boldsymbol{I}\boldsymbol{V}^{\mathrm{CD}}, \\
\lim_{k\to\infty} \left(\frac{1}{\lambda_{\max}^{\mathrm{CD}}}\boldsymbol{A}^{\mathrm{CD}}\right)^k \boldsymbol{X} &= \boldsymbol{I}\boldsymbol{V}^{\mathrm{CD}}.
\end{aligned} \tag{6.14}$$

This equation indicates that the value converges to the same value in the steady state. This signifies that the value converges regardless of any input. Moreover, as mentioned previously, the index of one system is affected by other systems; therefore, it can be interpreted as the relative influence of one system to other systems.

6.3 Topology Selection Based on Influence Value

This subsection proposes the method of obtaining the desired topology in multilateral control by using the IV. The desired topology changes depending on the delay time in each link. At first, the relationship that each system has to fulfill is described.

6.3.1 Desired Relationship for Master and Slave Systems

As it is analyzed in Chapter 4, relative motion controllers which are position controllers deteriorate the transparency in multilateral teleoperation. One of the reason of it is because existing methods connected all systems for transmitting force and position responses. The report in [101] shows removing the connection for controlling the relative motion can enhance the performance of the overall system. The report gives strong evidence of the necessity of selecting the relative motion topology for regaining the tactile sensation transmission performance. However, at the same time, one of the important points in multilateral control is to translate the information from the slave system to the master systems. In multilateral teleoperation, operators want to perceive the impedance of the contact object at the slave system. Therefore, both the force and position responses of the slave system need to be transmitted precisely. The transmission ability regarding the position response of the slave system can be enhanced by making the influence the strongest of all the systems, and the index that shows the relative influence between

the systems is the influence value. In order to make the slave system to have the most influence of all the systems, the IV of the slave system must be the largest. Therefore, connection links are selected to achieve the following inequality:

$$IV_S^{\mathrm{CD}} > IV_{M_i}^{\mathrm{CD}} \ \ (i = 1, 2, \cdots, n-1) \ \ \text{with the largest} \ \lambda_{\max}^{\mathrm{CD}}, \tag{6.15}$$

where IV_S^{CD} is the IV of the slave system, and $IV_{M_i}^{\mathrm{CD}}$ is the IV of the ith master system. The inequality realizes for the slave system to have the largest influence in the system. Since removing communication links regarding force information precludes the realization of the law of action and reaction in every system, only the topology regarding the relative motion is removed based on the IV. As mentioned above, when $\lambda_{\max}^{\mathrm{CD}}$ is large, the overall system transmits more information to others. Therefore, the least number of link is needed to be removed to achieve the goal (6.15). This is a constraint satisfaction problem.

When a link from the slave system to a master system is disconnected, the master system cannot receive the response of the slave system directly. Moreover, IV_S^{CD} becomes small when a link from a master system to the slave system is removed because it equivalently reduces the amount of the information that the system receives. Therefore, the connection link to remove is the one between the master systems.

When there are several slave systems, the best performance is obtained by switching the topology depending on which environmental information the operators want to perceive at the moment.

6.3.2 Removing the Links

The following subsection describes the procedure of removing the unnecessary links for achieving the goal.

To begin with, $\boldsymbol{IV}^{\mathrm{CD}}$ is calculated from the adjacency matrix. Then, whether IV_S^{CD} is larger than any other $IV_{M_i}^{\mathrm{CD}}$ is checked. If not, one of the link between the master systems is removed. Based on the fact noted in the previous section, removing the link from the master system that has the smallest IV to the master system that has the largest IV is the effective way of averaging the IV of each system. Therefore, the link from the master system with the smallest IV that is expressed as M^{min} to the master system with the largest IV which is expressed as M^{max} is removed. Disconnecting the link changes the adjacency matrix; therefore, the IV is calculated again based on the renewed adjacency matrix. The process repeats until the desired relation between the slave and the masters regarding the IV which is shown in (6.15) is achieved. Fig. 6-4 describes the flow chart of the process.

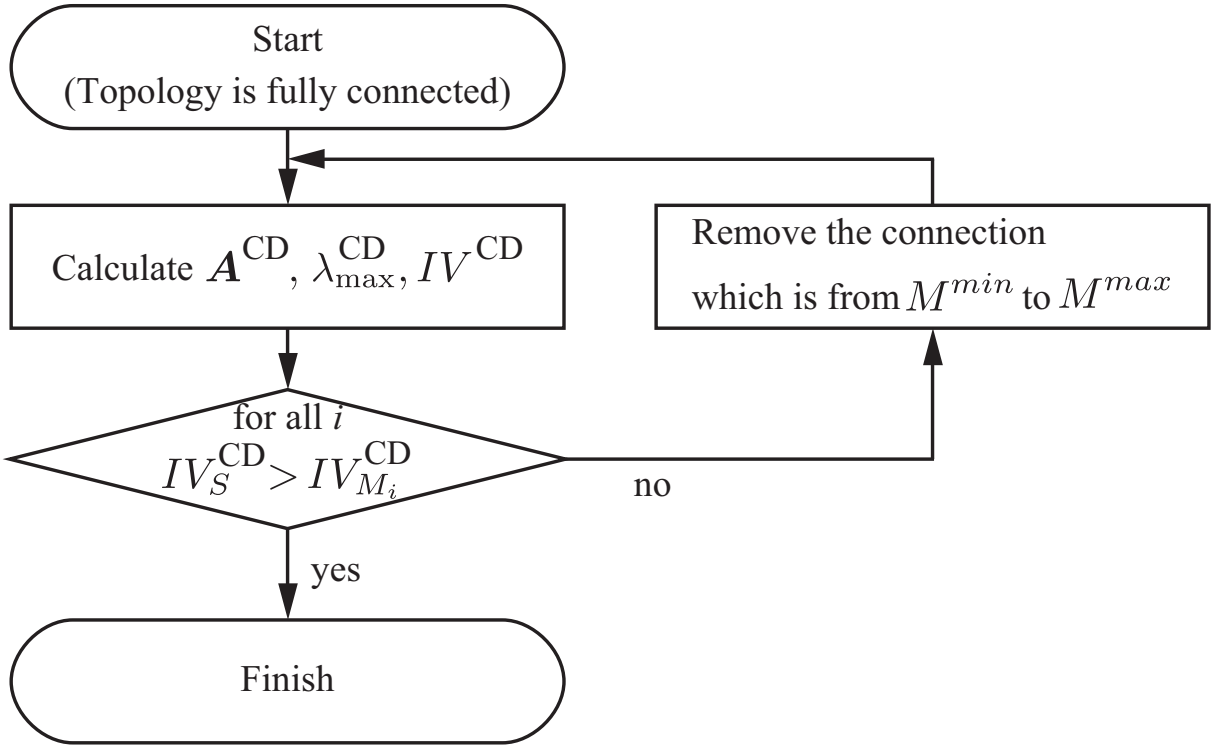

Fig. 6-4: Flow chart for realizing the designed topology.

The best way to derive the designed topology is to fully search all topology. Whether the flow chart does not give the optimized topology; however, it at least gives one of the topology that is near the optimal because of the characteristics. The flow chart is aimed to use in real time systems in future whose calculation cost is small compared to other methods.

When the number of a system becomes large, there is a situation where the IV of the slave system becomes the same as the IV of master systems. According to [79], links between master systems should be removed even if all of the IV is the same. Therefore, the IV in the slave system should be the largest in the overall system. This is the reason why (6.15) does not have an equal sign. Therefore, by using the flow chart, it is able to derive the topology that satisfies (6.15).

The following shows an example of selecting the best topology for relative motion. Assume that there are 4 agents in a system and the delay times in each link are $T_{12} = T_{21} = 0.04$ s, $T_{23} = T_{32} = 0.15$ s, $T_{34} = T_{43} = 0.12$ s, $T_{14} = T_{41} = 0.16$ s, $T_{13} = T_{31} = 0.04$ s, $T_{24} = T_{42} = 0.24$ s. The initial

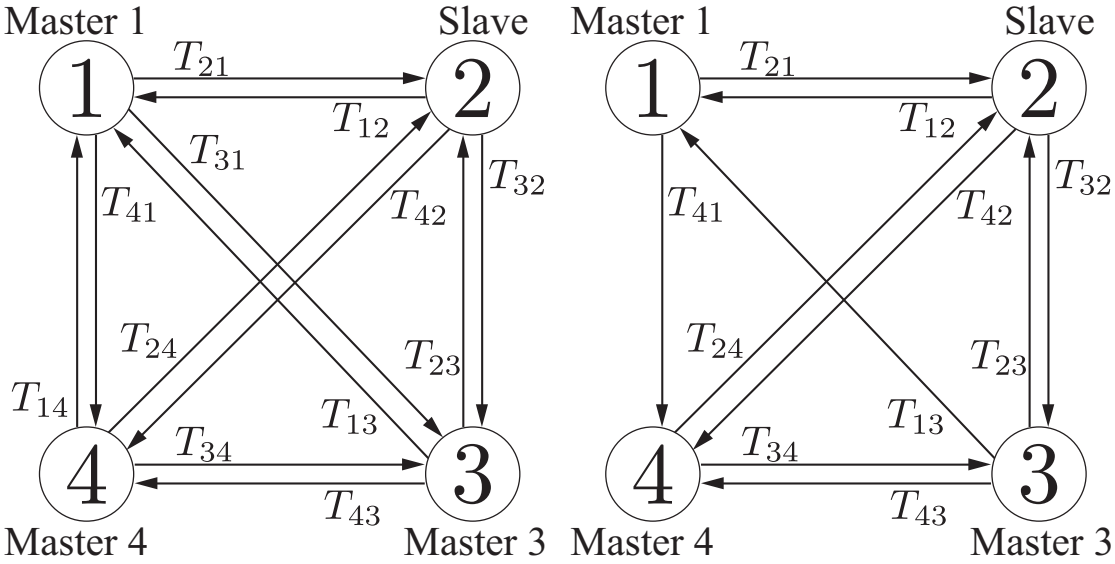

(a) Initial topology. (b) Designed topoloty.

Fig. 6-5: Connection link selection to fit the goal relation.

condition is described in Fig. 6-5(a). In the condition, the IV is calculated as follows:

$$\boldsymbol{IV}^{\mathrm{CD}^{1st}} = [0.258, 0.246, 0.270, 0.243]^T . \tag{6.16}$$

System 2 is assumed to be the slave system in the example, and IV_S^{CD} is not the largest. M^{max}, M^{min} is system 1 and 4, respectively. Therefore, the link from system 4 to system 1 is disconnected. Being the adjacency matrix updated, the value changes into

$$\boldsymbol{IV}^{\mathrm{CD}^{2nd}} = [0.21, 0.262, 0.27, 0.258]^T . \tag{6.17}$$

IV_S^{CD} is still not the largest, and M^{max}, M^{min} are system 3 and 1, respectively. Removing the connection from system 3 to 1, the renewed $\boldsymbol{IV}$ based on the updated adjacency matrix is calculated as

$$\boldsymbol{IV}^{\mathrm{CD}^{final}} = [0.220, 0.282, 0.222, 0.276]^T . \tag{6.18}$$

IV_S^{CD} is the largest; therefore, the goal relationship is achieved.

Based on the topology design, the control goals for the trajectory tracking is changed which is explained in the following. Since the COG mode equation does not change, only the relative motion mode equations change. The control goals of each system regarding the relative motion in the conventional

method are

$$\left\{\begin{array}{lcl} x_{d_1} &=& 3x_1 - x_2 - x_3 - x_4 \\ x_{d_2} &=& 3x_2 - x_3 - x_4 - x_1 \\ x_{d_3} &=& 3x_3 - x_4 - x_1 - x_2 \\ x_{d_4} &=& 3x_4 - x_1 - x_2 - x_3 \end{array}\right. = \left\{\begin{array}{l} 0 \\ 0 \\ 0 \\ 0 \end{array}\right. . \tag{6.19}$$

As for the proposed method, since some connections are removed, the control goals also changes. It is given as

$$\left\{\begin{array}{lcl} x_{d_1} &=& 2x_1 - x_2 - x_3 \\ x_{d_2} &=& 3x_2 - x_3 - x_4 - x_1 \\ x_{d_3} &=& 2x_3 - x_4 - x_2 \\ x_{d_4} &=& 3x_4 - x_1 - x_2 - x_3 \end{array}\right. = \left\{\begin{array}{l} 0 \\ 0 \\ 0 \\ 0 \end{array}\right. . \tag{6.20}$$

System 1 receives position responses from system 2 and 3; however, the system does not receive the response from system 4 because the connection is removed so that the desired topology in the relative motion is realized.

The control goals of the multilateral teleoperation shows that all master and slave systems actuates in the same direction. When a different operator in a different place try to operate each system differently, the motion of the master systems interferes. The main focus of the proposed method is to enhance the transmission ability of the tactile sensation from the slave system; therefore, it cannot reduce the interference when operators tried to actuate the system in the opposite direction. There are other reports which solve the problem of the interference by introducing identity ratio to separate the motion of master systems [102]; therefore, the interference of the master systems can be suppressed by using the method.

Final acceleration reference in this example is obtained as

$$\begin{aligned} \begin{bmatrix} \ddot{x}_1^{\mathrm{ref}} \\ \ddot{x}_2^{\mathrm{ref}} \\ \ddot{x}_3^{\mathrm{ref}} \\ \ddot{x}_4^{\mathrm{ref}} \end{bmatrix} = &- C_{\mathrm{f}} \begin{bmatrix} 1 & e^{-T_{12}s} & e^{-T_{13}s} & e^{-T_{14}s} \\ e^{-T_{21}s} & 1 & e^{-T_{23}s} & e^{-T_{24}s} \\ e^{-T_{31}s} & e^{-T_{32}s} & 1 & e^{-T_{34}s} \\ e^{-T_{41}s} & e^{-T_{42}s} & e^{-T_{43}s} & 1 \end{bmatrix} \begin{bmatrix} f_1 \\ f_2 \\ f_3 \\ f_4 \end{bmatrix} \\ &- C_{\mathrm{p}} \begin{bmatrix} 2 & -e^{-T_{12}s} & -e^{-T_{13}s} & 0 \\ -e^{-T_{21}s} & 3 & -e^{-T_{23}s} & -e^{-T_{24}s} \\ 0 & -e^{-T_{32}s} & 2 & -e^{-T_{34}s} \\ -e^{-T_{41}s} & -e^{-T_{42}s} & -e^{-T_{43}s} & 3 \end{bmatrix} \begin{bmatrix} x_1 \\ x_2 \\ x_3 \\ x_4 \end{bmatrix} . \end{aligned} \tag{6.21}$$

6.4 Performance Analysis

The performance of the proposed multilateral teleoperation is analyzed by using the fundamental matrix. The fundamental matrix in multilateral teleoperation is expressed as

$$\begin{bmatrix} f_1 \\ x_2 \\ x_3 \end{bmatrix} = \frac{1}{F_{\mathrm{den}}} \begin{bmatrix} F_{11} & F_{12} & F_{13} \\ F_{21} & F_{22} & F_{23} \\ F_{31} & F_{32} & F_{33} \end{bmatrix} \begin{bmatrix} x_1 \\ f_2 \\ f_3 \end{bmatrix}. \tag{6.22}$$

In an ideal condition where there is no delay between any system, the fundamental matrix should be as follows:

$$\boldsymbol{F}_{ideal} = \begin{bmatrix} 0 & -1 & -1 \\ 1 & 0 & 0 \\ 1 & 0 & 0 \end{bmatrix}. \tag{6.23}$$

Each element of the matrix can be obtained by using the acceleration reference of the system.For the simplicity, the delay time of the upstream and downstream are assumed to be the same as

$$T_{12} = T_{21} = T_1 \tag{6.24}$$

$$T_{23} = T_{32} = T_2 \tag{6.25}$$

$$T_{13} = T_{31} = T_3. \tag{6.26}$$

As for the conventional method, the elements are calculated as

$$F_{11} = -\frac{1}{C_{\mathrm{f}}}\left(s^2 + 2C_{\mathrm{p}}\right)^3 - \left(e^{-2T_1 s} + e^{-2T_2 s} + e^{-2T_3 s}\right) {C_{\mathrm{p}}}^2 (s^2 + 2C_{\mathrm{p}}) - 2e^{-(T_1+T_2+T_3)s} {C_{\mathrm{p}}}^3 \tag{6.27}$$

$$F_{12} = -C_{\mathrm{f}}(s^2 + 3C_{\mathrm{p}}) \left(e^{-T_1 s}(s^2 + 2C_{\mathrm{p}}) + e^{-(T_2+T_3)s} C_{\mathrm{p}}\right) \tag{6.28}$$

$$F_{13} = -C_{\mathrm{f}}(s^2 + 3C_{\mathrm{p}}) \left(e^{-T_2 s}(s^2 + 2C_{\mathrm{p}}) + e^{-(T_1+T_2)s} C_{\mathrm{p}}\right) \tag{6.29}$$

$$F_{21} = (s^2 + 3C_{\mathrm{p}}) \left(e^{-T_1 s}(s^2 + 2C_{\mathrm{p}}) + e^{-(T_2+T_3)s} C_{\mathrm{p}}\right) \tag{6.30}$$

$$F_{22} = -C_{\mathrm{f}} \left\{(1 - e^{-2T_1 s})(s^2 + 2C_{\mathrm{p}}) + \left(2^{-(T_1+T_2+T_3)s} - e^{-2T_2 s} - e^{-2T_3 s}\right) C_{\mathrm{p}}\right\} \tag{6.31}$$

$$F_{23} = \left(e^{-(T_1+T_3)s} - e^{-T_2 s}\right) C_{\mathrm{f}}(s^2 + 3C_{\mathrm{p}}) \tag{6.32}$$

$$F_{31} = (s^2 + 3C_{\mathrm{p}}) \left(e^{-T_3 s}(s^2 + 2C_{\mathrm{p}}) + e^{-(T_1+T_2)s} C_{\mathrm{p}}\right) \tag{6.33}$$

$$F_{32} = \left(e^{-(T_1+T_3)s} - e^{-T_2 s}\right) C_{\mathrm{f}}(s^2 + 3C_{\mathrm{p}}) \tag{6.34}$$

$$F_{33} = -C_{\mathrm{f}} \left\{(1 - e^{-2T_3 s})(s^2 + 2C_{\mathrm{p}}) - \left(e^{-(T_1+T_2+T_3)s} - e^{-2T_1 s} - e^{-2T_2 s}\right) C_{\mathrm{p}}\right\} \tag{6.35}$$

$$F_{\mathrm{den}} = (s^2 + 2C_{\mathrm{p}})^2 + \left(e^{-2T_1 s} + e^{-2T_3 s}\right) C_{\mathrm{p}}(s^2 + 2C_{\mathrm{p}}) + e^{-T_2 s} \left(2e^{-(T_1+T_3)s} - e^{-T_2 s}\right) {C_{\mathrm{p}}}^2 \tag{6.36}$$

Table 6.1: Controller parameters.

Parameter	Description	Value
K_p	Proportional gain (position controller)	900
K_d	Differential gain (position controller)	60
C_f	Proportional gain (force controller)	1

As for the proposed method, the elements are obtain as

$$F_{11} = -\frac{1}{C_\mathrm{f}}(s^2+2C_\mathrm{p})^2(s^2+C_\mathrm{p}) - \left(e^{-2T_1 s}+e^{-2T_2 s}\right){C_\mathrm{p}}^2(s^2+2C_\mathrm{p}) - e^{-(T_1+T_2+T_3)s}{C_\mathrm{p}}^3 \tag{6.37}$$

$$F_{12} = -e^{-T_1 s}C_\mathrm{f}(s^2+C_\mathrm{p})(s^2+5C_\mathrm{p}) \tag{6.38}$$

$$F_{13} = -C_\mathrm{f}\left\{e^{-T_3 s}(s^2+2C_\mathrm{p})^2 + e^{-(T_1+T_2)s}C_\mathrm{p}(s^2+3C_\mathrm{p}) - e^{-(2T_2+T_3)s}{C_\mathrm{p}}^2\right\} \tag{6.39}$$

$$F_{21} = e^{-T_1 s}(s^2+2C_\mathrm{p})^2 \tag{6.40}$$

$$F_{22} = -C_\mathrm{f}\left\{(1-e^{-2T_1 s})(s^2+2C_\mathrm{p})^2 + e^{-T_2 s}\left(e^{-(T_1+T_3)s} - e^{-T_2 s}\right)C_\mathrm{p}\right\} \tag{6.41}$$

$$F_{23} = -C_\mathrm{f}\left\{e^{-T_2 s}(s^2+3C_\mathrm{p}) - e^{-(T_1+T_3)s}(s^2+2C_\mathrm{p}) - e^{-(T_2+2T_3)s}C_\mathrm{p}\right\} \tag{6.42}$$

$$F_{31} = e^{-T_3 s}(s^2+2C_\mathrm{p})^2 + e^{-(T_1+T_2)s}C_\mathrm{p}(s^2+2C_\mathrm{p}) \tag{6.43}$$

$$F_{32} = \left(e^{-(T_1+T_3)s} - e^{-T_2 s}\right)C_\mathrm{f}(s^2+3C_\mathrm{p}) \tag{6.44}$$

$$F_{33} = -C_\mathrm{f}\left\{(1-e^{-2T_3 s})(s^2+2C_\mathrm{p}) - \left(e^{-(T_1+T_2+T_3)s} - e^{-2T_1 s} - e^{-2T_2 s}\right)C_\mathrm{p}\right\} \tag{6.45}$$

$$F_\mathrm{den} = (s^2+2C_\mathrm{p})^2 + e^{-2T_1 s}C_\mathrm{p}(s^2+2C_\mathrm{p}) + e^{-T_2 s}\left(e^{-(T_1+T_3)s} - e^{-T_2 s}\right){C_\mathrm{p}}^2 \tag{6.46}$$

It is important to analyze the relation between master and slave systems regarding the force and position responses because it directly shows the tactile sensation transmission performance. Putting it another way, the important point is how much the transfer function from the slave system to the master systems is close to 1. Therefore, the following part analyzes the transfer functions from the slave position response to the master position response and the slave force response to the master force response. To begin with, the transfer function of the force response of the slave system to the force response of the master system, which is the element F_{12}, is compared. In order to correspond the relationship between the IV and the transfer function, the dissertation compares the pole placement of the transfer function. Table 6.1 shows the parameters for each controller. Fig. 6-6 shows the conventional and proposed pole-zero placement of F_{12} near the origin. Comparing the damping ratio ξ of the dominant pole, it is smaller in the proposed method, meaning that it less causes vibration. That is proved by the fact that the biggest angle from the real axis becomes small in the proposed method.

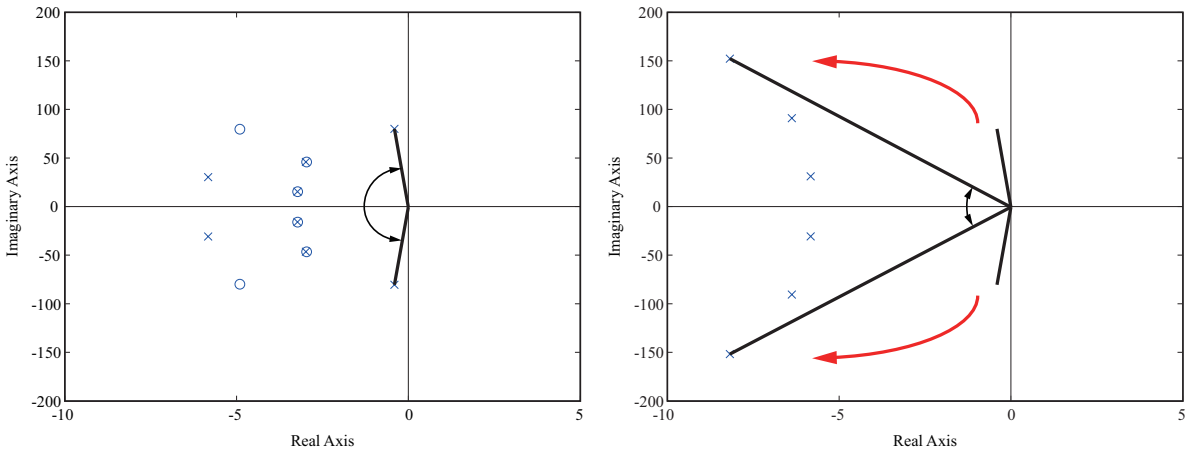

(a) Conventional method. (b) Proposed method.

Fig. 6-6: Pole-zero assignment of parameter F_{12}.

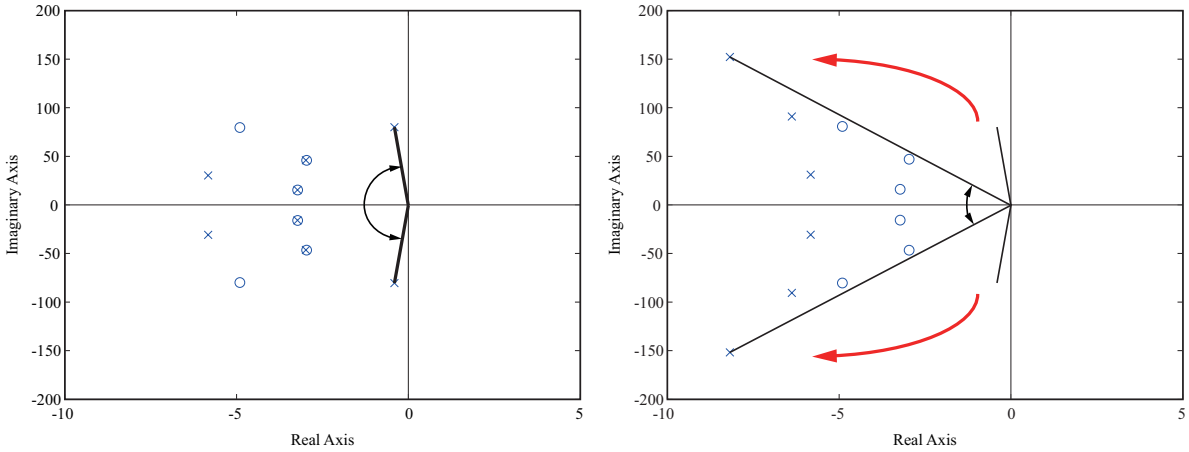

(a) Conventional method. (b) Proposed method.

Fig. 6-7: Pole-zero placement of parameter F_{21}.

At next, the transfer function from the position response of the slave system to the position response of the master system is compared. The delay time was approximated by using a pade approximation of 10th order in the analysis. Fig. 6-7 shows the conventional and proposed pole placement of F_{21} near the origin. The dominant damping ratio ξ is small in the proposed method which is Similar to the results of the F_{12}. Both transfer functions showed that proposed method shows better vibration suppression ability than the conventional method.

The operationality P_{o} and reproductivity P_{r} is also analyzed. Assuming the impedance of the environment as Z_2 and system 3 is not touched, the transfer function from the force input to the position

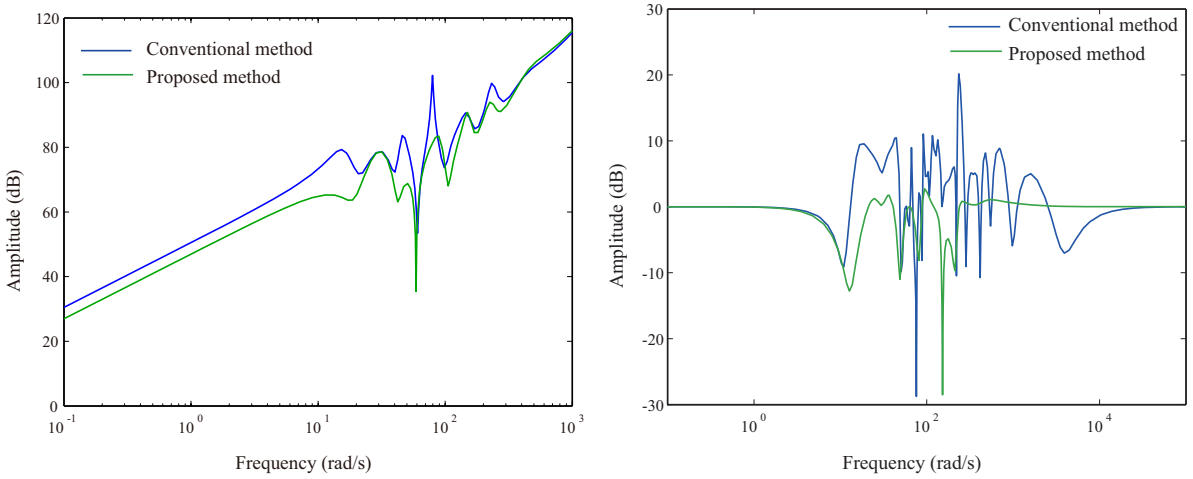

(a) Operationality. (b) Reproducibility.

Fig. 6-8: Bode diagram of the Operationality and Reproducibility.

response of system 1 is as follows:

$$\begin{aligned} f_1 &= \left(\frac{F_{11}}{1 - F_{22}Z_2} + \frac{F_{12}F_{21} - F_{11}F_{22}}{1 - F_{22}Z_2} Z_2 \right) x_1 \\ &= (P_\mathrm{o} + P_\mathrm{r} Z_2) x_1. \end{aligned} \tag{6.47}$$

The Bode diagram of each parameter is shown in Fig. 6-8. The amplitude of the operationality is smaller in the proposed method, which means that operator can manipulate the motor with less force in non-contact motion. On the other hand, the resonance of the reproductivity in the low frequency of the conventional method is attenuated in the proposed method which is around 30 to 150 rad/s.

6.5 Experiments

In order to confirm the validity of the proposed method, experiments are conducted. The experimental setup is shown in Fig. 6-9. Controller parameters are the same as Table 6.1. Both of the cut-off frequencies of DOB and RFOB are set as 1000 rad/s. An input motor is used to analyze the performance of the methods quantitatively. As for the conventional method, the topology that is fully connected is used. At

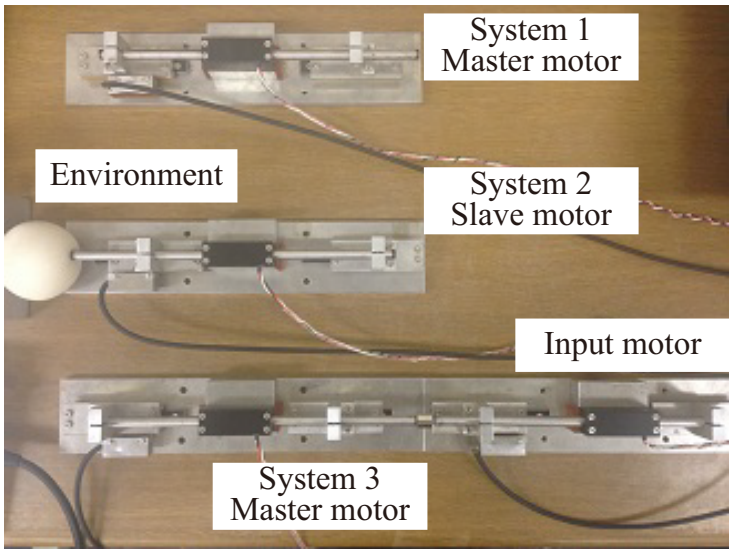

Fig. 6-9: Experimental setup.

first, the situation where there are three systems is assumed. The delay time are given as

$$T_{12} = T_{21} = 0.05 \text{ s}, \tag{6.48}$$

$$T_{23} = T_{32} = 0.15 \text{ s}, \tag{6.49}$$

$$T_{13} = T_{31} = 0.1 \text{ s}. \tag{6.50}$$

The initial topology (conventional method) is shown in Fig. 6-1(a), and the designed topology (proposed method) is shown in Fig. 6-1(b).

At first, free motion was compared between the conventional and proposed method. The same sinusoidal was used as an input to the input motor. The result is shown in Fig. 6-10. The input motor was attached to system 3. The amplitude of the position response is larger in the proposed method compared to the conventional method. This indicates the operational force is smaller in the proposed method.

At next, contact motion was compared. A step input was applied to the input motor, and a soft ball was selected as a contact object. F_{err} is a force error at the operating system, while x_{err1} indicates a position error of the system 1 and 2 and x_{err2} stands for the error of the system 1 and 3. Experimental results of the conventional topology are shown in Figs. 6-11 and 6-13. It has oscillation in the force response and the convergence of the position response is slow. On the other hand, by using the proposed system shown in Figs. 6-12 and 6-14, the force response less oscillates, and the convergence speed of the position response is fast meaning that systems have less interference in the proposed method.

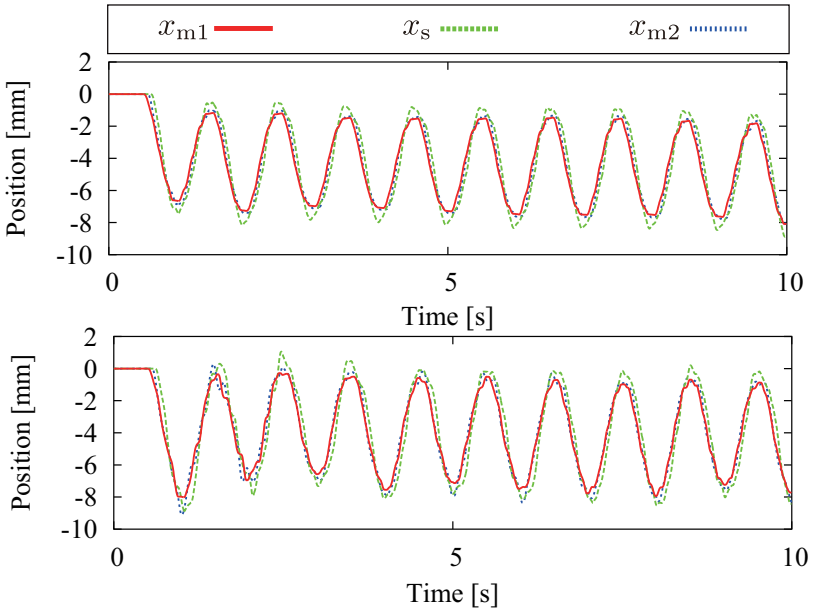

Fig. 6-10: Comparison of free motion results (upper result: conventional method, lower result: proposed method).

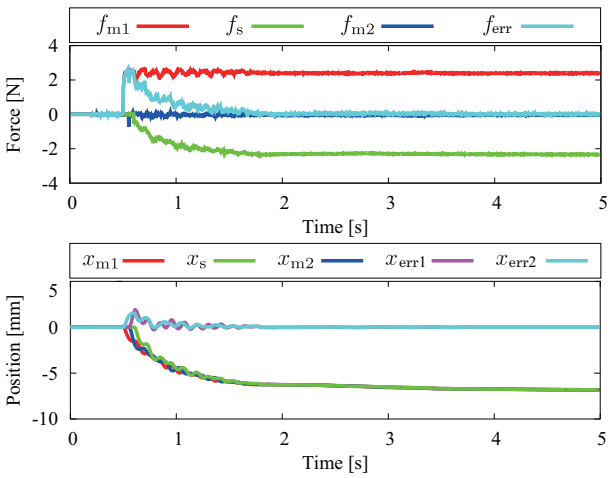

Fig. 6-11: Conventional method pushing system 1.

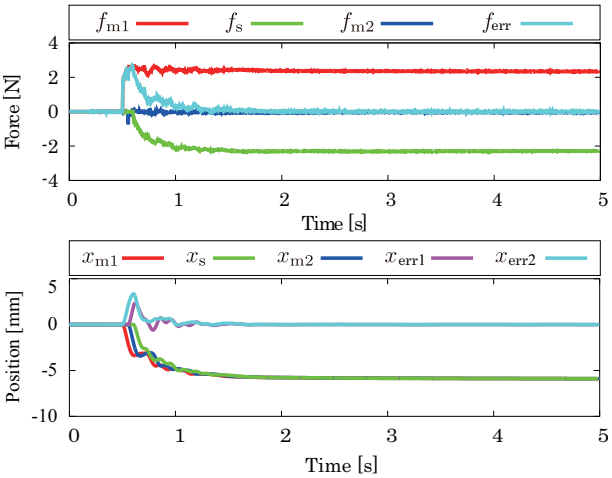

Fig. 6-12: Proposed method pushing system 1.

Both position and force responses from Figs. 6-11 to 6-14 show the same outcomes. The following part compares the convergence speed by approximating force error at the operating system as $f_{\mathrm{err}} = Ae^{-Bt}$ and the position error between system 1 and 2 as $x_{\mathrm{err1}} = Ae^{-Bt}$ respectively. At first, the force

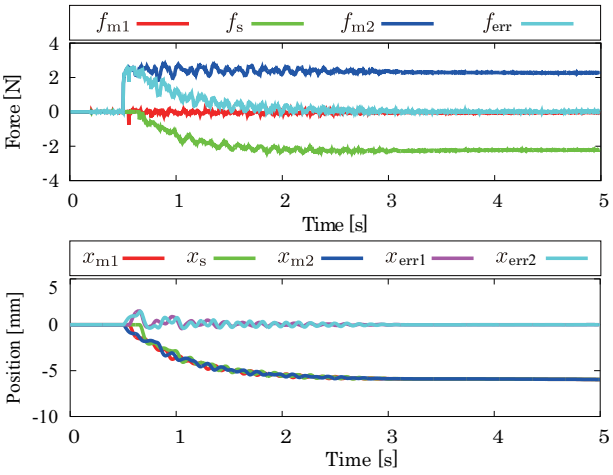

Fig. 6-13: Conventional method pushing system 3.

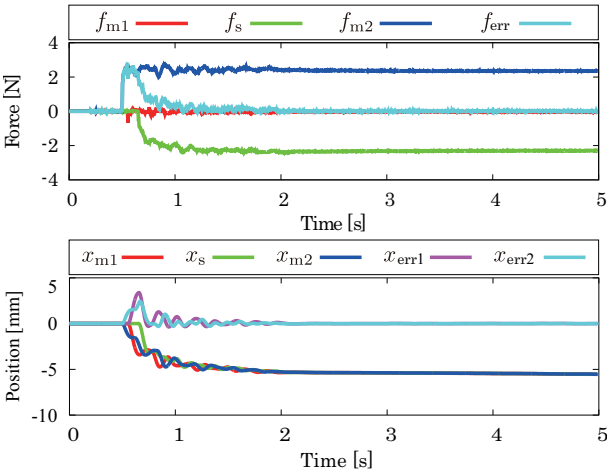

Fig. 6-14: Proposed method pushing system 3.

error is analyzed.

$$\begin{cases} f_{\mathrm{err}}^{\mathrm{Fig.9}} &= 1.891e^{-2.834t} \\ f_{\mathrm{err}}^{\mathrm{Fig.10}} &= 1.254e^{-3.145t} \\ f_{\mathrm{err}}^{\mathrm{Fig.11}} &= 1.899e^{-1.901t} \\ f_{\mathrm{err}}^{\mathrm{Fig.12}} &= 0.678e^{-2.437t} \end{cases}. \tag{6.51}$$

Both the amplitude A and time constant B are improved by comparing the conventional method and the proposed method. As for the position errors, they were obtained as

$$\begin{cases} x_{\mathrm{err1}}^{\mathrm{Fig.9}} &= 0.0005e^{-2.471t} \\ x_{\mathrm{err1}}^{\mathrm{Fig.10}} &= 0.0006e^{-3.145t} \\ x_{\mathrm{err1}}^{\mathrm{Fig.11}} &= 0.0005e^{-1.489t} \\ x_{\mathrm{err1}}^{\mathrm{Fig.12}} &= 0.001e^{-2.223t} \end{cases}. \tag{6.52}$$

The amplitude of the error is larger in the proposed method than that of the conventional method; however, the time constant of the proposed method is smaller than that of the conventional method.

To verify the topology in the proposed method is the best, the following results show when different communication links are removed. Firstly evaluates the topology shown in Fig. 6-15(a). One additional connection link is disconnected from the proposed method, which is from system 1 to 3.

Figs. 6-16 and 6-17 show the results of pushing each master system in topology 1. Comparing the experimental result of pushing system 1 with the conventional and proposed method, the convergence speed in the force error was fast compared with the conventional method and was almost the same with the proposed method; however, the oscillation regarding the position response was the largest in the three. The same explanation can be made to the result when pushing system 3. The position response oscillation

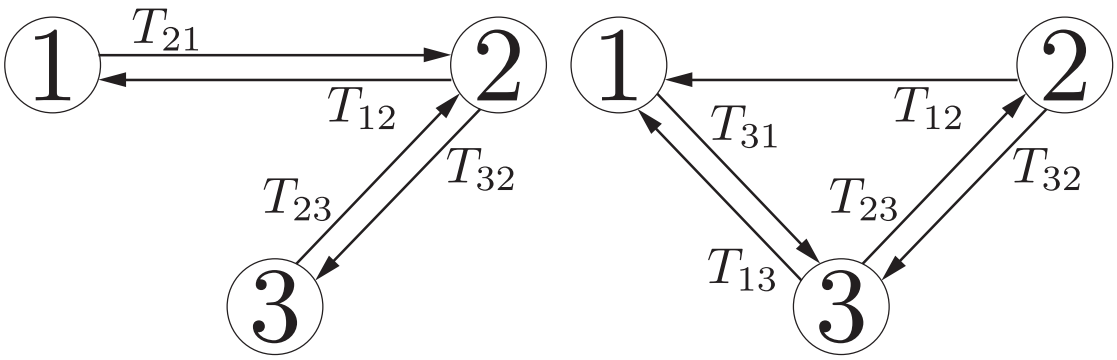

(a) Comparison topology 1. (b) Comparison topology 2.

Fig. 6-15: Topologies for comparison.

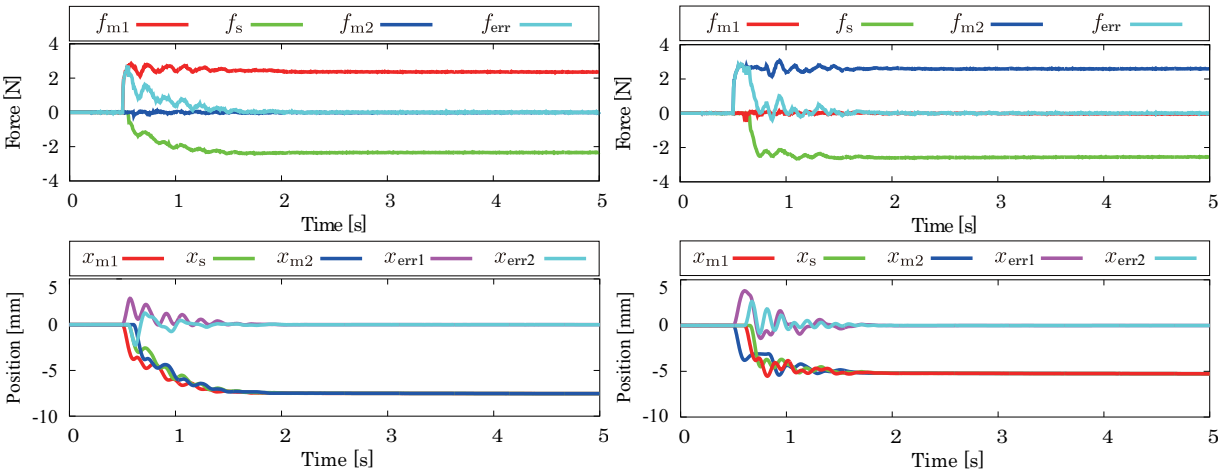

Fig. 6-16: Comparison topology 1 when pushing system 1.

Fig. 6-17: Comparison topology 1 when pushing system 3.

is caused by removing too much connection links. This results support the fact that the number of links to remove should be minimum.

At next, the experimental results of topology 2 are shown in Figs. 6-18 and 6-19. Topology 2 is shown in Fig. 6-15(b). The IV for this topology in each system is calculated as

$$\boldsymbol{IV}^{\mathrm{CD}}_{\mathrm{topology2}} = [0.462, 0.312, 0.226]^T . \tag{6.53}$$

This topology is designed so that the slave system contains the least IV. The IV of the slave system is the second largest in the conventional topology and is the largest in the designed topology.

Fig. 6-18 shows the result when pushing system 1. The position response error was almost zero because the IV of system 1 was the largest. The IV represents the amount of the influence to other systems

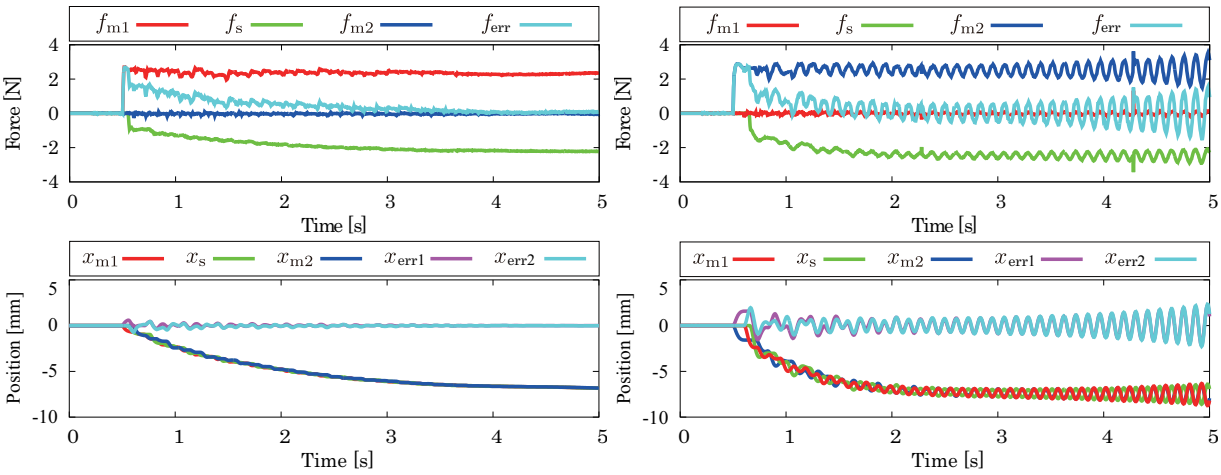

Fig. 6-18: Comparison topology 2 pushing system 1.

Fig. 6-19: Comparison topology 2 pushing system 3.

Table 6.2: Experimental parameters using four agents.

Parameter	Description	Value
T_s	Sampling time	0.5 ms
M_{n}	Nominal motor mass	0.23 kg
K_{p}	Proportional gain for position control	1200
K_{d}	Differential gain for position control	34.6
C_{f}	Proportional gain for force control	0.7
g_{dis}	Cut-off frequency of DOB	500 rad/s
g_{reac}	Cut-off frequency of RFOB	500 rad/s

as it is previously mentioned. Every system mostly followed the position response of the system 1 than system 2 that is the slave system; therefore, although the position error during in the transient response was the smallest, the convergence speed of the force error was slower than that of the conventional method. Fig. 6-19 shows the result of pushing system 3. The oscillation did not converge, and the stable result could not be obtained.

In the following, experimental results when there are four agents are compared between the conventional method and the proposed method. Experimental parameters are shown in Table 6.2. Both free motion and contact motion were compared between the conventional and proposed method. Contact motion is expressed as the gray zone in the experimental results, while free motion is described before the gray area. Fig. 6-5(a) shows the conventional system connection and Fig. 6-5(b) shows the proposed system connection. Figs. 6-20 and 6-21 show the experimental results where the master systems were

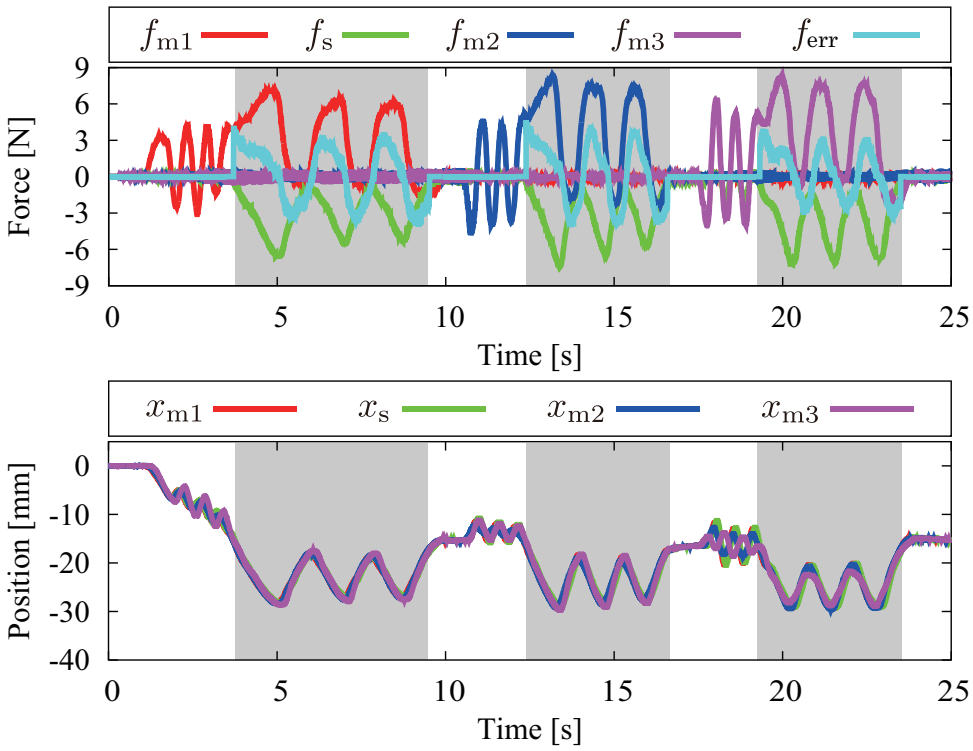

Fig. 6-20: Conventional multilateral teleoperation using four systems.

operated by a human.

At first, the experimental result of free motion is compared. When almost same force is applied, the amount of the movement in the proposed method is larger than that of the conventional method. It means that the proposed method have operational force compared to the conventional method.

At next, the experimental result of contact motion is compared by using f_{err}. f_{err} in Fig.6-20 and 6-21 show the force error during contact motion from the operating system. The smaller the value is, the more the law of action and reaction is realized. The value is evaluated by the root mean square error (RMSE). While the RMSE of the conventional method was 3.98 N, the RMSE of the proposed method was 2.16 N. The results show that the force error during the contact motion reduced to 54%. It indicates that the operator can perceive the tactile sensation of the contact object (a soft ball) more precisely. In this experiment, system 4 was set to be the most distant system from the slave system. The experimental result demonstrates that the proposed method can transmit precise tactile sensation to a master system that is located further from the slave system since the force error was reduced to 47 % in system 4.

The links are disconnected to enhance the transmission ability of sharing tactile sensation in the slave

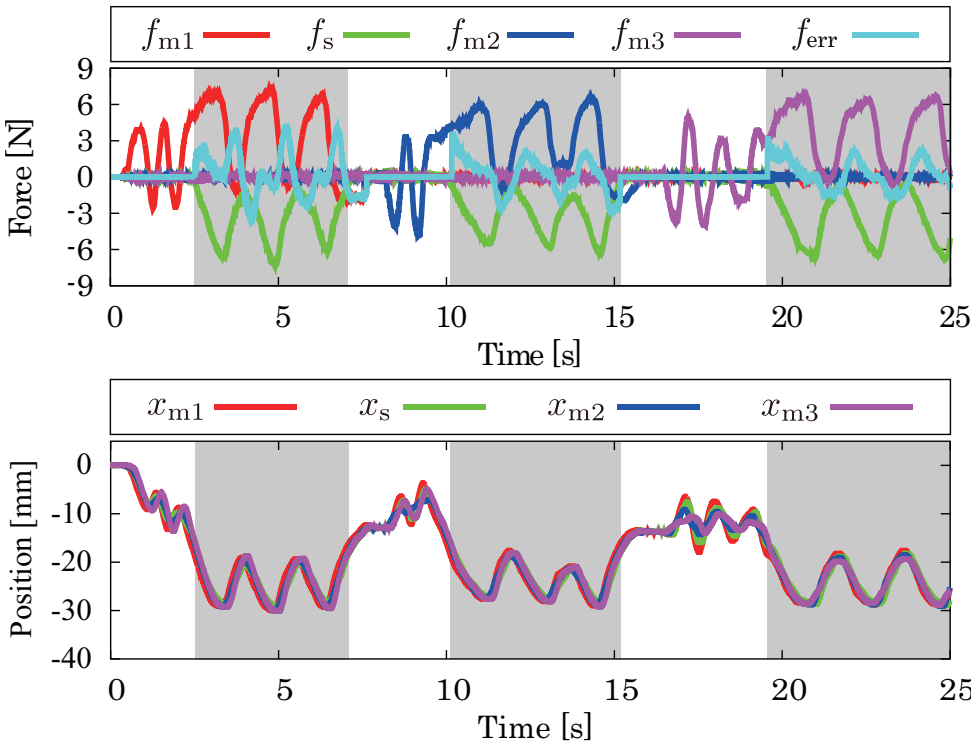

Fig. 6-21: Proposed multilateral teleoperation using four systems.

system. The experimental results show that the proposed method reduced the operational force and regained the reproductivity of the environment. Therefore, the results show that there are no disadvantages caused by removing the appropriate links based on the chart shown in Fig. 6-4.

The results indicate that the proposed system whose topology for the relative motion mode is designed have good tactile sensation transmission performance because the proposed system offers more vivid response than the conventional method.

6.6 Summary of Chapter 6

In this chapter, the topology for the relative motion was designed in multilateral teleoperation. The index that quantifies the equivalent amount of information that each system contains was proposed. It was defined as information value in this chapter, and it can be calculated by obtaining the eigenvectors of the maximum eigenvalue of the adjacency matrix that contains a delay element. The most important part in tactile sensation transmission is to transmit precise impedance of a contact object to master systems. Therefore, the topology of the relative motion was designed so that the information value of the slave system becomes the largest among all systems. The design flow to design the topology was proposed, and the experimental results showed that the convergence of position and force response were faster compared to the multilateral teleoperation system whose topology is not modified.

Chapter 7

Simultaneous Presentation of Thermal and Tactile Sensations Using Multilateral Teleoperation

---

This chapter proposes a multilateral teleoperation system that simultaneously presents tactile and thermal sensations. For more realistic communication with remote places, it is important to transmit not only tactile sensation but also thermal sensation so that the operator could obtain more information about the remote system.

7.1 Introduction of Chapter 7

The contents of this chapter are given as follows. In Section 7.1, the Peltier device is modeled by using a thermal network method, and then, the disturbance observer was applied to realize robust heat flow control. Section 7.2 describes the design methodology to realize simultaneous presentation of tactile and thermal sensations. Since the response speed of each actuator is different, an artificial buffer is inserted to correct the timing of the presentation. The experimental results are shown in Section 7.3 to verify the validity of the proposed method. Section 7.4 concludes this chapter.

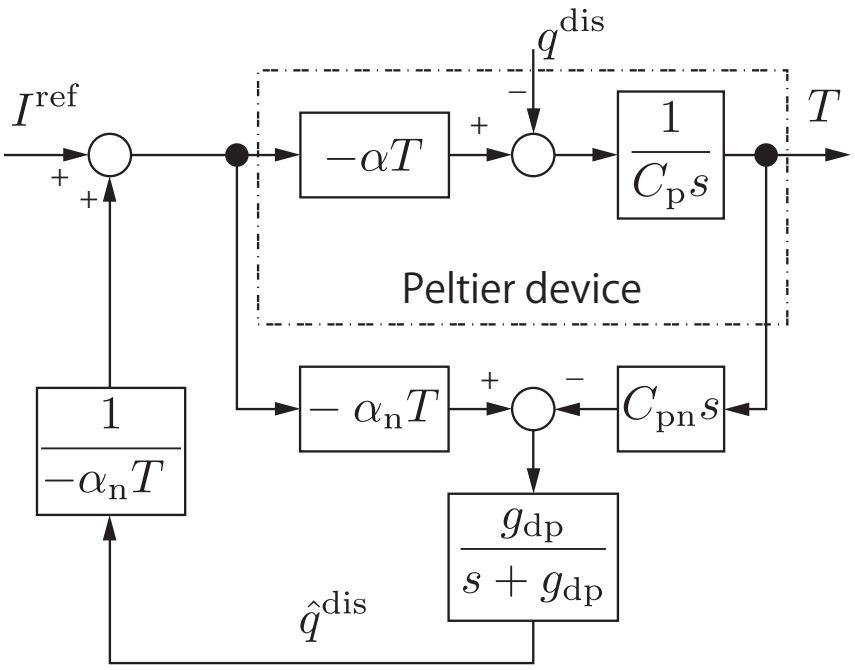

Fig. 7-1: Peltier device with disturbance observer.

7.2 Modeling and Robust Heat Flow Control of Peltier Device

7.2.1 Modeling of Peltier Device

In this section, the Peltier device is used as an actuator for presenting thermal sensation. As for the tactile sensation presentation, a robot manipulator is used. Since robust acceleration control using the DOB is already explained in Chapter 2, in the following, the DOB is applied to the Peltier device to construct the robust heat flow control system.

Firstly, the following part models the Peltier device. The Peltier device is actuated by applying DC current to generate heat transfer as

$$q = -\alpha T I + \frac{1}{2} R_{\mathrm{p}} I^2, \tag{7.1}$$

where I, α, T, R_{p} stand for applied current, Seebeck coefficient, the temperature of the Peltier device, and the electrical resistance inside the Peltier device, respectively. The Peltier device absorbs heat when forward current is applied; therefore, there is a minus sign in (7.1). The second term in (7.1) represents the Joule heat.

The modeling of the Peltier device is done using the thermal network method [103]. By using the

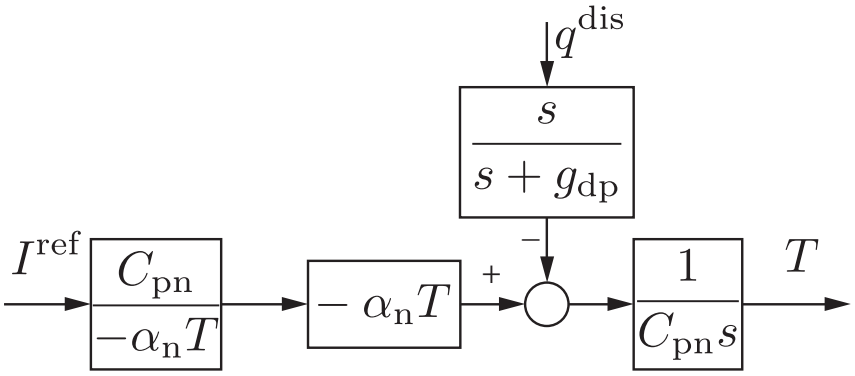

Fig. 7-2: Robust heat flow control of a thermal system.

method, the temperature difference of the Peltier device can be expressed as

$$C_{\mathrm{p}}\frac{dT}{dt} = -q^{\mathrm{ref}} + q^{\mathrm{dis}}, \tag{7.2}$$

where C_{p}, q_{in}, and q_{dis} stand for the heat conductance, heat flow reference, and the disturbance heat flow of the Peltier device, respectively.

7.2.2 Robust Heat Flow Control Using Disturbance Observer

The block diagram when the disturbance observer is applied to the Peltier device is shown in Fig. 7-1 and the equivalent transformation is shown in Fig. 7-2. By using the disturbance observer, the control structure which is robust against modeling errors, Joule heat, and disturbance heat flow is constructed.

The block diagram of the Peltier devices can be treated as Fig. 7-2 by applying the disturbance observer.

7.3 Modal Transformation Matrix for Simultaneously Presenting Thermal and Tactile Sensations

As mentioned in previous sections, when there is a time delay between subsystems, each controller interfere. In this section, subsystem 1 is the slave system, and subsystem 2 and 3 are master systems, and in order to compensate the limitation of motion area, the movement of master systems are scaled by using a scaling gain. The mode decoupling matrix $\boldsymbol{\mathcal{Q}}_{\mathrm{SIM}}$ that is used regarding tactile sensation is

defined as

$$\boldsymbol{\mathcal{Q}}_{\mathrm{SIM}}^{\mathrm{f}} = \begin{bmatrix} 1 & ae^{-T_{12}s} & be^{-T_{13}s} \\ -e^{-T_{21}s} & 2a & -be^{-T_{23}s} \\ -e^{-T_{31}s} & -ae^{-T_{32}s} & 2b \end{bmatrix}, \tag{7.3}$$

where a and b stand for the scaling gain of system 2 and 3, respectively. The subscript $_{\mathrm{SIM}}$ stands for the matrix for simultaneous presentation. However, the response speed of a Peltier device is slower than a robot manipulator. Therefore, the quarry matrix for force sensation transmission artificially inserts a buffer time to correct the timing for the simultaneous presentation. The proposed quarry matrix is written as

$$\boldsymbol{\mathcal{Q}}_{\mathrm{SIM}}^{\mathrm{f}} = \begin{bmatrix} 1 & ae^{-(T_{12}+T_{\mathrm{b}})s} & be^{-(T_{13}+T_{\mathrm{b}})s} \\ -e^{-(T_{21}+T_{\mathrm{b}})s} & 2a & -be^{-(T_{23}+T_{\mathrm{b}})s} \\ -e^{-(T_{31}+T_{\mathrm{b}})s} & -ae^{-(T_{32}+T_{\mathrm{b}})s} & 2b \end{bmatrix}, \tag{7.4}$$

where T_{b} stands for the buffered time. The timing that human recognizes the hardness and hotness of a contact object can be corrected by additionally inserting a delay element. The method has a high affinity to network systems because it naturally includes a time delay element inside the control system. The buffer can also be used for jitter buffering.

As for thermal sensation transmission, the modal transformation matrix is defined as

$$\boldsymbol{\mathcal{Q}}_{\mathrm{SIM}}^{\mathrm{t}} = \begin{bmatrix} 1 & e^{-T_{12}s} & e^{-T_{13}s} \\ -e^{-T_{21}s} & 2 & -e^{-T_{23}s} \\ -e^{-T_{31}s} & -e^{-T_{32}s} & 2 \end{bmatrix}, \tag{7.5}$$

The control goals are thus defined as

$$\begin{cases} F_1 + ae^{-(T_{12}+T_{\mathrm{b}})s}F_2 + be^{-(T_{13}+T_{\mathrm{b}})s}F_3 &= 0 \\ -e^{-(T_{21}+T_{\mathrm{b}})s}X_1 + 2aX_2 - be^{-(T_{23}+T_{\mathrm{b}})s}X_3 &= 0 \\ -e^{-(T_{31}+T_{\mathrm{b}})s}X_1 - ae^{-(T_{32}+T_{\mathrm{b}})s}X_2 + 2bX_3 &= 0 \end{cases}, \tag{7.6}$$

$$\begin{cases} q_1 + e^{-T_{12}s}q_2 + e^{-T_{13}s}q_3 &= 0 \\ -e^{-T_{21}s}T_1 + aT_2 - e^{-T_{23}s}T_3 &= 0 \\ -e^{-T_{31}s}T_1 - e^{-T_{32}s}T_2 + 2T_3 &= 0 \end{cases}. \tag{7.7}$$

The inverse matrix of (7.3) is calculated as

$$\boldsymbol{\mathcal{Q}}_{\mathrm{SIM}}{}^{-1} = \begin{bmatrix} -ab(e^{-(T_{23}+T_{32}+2T_{\mathrm{b}})s} - 4) & -ab(2e^{-(T_{12}+T_{\mathrm{b}})s} + e^{-(T_{13}+T_{32}+2T_{\mathrm{b}})s}) & -ab(2e^{-(T_{13}+T_{\mathrm{b}})s} + e^{-(T_{12}+T_{23}+2T_{\mathrm{b}})s}) \\ b(2e^{-(T_{21}+T_{\mathrm{b}})s} + e^{-(T_{23}+T_{31}+2T_{\mathrm{b}})s}) & b(2 + e^{-(T_{13}+T_{31}+2T_{\mathrm{b}})s}) & b(e^{-(T_{23}+T_{\mathrm{b}})s} - e^{-(T_{13}+T_{21}+2T_{\mathrm{b}})s}) \\ a(2e^{-(T_{31}+T_{\mathrm{b}})s} + e^{-(T_{21}+T_{32}+2T_{\mathrm{b}})s}) & a(e^{-(T_{32}+T_{\mathrm{b}})s} - e^{-(T_{12}+T_{31}+2T_{\mathrm{b}})s}) & a(2 + e^{-(T_{12}+T_{21}+2T_{\mathrm{b}})s}) \end{bmatrix} \tag{7.8}$$

Transparency of the proposed method for tactile sensation is analyzed using the fundamental matrix which is calculated as

$$\boldsymbol{F}^{\mathrm{f}} = \begin{bmatrix} \dfrac{3s^2}{e^{-(T_{31}+T_{\mathrm{b}})s}C_{\mathrm{f}}} & -a\dfrac{e^{-(T_{32}+T_{\mathrm{b}})s}}{e^{-(T_{31}+T_{\mathrm{b}})s}} & -b\dfrac{1}{e^{-(T_{31}+T_{\mathrm{b}})s}} \\ \dfrac{1}{a}\dfrac{e^{-(T_{21}+T_{13}+2T_{\mathrm{b}})s}+2e^{-(T_{23}+T_{\mathrm{b}})s}}{e^{-(T_{12}+T_{23}+2T_{\mathrm{b}})s}+2e^{-(T_{13}+T_{\mathrm{b}})s}} & 0 & 0 \\ \dfrac{1}{b}\dfrac{4-e^{-(T_{12}+T_{21}+2T_{\mathrm{b}})s}}{e^{-(T_{12}+T_{23}+2T_{\mathrm{b}})s}+2e^{-(T_{13}+T_{\mathrm{b}})s}} & 0 & 0 \end{bmatrix}. \tag{7.9}$$

Eq. (7.9) indicates that even artificial buffer and scaling gains are inserted, the transparency does not change in the proposed method.

7.4 Experiments

In order to confirm the validity of the proposed method, experiments were conducted. The experimental setup is shown in Fig. 7-3. Assuming the sensation transmission to a remote place, delay time was 50 ms constant delay with jitter in the experiments. The response of each subsystem is transmitted to each subsystem through UDP communication. 6 DOF robot manipulators were placed as an actuator for transmitting force sensation, and the Peltier devices are placed at the end effector of the manipulators for thermal sensation transmission. A temperature and heat flow sensors are attached to the Peltier device, and a position encoder is used to detect the position of each motor. As for the force response, a reaction force observer is used to estimate the external force.

The parameters used in the experiments are shown in Table 7.1.

At first, experiment using only manipulators are shown. The time delay between master systems are shown in Fig. 7-4. 50 ms delay was artificially buffered in the program. Since each response is transmitted by using UDP communication, jitter occurs between the communication.

Contact motion results are shown in Fig. 7-5. After the steady contact, pushing motion was conducted. Human operated master 1 in the experiment. In the conventional method, there are significant position errors, especially in the pushing motion. This is because force response interferes the position control loop to deteriorate the trajectory tracking performance. On the other hand, position error in the proposed method is well attenuated. It means the operator can feel much precise impedance of the contact object in the proposed method.

The modal space response is compared to see whether modal space response is decoupled. The results are given from Fig. 7-6 to Fig. 7-8. Fig. 7-6 shows the force response of the COG motion in each

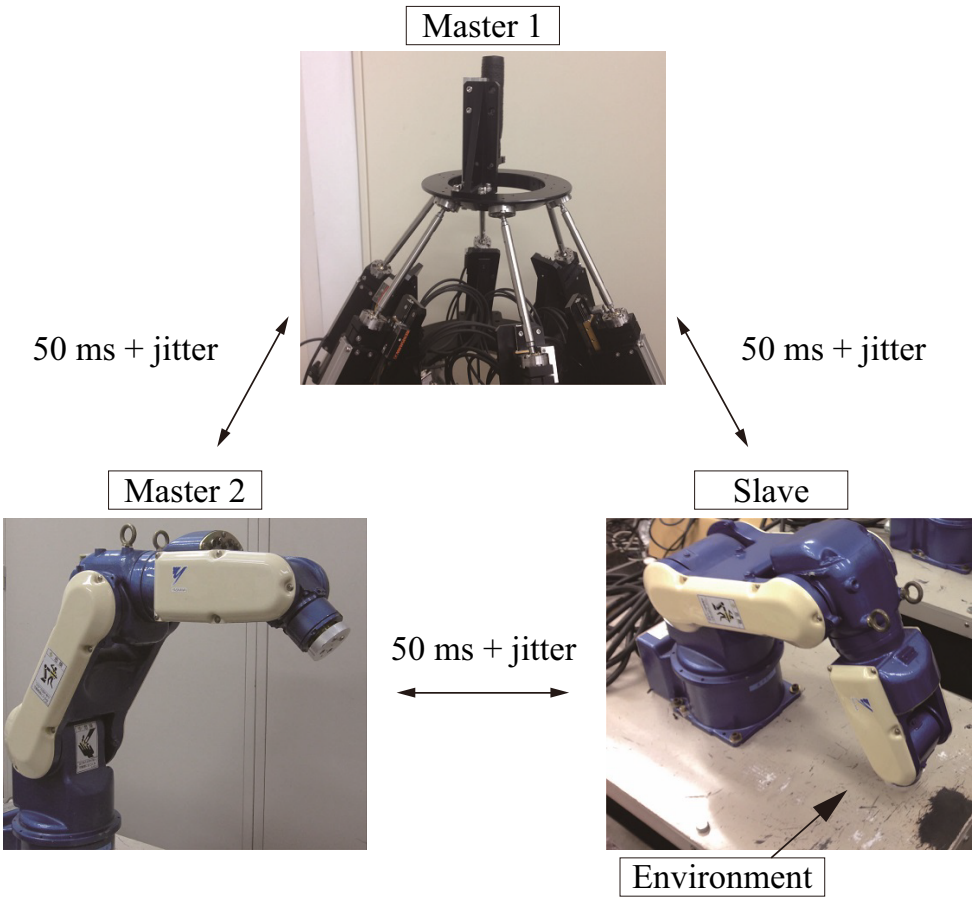

Fig. 7-3: Experimental setup.

subsystem, while Figs. 7-7 and 7-8 show the response of the relative motion modes in each subsystem. Since there are three subsystems, two relative motions can be defined. The control goals in multilateral teleoperation are to reduce the modal response errors to zero. Overall, the errors in the conventional method are much larger compared to the proposed method. As for each mode, the same acceleration reference is applied to each motor in the proposed method. This is the reason of the relative motion responses being symmetric. The acceleration reference of every mode in the conventional method is generated in each subsystem; therefore, the modal space response is not symmetric to each other.

In the following, experimental results of simultaneous presentation are explained. A cold aluminum plate was used as a contact object. After the contact motion becomes steady, pushing motion to the environment was conducted to examine whether each controller is decoupled from the other controllers.

The method which does not decouple the modes was selected as a conventional method. The exper-

Table 7.1: Experimental parameters for simultaneous sensation presentation.

Parameter	Description	Value
T_s	Sampling time	0.5 ms
K_{pm}	Proportional gain for position control	160
K_{dm}	Differential gain for position control	25.3
C_{fm}	Proportional gain for force control	1.0
g_{dm}	Cut-off frequency of DOB for motor	1000 rad/s
g_{rm}	Cut-off frequency of RFOB for motor	1000 rad/s
K_{pt}	Proportional gain for temperature control	0.7
K_{pf}	Proportional gain for heat flow control	1.0
g_{dp}	Cut-off frequency of DOB for Peltier device	1.0 rad/s
g_{rp}	Cut-off frequency of HIOB for Peltier device	6.28 rad/s
a	Scaling gain for system 2	6
b	Scaling gain for system 3	6
T_{b}	Artificial buffer for presentation timing correction	50 ms

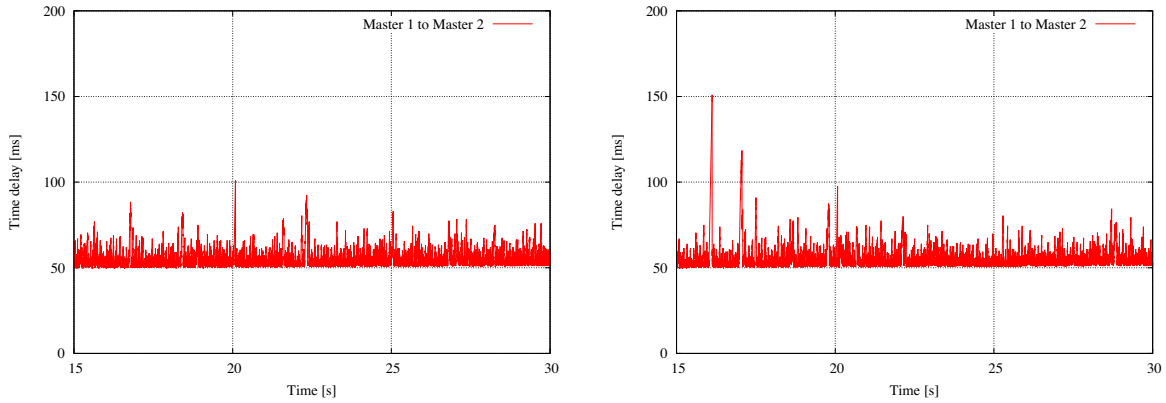

(a) Conventional method.

(b) Proposed method.

Fig. 7-4: Measured delay time between master system (one way).

imental results of the conventional method are shown in Fig. 7-9. Red and green lines represent the response of master systems, while blue lines show the response of the slave system. The effect of the modes not decoupled can especially be seen in the position and temperature responses. It takes several seconds for each response to converging to the same response, especially, the temperature response takes about 10 seconds for the convergence. The reason is the controllers in the conventional method is interfering with each other. The effect of external force appears inside the position control loop, and the external force affects the response of temperature control.

On the contrary, the experimental results of the proposed method are shown in Fig. 7-10. Compared to

the conventional method, position and temperature errors between subsystems are well suppressed. It is because the modes are decoupled. As for the temperature response, the convergence time was shortened up to 3 seconds which is three times faster compared to the conventional method. It can also be seen that the timing of presenting each sensation was collected by inserting the buffer to the modal transformation matrix of force sensation. The operator was able to feel the hardness and the coldness of the contacting object more naturally in the proposed method. Therefore, it can be said that precise multimodal sensation transmission was realized in the proposed method.

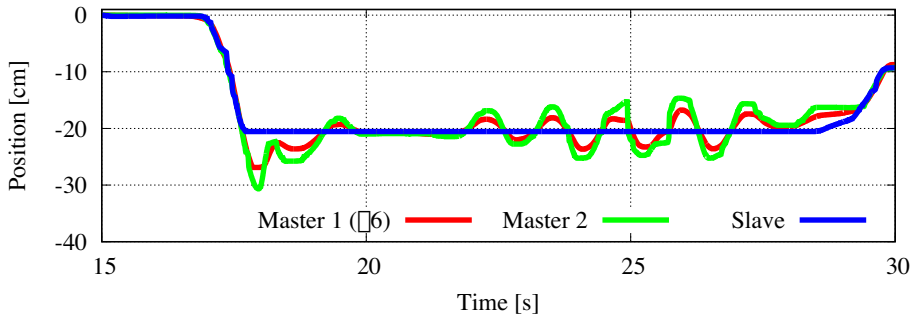

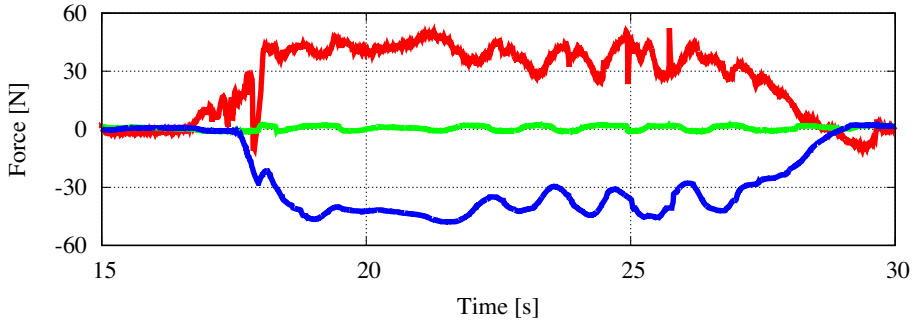

(a) Conventional method.

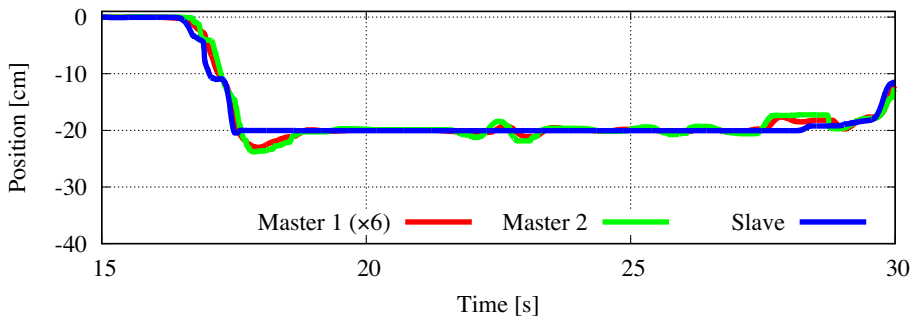

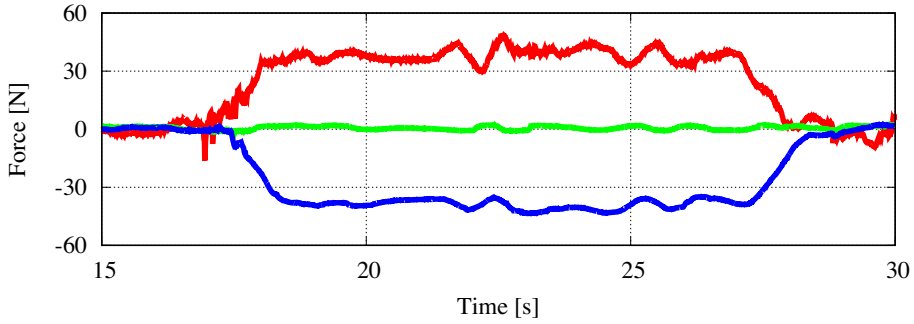

(b) Proposed method.

Fig. 7-5: Contact motion result to aluminum plate.

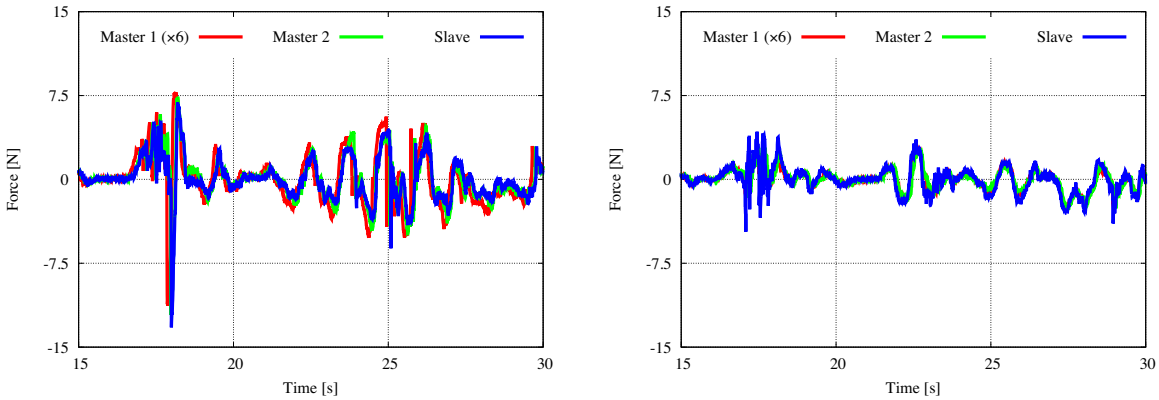

(a) Conventional method. (b) Proposed method.

Fig. 7-6: Force response of the COG motion in contact motion.

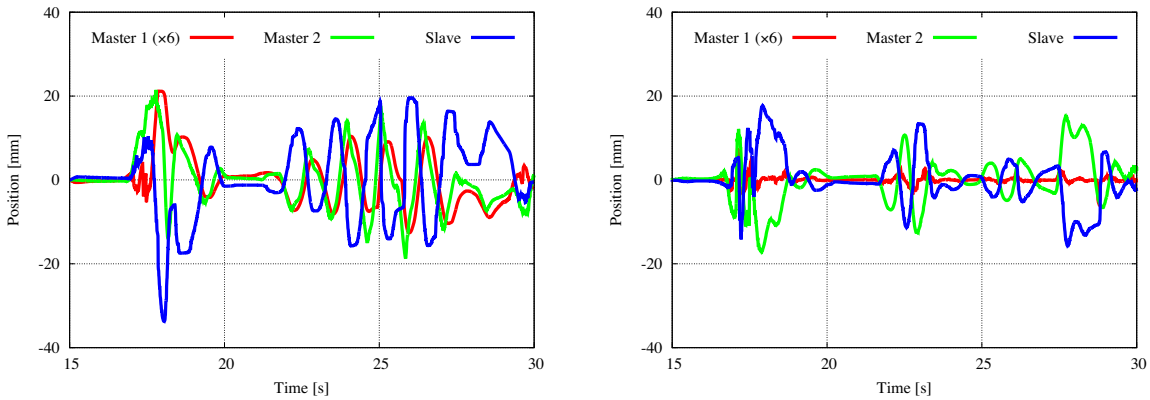

(a) Conventional method. (b) Proposed method.

Fig. 7-7: 1st relative motion mode response in contact motion.

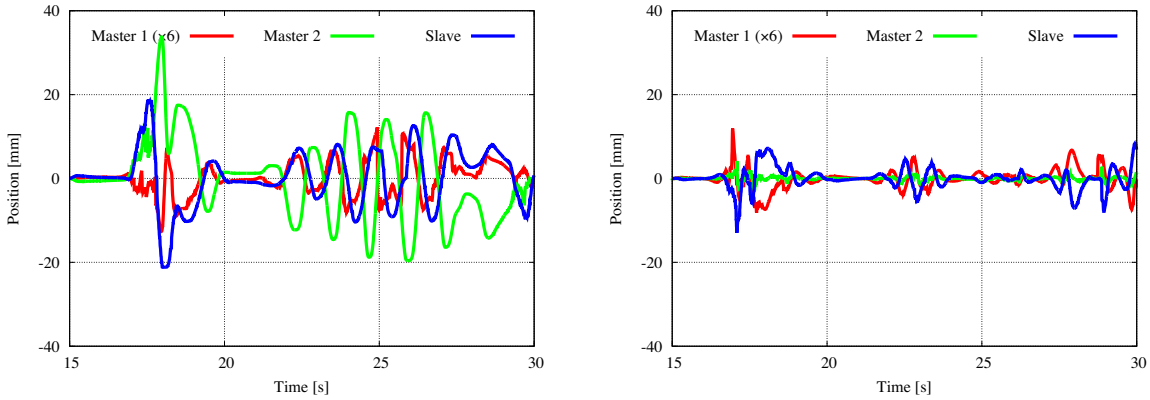

(a) Conventional method. (b) Proposed method.

Fig. 7-8: 2nd relative motion mode response in contact motion.

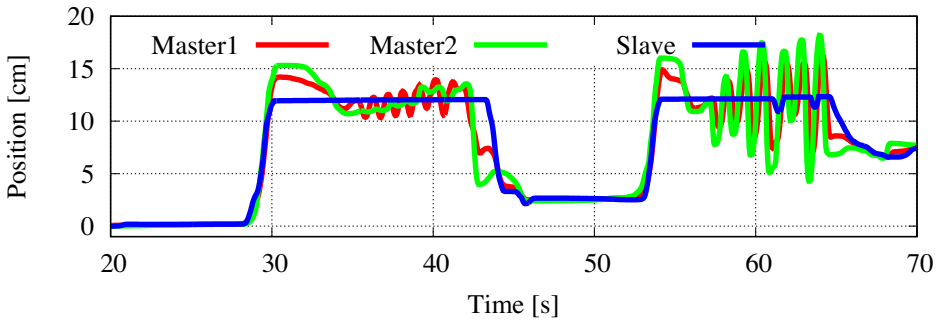

(a) Tactile sensation transmission response.

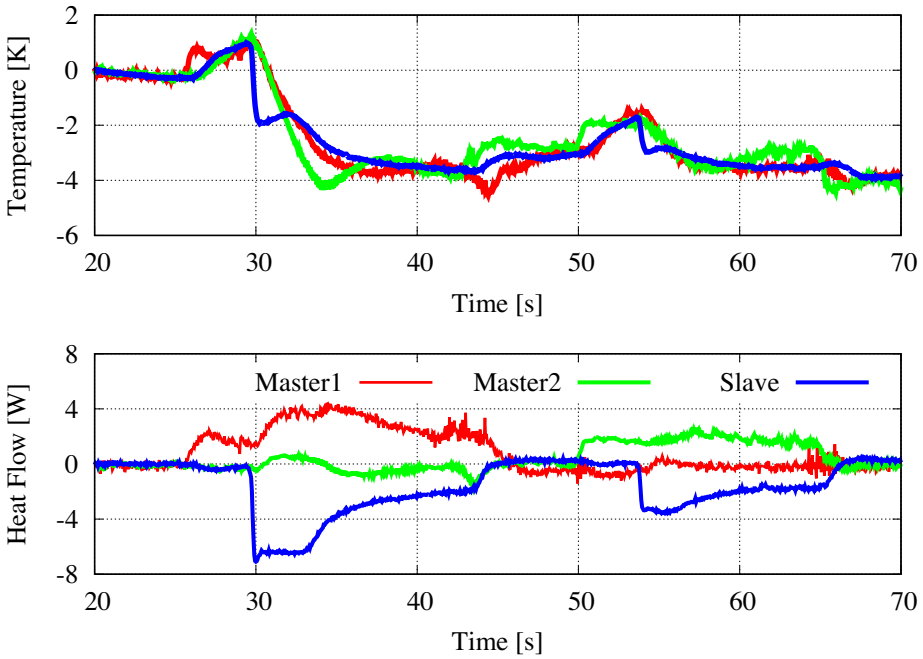

(b) Thermal sensation transmission response.

Fig. 7-9: Experimental results of the simultaneous presentation in the conventional method.

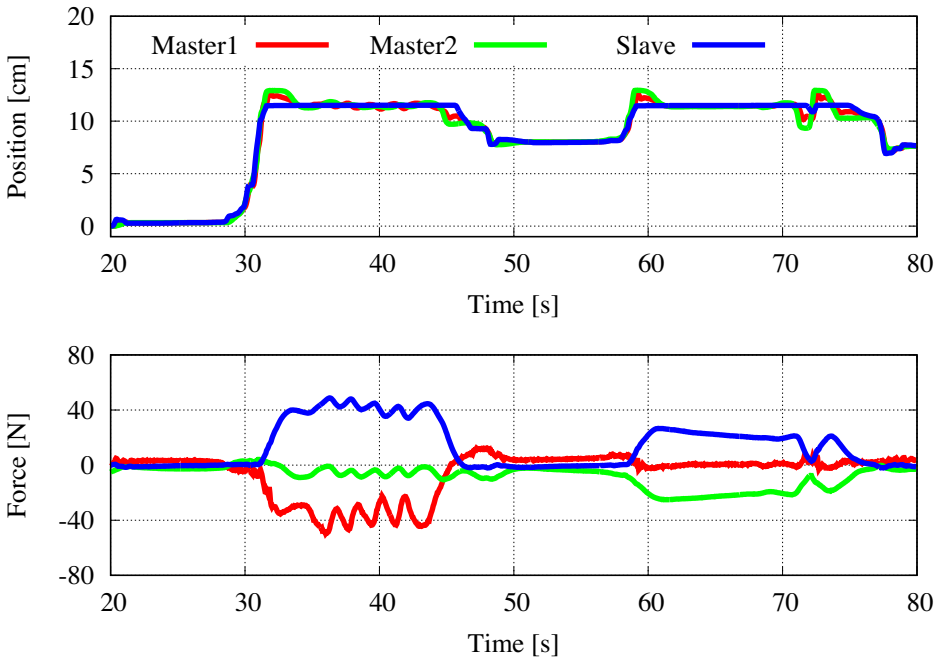

(a) Tactile sensation transmission response.

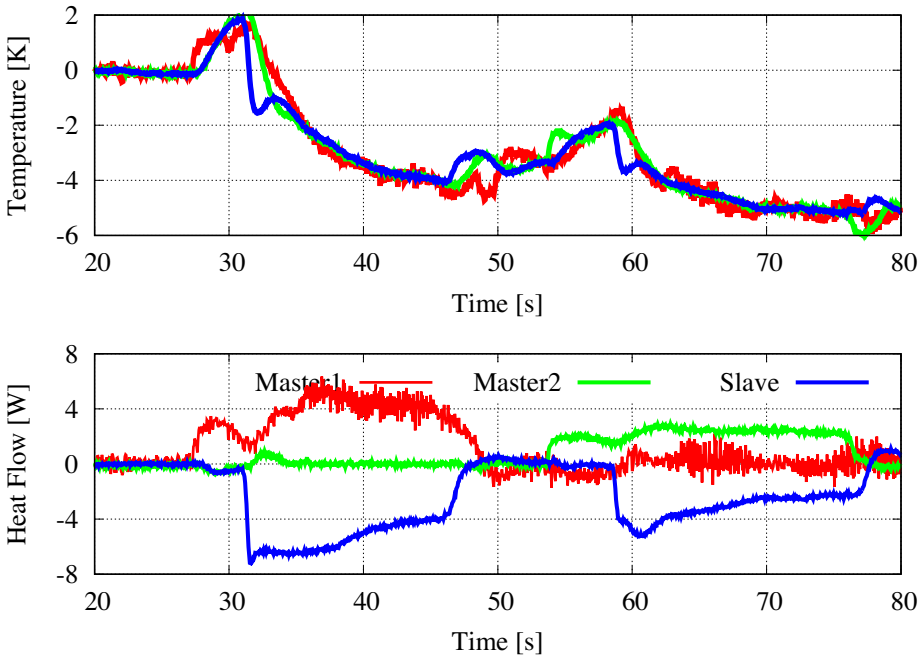

(b) Thermal sensation transmission response.

Fig. 7-10: Experimental results of the simultaneous presentation in the proposed method.

7.5 Summary of Chapter 7

In this chapter, multilateral teleoperation for presenting thermal and tactile sensations was proposed. By the use of the DOB to the Peltier device, the same connectivity design can be conducted to thermal systems. Since the time constant of the Peltier device is slow compared to robot manipulators, the artificial buffer was inserted in the modal transformation matrix of the tactile presentation system. The scaling gain was also used to compensate the difference in the motion range of manipulators. The experiments were conducted in a situation where there is a jitter between every system, and the results showed that the motion decoupling method was also effective in thermal systems. The inserted buffer corrected the timing of the presentation.

Chapter 8

Conclusions

This dissertation proposed connectivity design method to place controllers for each motion in multilateral systems separately. The connectivity is how to connect with other systems. Connectivity matrices for both COG and relative motions are designed so that each controller controls each motion separately. One of the interesting aspects of this dissertation was that it showed that how information is sent between systems can change the poles of a system without any use of controllers. The connectivity matrix showed how to route the information to control the defined motion in network systems explicitly. Based on the information routing, clear controller design was realized.

The method is able to realize the control goals of each motion in wide bandwidth. In order to realize wide bandwidth motion, controller parameters must be adequately tuned within the stable region. Even though some structures did not require a delay model, the method requires the round trip time delay to determine the controller gains. The control structure is more centralized rather than decentralized.

Chapter 2 proposed the connectivity design method of the relative motion in multilateral systems. The dissertation firstly showed that the COG motion was affected by the controllers for the relative motion because of the time delay between the systems when the number the system is two. The effect was mathematically observed by calculating the determinant of the connectivity matrix. If the determinant of the matrix is not 0, the controllers for the relative motion affects the COG motion. In order to regain the double integrator characteristics, the timing of the response used for the input to the relative motion controller was changed so that the determinant of the proposed graph Laplacian becomes 0. It revealed that there are two ways of realizing the condition: the first structure is the one which does not require the

delay model and the second one requires the delay model. The connectivity method was extended to a system that the number of an agent is n. The method was applied to several topologies, and it showed that the determinant of the graph Laplacian regarding the connectivity designed structure is 0. The dissertation revealed that the system that was constructed by the proposed method is similar to a multi-mass resonant system. Based on this notation, the controller parameter was designed by using the parameter design method of resonant ratio control. Impulse response was applied to see whether the system regains the double integrator characteristics in the COG motion. Sinusoidal and step commands were applied to the structures to see the proposed method can realize high command tracking performance because of the connectivity design.

The connectivity design using Type 2 can be extended to loop structured MAS while the structure designed using Type 1 cannot. The reason why the design using Type 1 cannot decouple COG/relative motions is because it assumes the propagation of the COG motion as one direction. In a loop structure, there are two ways to propagate information which is clockwise and counter-clockwise. As for a future work, a relative motion connectivity design method which does not require a delay time model should be established.

In Chapter 3, the connectivity design method of the COG motion in bilateral teleoperation was proposed. In bilateral teleoperation, it is well known that the controllers for COG and relative motions interfere because of the time delay between the systems. The reason for the interference was revealed first. It was because the number of the motion that the conventional method tried to control was larger than the number of the controllable motion. Based on the fact, connectivity of the force response was designed so that the force controller does not have the influence to the relative motion. It was realized by inserting the artificial buffer to the force response of the own system. The dissertation also revealed that the determinant of the connectivity matrix for COG motion is required to be 0 in order not to affect the relative motion. Since the connectivity design requires the delay model, the effect of the modeling error was analyzed by using the fundamental matrix. The matrix is used to express the relationship between four variables, and it was revealed that the model time should set as smaller value when there exists a modeling error. In order to compensate the effect of the modeling error, the phase-lag compensator and the phase lead compensator were used in COG motion and relative motion controllers, respectively. The phase-lag compensator was inserted not to affect the operational force in low-frequency area and also attenuate the interference from force controllers to position controllers. As for the phase lead controller, it realized to enlarge the phase margin in the relative motion control. The final performance was an-

alyzed by using the index which is called operationality and reproducibility. The experimental results showed that the proposed method has less operational force compared to FDD system, which is one of the famous methods to stabilize bilateral control systems under time delay. The convergence of position and force responses was also faster than the FDD method. Experiments of bilateral teleoperation under time-varying delay were also conducted, and it showed stable contact motion could be realized.

In Chapter 4, integrated design of connectivity for COG and relative motions in bilateral/multilateral teleoperation was proposed. As same as the design in Chapter 2, the dissertation showed that there are two ways to realize motion decoupling in bilateral teleoperation. The interesting characteristics of the proposed method is that the modal transformation matrix determines the route to realize motion decoupling. In bilateral teleoperation, the structure without the use of delay model was proposed. The design method was then extended to multilateral teleoperation. The determinant of the connectivity matrix for both motions became 0 in the proposed method. It indicates that the double integrator characteristics in COG motion is realized. The performance analysis showed that the proposed method has complete transmissibility even in the presence of time delay. The experimental results showed that the proposed method has the small operational force and the impedance reproduction performance is high.

In Chapter 5, bilateral control using flexible manipulators was proposed. Flexible manipulators are often used to mechanically enhance the safety; however, the control becomes difficult since the flexibility generates resonant peaks in the system. In order to compensate the effect of the resonance, the system was modeled by using the wave equation. By rejecting the reflected wave inside the system, the system becomes an equivalent input time delay system. In order to compensate the interference that will be caused by the equivalent time delay, modal transformation matrix for input delay systems was proposed. The experimental results showed that the proposed method was able to transmit precise motion without the vibration caused by the flexibility of the slave system.

In Chapter 6, the topology of the relative motion was optimized in multilateral teleoperation. Information value can be calculated from an adjacency matrix. In other methods, the value was obtained when there is no delay between the systems. This dissertation extended the definition of the value to network systems by putting a delay time into the elements of an adjacency matrix. The dissertation revealed that the relationship of the value between systems. The aim of using multilateral teleoperation to realize tactile sensation transmission is because operators want to receive precise impedance of an object that is in contact with the slave system. Based on this fact, the topology of multilateral teleoperation was optimized so that the slave system has the most influence on all systems. The design procedure of the

connectivity modification was shown, and the experimental results showed that the proposed method has better impedance transmission performance compared to the structure where the slave system does not have the largest influence. In real networks, the amount of time delay varies. Since the method assumes a constant delay to derive quantitative importance of each system, it is not clear whether the index can be applied to time-varying delay. As a future work, the index should be extended to evaluate the importance even when the delay is time-varying.

In Chapter 7, multimodal communication using multilateral teleoperation was proposed. Not only tactile sensation but also thermal sensation were transmitted through the network to realize a realistic feeling. Robot manipulators were used to transmitting tactile sensation, and the Peltier device was used to present thermal sensation in this chapter. The response speed of the Peltier device is slow compared to that of the robot manipulators. It means that even if motion decoupled control was realized by each system, the timing of the presentation varies. The difference of the response speed was modeled as a delay in this chapter, and to present the natural feeling of the remote object, the timing of the presentation was corrected by artificially inserting a delay element to the modal transformation matrix. Even though the delay time is equivalently enlarged for tactile sensation presentation, experimental results showed that the presentation timing was corrected between two sensations, realizing a much realistic feeling of a contact object placed at the slave system.

The method proposed in Chapter 2 realizes a structure that the relative motion does not affect the COG motion. The interference of the COG motion appears to the relative motion as some vibration between the systems. The method proposed in Chapter 3 realizes a structure that the COG motion does not affect the relative motion. The interference of the relative motion to the COG motion appears as a velocity constraint. The method proposed in Chapter 4 realizes a complete motion decoupling. The method is applicable for realizing delicate motions. Usually, it is desired to decouple each motion; however, the stability margin of the method is limited compared to the methods proposed in Chapter 2 and 3. In this situation, the method to use should be selected based on the priority of the motion the designer want to realize.

Although this dissertation succeeded in developing the fundamental theory for designing the connectivity in multilateral systems, the dissertation assumed to be the delay time as constant in the theoretical part even though the effect of time-varying delay was experimentally analyzed. Controller design in the time domain will enlarge the utility of the proposed method.

The local system has double integrator characteristics thanks to the DOB. However, this dissertation

did not considered other situations such as a system that has non-holomic constraint. As for the future work, the method should be extended to a situation where there are some constraints in local systems.

References

[1] R. A. Gupta and M.-Y. Chow, "Networked control system: Overview and research trends," *IEEE Transactions on Industrial Electronics*, Vol. 27, No. 7, pp. 2527–2535, July 2010.

[2] W. Zhang, M. S. Branicky, and S. M. Phillips, "Stability of networked control systems," *IEEE Control Systems Magazine*, Vol. 21, No. 1, pp. 84–99, February 2001.

[3] M. Krstic and A. Smyshlyaev, "Backstepping boundary control for first-order hyperbolic PDEs and application to systems with actuator and sensor delays," *Systems and Control Letters*, Vol. 57, No. 9, pp. 750 – 758, September 2008.

[4] O. J. Smith, "A controller to overcome dead time," *ISA Journal*, Vol. 6, No. 2, pp. 28–33, 1959.

[5] K. J. Astrom, C. C. Hang, and B. C. Lim, "A new smith predictor for controlling a process with an integrator and long dead-time," *IEEE Transactions on Automatic Control*, Vol. 39, No. 2, pp. 343–345, February 1994.

[6] W. Zhang and C. Lin, "Multivariable smith predictors design for nonsquare plants," *IEEE Transactions on Control Systems Technology*, Vol. 14, No. 6, pp. 1145–1149, November 2006.

[7] B. Oklander and M. Sidi, "Jitter buffer analysis," in *Proceedings of the International Conference on Computer Communications and Networks, ICCCN*, pp. 1–6, August 2008.

[8] L. Repele, R. Muradore, D. Quaglia, and P. Fiorini, "Improving performance of networked control systems by using adaptive buffering," *IEEE Transactions on Industrial Electronics*, Vol. 61, No. 9, pp. 4847–4856, September 2014.

[9] D. Yashiro and T. Yakoh, "Feedback controller with low-pass-filter-based delay regulation for networked control systems," *IEEE Transactions on Industrial Electronics*, Vol. 61, No. 7, pp. 3744–3752, July 2014.

[10] K. Natori and K. Ohnishi, "A design method of communication disturbance observer for time-delay compensation, taking the dynamic property of network disturbance into account," *IEEE Transactions on Industrial Electronics*, Vol. 55, No. 5, pp. 2152–2168, May 2008.

[11] K. Natori, R. Oboe, and K. Ohnishi, "Stability analysis and practical design procedure of time delayed control systems with communication disturbance observer," *IEEE Transactions on Industrial Informatics*, Vol. 4, No. 3, pp. 185–197, August 2008.

[12] A. Suzuki and K. Ohnishi, "Improvement in steady-state accuracy of time-delayed control systems with communication disturbance observer by low-frequency model error feedback," *IEEJ Transactions on Industry Applications*, Vol. 133, No. 9, pp. 861–867, September 2013 (in Japanese).

[13] N. Uematsu, T. Suhara, and Y. Uchimura, "Model-error feedback for systems with time-varying delay based on mixed H_2/H_∞ control," *IEEJ Journal of Industry Applications*, Vol. 5, No. 3, pp. 245–252, May 2016.

[14] R. Imai and R. Kubo, "Introducing jitter buffers in networked control systems with communication disturbance observer under time-varying communication delays," in *Proceedings of the Annual Conference of IEEE Industrial Electronics Society, IECON*, pp. 2956–2961, November 2015.

[15] R. Yang, G.-P. Liu, P. Shi, C. Thomas, and M. Basin, "Predictive output feedback control for networked control systems," *IEEE Transactions on Industrial Electronics*, Vol. 61, No. 1, pp. 512–520, January 2014.

[16] F. Liu, H. Gao, J. Qiu, S. Yin, J. Fan, and T. Chai, "Networked multirate output feedback control for setpoints compensation and its application to rougher flotation process," *IEEE Transactions on Industrial Electronics*, Vol. 61, No. 1, pp. 460–468, January 2014.

[17] Y. Xu and Z. Li, "Distributed optimal resource management based on the consensus algorithm in a microgrid," *IEEE Transactions on Industrial Electronics*, Vol. 62, No. 4, pp. 2584–2592, April 2015.

[18] S. Chen, D. Ho, and C. Huang, "Fault reconstruction and state estimator design for distributed sensor networks in multitarget tracking," *IEEE Transactions on Industrial Electronics*, Vol. 62, No. 11, pp. 7091–7102, November 2015.

[19] D. Lee and P. Y. Li, "Formation and maneuver control of multiple spacecraft," in *Proceedings of the American Control Conference, ACC*, Vol. 1, pp. 278–283, June 2003.

[20] R. Olfati-Saber, J. Fax, and R. Murray, "Consensus and cooperation in networked multi-agent systems," *Proceedings of the IEEE*, Vol. 95, No. 1, pp. 215–233, January 2007.

[21] L. Bakule, "Decentralized control: An overview," *Annual Reviews in Control*, Vol. 32, No. 1, pp. 87–98, April 2008.

[22] K. Movric and F. Lewis, "Cooperative optimal control for multi-agent systems on directed graph topologies," *IEEE Transactions on Automatic Control*, Vol. 59, No. 3, pp. 769–774, March 2014.

[23] H. G. Tanner, A. Jadbabaie, and G. J. Pappas, "Stable flocking of mobile agents, part i: Fixed topology," in *Proceedings of the IEEE Conference on Decision and Control, CDC*, Vol. 2, pp. 2010–2015, December 2003.

[24] W. Ren, R. W. Beard, and E. M. Atkins, "A survey of consensus problems in multi-agent coordination," in *Proceedings of the American Control Conference, ACC*, Vol. 3, pp. 1859–1864, June 2005.

[25] R. Olfati-Saber and R. Murray, "Consensus problems in networks of agents with switching topology and time-delays," *IEEE Transactions on Automatic Control*, Vol. 49, No. 9, pp. 1520–1533, September 2004.

[26] R. Olfati-Saber and R. M. Murray, "Consensus protocols for undirected networks of dynamic agents with communication time-delays," in *Proceedings of the Technical Report on California Institute of Technology Control and Dynamical Systems, CIT-CDS*, pp. 1–12, March 2003.

[27] M. Arcak, "Passivity as a design tool for group coordination," *IEEE Transactions on Automatic Control*, Vol. 52, No. 8, pp. 1380–1390, August 2007.

[28] L. Moreau, "Stability of multiagent systems with time-dependent communication links," *IEEE Transactions on Automatic Control*, Vol. 50, No. 2, pp. 169–182, February 2005.

[29] H. Zhang, G. Feng, H. Yan, and Q. Chen, "Observer-based output feedback event-triggered control for consensus of multi-agent systems," *IEEE Transactions on Industrial Electronics*, Vol. 61, No. 9, pp. 4885–4894, September 2014.

[30] T. Namerikawa and C. Yoshioka, "Consensus control of observer-based multi-agent system with communication delay," in *Proceedings of the SICE Annual Conference*, pp. 2414–2419, August 2008.

[31] P.-A. Bliman and G. Ferrari-Trecate, "Average consensus problems in networks of agents with delayed communications," *Automatica*, Vol. 44, No. 8, pp. 1985–1995, August 2008.

[32] D. Lee and M. Spong, "Stable flocking of multiple inertial agents on balanced graphs," *IEEE Transactions on Automatic Control*, Vol. 52, No. 8, pp. 1469–1475, August 2007.

[33] R. C. Goertz, "Mechanical master-slave manipulator," *Nucleonics*, Vol. 12, No. 11, pp. 45–46, 1954.

[34] D. Lawrence, "Stability and transparency in bilateral teleoperation," *IEEE Transactions on Robotics and Automation*, Vol. 9, No. 5, pp. 624–637, October 1993.

[35] W. Iida and K. Ohnishi, "Reproducibility and operationality in bilateral teleoperation," in *Proceedings of the IEEE International Workshop on Advanced Motion Control, AMC*, pp. 217–222, March 2004.

[36] K. Natori, S. Katsura, T. Tsuji, and K. Ohnishi, "Analysis of bilateral systems with time delay," in *Proceedings of the IEEE International Symposium on Industrial Electronics, ISIE*, Vol. 4, pp. 1511–1516, June 2005.

[37] P. F. Hokayem and M. W. Spong, "Bilateral teleoperation: An historical survey," *Automatica*, Vol. 42, No. 12, pp. 2035–2057, December 2006.

[38] D. Sun, F. Naghdy, and H. Du, "Application of wave-variable control to bilateral teleoperation systems: A survey," *Annual Reviews in Control*, Vol. 38, No. 1, pp. 12–31, 2014.

[39] G. Leung, B. Francis, and J. Apkarian, "Bilateral controller for teleoperators with time delay via μ-synthesis," *IEEE Transactions on Robotics and Automation*, Vol. 11, No. 1, pp. 105–116, February 1995.

[40] V. Chawda and M. O'Malley, "Position synchronization in bilateral teleoperation under time-varying communication delays," *IEEE/ASME Transactions on Mechatronics*, Vol. 20, No. 1, pp. 245–253, February 2015.

[41] B. Yalcin and K. Ohnishi, "Stable and transparent time-delayed teleoperation by direct acceleration waves," *IEEE Transactions on Industrial Electronics*, Vol. 57, No. 9, pp. 3228–3238, September 2010.

[42] L. Bate, C. D. Cook, and Z. Li, "Reducing wave-based teleoperator reflections for unknown environments," *IEEE Transactions on Industrial Electronics*, Vol. 58, No. 2, pp. 392–397, February 2011.

[43] B. Hannaford and J.-H. Ryu, "Time-domain passivity control of haptic interfaces," *IEEE Transactions on Robotics and Automation*, Vol. 18, No. 1, pp. 1–10, February 2002.

[44] J.-H. Ryu, D.-S. Kwon, and B. Hannaford, "Stable teleoperation with time-domain passivity control," *IEEE Transactions on Robotics and Automation*, Vol. 20, No. 2, pp. 365–373, April 2004.

[45] A. Aziminejad, M. Tavakoli, R. V. Patel, and M. Moallem, "Transparent time-delayed bilateral teleoperation using wave variables," *IEEE Transactions on Control Systems Technology*, Vol. 16, No. 3, pp. 548–555, May 2008.

[46] D. Sun, F. Naghdy, and H. Du, "Transparent four-channel bilateral control architecture using modified wave variable controllers under time delays," *Robotica*, Vol. 34, No. 4, pp. 859–875, April 2016.

[47] D. Sun, F. Naghdy, and H. Du, "Wave-variable-based passivity control of four-channel nonlinear bilateral teleoperation system under time delays," *IEEE/ASME Transactions on Mechatronics*, Vol. 21, No. 1, pp. 238–253, February 2016.

[48] B. Hannaford, "A design framework for teleoperators with kinesthetic feedback," *IEEE Transactions on Robotics and Automation*, Vol. 5, No. 4, pp. 426–434, August 1989.

[49] A. Smith and K. Hashtrudi-Zaad, "Neural network-based teleoperation using smith predictors," in *Proceedings of the IEEE International Conference on Mechatronics and Automation, ICMA*, Vol. 3, pp. 1654–1659, July 2005.

[50] S. Sirouspour and A. Shahdi, "Model predictive control for transparent teleoperation under communication time delay," *IEEE Transactions on Robotics*, Vol. 22, No. 6, pp. 1131–1145, December 2006.

[51] Y. Maddahi, S. Liao, W. Fung, E. Hossain, and N. Sepehri, "Selection of network parameters in wireless control of bilateral teleoperated manipulators," *IEEE Transactions on Industrial Electronics*, Vol. 11, No. 6, pp. 1445–1456, December 2015.

[52] K. Natori, T. Tsuji, K. Ohnishi, A. Hace, and K. Jezernik, "Time-delay compensation by communication disturbance observer for bilateral teleoperation under time-varying delay," *IEEE Transactions on Industrial Electronics*, Vol. 57, No. 3, pp. 1050–1062, March 2010.

[53] H. Kawada and T. Namerikawa, "Bilateral control of nonlinear teleoperation with time varying communication delays," in *Proceedings of the American Control Conference, ACC*, pp. 189–194, June 2008.

[54] P. Shull and G. Niemeyer, "Open-loop bilateral teleoperation for stable force tracking," in *Proceedings of the IEEE/RSJ International Conference on Intelligent Robots and Systems, IROS*, pp. 5121–5126, October 2009.

[55] D. Yashiro and K. Ohnishi, "Performance analysis of bilateral control system with communication bandwidth constraint," *IEEE Transactions on Industrial Electronics*, Vol. 58, No. 2, pp. 436–443, February 2011.

[56] J. Azorin, O. Reinoso, R. Aracil, and M. Ferre, "Generalized control method by state convergence for teleoperation systems with time delay," *Automatica*, Vol. 40, No. 9, pp. 1575–1582, September 2004.

[57] R. Kubo, N. Iiyama, K. Natori, K. Ohnishi, and H. Furukawa, "Performance analysis of a three-channel control architecture for bilateral teleoperation with time delay," *IEEJ Journal of Industry Applications*, Vol. 127, No. 12, pp. 1224–1230, December 2007.

[58] B. Hannaford and R. Anderson, "Experimental and simulation studies of hard contact in force reflecting teleoperation," in *Proceedings of the IEEE International Conference on Robotics and Automation, ICRA*, Vol. 1, pp. 584–589, April 1988.

[59] A. Suzuki and K. Ohnishi, "Frequency-domain damping design for time-delayed bilateral teleoperation system based on modal space analysis," *IEEE Transactions on Industrial Electronics*, Vol. 60, No. 1, pp. 177–190, January 2013.

[60] A. Suzuki and K. Ohnishi, "Novel four-channel bilateral control design for haptic communication under time delay based on modal space analysis," *IEEE Transactions on Control Systems Technology*, Vol. 21, No. 3, pp. 882–890, May 2013.

[61] D. Tian, D. Yashiro, and K. Ohnishi, "Wireless haptic communication under varying delay by switching-channel bilateral control with energy monitor," *IEEE/ASME Transactions on Mechatronics*, Vol. 17, No. 3, pp. 488–498, June 2012.

[62] S. Nishimura and S. Katsura, "Realization of simultaneity in bilateral teleoperation system under time delay," in *Proceedings of the IEEE International Workshop on Advanced Motion Control, AMC*, pp. 770–775, March 2014.

[63] S. Hyodo and K. Ohnishi, "A bilateral control system to synchronize with haptic and visual sense for teleoperation over network," in *Proceedings of the IEEJ International Workshop on Sensing, Actuation, and Motion Control, SAMCON*, March 2015.

[64] C. R. Carignan and H. I. Krebs, "Telerehabilitation robotics: Bright lights, big future?" *Journal of Rehabilitation Research and Development*, Vol. 43, No. 5, pp. 695–710, September 2006.

[65] Y. Ishibashi, T. Hasegawa, and S. Tasaka, "Group synchronization control for haptic media in networked virtual environments," in *Proceedings of the IEEE Haptics Symposium, HAPTICS*, pp. 106–113, March 2004.

[66] A. Drif, J. Citerin, and A. Kheddar, "Thermal bilateral coupling in teleoperators," in *Proceedings of the IEEE/RSJ International Conference on Intelligent Robots and Systems, IROS*, pp. 1301–1306, August 2005.

[67] S. Katsura, Y. Matsumoto, and K. Ohnishi, "Realization of "law of action and reaction" by multilateral control," *IEEE Transactions on Industrial Electronics*, Vol. 52, No. 5, pp. 1196–1205, October 2005.

[68] P. Malysz and S. Sirouspour, "A kinematic control framework for single-slave asymmetric teleoperation systems," *IEEE Transactions on Robotics*, Vol. 27, No. 5, pp. 901–917, October 2011.

[69] T. Shimono, R. Kubo, K. Ohnishi, S. Katsura, and K. Ohishi, "Multilateral control with haptic transmission ratio," *IEEJ Transactions on Industry Applications*, Vol. 127, No. 8, pp. 875–883, September 2007 (in Japanese).

[70] B. Khademian and K. Hashtrudi-Zaad, "A four-channel multilateral shared control architecture for dual-user teleoperation systems," in *Proceedings of the IEEE/RSJ International Conference on Intelligent Robots and Systems, IROS*, pp. 2660–2666, October 2007.

[71] B. Khademian and K. Hashtrudi-Zaad, "Dual-user teleoperation systems: New multilateral shared control architecture and kinesthetic performance measures," *IEEE/ASME Transactions on Mechatronics*, Vol. 17, No. 5, pp. 895–906, October 2012.

[72] H. Morimitsu and S. Katsura, "Construction of thermal multilateral control system based on quarry matirx," in *Proceedings of the IEEJ Annual Meeting*, No. 4, pp. 386–387, March 2013.

[73] M. Panzirsch, J. Artigas, J.-H. Ryu, and M. Ferre, "Multilateral control for delayed teleoperation," in *Proceedings of the International Conference on Advanced Robotics, ICAR*, pp. 1–6, November 2013.

[74] M. Shahbazi, H. A. Talebi, S. F. Atashzar, F. Towhidkhah, R. V. Patel, and S. Shojaei, "A novel shared structure for dual user systems with unknown time-delay utilizing adaptive impedance control," in *Proceedings of the IEEE International Conference on Robotics and Automation, ICRA*, pp. 2124–2129, May 2011.

[75] H. V. Quang and J.-H. Ryu, "Stable multilateral teleoperation with time domain passivity approach," in *Proceedings of the IEEE/RSJ International Conference on Intelligent Robots and Systems, IROS*, pp. 5890–5895, November 2013.

[76] T. Kanno and Y. Yokokohji, "Multilateral teleoperation control over time-delayed computer networks using wave variables," in *Proceedings of the IEEE Haptics Symposium, HAPTICS*, pp. 125–131, March 2012.

[77] D. Sun, F. Naghdy, and H. Du, "Stability control of force-reflected nonlinear multilateral teleoperation system under time-varying delays," *Journal of Sensors*, pp. 1–17, 2016.

[78] J. Li, M. Tavakoli, and Q. Huang, "Absolute stability of a class of trilateral haptic systems," *IEEE Transactions on Haptics*, Vol. 7, No. 3, pp. 301–310, July 2014.

[79] A. Yamaguchi, K. Natori, and K. Ohnishi, "Operationality of multilateral control system under constant communication time delay," *IEEJ Transactions on Industry Applications*, Vol. 129, No. 8, pp. 802–810, August 2009 (in Japanese).

[80] S. Nishimura and S. Katsura, "An evaluation of connectivity and a control in a multilateral communication system," *IEEJ Journal of Industry Applications*, Vol. 3, No. 2, pp. 164–173, March 2014.

[81] M. Panzirsch, R. Balachandran, and J. Artigas, "Cartesian task allocation for cooperative, multilateral teleoperation under time delay," in *Proceedings of the IEEE International Conference on Robotics and Automation, ICRA*, pp. 312–317, May 2015.

[82] S. Nishimura and S. Katsura, "Multilateral control under time delay for decoupling force and velocity controllers," in *Proceedings of the IEEE International Symposium on Industrial Electronics, ISIE*, pp. 1258–1263, June 2016.

[83] U. Farooq, J. Gu, M. El-Hawary, M. U. Asad, and J. Luo, "An extended state convergence architecture for multilateral teleoperation systems," *IEEE Access*, Vol. 5, pp. 2063–2079, January 2017.

[84] Z. Li, Y. Xia, D. Wang, D. H. Zhai, C. Y. Su, and X. Zhao, "Neural network-based control of networked trilateral teleoperation with geometrically unknown constraints," *Transactions on Cybernetics*, Vol. 46, No. 5, pp. 1051–1064, May 2016.

[85] Z. Chen, Y.-J. Pan, and J. Gu, "Integrated adaptive robust control for multilateral teleoperation systems under arbitrary time delays," *International Journal of Robust and Nonlinear Control*, Vol. 26, No. 12, pp. 2708–2728, July 2016.

[86] S. Katsura and K. Ohishi, "Modal system design of multirobot systems by interaction mode control," *IEEE Transactions on Industrial Electronics*, Vol. 54, No. 3, pp. 1537–1546, June 2007.

[87] S. Nishimura and S. Katsura, “Connectivity design and control of multi agent systems based on average/torsional mode,” in *Proceedings of the International Symposium on Applied Abstraction and Integrated Design, AAID*, pp. 1–6, March 2017.

[88] S. Nishimura and S. Katsura, “Realization of simultaneity in bilateral control system under communication delay,” *IEEJ Journal of Industry Applications*, Vol. 4, No. 3, pp. 253–261, May 2015.

[89] S. Nishimura and S. Katsura, “Comparison of control structures of bilateral control under time delay without velocity constraint in force control,” in *Proceedings of the IEEJ Technical Meeting on Mechatronics Control, MEC*, pp. 55–60, August 2015.

[90] E. Saito, S. Nishimura, and S. Katsura, “Bilateral control of mechanical resonant system based on reflected wave rejection,” in *Proceedings of the IEEJ Technical Meeting on Mechatronics Control, MEC*, pp. 59–64, September 2015.

[91] S. Brin and L. Page, “Reprint of: The anatomy of a large-scale hypertextual web search engine,” *Computer Networks*, Vol. 56, No. 18, pp. 3825–3833, December 2012.

[92] K. Ohnishi, M. Shibata, and T. Murakami, “Motion control for advanced mechatronics,” *IEEE/ASME Transactions on Mechatronics*, Vol. 1, No. 1, pp. 56–67, March 1996.

[93] F. L. Lewis, H. Zhang, K. Hengster-Movric, and A. Das, “Cooperative control of multi-agent systems -optimal and adaptive design approaches-,” Ser. Communications and Control Engineering. Springer, 2014.

[94] K. Yuki, T. Murakami, and K. Ohnishi, “Vibration control of a 2 mass resonant system by the resonance ratio control,” *IEEJ Transactions on Industry Applications*, Vol. 113, No. 10, pp. 1162–1169, October 1993 (in Japanese).

[95] K. Ohishi, K. Ohnishi, and K. Miyachi, “Torque-speed regulation of DC motor based on load torque estimation method,” in *Proceedings of the IEEJ International Power Electronics Conference, IPEC*, pp. 1209–1218, March 1983.

[96] T. Murakami, F. Yu, and K. Ohnishi, “Torque sensorless control in multidegree-of-freedom manipulator,” *IEEE Transactions on Industrial Electronics*, Vol. 40, No. 2, pp. 259–265, April 1993.

[97] E. Saito and S. Katsura, “Wave-based load disturbance observer for robust enhancement of reflected wave rejection-based vibration control,” in *Proceedings of the IEEE International Conference on Advanced Intelligent Mechatronics, AIM*, pp. 1114–1119, July 2015.

[98] E. Saito and S. Katsura, “Vibration suppression of resonant system by using wave compensator,” in *Proceedings of the Annual Conference of IEEE Industrial Electronics Society, IECON*, pp. 4250–4255, November 2011.

[99] K. Akuzawa and K. Ohnishi, “Design indices for information connection in decentralized system,” in *Proceedings of the Annual Conference of IEEE Industrial Electronics Society, IECON*, Vol. 3, pp. 2417–2422 Vol.3, November 2003.

[100] Y. Uchimura, T. Yakoh, and K. Ohnishi, “A controller design method for mutually interacted decentralized systems,” *Transactions of the Society of Instrument and Control Engineers*, Vol. 41, No. 7, pp. 547–554, March 2005.

[101] A. Yamaguchi and K. Ohnishi, “Improvement of operationality for multilateral control system under constant time delay,” in *Proceedings of the IEEE International Workshop on Advanced Motion Control, AMC*, pp. 538–543, March 2008.

[102] T. Suzuyama, S. Katsura, and K. Ohishi, “Decoupling type multilateral control by using identity ratio,” *IEEJ Transactions on Industry Applications*, Vol. 127, No. 6, pp. 571–578, September 2007.

[103] H. Morimitsu and S. Katsura, “Control of thermal conductance of peltier device using heat disturbance observer,” *IEEJ Journal of Industry Applications*, Vol. 132, No. 3, pp. 333–339, March 2012.

List of Achievements

Journals (As a first author)

[1] Satoshi Nishimura and Seiichiro Katsura, "An Evaluation of Connectivity and a Control in a Multilateral Communication System," *IEEJ Journal of Industry Applications*, Vol. 3-D, No. 2, pp. 164–173, March 2014.

[2] Satoshi Nishimura and Seiichiro Katsura, "Realization of Simultaneity in Bilateral Control System under Communication Delay," *IEEJ Journal of Industry Applications*, Vol. 4-D, No. 3, pp. 253–261, May 2014.

International Conference (As a first author)

[1] Satoshi Nishimura and Seiichiro Katsura, "Topology Analysis of Position Information in Multilateral Communication System," *Proceedings of the 39th Annual Conference of IEEE Industrial Electronics Society, IECON'13-VIENNA*, pp. 6569–6574, November 2013.

[2] Satoshi Nishimura and Seiichiro Katsura, "Realization of Simultaneity in Bilateral Teleoperation System under Time Delay," *Proceedings of the 13th IEEE International Workshop on Advanced Motion Control, AMC'14-YOKOHAMA*, pp.770–775, March 2014.

[3] Satoshi Nishimura and Seiichiro Katsura, "Reduction of an Operational Force in a Simultaneity Realized Bilateral Telecommunication System," *Proceedings of the 23rd IEEE International Symposium on Industrial Electronics, ISIE'14-ISTANBUL*, pp. 2252–2257, June 2014.

[4] Satoshi Nishimura and Seiichiro Katsura, "Performance Enhancement Method for Bilateral Telecommunication System utilizing Buffered Information," *Proceedings of the 40th Annual Conference of IEEE Industrial Electronics Society, IECON'14-DALLAS*, pp. 4793–4798, October 2014.

[5] Satoshi Nishimura and Seiichiro Katsura, "Contact Motion Stabilization Using Equivalent Future Response in Synchronized Bilateral Teleoperation," *Proceedings of the 12th International Conference on Ubiquitous Robots and Ambient Intelligence, URAI'15-GOYANG*, pp. 66–71, October 2015.

[6] Satoshi Nishimura and Seiichiro Katsura, "Analysis and Compensation of Modeling Error for Synchronized Bilateral Teleoperation," *Proceedings of the 41st Annual Conference of IEEE Industrial Electronics Society, IECON'15-YOKOHAMA*, pp. 5279–5284, November 2015.

[7] Satoshi Nishimura and Seiichiro Katsura, "Modal Space Selection and Control in Bilateral Control under Time Delay," *Proceedings of the 2nd International Workshop on Sensing, Actuation, Motion Control, and Optimization, SAMCON'16-TOKYO*, TT7-6, pp. 1–6, March 2016.

[8] Satoshi Nishimura and Seiichiro Katsura, "Multilateral Control under Time Delay for Decoupling Force and Velocity Controllers," *Proceedings of the 25th IEEE International Symposium on Industrial Electronics, ISIE'16-SANTA CLARA*, pp. 1258–1263, June 2016.

[9] Satoshi Nishimura and Seiichiro Katsura, "Multilateral Transmission of Thermal and Force Sensations for Skill Acquisition," *Proceedings of the IEEE/RSJ International Conference on Intelligent Robots and Systems, IROS'16-DAEJEON*, No. 10, pp. 1–2, October 2016.

[10] Satoshi Nishimura, Yukiko Osawa, Hiroki Kurumatani, Yuki Nagatsu, Kazumasa Miura, and Seiichiro Katsura, "Simultaneous Presentation of Thermal and Tactile Sensations Using Multilateral Control under Time Delay," *Proceedings of the 3rd International Workshop on Sensing, Actuation, Motion Control, and Optimization, SAMCON'17-NAGAOKA*, SS2-4, pp. 1–6, March 2017.

[11] Satoshi Nishimura and Seiichiro Katsura, "Connectivity Design and Control of Multi Agent Systems Based on Average/Torsional Mode," *Proceedings of the 1st International Symposium on Applied Abstraction and Integrated Design, AAID'17-YOKOHAMA*, RS2-6, March 2017.

International Conference (As a co-author)

[1] Ayaka Matsui, Satoshi Nishimura, and Seiichiro Katsura, "A Classification Method of Motion Database Using Hidden Markov Model," *Proceedings of the 23rd IEEE International Symposium on Industrial Electronics, ISIE'14-ISTANBUL*, pp. 2228–2233, June 2014.

Domestic Conference (As a first author)

[1] Satoshi Nishimura and Seiichiro Katsura, "An Evaluation of Connectivity and a Control in a Multilateral Communication System," *Proceedings of Technical Meeting on Industrial Instrumentation and Control, IIC'13-CHIBA*, Vol. 5, pp. 91–96, March 2013.

[2] Satoshi Nishimura and Seiichiro Katsura, "An Analysis of Multilateral System under Time Delay Considering the Information Volume," *Proceedings of the 2013 IEEJ Annual Meeting, Aichi*, Vol. 4, pp. 397–398, March 2013 (in Japanese).

[3] Satoshi Nishimura and Seiichiro Katsura, "Realization of Simultaneity Property in Bilateral Control under Time Delay," *Proceedings of the 31st Annual Conference of the Robotics Society of Japan, RSJ 2013, Tokyo*, pp. 1–4, September 2013 (in Japanese).

[4] Satoshi Nishimura and Seiichiro Katsura, "Force Sensation Transmission Performance Enhancement for Multilateral Control System under Time Delay," *Proceedings of the 2013 Annual Conference of the Japan Society of Mechanical Engineers, JSME, Okayama*, pp. 1–5, September 2013 (in Japanese).

[5] Satoshi Nishimura and Seiichiro Katsura, "A Control Design Method to Realize Simultaneity in Bilateral Control System under Communication Delay," *Proceedings of Technical Meeting on Mechatronics Control, MEC'13-NAGAOKA*, pp. 87–92, November 2013.

[6] Satoshi Nishimura and Seiichiro Katsura, "Reducing the Operational Force in a Simultaneity Realized Bilateral Teleoperation System," *Proceedings of Technical Meeting on Industrial Instrumentation and Control, IIC'14-TOKYO*, Vol. 5, pp. 97–102, March 2014.

[7] Satoshi Nishimura and Seiichiro Katsura, "Stabilization Method of Contact Motion in Bilateral Teleoperation System Utilizing Impulse Damping," *Proceedings of the 32nd Annual Conference of the Robotics Society of Japan, RSJ'14-FUKUOKA*, September 2014 (in Japanese).

[8] Satoshi Nishimura and Seiichiro Katsura, "Comparison of Control Structures of Bilateral Control under Time Delay without Velocity Constraint in Force Control," *Proceedings of Technical Meeting on Mechatronics Control, MEC'15-TOKYO*, pp. 65–70, August 2015.

[9] Satoshi Nishimura, Yukiko Osawa, Hiroki Kurumatani, Yuki Nagatsu, Kazumasa Miura, and Seiichiro Katsura, "Kinesthetic and Thermal Sensation Presentation Using Multilateral Control under Time Delay," *Proceedings of Technical Meeting on Mechatronics Control, MEC'16-TOKYO*, pp. 55–60, September 2016 (in Japanese).

[10] Satoshi Nishimura and Seiichiro Katsura, "Vibration Suppression Control Based on Reflected Wave Rejection Using Acceleration Sensor," *Proceedings of the Spring Meeting on Japan Society for Precision Engineering, Yokohama*, pp. 313–314, March 2017 (in Japanese).

[11] Satoshi Nishimura and Seiichiro Katsura, "Mode Decoupling Control for Networked Multi Agent System Based on Connectivity Design," *Proceedings of the 2017 IEEJ Annual Meeting, Toyama*, pp. 128–129, March 2017 (in Japanese).

Domestic Conference (As a co-author)

[1] Eiichi Saito, Satoshi Nishimura, and Seiichiro Katsura, "Bilateral Control of Mechanical Resonant System Based on Reflected Wave Rejection," *Proceedings of Technical Meeting on Mechatronics Control, MEC'15-TOKYO*, pp. 59–64, September 2015.

Awards

[1] "IECON 2015 Best Presentation Recognition"
The 41st Annual Conference of IEEE Industrial Electronics Society, IECON'15
November 2015

[2] "IES Student Paper Travel Award"
The 25th International Symposium on Industrial Electronics, ISIE'16
June 2016

[3] "Student Forum Best Paper & Presentation Award"
The 25th International Symposium on Industrial Electronics, ISIE'16
June 2016

Career

[1] April 2015∼March 2016
Research Associate
The Graduate School of Keio University

[2] April 2016∼
Research Fellow (DC2)
The Japan Society for the Promotion of Science